Small molecules: Where do they go to on tea leaves?

Declan Cummins BSc.

Thesis submitted to the University of Nottingham

for the degree of Doctor of Philosophy

Abstract

The aims of this project were to investigate the surface chemistry and morphology of processed tea leaves the techniques of atomic force microscopy (AFM), scanning electron microscopy (SEM) and time of flight secondary ion mass spectrometry (ToF-SIMS). Data from the spectra obtained by ToF-SIMS was also analysed using principal component analysis (PCA). Further experimentation was performed on tea leaves by the addition of diluted samples of aromas, methyl salicylate, trans-2-hexenal and linalool and examining these leaves using depth profiling to discover how far into the leaf the aroma had penetrated and if there was any connection between the chemistry and size of the aromas and how far they penetrated.

A general characterisation of the tea leaves was performed in Chapter 3 where layers of waxes of a comparable size were observed on both green and black tea leaves with AFM, as were micro-crystals on black tea and areas showing two distinct types of interaction between the cantilever tip and the surface of a green tea leaf indicating different surface properties. SEM images revealed a visual difference between green and black tea leaves, where the black tea leaves had more debris on the surface and greater changes in topography due to the different processing methods.

The presence of lipids and epicuticular waxes were observed on the surface of the tea leaves using the ToF-SIMS.

In Chapter 4 the effects of infusion in hot water on the morphology and surface chemistry of the tea leaves are examined. SEM revealed structural damage to the leaves from 30 seconds of infusion and this increased with infusion time, resulting in the formation of holes in the cutin on the adaxial surface of the tea leaf. By examining positive and negative ToF-SIMS spectra and using PCA, a change in surface chemistry could be detected from 15 seconds of infusion. The intensity of $C_3H_5O_2^+$ peaks in the spectra increased as infusion time increased, indicating that the waxy cuticle of the leaf surface had been removed revealing the underlying epidermal cell layer. Peaks associated with octadecenoic and octadecanoic acids were shown to have a reproducible effect on the positioning of the different infusion times within the PCA plots. Though chemical changes can be detected at 15 seconds, the first 30 seconds of infusion were found to be responsible for the majority of the chemical changes on the surface. Taken together these data indicate that the melting of the cutin layer, primarily within the first 30 seconds of infusion may be related to the release of flavour, aroma and constituents such as polyphenols.

The penetration into the leaf of aroma molecules was examined in Chapter 5. Diluted solutions of methyl salicylate, linalool and trans-2-hexenal were added to tea leaves and then examined using depth profiling with ToF-SIMS. For the first time a leaf was depth profiled using a C_{60}. The

presence of trans-2-hexenal was detected in the palisade mesophyll layer of the leaf as was methyl salicylate, but to a smaller intensity. Methyl salicylate showed partitioning in diffusion across the cuticle with a large intensity in the cuticle and also in the interface between the epidermis and palisade mesophyll layers. Linalool was present on the surface of the leaf and showed partitioning in the cuticle of the tea leaves. As trans-2-hexenal was the smallest and least lipophilic of the three aromas examined it is theorized that the smaller the size of the aroma molecule plays a key role in the penetration of the dehydrated leaves.

Acknowledgements.

I would like to thank my supervisors, Professor Clive Roberts and Professor Martyn Davies, for their support, guidance and advice during my PhD. Thanks also go to Doctor Allen Griffiths from Unilever for their input and to all members of the LBSA in Nottingham, with a special mention to Doctor Xingyong Chen for AFM training and help and Doctor David Scurr for training on the ToF-SIMS and analysis and help and advice.

Funding for this project came from the BBSRC and Unilever and I would like to thank them for that.

I would like to thank my mother, Margaret Brown, my brother and sister, Brendan and Regina Brown for listening to me talk about tea far too much and supporting me during this process.

I would finally like to thank my friends, Matthew Williams, Lee Binding, Zoe Ridley and Martin Bushell for allowing me to talk to them endlessly when I needed to about the experiments, results and the whole writing process.

Finally, this thesis is in memory of Archie, gone far too early.

Table of contents

Table of figures

Chapter 1

Chapter 3

Chapter 4

Chapter 5

Chapter 1.

Introduction

1.1 Introduction

To characterise and examine the surface properties of tea leaves, several techniques will be used. Atomic force microscopy (AFM) will be used to map the topography of the surface and also to examine if there are any differences in the surface properties due to force interactions between the cantilever tip and the tea leaf surface.

Time of flight secondary ion mass spectrometry (ToF-SIMS) will be used to examine the chemical composition of the tea leaves and to also examine changes in the leaves during infusion with boiling water. When specific aromas are added to the surface of the tea leaves depth profiling will be performed to determine when the aroma is in the leaves by removing layers of the surface and scanning to identify aroma molecules and constituents within the leaf.

Principle component analysis (PCA) will be used to analyse ToF-SIMS data for the infusion of tea leaves to examine if different infusion times affect the surface chemistry of the tea leaves.

1.2. General introduction to tea

1.2.1 General introduction to tea

The leaves of the plant *Camellia sinensis* are a crop of major economic importance. When processed and infused with boiling water tea is produced. Tea is the second most commonly drunk liquid after water (Graham. 1992; McKay et al. 2002). It is clear that the production of tea has had a major impact on society, whether as the formation of elaborate rituals for tea drinking ceremonies in the East or the spark that started the American Revolution with the Boston tea party.

Originally all tea came from China. The Chinese plants were *Camellia sinensis* var. *sinensis*. Original attempts to transplant these plants in India failed. During the Chinese opium wars the production of tea was greatly destabilised, fortunately a variant breed *Camellia sinensis* var. *assamica* was discovered in the hills of Assam in India by Major Robert Bruce, it took years for official identification to be performed, even when a second sample was sent in by Lieutenant Charlton. It was only after the death of Bruce, when his brother requested identification that it was confirmed to be tea. The discovery of this variant led to the foundation of tea plantations all over the Asian and African highlands. The main product of these plantations is black tea.

Both varieties of the plant grow best in warm, humid climates and in its wild state can grow up to a metre a year. The plant prefers a weakly acidic and well drained soil, with diffuse light (Zhang et al. 2008). The evergreen shrub can grow up to 17 metres in height but is usually pruned to between 1 and 2 metres to make harvesting easier.

The growth conditions of the plants, such as type of soil, climate and altitude of growth, have an effect on the characteristics and flavour of the tea.

Harvesting is still a very manual job and happens every 7 to 14 days; the top two leaves and the bud are typically plucked. At sea level the bush will replace the plucked leaves at a much quicker rate than if the bush is at a higher altitude (Tea council. 2003). It is possible for mechanical plucking but this is seen as giving a product that is less uniform and of a lower quality (Zhang et al. 2008).

1.2.2 Economic importance of tea

Considering the industry that has surrounded the growing and processing of tea as a commodity it is important to consider the economic importance of this crop. Figure 1.1 shows the top twenty countries producing tea in 2009, where the amount of tea produced per country is shown. China and India are still the highest producers of tea but some of the third world

developing countries are included in this list showing the importance of the growth and export of this crop for these poorer regions.

Figure 1.2 shows the 2008 import figures for the top twenty tea importing areas. Previously the United Kingdom was the largest importer of tea, until 2004, the Russian Federation and the United Arab Emirates now spend more money on importing tea than the UK. Both import and export figures were not available for 2009. With regards to the export of tea, figure 1.3 shows the top 20 nations of tea exporters for 2008.

The Russian Federation, United Arab Emirates, United Kingdom, United States of America, France, the Netherlands and Poland all export a larger value of tea than they import. It can be assumed that these countries are resellers. Given the location of these countries and the wealth of them it would be likely that these are selling specific brands and blends which account for the large volumes imported and exported.

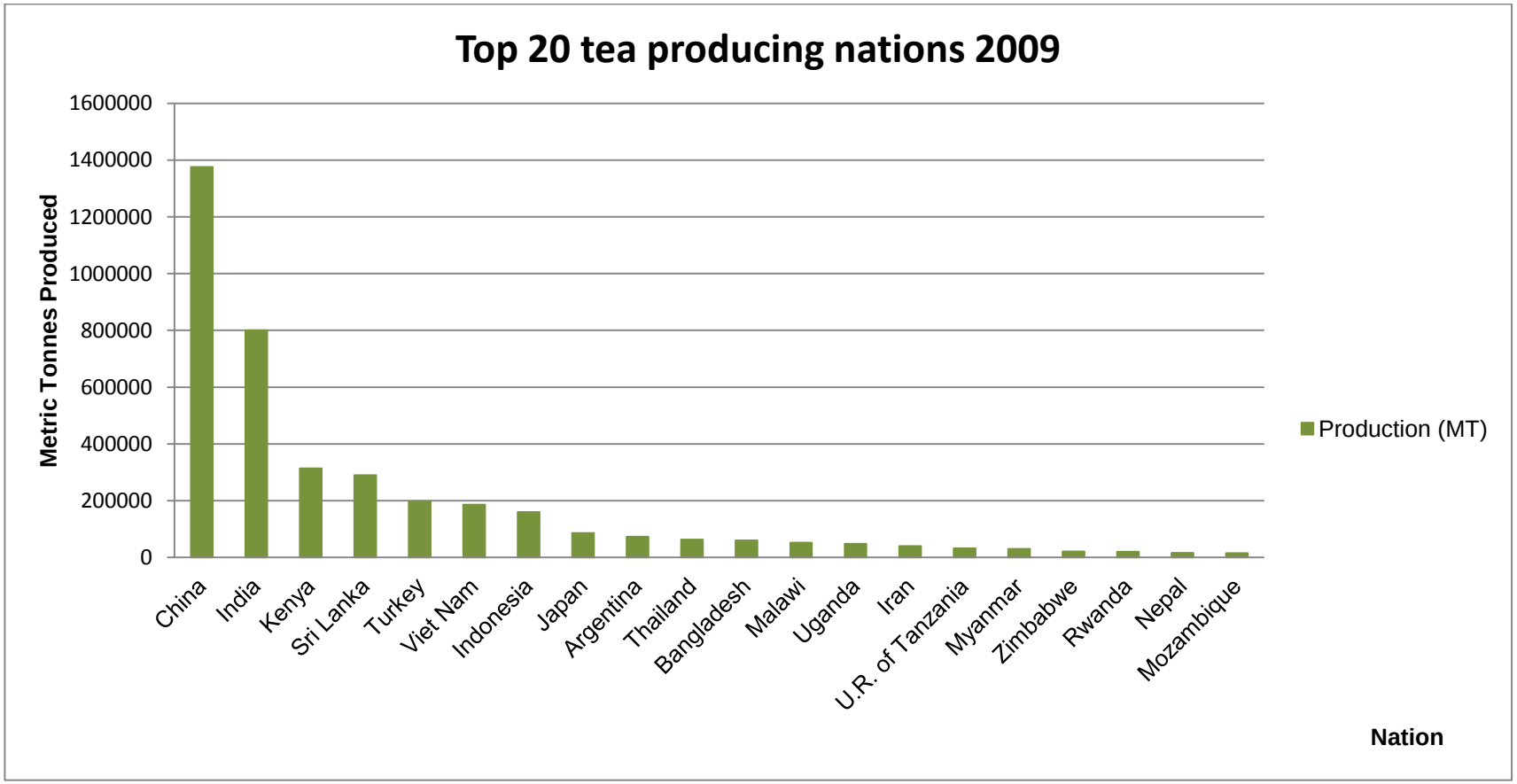

Figure 1.1 – Top 20 tea producing nations world wide (estimated metric tonnage). (Source Food and Agriculture Organization of the United Nations).

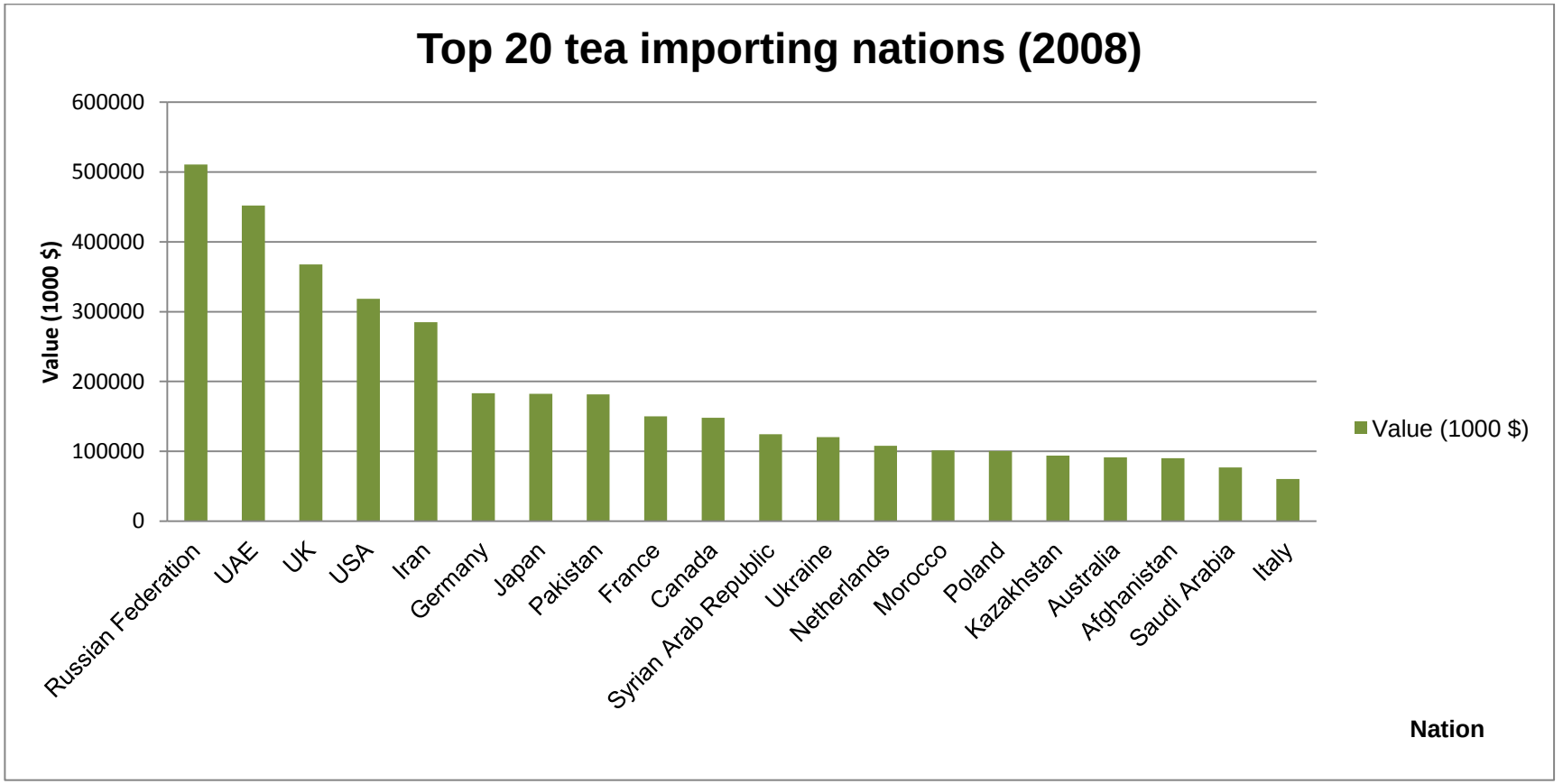

Figure 1.2 – Top 20 tea importing nations world wide (based on cost of tea imported). (Source Food and Agriculture Organization of the United Nations).

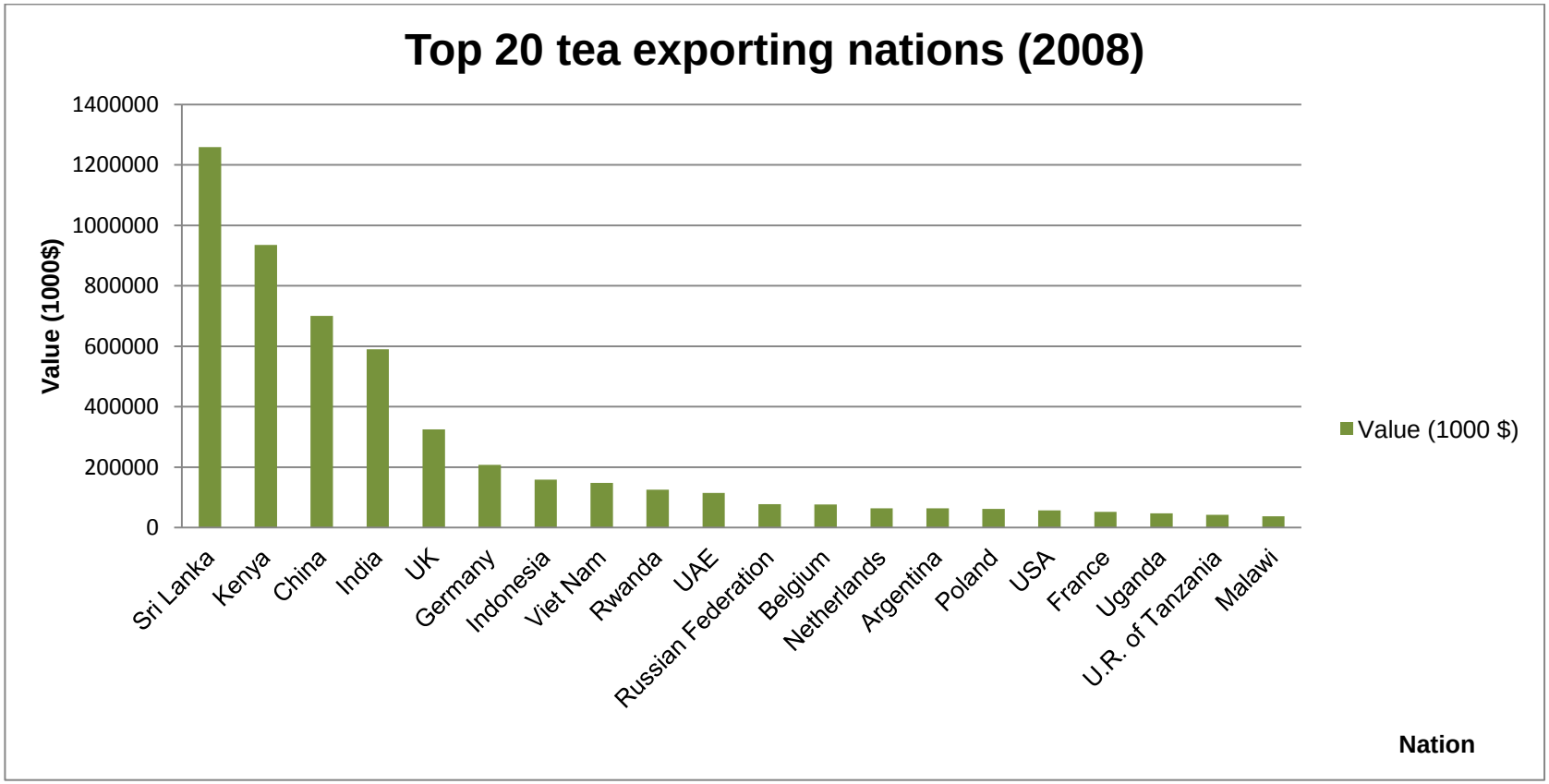

Figure 1.3 – Top 20 tea exporting nations world wide (based on value of tea exported) (Source Food and Agriculture Organization of the United Nations).

Specific trade figures for the United Kingdom show that tea is a large business. Figure 1.4 a shows the manufacturer sales for 4 years in the UK in tea products (under 3kg). In 2007 the tea export trade made £674,282,000. Though this is a decrease in the £710,648,000 export figure from the previous year it is still a large sales figure. Given the variable price of tea and the state of the global economy, fluctuations are bound to be seen in any commodity. The variability of the price is seen in figure 1.4b which shows the price per tonne of tea exports.

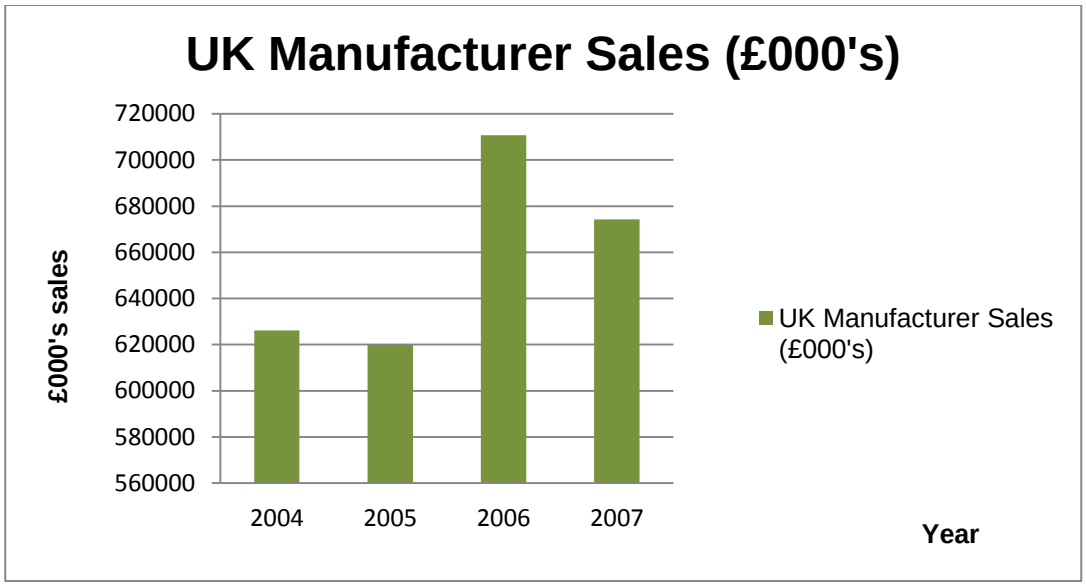

Figure 1.4a – Sales of tea from UK manufacturers (£000's) for 2004 to 2007 (Source Office of National Statistics PRA 15860 Processing of Tea and Coffee 2007).

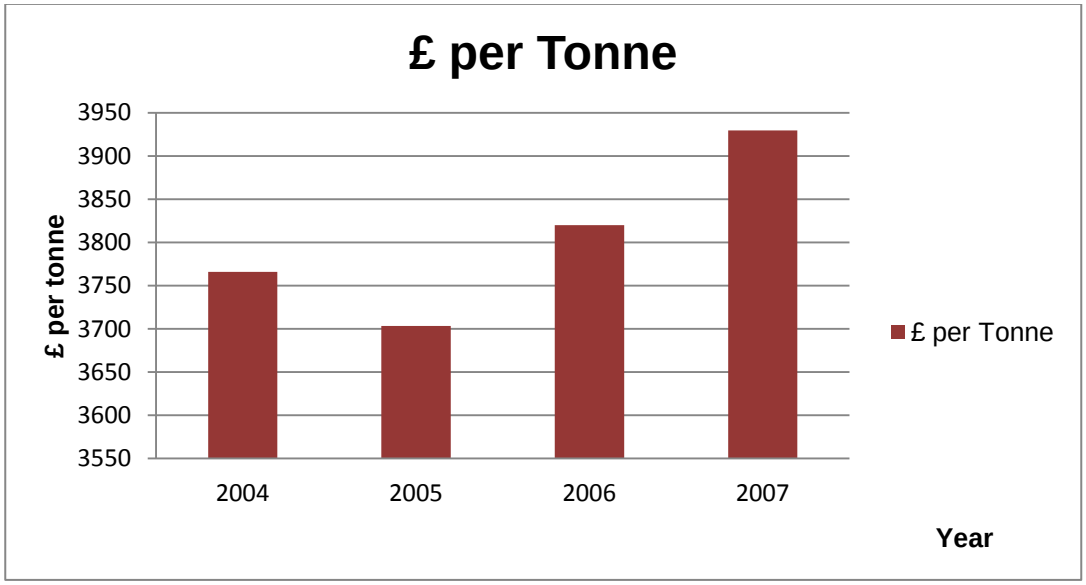

Figure 1.4b - £ per tonne of tea based on UK manufacturer sales for 2004 to 2007 (Source Office of National Statistics PRA 15860 Processing of Tea and Coffee 2007).

Black tea has the largest share of the tea market in terms of sales, quantities consumed and production so most tea factories will produce this variant (Approximately 70.09% of the market share).

The apocryphal story of the origin of the tea drink as we know it today is that leaves from the tea plant, *Camellia sinensis* va r. *sinensis* fell in the boiled drinking water of Emperor Shen Nung in 2737BC, the second emperor of China. After drinking the infusion the Emperor is said to have found the drink delicious and refreshing and is listed as having accidentally discovering the stimulating and beneficial properties of a tea infusion (Chopra et al. 2000).

1.2.3 General production of tea

Camellia sinensis, also commonly known as the tea plant, tea bush and tea tree, is the plant whose leaves are harvested for the production of the majority of tea products sold around the world.

The evergreen shrub is usually trimmed to keep the height below six feet to allow the easy harvesting of the buds and top two leaves of the plant. It is able to grow in tropical and subtropical climates, but some varieties are able to grow in much harsher conditions. The ranges in which the plant

can grow extend from the outer Carpathians and Russia in the Northern hemisphere to the Indian subcontinent, Japan, China and Africa in the Southern hemisphere.

The younger leaves are preferentially harvested for the production of tea. This is because different leaf ages can have an effect on the quality of the tea produced due to differences in the chemical composition of the leaf. Given the rate of growth for the plant, harvesting can occur every week to two weeks to ensure only new growth is plucked.

The production of tea begins with the picking of the leaves. The picking season depends upon the country in which the tea is being produced. For example African teas will be picked all year round, whereas the Asian countries have a specific season of May through to August. Only the bud of the plant and the top two leaves are picked. Some plantations also include the flower to be added to the blend as an aroma supplement.

After picking the leaves are processed to produce the tea. The amount of processing varies on which type of tea is to be produced (Wilson et al. 1991; Wilson et al. 2003; Zhang et al. 2008).

1.2.3.1 Black tea

Black tea is the most processed form of tea and goes through a number of production stages. The term black tea derives from its colour, which is characteristic of the fermentation process that the leaf goes through. This type of fermentation is not the same as in the brewing industry of alcohol.

The leaves are first withered. This is to reduce the moisture content of the tea leaf. The withering process is where the leaves are laid out on a wire mesh and hot air is passed through the mesh and leaves. The mesh ensures that all leaves are dried in a uniform fashion. The final withered leaves are pliable and limp and this process can take up to 17 hours.

After withering the leaves are then rolled in a machine. The reason for this process is to break the structure of the leaves and to release the oxidative enzymes within the leaf to start the next processing step of oxidation. In oxidation the leaves are left in troughs or laid out on tables to allow the oxidative enzymes within the leaf to come into contact with the atmosphere. The oxidation process produces the colour, flavour and aroma of the final tea product. During this process the leaves will change from a green colour to a light brown and finally a dark brown colour. This process is time dependent as the tea can be spoilt if it is left to oxidise for too long. Usual oxidation times are from half an hour to 2 hours at a specified temperature of approximately 26 ^{o}C. This step is constantly monitored to ensure the temperature is constant and the tea is not spoilt.

The oxidation step is where catechins are condensed and oxidatively polymerised by the catalisation of polyphenol oxidase and peroxidise. The final products of this oxidative step include theaflavins and thearubigens which affect the colour and the taste of the tea (Zhang et al. 2008).

To stop the oxidation process the tea is dried. This is done by passing the oxidising leaves through hot air driers again to degrade the oxidative enzymes. At the end of the final drying stage the moisture content of the tea leaves is reduced to 3% of the original moisture content. The leaves can then be graded according to size and quality (Chen 1984; Wilson et al. 1991; Wilson et al. 2003; Zhang et al. 2008).

1.2.3.2 Green tea

Green tea is produced in a different way to black tea to ensure the oxidation step doesn't occur. By denaturing the oxidative enzymes and also keeping the leaf whole this processing step is completely omitted.

The leaves are usually first sun dried on trays for a few hours. After this they are usually roasted. The roasting process involves either steaming of the leaves or pan frying to inactivate the oxidative enzymes. Techniques involved in this step include the use of microwaves, far infrared, rotary heated drums, steaming machines and less technological solutions such as wood burning pans. The leaves are then rolled. To reduce the stress

and damage to the leaf these can be manually rolled as opposed to the black tea manufacturing where a machine roller is generally used.

Following on from the rolling the leaves are dried again to reduce moisture content and can then either be rolled for a final time to give the leaf it distinctive shape and then sorted into it grade or just sorted into its grade without the final rolling stage. The final moisture content should be below 6% of its original content (Chen 1984; Wilson et al. 1991; Zhang et al. 2008).

The tea is generally divided into two groups depending on the method of fixation. China mainly produces pan-fried green tea and Japan mainly produces steamed green tea. The pan-fried tea is usually for export whilst the steamed tea is for consumption within Japan rather than export (Zhang et al. 2008).

1.2.3.3 Other teas

Many other types of tea are also commercially available. With the exception of herbal and fruit teas these all are made from the leaves of the *Camellia sinesis* plant. The only difference between these types of tea is how they are produced. Figure 1.5 shows how these different teas are produced. With fruit and herbal teas, the ingredients are made of combinations of dried parts of plants and fruits. These are caffeine free and are sweetened with the sugars naturally found in fruits.

Oolong tea is a traditional Chinese tea which is partially oxidised. There is a range of 10% to 70% oxidation in production of Oolong. This variation is not in the plant but in the production of the finished tea product and it is not stated if the original leaves are from sources usually used for the production of green or black tea (Lee 2006).

White tea is made from young leaves and new growth buds of *Camellia sinensis,* but from the cultivars (a cultivated plant given a specific name because of it desirable characteristics) *Da Bai*, *Xiao Bai*, *Narcissus* and *Chaicha*. It is a speciality of the Chinese province of Fujian (Chow et al. 1990).

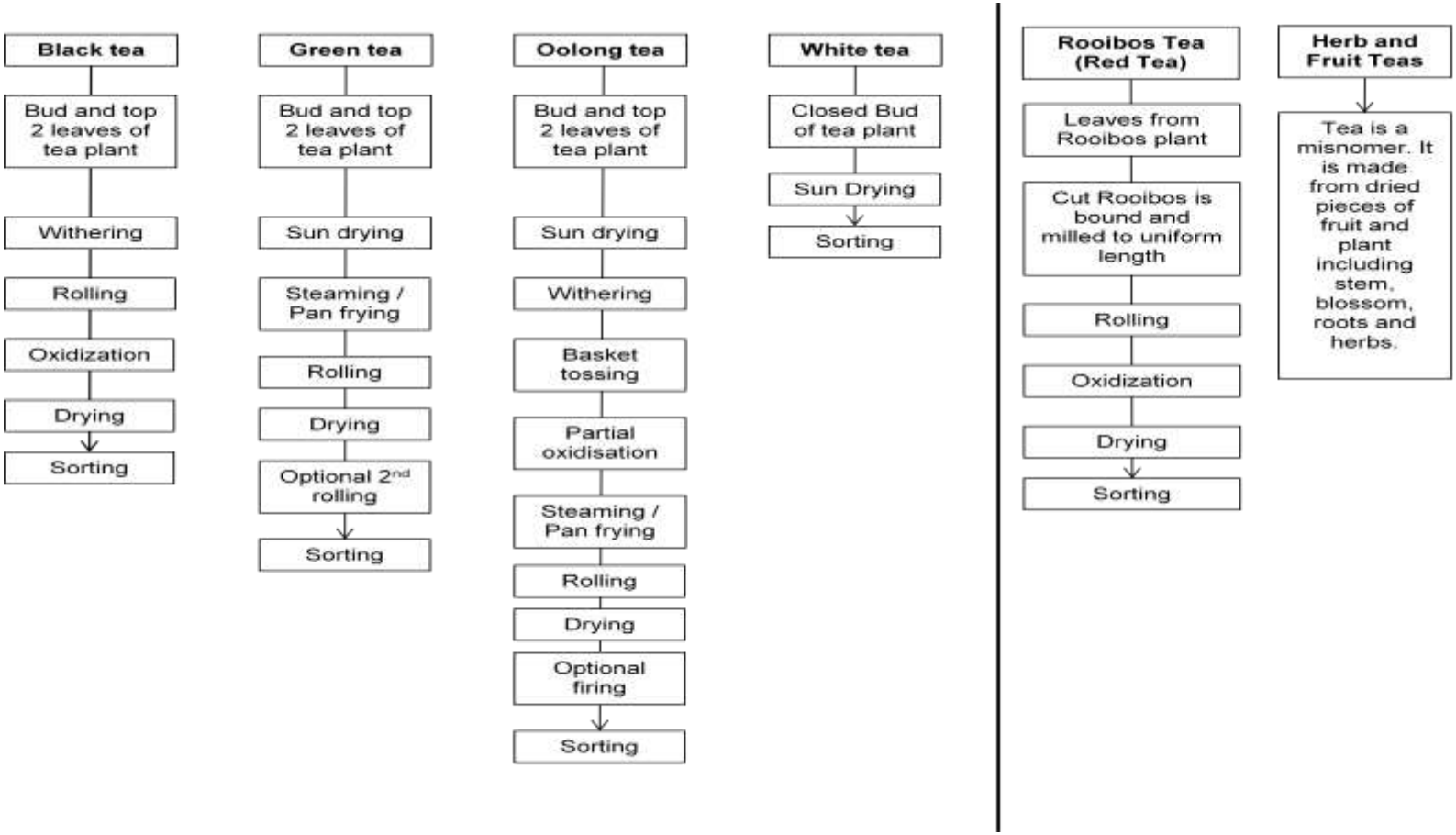

Figure 1.5 – Overview of methods for producing different tea types (including drinks that are commonly referred to as tea).

1.2.4 Chemical constituents of tea

The constituents of tea depend on the production process used. It is generally seen that the darker the tea variety the less the efficacy of the antibacterial and antioxidising activities. All leaves contain vitamins, minerals, alkaloids (such as caffeine) and polyphenols (flavonoids and catechins) (Kaplan et al. 1974; Ikegaya et al. 1987; Balentine et al. 1997; Zhu et al. 1997; Wang et al. 2000; Friedman et al., 2005; Friedman 2007; Chin et al. 2008; Freeman et al. 2008; Arab et al. 2010; Castro et al. 2010; Chen et al. 2010; Hodgson et al. 2010).

The flavonoids have a variety of medicinal properties. These include anti-allergic, anti-inflammatory, antibacterial, antiviral and antioxidant effects. There is also the ability to decrease vein permeability and to increase the strength of the veins (Weber et al. 2003; Friedman 2007; Jariwalla et al. 2007; Garcia-Lafuente et al. 2009; Yoshino et al. 2010; Cushnie et al. 2011; Ferrario et al. 2011; Shen et al. 2011; Tzellos et al. 2011).

Tea is also a good source of vitamin C and it has been found that 2 cups of tea a day provide the equivalent of 3 glasses of orange juice (du Toit et al. 2001).

Catechins (tea tannins) have antiseptic and antioxidant properties. They are also claimed to have a detoxifying effect by forming complexes with other molecules. A quarter of fresh dried green tea leaves are composed of catechins. Catechins are plant metabolites which are present in numerous plant species, the largest source in the human diet comes from tea. Catechins can also be found in wine, fruits, vegetables and chocolate. The most common tea catechin is epigallocatechin gallate (EGCG) (Figure 1.6a) which is gallic acid ester of a catechin (Figure 1.6b). Other catechins found in tea include epicatechin (EG) (Figure 1.6c) and Epigallocatechin (EGC). Though the fermentation of black tea reduces the amount of catechins present in finished product these three catechins are still present. White tea has a higher concentration of catechins much like green tea (Zhu et al. 1997).

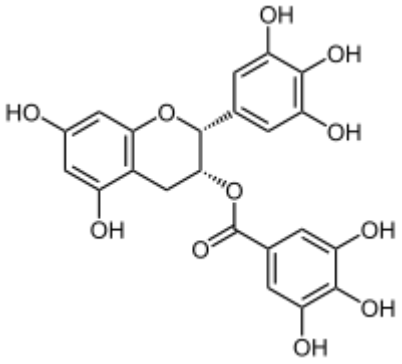

Figure 1.6a – Chemical structure of epigallocatechin gallate (EGCG)

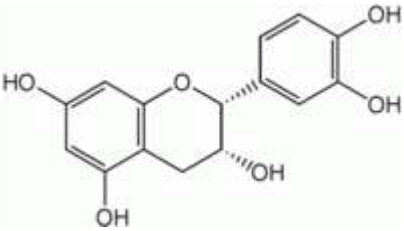

Figure 1.6b – Chemical structure of epicatechin (EG)

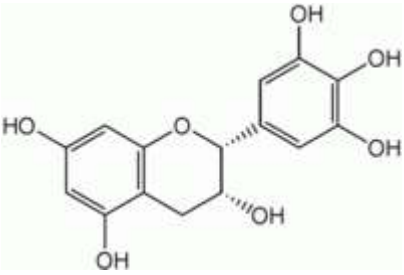

Figure 1.6c – Chemical structure of epigallocatechin (EGC)

1.2.5 Medicinal benefits of tea

Tea has been used as a home remedy for a long time and has some proven medical benefits.

There are two known benefits from all tea types. The antiseptic properties of flavonoids and tannins have meant that tea has been used as a way of fighting infections. As mentioned earlier tannins also have anti inflammatory properties and flavonoids bind with complex molecules meaning they can help detoxify a system. A compress of tea is used to stem bleeding, a poultice of green tea is used to combat itching and inflammation of insect bites (Van-Wyk et al. 2002).

Tea has also been used to treat inflammatory bowel disease and infectious dysentery because of these same properties (Jurjus et al. 2004). Whilst green tea has been seen to have more medicinal properties than black tea, and the uses of it are being investigated. For example, green teas are seen as immune boosters with their antioxidant and detoxifying properties, as well as the mineral and vitamin content.

Laboratories have been studying the effects of an extract of green tea on skin tumour formation using animal models. If taken orally or applied to the skin the extract has been shown to inhibit skin tumour formation when it is formed by ultra-violet B radiation (UVB) or by chemical carcinogens. The extracts contain polyphenols (catechins), and the predominant polyphenol to have an effect is epigallocatechin-3-gallate (EGCG). This was applied to mouse skin and prevented UVB-induced oxidative stress and suppression of the immune system. The trials with mouse skin models have extensively illustrated benefits of green tea extracts (Katiyar et al. 1997). Only a few studies have been performed on human skin cells. Currently pharmaceutical and cosmetic companies have been using green tea extracts to supplement skin care products (Katiyar et al. 1997).

Surprisingly, green tea is very rich in fluoride and a study has been performed using natural toothpaste containing zinc ascorbate and green tea bioflavonoid. The aim of this study of natural toothpaste was to determine the effect on bacterial plaque accumulation. The results showed a significant decrease in total plaque biomass when compared with control toothpaste (Wolinsky et al. 2000). Other studies are ongoing into the effects of tea drinking on health of teeth. If these studies produce

substantiated results the hope is that tea could play a larger role in public health.

The role of tea in cancer prevention is of major current interest. Catechins have shown an ability to inhibit the proliferation of tumour cells and can also promote the destruction of leukaemia cells. Both green and black teas have also been shown to suppress DNA reproduction (Olaku et al. 2011; Yang et al. 2011).

1.2.6 Potential health risks of tea ingestion

As with most compounds ingested by humans, there is the potential for health risks with a large intake of tea. Fortunately the caffeine content of tea is less than coffee. It is estimated that a cup of tea that has been brewed for one minute will contain half the caffeine than a cup of coffee (Bunker 1979). Green tea has the least caffeine in it. Caffeine can cause insomnia, nervousness and in some cases migraines in people who drink large amounts of it or are sensitive to it. White tea has a high amount of caffeine in it compared to other teas due to the process of production. Also, because tea can have an antioxidant effect, it can cause a reduction in the ability to use iron from the diet and can be a problem for people who suffer from anaemia (Samman et al. 2001).

1.3 Introduction to leaves

The basic functions of a leaf is to increase the surface area of the plant to allow photosynthesis, to provide a place where gas exchange can occur (CO_2 into the leaf and O_2 out) and to be a site of transpiration where the evaporation of water from the leaf helps with the uptake of water from the roots into the plant.

A general structure of a leaf is shown in figure 1.7.

The cuticle is a waxy waterproofing layer on the upper side of the leaf (the adaxial side). The cuticular layer varies in thickness with plant species. This layer helps the plant to reduce water loss. Though the bottom side (the abaxial side) of the leaf also has a waxy cuticular layer the adaxial layer tends to be thicker for the cuticle than it does for the lower epidermis.

The cuticle is the main barrier to foliar penetration of compounds. The cuticle can be considered as a lipid membrane composed of a cutin polymer, which has waxes embedded into it or surrounding it. It has a high capacity for the adsorption of lipophilic compounds (Riederer et al. 1984; Reiderer et al. 1985). The membrane has been seen to be heterogenous in structure and chemical composition. The cuticle is composed of a layer of epicuticular waxes on top of a cutin membrane or embedded within it, cuticular waxes.

For compounds to penetrate the cuticle there must be sorption into the lipids in the cuticle, diffusion of the compound over the cuticular membrane

and then desorption of the compound into the cells in the epidermal layer (Kirkwood 1999; Schoenherr et al. 1999).

The second layer is the upper epidermis. This is a protective layer which contains no chloroplasts within it. The upper epidermis secretes the non-cellular wax layer of the cuticle. An interesting adaptation within the upper epidermis is that the cell wall on the adxial side of the epidermal cell is thicker than the abaxial side.

The palisade mesophyll is a layer of tightly packed parenchyma cells which contain chloroplasts. The chloroplasts are needed for photosynthesis. The structure within this layer is more organised than the spongy mesophyll layer below it. This is to give the leaf a rigid structure. The spongy mesophyll layer is also composed of parenchyma cells but also has air spaces between these.

The lower epidermis on the abaxial side of the leaf contains stomatal guard cells and an aperture for gas and water exchange known as the stoma. The stomatal guard cells surround the stoma in pairs and are used to control the rate of gas exchange and transpiration. These are usually the only cells in the epidermal layer that contain chloroplasts.

The xylem and phloem are also known as the bundle sheath cells and are used as a transport mechanism within the leaf. The xylem is responsible for the transport of minerals and water within the plant, whereas the

phloem transports organic compounds and dissolved sugars (Toole et al. 1999).

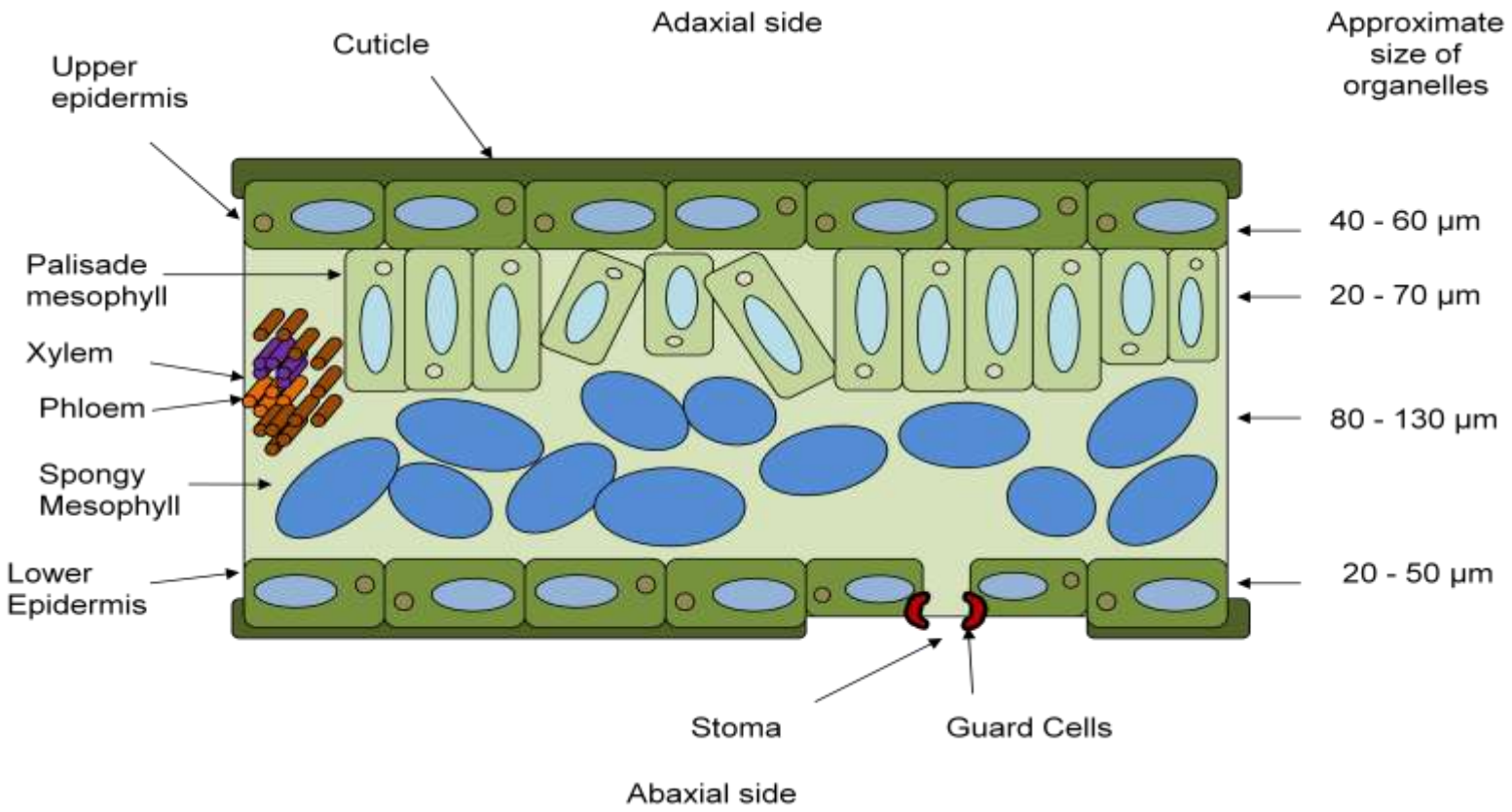

Figure 1.7 – The cross section of a typical leaf.

1.4 Tea Aroma

1.4.1 Importance of Aroma

When tea is processed from its fresh leaf form to the tea leaves that are used for infusion, a proportion of the aroma is lost (Ravichandran et al. 1998). During the processing of the tea the lost aroma is captured by condensation of the aroma during heating stages, mixed with water and re-sprayed back onto the dry leaves. As a method of replacing lost aroma it is still very inefficient.

Aroma is one of the major stimuli that contribute to the perception of flavour, along with taste, texture and general “mouth feel”. The stimulation occurs when the food or liquid encounter the mucous membranes of the mouth (stimulating taste) or nose (stimulating odour). It can also occur when the compounds from the ingested material interact with the lining of the mouth (“mouth feel”) and when the chewing process is affected by the material ingested (texture) (Ruth et al. 2002).

The combination of these stimuli affects how we perceive the taste of a foodstuff and this is generally known as the flavour of the foodstuff. Of all of these stimuli, aroma is generally considered to have the largest effect on the flavour perceived.

Quantifying flavour can be quite difficult experimentally. There are problems in the comparison of data collected from live subjects when compared to quantitative and qualitative data obtained by a machine. A

sample could have all the favourable ingredients for what could be perceived as a good flavour but an instrument cannot quantitatively or qualitatively express results for mouth feel.

For the aroma to be perceived, it must enter the airways, either by direct inhalation (the first sniff of a beverage) or release through the mouth (when a foodstuff is chewed and volatile aroma molecules are released), and contact the olfactory receptors (Buettner et al. 2000; Beuttner et al 2000).

1.4.2 Tea Aromas

The study of tea aromas has focussed on the aromas present either in the raw leaf before processing or the finished processed tea product.

The formation of black tea aroma was found to occur during the time taken to process green tea leaves to the finished black tea product. The oxidative flavanols were thought to form volatile aroma products. The final drying stage was thought to be responsible for further oxidation (Sanderson et al. 1973).

By incubation of glycoside fractions of methanol extract of two varieties of fresh tea leaves with different enzymes the formation of aromas and aroma precursors were observed. (Z)-3-Hexenol, methyl salicylate, geraniol, 2-phenylethanol, benzyl alcohol, linalool and linalool oxides were

all identified following the enzymatic treatment by gas chromatography. A calculation of comparison of the aroma products showed that the different samples had different amounts of aroma in the samples which corresponded with previous experiments on the growing conditions of *Camellia sinensis*. The conditions in which the plant is cultivated will lead to a difference in the aroma constituents found in the plant (Takeo 1981; Takeo 1981; Morita et al. 1994).

The effects of tea processing were examined in relation to the aroma content. Fresh leaves were collected from 3 cultivars of tea and subjected to the usual processing of green and black tea leaves. Solvent extraction was used to collect volatile flavour compounds (VFC) and samples were examined using gas chromatography. The VFCs were sorted into two groups, VFC group 1 consisted of 1-penten-3-ol, n-hexanal, n-hexanol, cis-3-hexenal, trans-2-hexenal, cis-3-hexenol, trans-2-hexenol and pentanol. Group 2 VFCs consisted of linalool and its oxides, methyl salicylate, phenylacetaldehyde, geraniol, benzyl alcohol, 2-phenylethanol, benzaldehyde, α- and β-ionone.

Withering of the leaf increased the amount of group 1 constituents present. There was some increase for group 2 but to a lower extent, with the exception of linalool. When fermentation occurred there was a reduction in the presence of group 1 alcohols and an increase in aldehydes. With the exception of methyl salicylate and α- and β-ionone, group 2 compound increased as well. The firing stage showed losses in

the amount of both group 1 and 2 compounds. Injury to the leaf before processing increased the group 1 content (Ravichandran 1998).

A comparison of oolong tea and black tea using a combination of gas chromatography and gas chromatography/FTIR spectrometry/mass spectrometry showed that black tea included linalool, 4 linalool oxides, geraniol and methyl salicylate (Kawakami et al. 1995).

The isolation of volatile components of black tea by simultaneous distillation extraction and hydro distillation and subsequent analysis by gas chromatography showed 50 different volatile compounds. These included geraniol, methyl salicylate, linalool and its oxides. Simultaneous distillation extraction was found to be a more effective technique for the examination of the volatile compounds (Rawat et al. 2007).

As well as examining the aroma found on the leaves, precursors for the aromas were also examined. Methyl salicylate glycosides, (z)-3-hexenyl-β-D-glucopyranoside and Cis and trans-linalool 3,7 oxides were identified following enzymatic hydrolysis and gas chromatography of oolong tea leaves (Moon et al. 1996).

A method of recovery of aroma components, pervaporation, was studied to see if there was an increase in the recovery of the components from tea aroma condensate that is generated in the production of tea. Pervaporation is a membrane based technique where components are separated by permeation through a membrane and then evaporation.

Differences in the type of membrane used allow the permeation of different desirable compounds through it. A model system was examined with a real tea leaf system and pervaporation performed on 8 compounds to examine if the technique would separate the aromas. These included methyl salicylate, linalool and trans-2-hexenal. The results showed that in model systems and a real tea system the pervaporation was able to separate the aromas with good yields but as it is a very selective process it could result in a change of the actual tea aroma. In the experiments only 8 volatiles were examined. Previous identification has show over 140 separate aroma components for black tea alone (Kanani et al. 2003).

These studies have identified tea aroma components, precursors and ways of separating the aromas during processing but ways of improving the reapplication of aromas onto the finished tea product have not been investigated.

1.5 Scanning probe microscopy

1.5.1 Introduction

The atomic force microscope (AFM) is a member of the scanning probe microscope family. The scanning tunnelling microscope (STM) was

developed in 1982 and was able to obtain images of a silicon sample with atomic resolution (Binnig et al. 1982). The main drawback of this system is that the sample being imaged had to be conducting. The AFM was developed to obtain high resolution images of surfaces that are not conductive, for example biological samples. It was developed by Binnig, Quate and Geber (Binnig et al. 1986).

1.5.2 Principle of AFM

The microscope is made up of a flexible cantilever with a sharp probe (a tip) mounted at its free end which can scan the surface of an object. To monitor cantilever deflection typically a laser is reflected from the cantilever on to a position sensitive photo detector. When the cantilever moves up or down, in response to surface forces or the topography of the sample, the laser beam deflection path changes, and this is sensed by the photo detector (Binnig et al. 1986). A piezo ceramic crystal in the scanner allows movement of the scanner or probe in 3 directions, x, y and z with sub-angström resolution. Figure 1.8 show a schematic set up of an AFM.

There are a variety of data aquisition modes which can be used in AFM. The two main modes are contact and non-contact mode. Non-contact

mode can be subdivided into two modes of operation, true non-contact mode and intermittent-contact or Tapping Mode ™ (TM-AFM) (Zhong et al. 1993). A recent mode of operation which has been developed for use with the AFM to address some of the shortcomings of Tapping Mode ™ is HarmoniX ™, which uses a novel torsional harmonic cantilever (THC) (Sahin et al. 2007; Sahin et al. 2008).

To use the AFM in contact mode, a constant interaction force is maintained between the sample being scanned and the tip on the cantilever. When the surface is scanned the motion of the probe can be monitored and recorded and a three dimensional image can be built up. When the tip of the probe comes into contact with a surface feature a feedback controller ensures that the vertical z position of the probe is adjusted so that a constant force is applied. Though this mode offers a high sensitivity for height of features of a sample, its success is dependent on the robustness of the sample surface and the accuracy of the force control used.

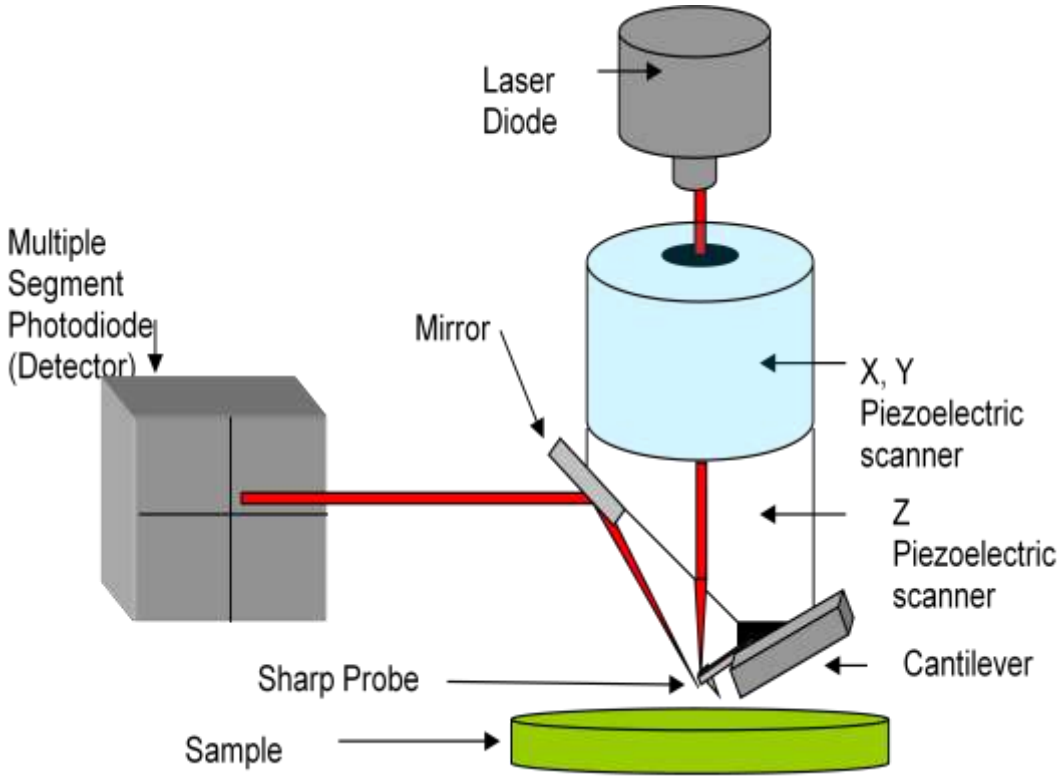

Figure 1.8 – AFM Schematic of a tip scanning system showing the main components of a typical system.

The basis of true non contact AFM imaging is to obtain topographical images from the measurement of long range attractive forces as opposed to short-range repulsive interactions as is typical for contact mode. The cantilever is vibrated at its resonant frequency (or close to it). This is done using either a piezoelectric ceramic contained within the AFM head (acoustic oscillation) or through an externally applied oscillating magnetic field (for a magnetized lever) in so called Mac-Mode^{TM} (Han et al. 1996). The probe is allowed to intermittently contact the surface during oscillation

of the cantilever whilst raster scanning across the sample surface. The contact with the surface alters both the phase and the amplitude of the vibrating cantilever. Similar to contact mode the feedback controller can adjust the height of the cantilever so the amplitude (or phase) of vibration is kept at pre-set set-point value. The feedback controller allows the TM-AFM to map the topography of the sample surface and to produce a phase image, taken simultaneously of the same area being scanned. The phase image is a measure of the energy dissipated when the sample surface and cantilever tip interact with each other (Magnov et al. 1997). This change in the interaction between the probe tip and sample can provide local information about chemical or physical properties of the sample, such as adhesion and elasticity and hence in the composition of the sample (Chen et al. 1998). There have been difficulties in relating the phase images to different material properties, so different modes of operation have been utilised to examine these individual properties (Chen et al. 2000).

All modes of AFM have different probes which are utilised in the operation of the machinery. Figure 1.9 shows the difference in the contact mode, non contact mode and harmoniX cantilevers which are used. From the images it can be seen that the cantilevers have different appearances. Contact mode cantilevers are typically triangular shaped and have a relatively low spring constant. When compared with a non contact mode cantilever, this cantilever is typically shaped as a beam with the tip at the end and is much stiffer to ensure a high enough oscillation resonant

frequency. Finally the harmoniX cantilever is also beam shaped but with the tip offset at one end of the beam. The offsetting of the probe is important in gathering data from other harmonics, hence the name of the technique.

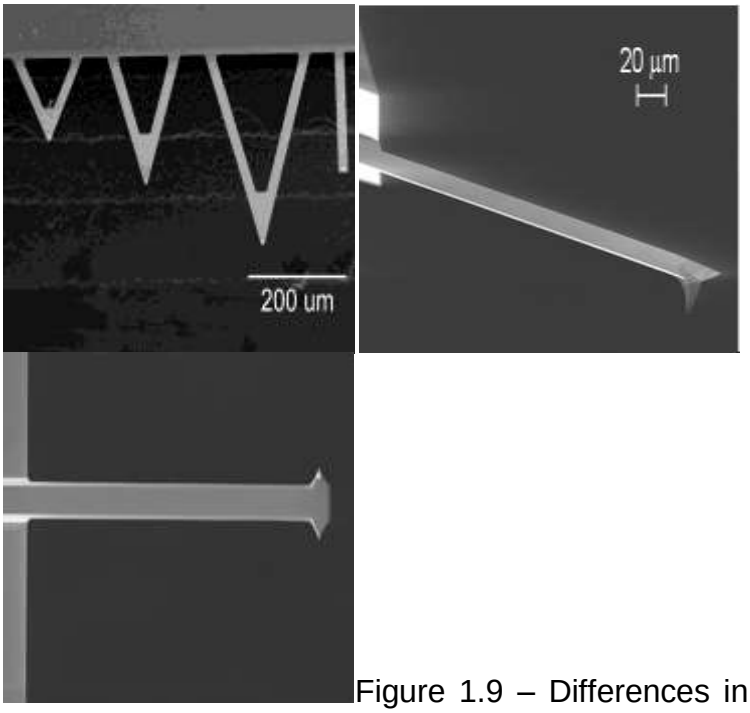

Figure 1.9 – Differences in cantilever design for the different modes of operation. (From left to right. Typical Contact mode Cantilever, Typical Non-contact mode cantilever and harmoniX cantilever.) Source www.acoustics.org, www.mobot.org and Veeco.

1.5.3 Use of AFM on leaves and tea

The AFM has been used to examine plant material in a variety of experiments. One of the earliest published uses of the AFM on plant material was to examine the stoma on a tree, *Lagerstroemia subcostata* and the abaxial side of a water lily leaf. Images obtained were able to reach 12nm detail (Butt et al. 1990).

The parenchyma of a variety of fruit species were examined in 1996. Homogenised samples were able to be imaged for about an hour, after this the sample dried out and images were unable to be obtained (Kirby et al. 1996). In this study samples were frozen for later experimentation. The freezing lead to alteration of the structure seen with the AFM when frozen compared with freshly prepared samples. Large pores appeared and polysaccharides started to associate due to the freeze thawing process.

Ageing in leaves were examined when leaves from *Vaccinium macrocarpon*, the American cranberry were studied. Younger leaves showed a large variation in topography and a larger amount of high plateaus when compared with the older leaves. The topography of the older leaves was observed to be less rough (Mechaber et al. 1996).

The regeneration and formation of the cuticle was observed using AFM. A live plant with and area on the leaf stripped of the waxy cuticle was continuously imaged. After 5 minutes the first patches of regenerated wax

were observed. 90 minutes after wax removal and 15% of the surface was covered in a regenerated wax layer. A complete layer of wax was observed at 10 hours and after 20 hours there was a multilayered wax film present (Koch et al. 2004).

The diagnostic power of the AFM was displayed with a study examining the properties of the *Prunus laurcerasus* leaves. The phase image from the AFM showed two different areas on the leaf. These two areas had different material properties and confirmed evidence seen by SEM micrographs of the same leaves (Perkins et al. 2005).

More recently there have been studies into constituents of tea rather than the leaf or the plant itself. A polysaccharide from Oolong tea was imaged to show a globular structure. Green tea polysaccharides were examined before and after the addition of an enzyme to show a morphological change due to the enzyme (Chen et al. 2009; Yi et al. 2001).

1.6 Time of flight secondary ion mass spectroscopy

1.6.1 Introduction to time of flight secondary ion mass spectroscopy (ToF-SIMS)

Time of flight secondary ion mass spectrometry (ToF-SIMS) measures the ionised particles that are released when a surface is bombarded with an

energetic primary particle. Sources used to date to generate the primary particle include caesium, gallium, gold, bismuth or carbon 60 (VanStipdonk et al. 1996; Kotter et al. 1998). The secondary particles are emitted from the surface after bombardment from the primary particle and can take the form of electrons, neutral atom or molecular species, cluster and atomic ions. Approximately 99 % of species emitted will be neutral and so cannot be analysed using standard ToF-SIMS. Only species with a positive or negative charge are analysed within the ToF-SIMS. To be able to detect the neutral species emitted another technique can be employed, for example MALDI ToF, where the neutral species are charged and thus able to be analysed (Karas et al. 1985). The secondary ions are detected and analysed by a mass spectrometer and give rise to a mass spectrum reflecting the chemical constituents of a given material's surface. In ToF-SIMS, assuming the primary ion dose density (PIDD) is kept below an established limit ($< 1 \times 10^{13}$ ions/cm^2), only the top surface layers, 1 – 2 nm are analysed. (Vickerman et al. 1997).

1.6.2 Theory of ToF-SIMS

ToF-SIMS uses a high energy beam of primary ions to bombard the surface of a material with the energy from these particles being transferred to the atoms in the solid. The energy is transferred through a cascade of collisions whereby some of these collisions will result in the release or emission of neutral or charged atoms, electrons and molecules from the surface. Although ToF-SIMS only obtains data from the upper 1-2

nanometres of a surface, the primary ions can penetrate 10s of nanometres into the surface that is being analysed. The further away from the impact point on the surface, the lesser the energy transferred and the greater the likelihood of molecular fragments being released as opposed to atoms. The release of these molecular fragments can give greater understanding of the chemistry of the surface.

When analysing a materials surface a technique known as static SIMS is used where the primary ion dose is kept below the PIDD limit. As previously mentioned this has been established experimentally as $< 1 \times 10^{13}$ ions/cm^2. This means that the region being analysed should not be struck by the primary ion no more than once during analysis. A reflectron is used in the instrumentation to ensure that all emitted ions of the same mass arrive at the detector at the same time, thus providing consistency of the mass resolution of the spectra. When analysed, ions can have a spread of energies which will lead to poor mass resolution for a secondary emitted ion. Ions with different energies will penetrate the reflectron to different depths, ie. The higher the energy of the ion, the deeper the penetration before being turned around towards the detector. This compensates for this difference in energy spread (Vickerman et al. 1997).

The ToF analyser can then separate out the secondary ions that have been produced by mass/charge (m/z). The mass, m, is dependent on the

time taken for the ion to travel the length of the flight tube, *L*, after they have accelerated to a common energy by the use of a reflectron, *E*.

$E = mv^2/2 = mL^2/2zt$ *Equation 1*

The time it takes for these ions to strike the detector (also described as the time of flight) is shown in equation 2.

$t=L(m/2zE)^{1/2}$ *Equation 2*

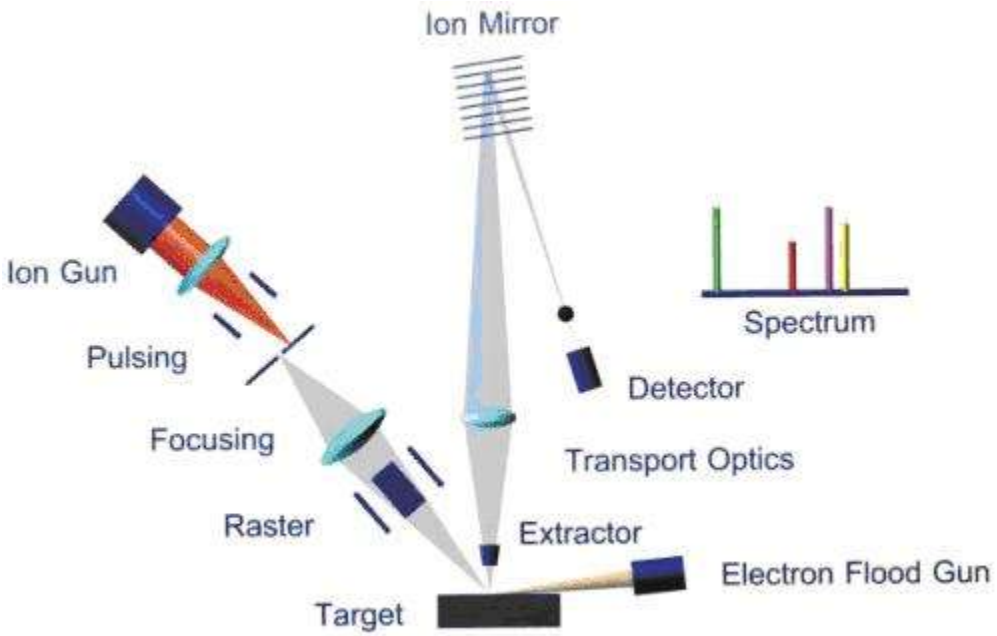

Figure 1.10 – Schematic of the ToF-SIMS machine and typical set up of IonTOF ToF-SIMS IV instrument.

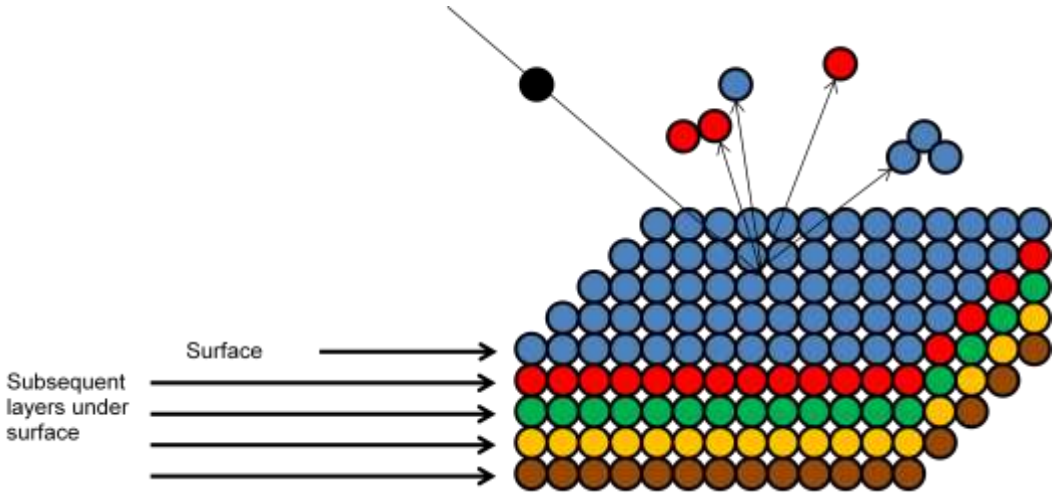

Figure 1.11 - Impact of the primary ion (black) releases secondary ion species and individual atoms for analysis.

1.6.3 Chemical mapping using ToF-SIMS

During the raster scan of the beam over the sample, as well as generating a spectra for the surface being analysed, ToF-SIMS can also generate a compositional map. For each point in the raster over the surface a spectra is generated and these individual spectra are combined to make the final spectra for the sample analysed. The functionality of the machine is such that when the total spectra is analysed and peaks assigned, these peaks can then be examined visually in a chemical map to examine where they originated from on the surface. The resolution of the chemical map is dependent on the primary ion used. For example if Bi^+ is used the

resolution is around 100 nm on suitable samples. The thickness of the sample, topography of roughness can affect the sample that is being mapped. Contamination of the sample also should be considered. If there is contamination it can alter the result so the contaminant appears more readily than ions that you wish to examine (Jones et al. 2006).

1.6.4 Depth Profiling using ToF-SIMS

As well as being able to scan the surface the ToF-SIMS instrument can produce a depth profile of the surface being examined. The sample is analysed in a dual beam mode where a scan of the area is taken, then the area is etched using a different energetic particle. Another scan is then taken of the area than has been etched and the process is repeated.

Different sources have been used for the etching process. The ideal source is one which has a high current but a lower energy source than the analysis beam.

Figure 1.12a and b show diagrammatically what is occurring in depth profiling.

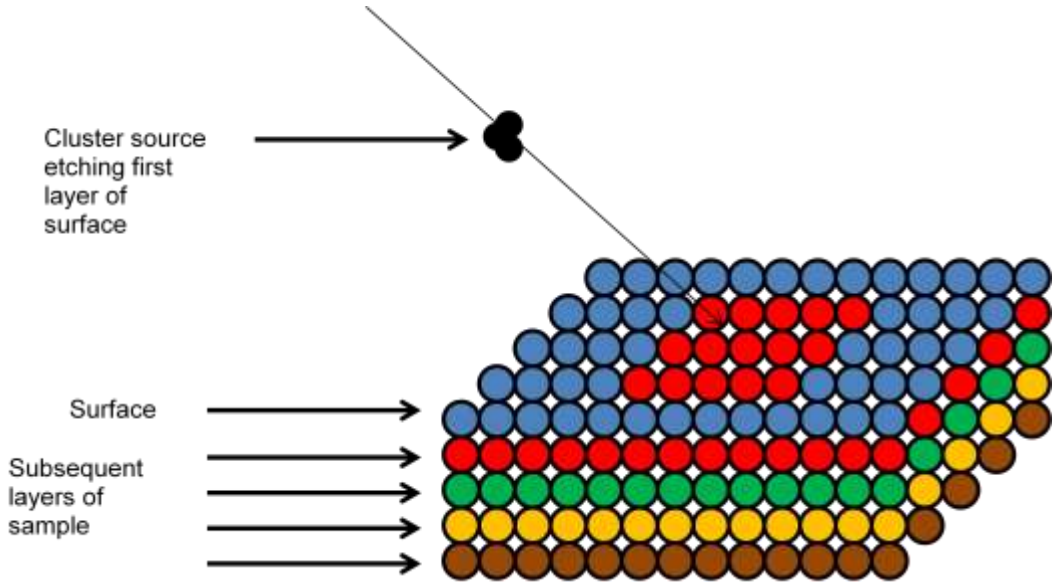

Figure 1.12a – Cluster source used to remove layer of surface

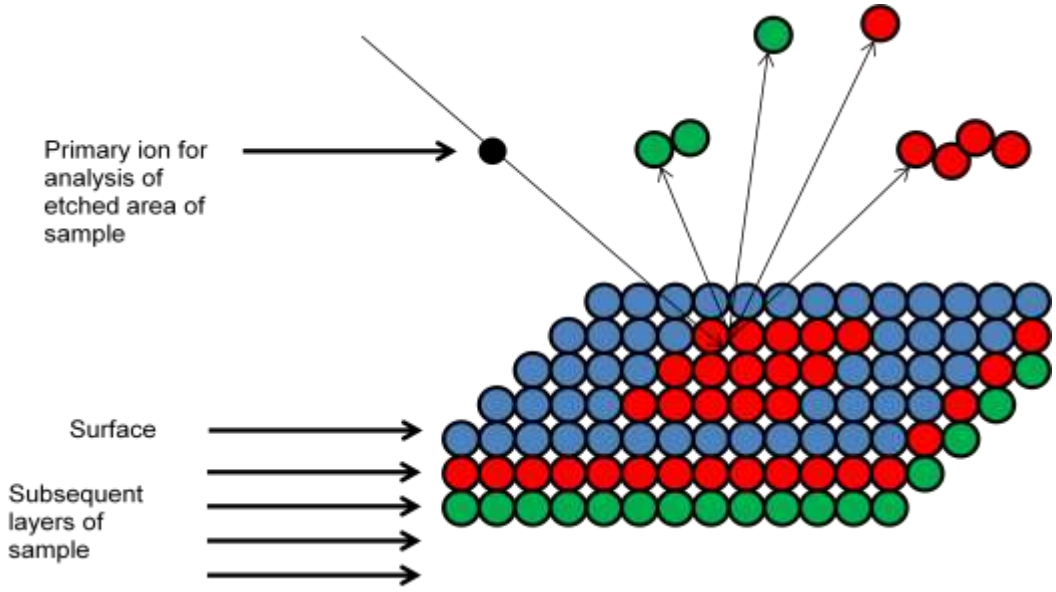

Figure 1.12b – Impact of the primary ion (black) releases secondary ion species and individual atoms for analysis. (Figure 1.12a and b repeated)

1.6.5 Use of ToF-SIMS on leaves

ToF-SIMS has been used in a variety of studies of plants and plant material. The technique was used to detect the presence of pesticides in fungus, the pesticide was seen on the surface but proved to be too volatile for long studies (Cliff 2001). A more successful study was able to trace the movement of surfactants, herbicides and mixtures of the compounds showed that there were differences in the penetration and diffusion of the compounds across the leaves of *Prunus laurocerasus* (Perkins et al. 2007; Perkins et al. 2008).

Differences in the distribution of carbohydrate, lignin and metal ions were investigated in aspen spruce wood tissue sections. There were differences in the location of these ions and lignins between the two species but carbohydrates were distributed evenly across all of the morphological regions (Tokareva et al. 2007). Examination of the distribution of sodium in rice plant roots was undertaken using cryo ToF-SIMS. Differences were seen in the distribution of sodium in two different cultivars, one salt sensitive and one salt resistant). The salt sensitive rice had a high salt content than the salt resistant plant with content being highest at the root tip in both plants (Ferdose et al. 2011).

Cryo ToF-SIMS was used to trace nutrient distribution in plant tissue with SEM. *Phaseolus vulgaris* stem samples were prepared with sodium,

potassium and rubidium tracers. As well as scanning for the tracers water calcium and magnesium were observed in the chemical mapping in xylem tissue (Metzner et al. 2008).

The movement of water between cells was examined by labelling water with deuterium in soybean plants. After 2 ½ minutes the labelled water was observed in the xylem vessels, the water was then detected in the phloem, cambium and cortex tissue from 30 to 60 minutes after absorption. Differences in the ion counts were observed in the cambium and phloem at different stages of transpiration. When transpiration was high the ion count was higher for the phloem, during the night, when transpiration is lower the ion count was higher in the cambium (Iijima et al. 2011).

The composition of the cuticle of *Kalanchoe daigremontiana* was examined and differences between the composition of the cuticle on the adaxial side and the abaxial side of leaves were observed. Glutinol and friedelin were present on the abaxial side. Three unidentified compound were found on the adaxial surface. All of the mapping showed a homogenous distribution (Jetter et al. 2010).

1.7 Principal component analysis

1.7.1 Introduction to principal component analysis (PCA)

Principle component analysis (PCA) is a mathematical procedure used to analyse large sets of data. PCA was invented in 1901 by Karl Pearson and is regularly used for making predictive models and investigating trends within data sets.

A data set of variables that could be related, are transformed into a smaller number of unrelated variables which are called principle components. The first principle component accounts for the largest percentage of variability within all of the original data set, with each successive principle component decreasing in percentage of variability.

The advantages of using this procedure are that the results are statistically valid, all information and data is used, any potential bias for samples is removed and the technique is both efficient and fast with the use of computers.

1.7.2 Theory of PCA

Principal component analysis can be used for the analysis of large amounts of data, for example ToF-SIMS spectra of samples which have been treated in different ways. The production of the principal components

is where factors from the original data inputted are used to create new variables. These principal components are selected in order to explain the variance in the original data set. The components produced remove any information that is deemed redundant and also filters the noise regularly seen in experimental data.

1.7.3 Use of PCA

ToF-SIMS and PCA has been used to analyse data from a variety of sources. Work has mainly been on the identification of films, structures and chemicals. Biological samples have been examined using these techniques together including cell work, and tissue samples.

Some studies have examined plant and fruit materials using both ToF-SIMS data and PCA. The effects of the addition of a fungicide and pesticide, and examination of the effects of washing were compared with untreated samples of olives and olive oil. Samples that had been treated and then washed were similar chemically to the untreated samples than the unwashed samples that had been treated. The chemical composition of the washed samples were different as there were changes apparent when compared to the untreated samples showing the washing step was not one hundred percent effective (Silvia et al. 2006).

Cellulose and holocelluose fractions of pine and extracted wood were analyzed using ToF-SIMS and PCA. Previously there had been 6 charateristic ions for identification in softwoods. This was increased to 44 with this study. The content of lignin was higher in wood samples than holocellulose which in turn was higher than cellulose. This differentiation in lignin content was exploited in the analysis. The experimental technique shows how these two methods used in conjunction with each other can increase knowledge of the chemical make up of woods and plants (Goacher et al. 2011).

PCA has been used to analyse experiments performed on tea. The use of visable and near infrared spectroscopy was used to examine different varieties of tea. The data collected was then examined using PCA and a library of 200 samples of 8 different varieties was collated. 40 unknown samples were then examined using vis/NIRS and this data was entered with the library. The 40 samples were identified with a 100% recognition rate (He et al. 2007).

Differentiation of tea drinks was observed using liquid chromatography. Catechin and alkaloid identification and determination were used to analyse black, green and instant tea drinks. PCA was used with Class Analogy to split the data into two different clusters. One cluster identified

green tea infusions whilst the second cluster comprised of black and red tea, instant teas and soft drinks (Fernandez et al. 2003).

The differences in fermentation and processing of tea types were examined using Nuclear Magnetic Resonance and the spectra of 176 types of tea were examined. Using PCA to analyse the spectra collected identified differences in the peaks for theanine and catechin content and allowed classification into different groups for green, black, yellow, white, hoji and oolong teas. The set of green tea data was further split into groups of Chinese and Japanese green teas (Fujiwara et al. 2006).

The quality of green tea using samples from a 2006 tea contest in the Kansai area of Japan were examined using a combination of Ultra-performance Liquid Chromatography and Time of Flight Mass Spectrometry. The metabolites of the samples were examined and the spectra examined. High and low ranking tea samples were separated by PCA dependent on the catechin content (Pongsuwan et al. 2008).

1.8 Aims

This project aimed to examine the surface chemistry and morphology of processed tea leaves using primarily TM-AFM, SEM and ToF-SIMS. The investigation of the cuticle of the tea leaves was to provide an understanding of any changes that could occur on the surface of the leaf during the processing from fresh leaf to the finished product.

The effects of hot water infusion on the morphology and chemistry of the leaf were examined at different time points to establish if there were any changes on the surface of the leaf during this process when compared to leaves which had not been infused.

Research was aimed to understand the effects of adding diluted aromas to the surface of the processed tea leaves and performing ToF-SIMS depth profiling to examine how far the aromas penetrated through the leaf and if the size and chemistry of the aroma had any effect on the penetration through the cuticle.

References

Arab, L., Liebeskind D. S. (2010). "Tea, flavonoids and stroke in man and mouse." Archives of Biochemistry and Biophysics 501(1): 31-36.

Balentine, D. A., Wiseman, S. A., Bouwens, L. C. (1997). "The chemistry of tea flavonoids." Critical Reviews in Food Science and Nutrition 37(8): 693-704.

Binnig, G., Quate, C. F., Gerber, Ch. (1986). "Atomic Force Microscope." Physical Review Letters 56(9): 930-933.

Binnig, G., Rohrer, H. (1982). "Scanning Tunneling Microscopy." Helvetica Physica Acta 55(6): 726-735.

Buettner, A., Schieberle, P (2000). "Influence of mastication on the concentrations of aroma volatiles - some aspects of flavour release and flavour perception." Food Chemistry 71(3): 347-354.

Buettner, A., Schieberle, P. (2000). "Quantification of the in-mouth release of heteroatomic odorants." Abstracts of Papers of the American Chemical Society 220: U36-U36.

Bunker, M. L., McWilliams, M. (1979). "Caffeine content of common beverages." Journal of the American Dietetic Association 74(1): 28.

Butt, H. J., Wolff, E. K., Gould, S. A. C., Dixon Northern, B., Peterson, C. M., Hansma, P. A. (1990). "Imaging cells with the Atomic Force Microscope." Journal of Structural Biology 105(1-3): 54-61.

Castro, J., Pregibon, T., Chumanov, K., Marcus, R. K. (2010). "Determination of catechins and caffeine in proposed green tea standard reference materials by liquid chromatography-particle beam/electron ionization mass spectrometry (LC-PB/EIMS)." Talanta 82(5): 1687-1695.

Chen, C. (1984). Theory in Tea Processing, Shanghai Science and Technological Press.

Chen, Q. S., Zhao, J. W., Zhiming, G., Wang, X. (2010). "Determination of caffeine content and main catechins contents in green tea (Camellia sinensis L.) using taste sensor technique and multivariate calibration." Journal of Food Composition and Analysis 23(4): 353-358.

Chen, X., Davies, M. C., Roberts, C. J., Tendler, S. J. B., Williams, P. M., Burnham, N. A. (2000). "Optimizing phase imaging via dynamic force curves." Surface Science 460(1-3): 292-300.

Chen, X., Davies, M. C., Roberts, C. J., Tendler, S. J. B., Williams, P. M., Davies, J., Dawkes, A.C., Edwards, J. C. (1998). "Interpretation of tapping mode atomic force microscopy data using amplitude-phase-distance measurements." Ultramicroscopy 75(3): 171-181.

Chin, J. M., Merves, M. L., Goldberger, B. A., Sampson-Cone, A., Cone, E. J. (2008). "Caffeine Content of Brewed Teas." Journal of Analytical Toxicology 32(8): 702-704.

Chopra, D., Simon, D. (2000). The Chopra Center Herbal Handbook:Forty Natural Prescriptions for Perfect Health. New York, Three Rivers Press.

Chow, K., Kramer, I. (1990). All the tea in China, China Books and Periodicals, Inc.

Cushnie, T. P. T., Lamb, A. J. (2011). "Recent advances in understanding the antibacterial properties of flavonoids." International Journal of Antimicrobial Agents 38(2): 99-107.

du Toit, R., Volsteedt, Y., Apostolides, Z. (2001). "Comparison of the antioxidant content of fruits, vegetables and teas measured as vitamin C equivalents." Toxicology 166(1-2): 63-69.

Ferdose, J., Kato, T., Kawasaki, M., Taniguchi, M., Miyake, H. (2011). "Vertical Distribution of Sodium in Roots of Rice Plants Exposed to Salinity as Analyzed by Cryo Time-of-Flight Secondary Ion Mass Spectrometry." Plant Production Science 14(3): 215-218.

Fernandez, P. L., Lopez, A., Pablos, F., Gonzalez, A. G., Martin, M. J. (2003). "The use of catechins and purine alkaloids as descriptors for the differentiation of tea beverages." Microchimica Acta 142(1-2): 79-84.

Ferrario, A., Luna, M., Rucker, N., Wong, S., Gomer, C. J. (2011). "Pro-Apoptotic and Anti-Inflammatory Properties of the Green Tea Constituent Epigallocatechin Gallate Increase Photodynamic Therapy Responsiveness." Lasers in Surgery and Medicine 43(7): 644-650.

Freeman, J. D. , Niemeyer, E. D. (2008). "Quantification of tea

flavonoids by high performance liquid chromatography." Journal of Chemical Education 85(7): 951-953.

Friedman, M. (2007). "Overview of antibacterial, antitoxin, antiviral, and antifungal activities of tea flavonoids and teas." Molecular Nutrition & Food Research 51(1): 116-134.

Friedman, M., Kim, S. Y., Lee, S. J., Han, G. P., Han, J. S., Lee., K. R., Kozukue, N. (2005). "Distribution of catechins, theaflavins, caffeine, and theobromine in 77 teas consumed in the United States." Journal of Food Science 70(9): C550-C559.

Fujiwara, M., Ando, I., Arifuku, K. (2006). "Multivariate analysis for H-1-NMR spectra of two hundred kinds of tea in the world." Analytical Sciences 22(10): 1307-1314.

Garcia-Lafuente, A., Guillamon, E., Villares, A., Rostagno, M. A., Martinez, J. A. (2009). "Flavonoids as anti-inflammatory agents: implications in cancer and cardiovascular disease." Inflammation Research 58(9): 537-552.

Goacher, R. E., Jeremic, D., Master, E. R. (2011). "Expanding the library of secondary ions that distinguish lignin and polysaccharides in time-of-flight secondary ion mass spectrometry analysis of wood." Anal Chem 83(3):804-812.

Graham, H. N. (1992). "Green tea composition, consumption, and polyphenol chemistry." Preventive Medicine 21(3): 334-350.

Han, W. H., Lindsay, S. M., Jing, T. (1996). "A magnetically driven oscillating probe microscope for operation in liquids." Applied Physics Letters 69(26): 4111-4113.

He, Y., Li, X. L., Deng, X. (2007). "Discrimination of varieties of tea using near infrared spectroscopy by principal component analysis and BP model." Journal of Food Engineering 79(4): 1238-1242.

Hodgson, J. M., Croft, K. D. (2010). "Tea flavonoids and cardiovascular health." Molecular Aspects of Medicine 31(6): 495-502.

Iijima, M., Yoshida, T., Kato, T., Kawasaki, M., Watanabe, T., Somasundaram, S. (2011). "Visualization of lateral water transport pathways in soybean by a time of flight-secondary ion mass spectrometry cryo-system." Journal of Experimental Botany 62(6):

2179-2188.

Ikegaya, K., Iwamoto, M., Uozumi, J., Nishinari, K. (1987). "Near-Infrared spectra of caffeine and its related-compounds and their application to determination of caffeine content in green tea." Journal of the Japanese Society for Food Science and Technology-Nippon Shokuhin Kagaku Kogaku Kaishi 34(4): 254-258.

Jariwalla, R. J., Roomi, M. W., Gangapurkar, B. Kalinovsky, T., Niedzwiecki, A., Rath, M. (2007). "Suppression of influenza A virus nuclear antigen production and neuraminidase activity by a nutrient mixture containing ascorbic acid, green tea extract and amino acids." Biofactors 31(1): 1-15.

Jetter, R., Sodhi, R. (2010). "Chemical composition and microstructure of waxy plant surfaces: triterpenoids and fatty acid derivatives on leaves of Kalanchoe daigremontiana." Surface and Interface Analysis 43(1-2): 326-330.

Jones, E. A., Fletcher, J. S., Thompson, C. E., Jackson, D. A., Lockyer, N. P., Vickerman, J. C. (2006). "ToF-SIMS analysis of bio-systems: Are polyatomic primary ions the solution?" Applied Surface Science 252(19): 6844-6854.

Jurjus, A. R., Khoury, N. N., Reimund, J. M. (2004). "Animal models of inflammatory bowel disease." Journal of Pharmacological and Toxicological Methods 50(2): 81-92.

Kanani, D. M., Nikhade, B. P., Balakrishnan, P., Singh, G., Pangarkar, V. G. (2003). "Recovery of valuable tea aroma components by pervaporation." Industrial & Engineering Chemistry Research 42(26): 6924-6932.

Kaplan, E., Holmes, J. H., Sapeika, N. (1974). "Caffeine content of tea and coffee." South African Medical Journal 48(12): 510-511.

Karas, M. Bachmann, D. Hillenkamp, F. (1985). “Influence of the wavelength in High-Irradiance Ultraviolet Laser Desorption Mass Spectrometry of Organic Molecules”. Anal. Chem. 57(14):2935-9.

Katiyar, S. K., Mukhtar, H. (1997). "Inhibition of phorbol ester tumor promoter 12-O-tetradecanoylphorbol-13-acetate-caused inflammatory responses in SENCAR mouse skin by black tea polyphenols."

Carcinogenesis 18(10): 1911-1916.

Kawakami, M., Ganguly, S. N., Banerjee, J., Kobayashi, A. (1995). "Aroma composition of Oolong tea and black tea by brewed extraction method and characterizing compounds of Darjeeling tea aroma." Journal of Agricultural and Food Chemistry 43(1): 200-207.

Kirby, A. R., Gunning, A. P., Waldron, K. W., Morris, V. J., Ng, A. (1996). "Visualization of plant cell walls by atomic force microscopy." Biophysical Journal 70(3): 1138-1143.

Kirkwood, R. C. (1999). "Recent developments in our understanding of the plant cuticle as a barrier to the foliar uptake of pesticides." Pesticide science 55(1): 69-77.

Koch, K., Neinhuis, C., Eniskat, H. J., Barthlott, W. (2004). "Self assembly of epicuticular waxes on living plant surfaces imaged by atomic force microscopy (AFM)." Journal of Experimental Botany 55(397): 711-718.

Kotter, F., Benninghoven, A. (1998). "Secondary ion emission from polymer surfaces under Ar+, Xe+ and SF5+ ion bombardment." Applied Surface Science 133(1-2): 47-57.

Lee, G. C. (2006). The Varieties of Formosa Oolong. The Art of Tea. 1.

Magonov, S. N., Elings, V., Whangbo, M. H. (1997). "Phase imaging and stiffness in tapping-mode atomic force microscopy." Surface Science 375(2-3): L385-L391.

McKay, D. L., Blumberg, J. B. (2002). "The role of tea in human health: An update." Journal of the American College of Nutrition 21(1): 1-13.

Mechaber, W. L., Marshall, D. B., Mechaber, R. A., Jobe, R. T., Chew, F. S. (1996). "Mapping leaf surface landscapes." Proceedings of the National Academy of Sciences of the United States of America 93(10): 4600-4603.

Metzner, R., Schneider,H. U.,Breuer, U., Schroeder, W. H. (2008). "Imaging nutrient distributions in plant tissue using time-of-flight secondary ion mass spectrometry and scanning electron microscopy." Plant Physiology 147(4): 1774-1787.

Moon, J. H., Watanabe, N. (1996). "Studies on aroma formation

mechanism in oolong tea .6. Cis- and trans-linalool 3,7-oxides and methyl salicylate glycosides and (Z)-3-Hexenyl beta-D-glucopyranoside as aroma precursors from tea leaves for oolong tea." Bioscience Biotechnology and Biochemistry 60(11): 1815-1819.

Morita, K., Wakabayashi, M., Kubota, K., Kobayashi, A., Herath, N. L. (1994). "Glycoside precursor of tea aroma .2. Aglycone constituents in fresh tea leaves cultivated for green and black tea." Bioscience Biotechnology and Biochemistry 58(4): 687-690.

Olaku, O., White, J. D. (2011). "Herbal therapy use by cancer patients: A literature review on case reports." European Journal of Cancer 47(4): 508-514.

Perkins, M. C., Bell, G., Briggs, D., Davies, M. C., Friedman, A., Hart, C. A., Roberts, C. J., Rutten, F. J. M. (2008). "The application of ToF-SIMS to the analysis of herbicide formulation penetration into and through leaf cuticles." Colloids and Surfaces B-Biointerfaces 67(1): 1-13.

Perkins, M. C., Briggs, D., Rutten, F. J. M., Roberts, C. J., Davies, M. C.. (2007). "Cationisation of oligiomeric alkylethoxylate surfactants in ToF-SIMS analysis." Surface and Interface Analysis 39(7): 644-647.

Perkins, M. C., Roberts, C. J., Briggs, D., Davies, M. C., Friedmann, A., Hart, C. A., Bell, G. A. (2005). "Surface morphology and chemistry of Prunus laurocerasus L. leaves: a study using X-ray photoelectron spectroscopy, time-of-flight secondary-ion mass spectrometry, atomic-force microscopy and scanning-electron microscopy." Planta 221(1): 123-134.

Pongsuwan, W., Bamba, T., Harada., K, Yonetani, T., Kobayashi, A., Fukusakim E. (2008). "High-Throughput Technique for Comprehensive Analysis of Japanese Green Tea Quality Assessment Using Ultra-performance Liquid Chromatography with Time-of-Flight Mass Spectrometry (UPLC/TOF MS)." Journal of Agricultural and Food Chemistry 56(22): 10705-10708.

Ravichandran, R., Parthiban, R. (1998). "The impact of processing techniques on tea volatiles." Food Chemistry 62(3): 347-353.

Rawat, R., Gulati, A., Kiran Babu, G. D., Acharya, R., Kaul, V. K., Singh, B. (2007). "Characterization of volatile components of Kangra

orthodox black tea by gas chromatography-mass spectrometry." Food Chemistry 105(1): 229-235.

Riederer, M., Schönherr, J. (1984). "Accumulation and transport of (2,4-dichlorophenoxy)acetic acid in plant cuticles: I. Sorption in the cuticular membrane and its components." Ecotoxicology and Environmental Safety 8(3): 236-247.

Riederer, M., Schönherr, J. (1985). "Accumulation and transport of (2,4-dichlorophenoxy)acetic acid in plant cuticles: II. Permeability of the cuticular membrane." Ecotoxicology and Environmental Safety 9(2): 196-208.

Ruth, S. M. V., Roozen, J. P. (2002). Food Flavour Technology - Delivery of flavours from food matrices, Sheffield.

Sahin, O., Erina, N. (2008). "High-resolution and large dynamic range nanomechanical mapping in tapping-mode atomic force microscopy." Nanotechnology 19(44).

Sahin, O., Magonov, S., Chanmin, S., Quate, C. F., Solgaard, O. (2007). "An atomic force microscope tip designed to measure time-varying nanomechanical forces." Nature Nanotechnology 2(8): 507-514.

Samman, S., Sandstrom, B., Toft, M. B., Bukhave, K., Jensen, M., Sorensen, S. S., Hansen, M. (2001). "Green tea or rosemary extract added to foods reduces nonheme-iron absorption." American Journal of Clinical Nutrition 73(3): 607-612.

Sanderson, G. W., H. N. Graham, H. N. (1973). "Formation of Black Tea Aroma." Journal of Agricultural and Food Chemistry 21(4): 576-585.

Schoenherr, J., Baur, P. (1999). "Modelling Foliar Penetration: Its Role in Optimising Pesticide Delivery." SPECIAL PUBLICATION- ROYAL SOCIETY OF CHEMISTRY 233: 134-154.

Shen, C. L., Samathanam, C., Tatum, O. L., Graham, S., Tubb, C., Cao, J. J., Dunn, D. M., Wang, J. S. (2011). "Green tea polyphenols avert chronic inflammation-induced myocardial fibrosis of female rats." Inflammation Research 60(7): 665-672.

Takeo, T. (1981). "Black tea aroma and its formation .1. Production of

linalol and geraniol by hydrolytic breakdown of bound forms in disrupted tea shoots." Phytochemistry 20(9): 2145-2147.

Takeo, T. (1981). "Black tea aroma and its formation .2. Variation in amounts of linalol and geraniol produced in tea shoots by mechanical injury." Phytochemistry 20(9): 2149-2151.

Tea Council (2003). "Tea Making from plantation to cup." from http://hollandbymail.co/tea/tea_manufacturing.html.

Tokareva, E. N., Pranovich, A. V., Fardim, P., Daniel, G., Holmbom, B. (2007). "Analysis of wood tissues by time-of-flight secondary ion mass spectrometry." Holzforschung 61(6): 647-655.

Toole, G., Toole, S. (1999). New Understanding Biology for Advanced Level, Nelson Thornes.

Tzellos, T. G., Sardeli, C., Lallas, A., Papazisis, G., Chourdakis, M., Kouvelas, D. (2011). "Efficacy, safety and tolerability of green tea catechins in the treatment of external anogenital warts: a systematic review and meta-analysis." Journal of the European Academy of Dermatology and Venereology 25(3): 345-353.

Van-Wyk, B., van-Oudtshoorn, B. (2002). Medicinal Plants of South Africa, Briza Publications.

VanStipdonk, M. J., Harris, R. D., Schweikert, E. A. (1996). "A comparison of desorption yields from C-60(+) to atomic and polyatomic projectiles at keV energies." Rapid Communications in Mass Spectrometry 10(15): 1987-1991.

Wang, H. F., Provan, G. J., Helliwell, K. (2000). "Tea flavonoids: their functions, utilisation and analysis." Trends in Food Science & Technology 11(4-5): 152-160.

Weber, J. M., Ruzindana-Umunyana, A., Imbwault, L. Sircar, S. (2003). "Inhibition of adenovirus infection and adenain by green tea catechins." Antiviral Research 58(2): 167-173.

Wilson, K. C., Clifford, M. N. (1991). Tea: Cultivation to Consumption, Springer.

Wolinsky, L. E., Cuomo, J., Quesada, K., Bato, T., Camargo, P. M. (2000). "A comparative pilot study of the effects of a dentifrice

containing green tea bioflavonoids, sanguinarine or triclosan on oral bacterial biofilm formation." J Clin Dent 11(2): 53-59.

Yang, H., Landis-Piwowar, K., Chan, T. H., Dou, Q. P. (2011). "Green Tea Polyphenols as Proteasome Inhibitors: Implication in Chemoprevention." Current Cancer Drug Targets 11(3): 296-306.

Yoshino, K., Yamazaki, K., Sano, M. (2010). "Preventive effects of black tea theaflavins against mouse type IV allergy." Journal of the Science of Food and Agriculture 90(12): 1983-1987.

Zhang, Z., Wan, X. (2008). Tea and Tea Products: Chemistry and Health Promoting Properties, CRC Press.

Zhong, Q., Inniss, D., Kjoller, K., Elings, V. B. (1993). "Fractured polymer silica fiber studied by Tapping Mode Atomic-Force Microscopy." Surface Science 290(1-2): L688-L692.

Zhu, Q. Y., Zhang, A., Tsang, D., Huang, T., Chen, Z. (1997). "Stability of green tea catechins." Journal of Agricultural and Food Chemistry 45(12): 4624-4628.

Chapter 2.

Experimental Methods

2.1 Introduction

Some of the procedures used in the experiments were the same for the different experiments. The most commonly used methodologies are listed below rather than in the experimental chapters.

2.2 Selection of leaves

Tea leaf samples were provided by Unilever. The tea was from a Kenyan plantation, with a medium size leaf grade (approximately 1mm in size). Small grades of tea are used in tea bags whereas the larger the medium and larger grading of tea leaves tend to be used in loose leaf tea. Leaves were examined using a light microscope to identify the adaxial, top, side of the leaf.

If stoma were present on the leaf surface this was the abaxial side of the leaf and the leaf was turned over.

The presence of veins also meant the leaf was rejected.

All leaves selected were free from veins, of a reasonable consistent topography and facing adaxially.

2.3 Piranha etching of glassware

All glassware to be used in experiments, beakers and slides, were soaked overnight in a 10% Decon solution to clean them. They were then washed thoroughly in distilled water and left to dry.

Piranha solution was prepared whilst the glassware was drying. Piranha solution was made at a ratio of 3:1 of concentrated sulphuric acid (H_2SO_4) and hydrogen peroxide (H_2O_2). The hydrogen peroxide was always added to the sulphuric acid. The piranha solution was left to cool down slightly for 15 minutes, but was still warm when used to clean. The glassware was placed in the solution for 30 minutes, then rinsed clean with 500 ml of deionised water and dried using nitrogen.

2.4 Infusion of tea leaves

Samples of tea leaves were infused for different times after they had been selected using the leaf selection method (Section 2.2). Glassware was first cleaned using a 10% Decon solution in water overnight. The glassware was then washed thoroughly with distilled water and left to dry. The final drying stage was performing by using a stream of nitrogen to remove any drops of water.

This glassware was then cleaned using piranha solution (Section 2.3).

After cleaning, 700ml of deionised water was heated on a hotplate to 100°C. 7 individual leaves were placed into a cleaned beaker. When the water was boiling 100ml was transferred into the beaker and a stop clock started. The water was agitated by hand to simulate the brewing process. After the allotted brewing time was completed the liquid containing the leaves was filtered using filter paper and the leaves were placed between two cleaned glass slides and placed in a labeled Petri dish.

The leaves were infused for 15, 30, 60, 150 or 300 seconds.

The leaves were transferred to a rotary oil pump vacuum oven for drying overnight (4pm-9am) at 40°C, as suggested by Unilever. After drying the leaves were re-examined under a light microscope to ensure the adaxial side was facing upwards for analysis and further experiments.

2.5 Preparation of aroma for experimentation

All aromas were diluted, 1 µl of aroma in a 1000 µl of deionised water. Methyl salicylate, trans-2-hexenal and linalool were purchased as pure samples from Sigma Aldrich UK, Gillingham, Dorset. These samples were then kept at 4°C. The pure aromas were poorly soluble in water so all aroma samples were vortex mixed to help ensure thorough mixing prior to experimentation. The chemical structures of these aromas are shown in figure 5.1 in chapter 5.

2.6 Preparation of samples and use of the Scanning Electron Microscope

Following leaf selection samples were placed on carbon discs which were stuck to aluminium stubs and were coated with a gold layer for 4 minutes using a Balzers SCD 030 gold sputter coater (Balzers Union Ltd., Leichtenstein, Germany) in argon at a vacuum of 0.15 mbar. The samples were then examined under the JEOL 6060LV variable pressure SEM (Jeol (UK) Ltd, Herts., UK).

2.7 Preparation of samples and use of the Atomic Force Microscope

2.7.1 Adhering leaves to slides and cover slips

Araldite epoxy resin was mixed as per the manufacturer's instructions and a small spot was placed on the slide using the tip of a syringe needle. This layer was then spread thinly using the needle to cover an area larger than the leaf to be experimented on. The leaf was then gently placed onto the thin layer of epoxy resin and another glass slide was placed on top and gentle pressure was placed on this top slide. The top slide was removed and the leaf was checked to ensure no resin has contaminated the adaxial surface that was to be scanned. The slide was left overnight for the resin to set before experimentation.

If the experiment was to be performed in the liquid tapping mode then the leaf was adhered to a glass cover slip rather than to a slide.

2.7.2 Experimental parameters

2.7.2.1 AFM imaging in air

All AFM experiments were performed on the Dimension D3000 AFM (Veeco, CA, USA) with a Nanoscope IIIa controller. A silicon tapping mode cantilever was placed in the tip holder and the tip holder was attached to the microscope.

The cantilever was then tuned, using the auto tune function, to find the resonant frequency of the cantilever. Each cantilever was tuned separately as there could be a difference in resonant frequency for cantilevers manufactured at the same time. After engaging the surface the cantilever was withdrawn slightly and retuned. This was to ensure proper tuning and allow imaging.

The cantilever was then moved back to the surface and the scan was taken.

2.7.2.1 AFM imaging in water

Following adhesion of the sample to a cover slip the sample was placed in a glass Petri dish and covered in deionised water. Initial scans showed the sample was unstable due to rehydration of the leaf, It was possible to obtain images using the AFM after 2 hours as the surface had stabilised. Following this observation the leaves were left for 2 hour to allow rehydration of the samples. The cantilever was attached to a liquid cell

holder for operation to protect the instrumentation. When the cantilever had broke the surface of the water it was tuned using the auto tune function and then moved to the surface of the sample. When the cantilever touched the surface it was withdrawn slightly and retuned to allow proper tuning for imaging.

The cantilever was then moved back to the surface and images were obtained.

2.8 Preparation of samples and use of the ToF-SIMS

2.8.1 General ToF-SIMS work

The leaves were then analysed using a ToF-SIMS IV Instrument (ION-TOF GmbH, Münster, Germany). A primary ion beam of Bi_3^+ was produced from a liquid metal ion source using an acceleration voltage of 25 kV and an AC target current of 1.26 pA with a bunched pulse width of less than 0.7 ns. Both positive and negative secondary ion species were analysed using a raster of 256 × 256 pixels. Data was collected from five randomly chosen areas for each leaf fragment. The total primary ion beam dose for every analysed area was kept below 10^{12} ions cm^{-2} throughout the analysis to ensure conditions stayed within the “static” regime.

The instrument was then set up so that the settings for each experiment were as similar as possible. After the emission of the LMIG had stabilized at 1.05 μA emitter for the primary ions was driven to a faraday cup on the

sample stage and the apertures of the emitter were centred. The current was then checked by ensuring the emissions were in the positive mode. The beam was set to pulsing in DC mode and the detector turned off. The target current was accepted if it was in the range of 10-15 nA. The DC mode was then turned off and the current checked again. At this stage it was accepted if it was approximately 1 pA. The emitter was then positioned over a clean fragment of silicon wafer and a scan was started. Whilst the emitter was over the silicon wafer the height was set, this was reset for every scan as the height of the samples was variable within the experiments. The flood gun was calibrated to the sample by adjustment for each individual scan. The reflector voltage was also optimized by adjustment before a spectra was obtained by adjusting the voltage when the emitter was over the area to be scanned so the best results were obtain. A short spectra was obtained of the silicon wafer and as long at the resolution for the silicon peak was over 6000 and the width of the hydrogen peak was at 0.7 nm the instrument was calibrated and ready for experimentation.

2.8.2 Preparation of samples

Following leaf selection all samples were adhered to a round glass cover slip with double-sided sticky tape. The samples were placed in the standard sample holder and placed in an airlock. The airlock was

subjected to UHV overnight. The stage holder was then moved into the main chamber, already at for experimentation.

2.8.3 Calibration of spectra

Once spectra had been collected they were calibrated. The calibration for both of the spectra was performed in IonSpec (Version 4) by the identification of 3 known peaks and then fitting the data to these peaks. For positive spectra the peaks used were H, CH_2, CH_3 and Na. For negative spectra the peaks were H, O and OH. Once calibrated the peaks could then be identified.

2.8.4 Identification of peaks

A peak list was produced within the IonSpec (Version 4). Peaks were identified automatically using the software. Each peak was then examined individually and assignments checked for what was known to be on the surface of tea leaves. Peaks were accepted only if the deviation from the expected mass was 100 ppm or below.

2.8.5 Normalisation of data

After identification of peaks data, processing could occur. The spectra obtained could be normalised in three ways.

The first was to normalise against a known peak. This can occur in two ways. Normalisation by a known peak can either be by the height of the

peak being used or by count for that peak. For example comparison of any peak identified in the positive spectra against the hydrogen peak in the positive spectra. With this normalisation the peak of interest would show a normalised intensity in relation to the count of hydrogen. If the count was higher, the intensity would be higher than 1, if the count was lower than hydrogen, then the intensity would be below 1. Given that the samples were variable in topography and also there was a possibility of differences due to the biological nature of the sample this type of normalisation was not used.

A second type of normalisation is by secondary ion intensity. The number of shots for the total ToF-SIMS scan is used to give a ratio of what is being detected as a secondary ion against the total amount of primary ions going into the surface. This tends to work best on longer acquisition times and larger areas of scanning.

Finally it is possible to normalise against the total count of the ToF-SIMS scan or the sum of the count for selected peaks. This would allow any biological differences to be taken into account as the normalised intensity would be shown as a proportion to the total intensity. If topography did have an effect on the sample, this would be taken into account with this method of normalisation.

The maximum mass of the positive scans for tea leaves was over 260 m/z but the identification of those peaks was very difficult. The highest mass

positive peak identified was at 222 m/z with $C_{15}H_{10}O_2$. The negative scans showed a maximum mass of over 260 m/.

For all experiments involving the ToF-SIMS, normalisation was performed against the total counts for each sspectrum (Wagner et al. 2004).

2.8.6 Preparation of samples for Cryo ToF-SIMS

The aromas used in the experiments were volatile and subjecting them to UHV could remove them from the surface. To allow the retention of aromas to the surface they were examined by attaching the sample to a cold stage. A square of aluminium foil was placed in the cold stage sample area and thermocouples were attached. The sample was then attached to the cold stage using double-sided sticky tape. The cold stage was placed into the air lock and a cold finger was moved into position to the cold stage. Liquid nitrogen was placed in a dewar, which is attached to the ToF-SIMS, and the temperature was monitored. When the temperature had reached -100°C the UHV in the airlock was engaged, the airlock was flushed with nitrogen (Perkins et al., 2005). Whilst the vacuum was reaching pressure a second dewar was filled with liquid nitrogen. This dewar was attached to a cold finger in the main chamber and would maintain the temperature of the samples when they were moved into it for experimentation.

The cold finger was removed and the cold stage was moved into the main chamber and the second cold finger attached. Experiments were then able to proceed.

2.8.7 Depth profiling using ToF-SIMS

All tea leaves were selected using the leaf selection process in section 2.2. For each sample condition three tea leaves were chosen and from these leaves, three sections were depth profiled. The sample conditions were:-

1. Control samples. No treatment to the leaves.
2. Methyl Salicylate. Diluted 1 µl in 1000 with dH_2O.
3. Trans-2-hexenal. Diluted 1 µl in 1000 with dH_2O.
4. Linalool. Diluted 1 µl in 1000 with dH_2O.

All aromas were supplied by Sigma Aldrich UK, Gillingham, Dorset. The purity was >99%

All aroma dilutions were prepared before initial experimentation as per section 2.5. 1 µl of diluted aroma was then placed on the surface of a leaf selected for analysis and left for 24 hours before experimentation. Depth profiling of all samples, including control were performed using Cryo ToF-SIMS to ensure the samples were treated in the same way and results were comparable.

2.9 PCA

2.9.1 PCA

All spectra were normalised to total ion count. The positive and negative spectra were collated and this was used as the total data set. The data from these spectra were then inputted into Matlab V7.0.4 and analysed using the PLS toolbox V5.2.1. (The Mathworks UK, Cambridge, UK).

2.9.2 Data Pre-processing

As with normalisation of the ToF-SIMS spectra, some preprocessing of data is needed when using PCA. The initial preprocessing step is to decide what information to include in the data set that is going to be used. One method is to select peaks of interest, this is for when the chemistry of the sample is known and the PCA is being used to examine if there are any differences between samples. Another method is to include all peaks that have been identified. If the chemistry is not fully known and the data is being analysed to examine if there are any differences this is useful. Instead of limiting the data set, a full comparison can be performed. In the experiments performed on the tea leaf fragments all identified peaks were included in the data set.

A secondary step in preprocessing is to either mean centre the data set or not. When the data is mean centred the mean spectrum intensity is subtracted from the sample. This allows the PCA, when complete, to show

variations from the mean. An examples of a loadings plot which hasn't been mean centred is shown if figure 4.22. When this is compared with the loadings plot of data that has been mean centred, for example 4.24, it can be seen that the peaks of interest which are identified by the PCA have a score of either above or below 0. The data is easier to interpret as the peaks which change very little and have no real effect on chemical changes appear on the zero line. All PCA analysis was performed using data that was mean centred.

When the data is inputted into Matlab it can create a scree test to view the eigenvalue log, this automatically suggests how many components are to be examined. When the PCA was performed data was exported and analysed using Excel (Lee et al. 2010).

References

Lee, J., Gilmore, I. (2010). "A guide to the practical use of Chemometrics - with applications for Static SIMS." 2010, from http://www.npl.co.uk/upload/pdf/Practical%20Chemometrics%20Guide%202010.pdf.

Perkins, M. C., Roberts, C. J., Briggs, D., Davies, M. C., Friedmann, A., Hart, C. A., Bell, G. A. (2005). "Surface morphology and chemistry of Prunus laurocerasus L. leaves: a study using X-ray photoelectron spectroscopy, time-of-flight secondary-ion mass spectrometry, atomic-force microscopy and scanning-electron microscopy." Planta 221(1): 123-134.

Wagner, M. S., Graham, D. J., Ratner, B. D., Castner, D. G. (2004). "Maximizing information obtained from secondary ion mass spectra of organic thin films using multivariate analysis." Surface Science 570(1-2): 78-97.

Chapter 3.

Preliminary characterisation of tea leaves.

3.1 Introduction

To understand more about the tea leaves an initial characterisation study utilizing the key equipment in this thesis was performed. Previous work with the AFM had been focused on the study of live leaves. This work has examined the presence of stomata on the bottom of the leaf, regeneration of the cuticle after removal of surface wax and examination of features such as chloroplasts and roots (Butt et al. 1990; Kirby et al. 1996; Koch et al. 2004).

Studies of the *Prunus laurocerasus* leaf showed a difference in AFM phase imaging leading to identification of two different surface wax regions one amorphous, the other crystalline (Perkins et al 2005).

The constituents of tea have been examined with the AFM. Oolong tea polysaccharide (OTP) was imaged using an AFM to show the OTP had a globular structure and more recently an investigation into the effects of green tea polysaccharides showed a morphological change in the polysaccharide after an enzyme reaction when compared to the original polysaccharide (Chen et al. 2009; Yi et al. 2011).

ToF-SIMS has been used to study a variety of plant material. The transport routes of minerals were observed using Cryo ToF-SIMS on stem samples of *Phaseolus vulgaris.* Mapping of the xylem was possible using water, calcium and magnesium. Sodium, rubidium and potassium markers supplemented these naturally occurring species to confirm the transport paths (Metzner 2008).

The study of *Prunus laurocerasus* using the ToF-SIMS identified components of the cuticle and a further study was able to trace active agrichemicals and their distribution through the cuticle (Perkins et al. 2005).

The detection of chlorinated pesticides was examined to see if the fungus would adsorb onto the surface of *Rhizopus arrizus.* Though the experiments were not successful, the pesticide was detected but it proved too unstable, the power of this technique was demonstrated in that adsorption could be detected (Cliff et al. 2003).

Molecular fragments of cellulose have also been detected in cotton fibres by ToF-SIMS after processing, from the original plant (Mitchell et al. 2005).

Given the diversity of applications of these techniques, the use of AFM and ToF-SIMS were selected as tools to start identification of the chemistry of the surface and surface properties of the tea leaves.

3.2 Experimental

3.2.1 Examination of tea leaves using AFM.

Tea leaf samples were examined using the leaf selection model as discussed in chapter 2 to ensure correct orientation. All tea leaf fragments were examined using the D3000 AFM either in tapping mode in air or in water. All settings were performed as described in chapter 2.

3.2.2 Examination of tea leaves using SEM.

The leaves were imaged using SEM, leaf samples were coated with a thin gold layer using a Balzers SCD 030 Gold Splutter coater (Balzers Union Ltd., Leichtenstein) in Argon at a vacuum of 0.15 mbar. The samples were examined using a JEOL 6060LV SEM (Jeol (UK) Ltd, Herts., UK). This was to compare visually any differences that may be present due to the different processing of the tea leaves and for comparing with AFM images.

3.2.3 ToF-SIMS of tea leaves with Bi_3^+ and C_{60}^+

The operational principal of ToF-SIMS is to bombard the surface being examined with a primary ion and then to detect the secondary ions that are emitted, if they are positive or negative. The introduction of cluster sources has improved the ability to detect and identify larger molecular fragments from organic compounds. When an atom hits the surface in ToF-SIMS some of the energy is transferred to the surface and molecular species can be released and detected. Unfortunately an atomic beam such as this

is more likely to destroy the sample by penetrating deeply into the sample. The use of molecular cluster sources allows the cluster ion to hit the surface and release molecular species by energy transfer but to not penetrate too deeply into the surface. There are a variety of cluster sources available, on the instrument used the options available was between C_{60}^{+} and Bismuth.

3.2.4 Examination of tea leaves using ToF-SIMS.

Tea leaf samples were examined using the leaf selection model as described in chapter 2. Multiple leaf fragments were used to allow for variation due to plant and processing conditions. Each sample was scanned in 5 randomly selected places to allow for variation on the leaf surface. The spectra were calibrated as described in chapter 2 for peak assignment using the ToF-SIMS software.

3.3 Results

3.3.1 Examination of tea leaves with AFM.

3.3.1.1 Black tea leaves with AFM – tapping mode in air.

Topographical and phase images of various tea leaves were taken with the D3000 AFM. Topographical, phase and 3D composite image of a black tea fragment are shown in figures 3.1a, b and c respectively.

Some of the scans of black tea also showed large areas of debris on the surface. These are shown in the height scan, corresponding phase image and 3D composite images in figures 3.2a, b and c.

A further type of image was also obtained with black tea leaves. A layered surface was seen and an example is shown in figure 3.3a where the topography is shown and 3.3b, for the corresponding phase image.

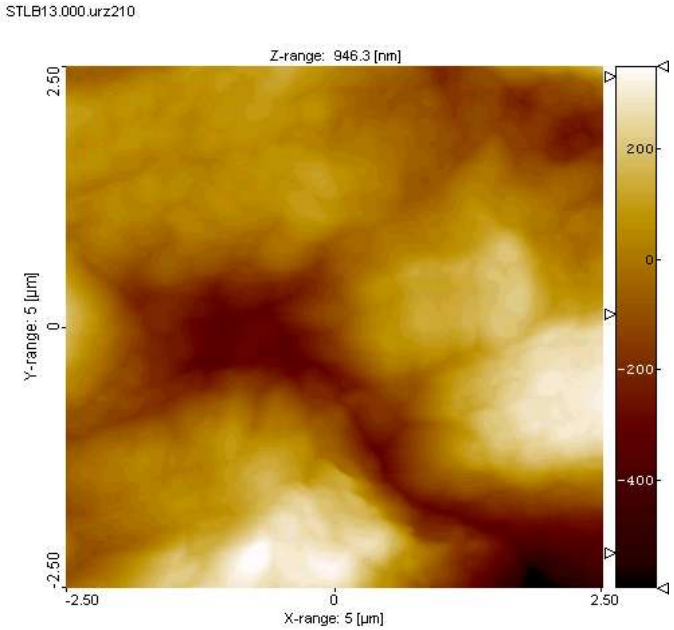

Figure 3.1a - Black untreated tea topography image (Scan size 5 μm^2)

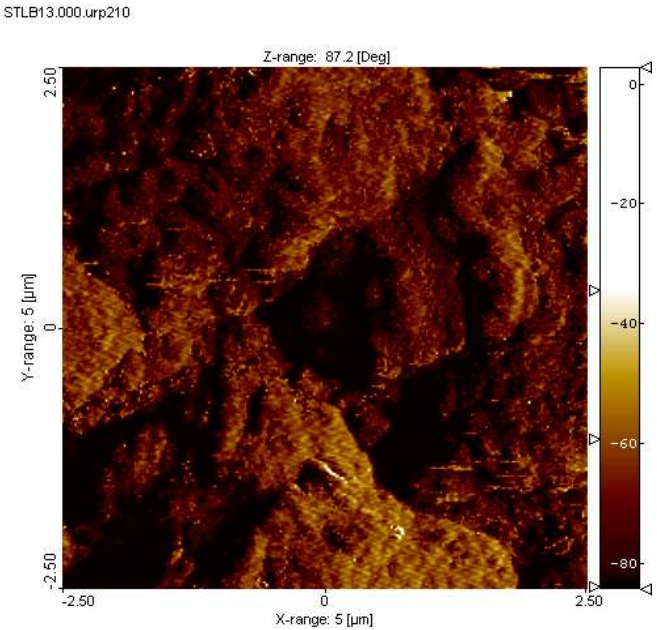

Figure 3.1b - Black untreated tea phase image (Scan size 5 μm^2)

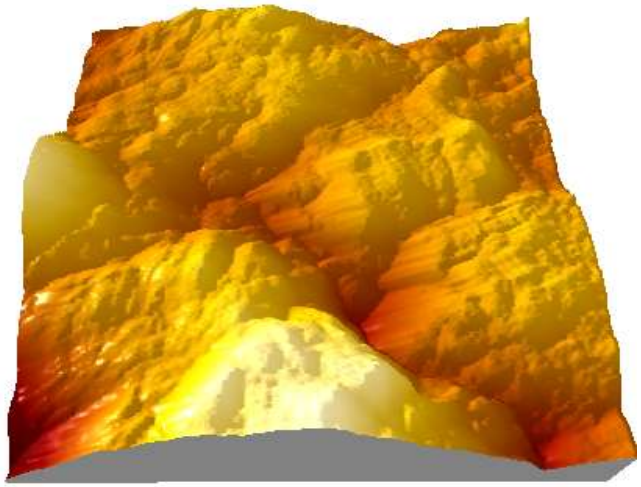

Figure 3.1c – 3D image of leaf (Scan size 5 μm^2)

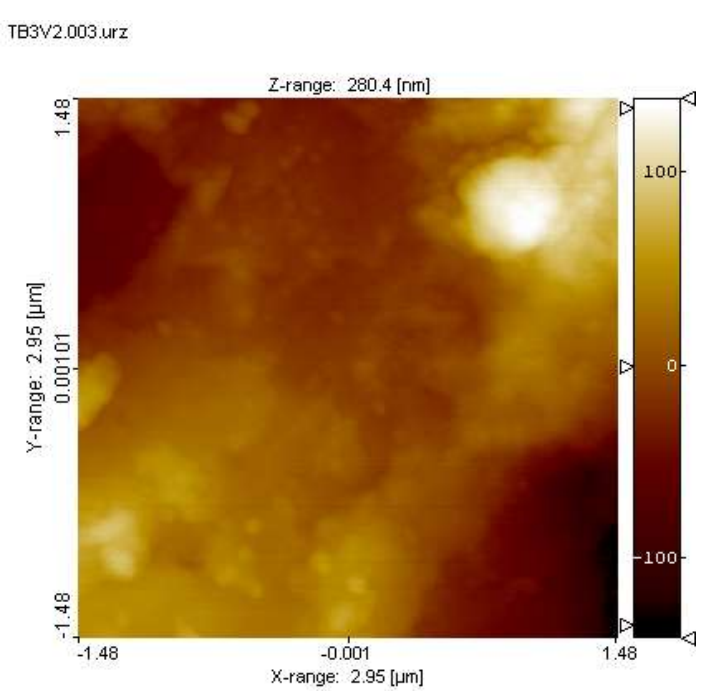

Figure 3.2a - Black untreated tea topography Image (Scan size 5 µm^2)

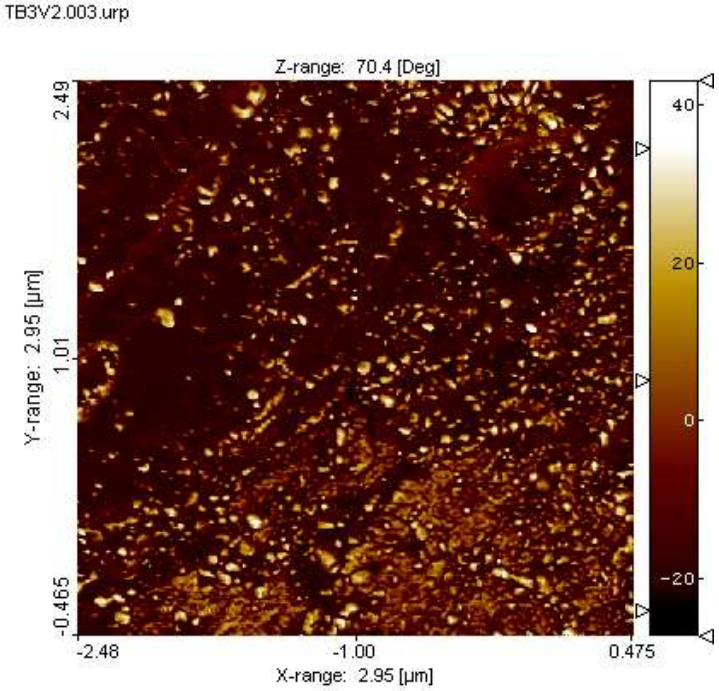

Figure 3.2b - Black untreated tea phase image (Scan size 5 µm^2)

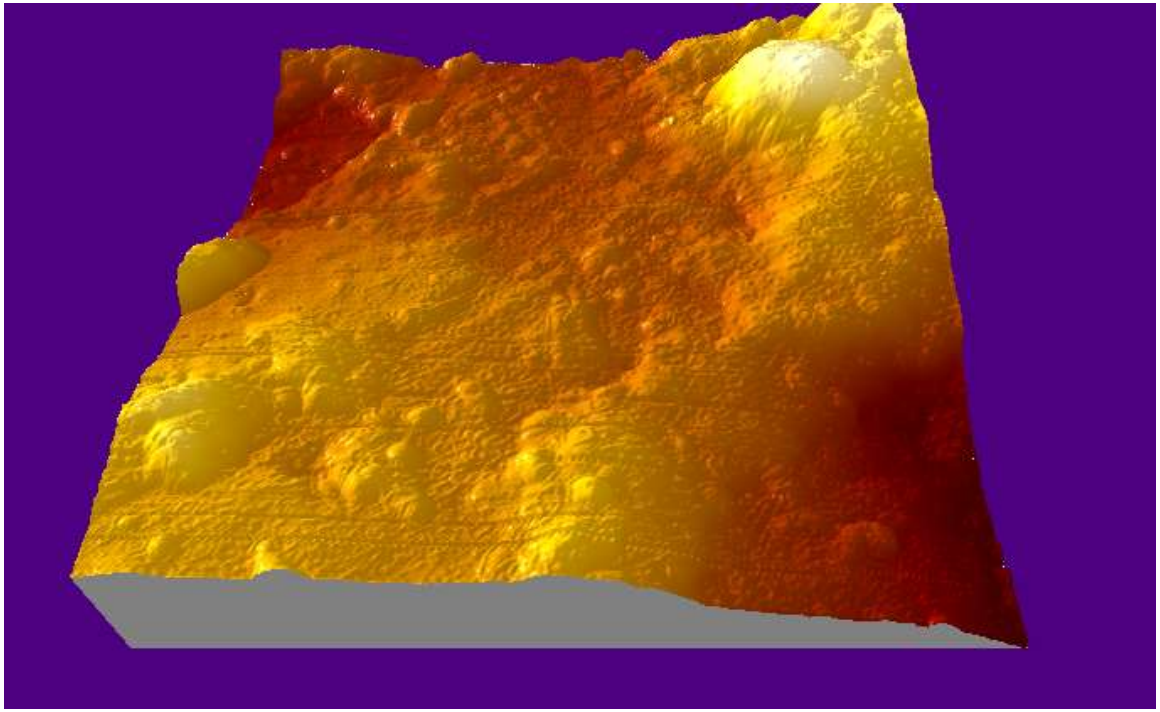

Figure 3.2c – 3D image of leaf (Scan size 5 μm^2)

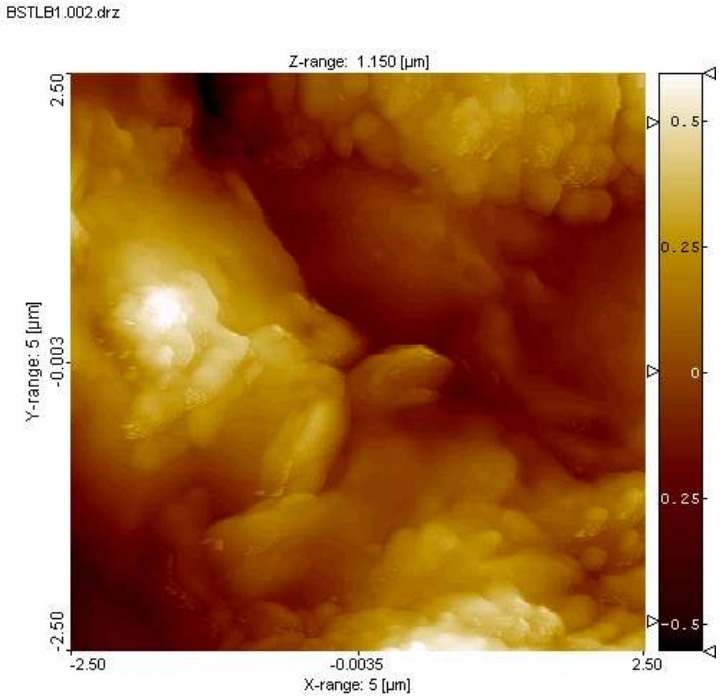

Figure 3.3a - Black untreated tea topography Image (Scan size 5 µm^2)

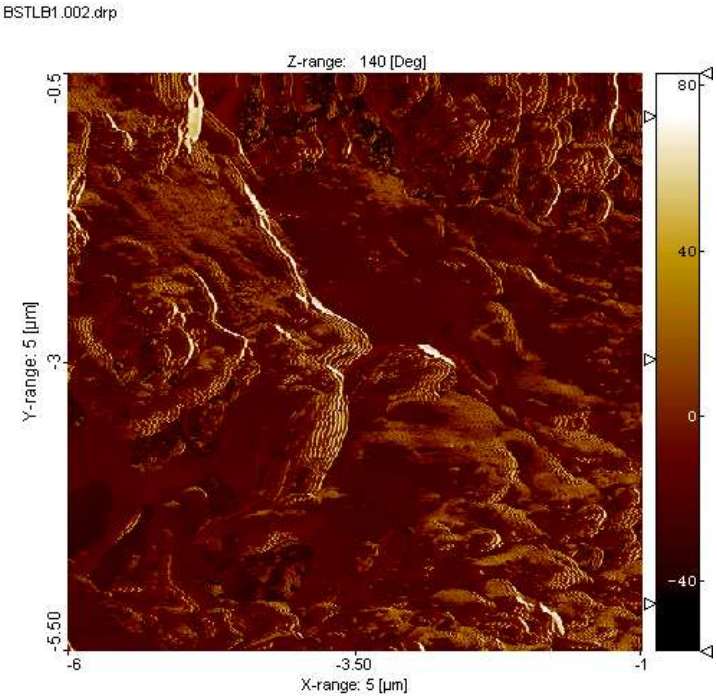

Figure 3.3b - Black untreated tea phase image (Scan size 5 µm^2)

3.3.1.2 Discussion of examination of black tea leaves with AFM – tapping mode in air.

Analysis of the sample images of black untreated tea leaves, Figures 3.1a, 3.1b and 3.1c shows that the leaf has a rough surface. Various sizes of scan were attempted and the largest stable images that were able to be obtained were 5 μm x 5 μm. Any larger than this and the scan was unstable as the vertical range exceeded that of the AFM piezo (approx. 1 μm). As the leaves had been processed, which includes drying stages, there is a clear potential for there to be large differences in the state of the tea leaf samples and also the topography of the samples in addition to the natural roughness of the leaf surface. Removal of water from the leaf system can, for example, alter the shape of the leaf. The AFM phase image can show if there are any interactions with the probe and the surface (Zhong et al. 1993). The image in 3.1b corresponds with the features seen in the topography image. This can be indicative that the phase data results from cross-talk from the topographic data due to changes in contact area of the probe with the leaf surface and therefore potential surface composition homogeneity on the leaf.

The topography image of another tea leaf fragment, shown in figure 3.2a, shows a large feature in the top right corner of the image. The height in the top left and bottom right of the image are lower and therefore darker in this representation than the rest of the leaf. When compared with the topography image in figure 3.1a the leaf fragment appears to be more

even and have fewer features. The phase image of this sample, in figure 3.2a initially shows a difference in the phase image to the surface topography. When the area where the large feature, seen in the topography image, in the top right of the image is examined initially there appears to be an area that corresponds with increased interaction between the tip and the surface. When the rest of the image is examined though, the contrast of this area is the same as the other parts of the leaf and so it cannot be said that this is any different from the rest of the leaf in composition. Other features can also be checked between the two images. There is more interaction between the tip and the surface in the top left of the image but there is interaction on the bottom right of the image. In the topography image these areas are of low topography. When the 3D image is also examined, in figure 3.2c, it can be seen that the surface has “bumps” on it which correspond to the phase image. The presence of these bumps could be an indication of a different surface property such as a change in the crystal structure of the epicuticular waxes on the surface of the leaf. The measurement of these features revealed that the largest was 180 nm x 80 nm whilst the rest were in the range of 60 nm x 50 nm.

A final example of the data produced by the AFM in air tapping mode

shows the topographical image in figure 3.3a and the corresponding phase image in figure 3.3b. The topographical image is different from those previously seen. It can be seen that the variation in topography is

1.15 μm from the highest feature on the scan to the lowest. As with the previous scans the phase image corresponds with the topographical image indicating a compositionally homogeneous surface as there are no changes in interactions between the tip and sample apart from the effect that topography has on the tip. When examined, these two images show that there appears to be a layered surface, where the layers overlap. Given that the leaf is covered in the cuticle which is composed of cuticular waxes and a cutin membrane and that the formation of the cuticular layer can occur in plate like structures, then these images could be indicative of the formation of waxy layer on the surface of the leaf. These layers ranged in size from approximately 300 nm x 20 nm to 60 nm x 40 nm. The overlapping of layers of wax has been seen previously in the work of Koch et al. 2004. The images of the regeneration of the cuticle of *Euphorbia lathyris* are shown here as a comparison of the layering of the wax on the cuticle of the tea leaf and can be seen in figure 3.4.

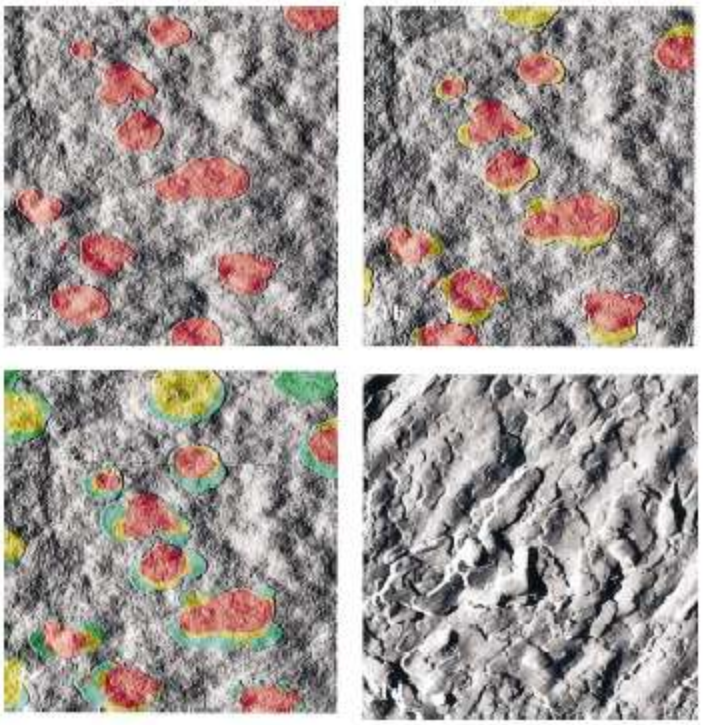

Figure 3.4 – The regeneration of cuticle of *Euphorbia lathyris.* (Scan size 3 x 3*μ*m). A – Regenerated waxes shown in red after 1h 38 min. B – Further wax accumulation shown after 2h 11min. C – At 3h 3 minutes additional accumulation of waxy cuticle shown in green. D – Multilayered regenerated wax film at 20h after wax removal. (Source Koch et al., 2004).

The three different types of images shown are examples of the images collected from various leaf samples when examined using air tapping mode. They all showed either the wax layer of the cuticle, large differences in topography across the 5000 nm scan range and the presence of debris on the surface.

3.3.1.3 Black tea leaves with AFM – tapping mode in water.

Black tea leaves were imaged using the D3000 AFM in water. A representative example of the examination of black tea leaf fragments in water is shown in figures 3.5a and b.

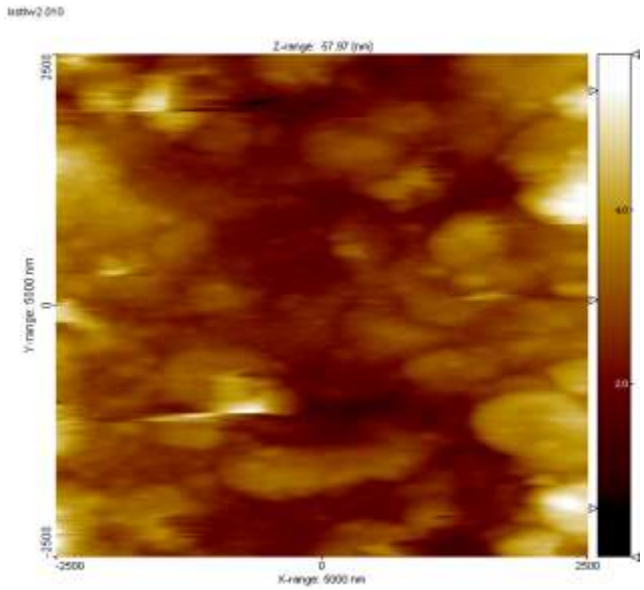

Figure 3.5a - Black untreated tea topography Image (Scan size 5 μm^2)

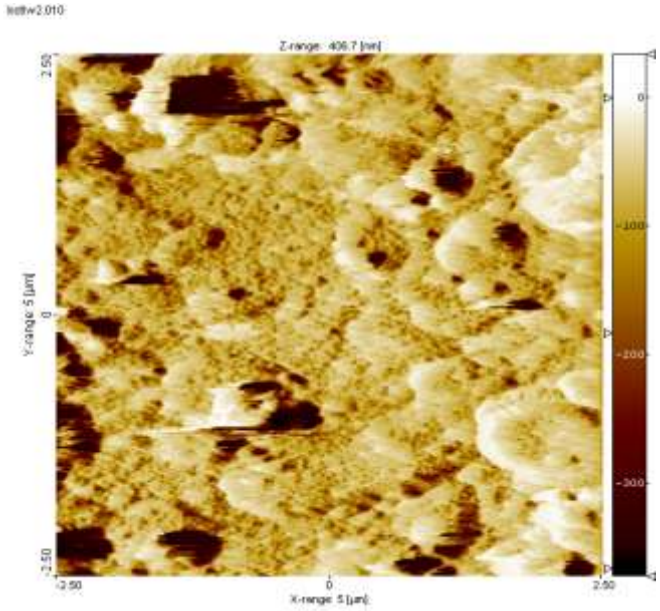

Figure 3.5b - Black untreated tea phase image (Scan size 5 μm^2)

3.3.1.4 Discussion of examination of black tea leaves with AFM – tapping mode in water.

Given that the results of scans of leaf fragments in air showed a homogeneous surface it was decided to examine the leaf fragments when in liquid to identify if changes occurred in this media. The topography and phase image of an example of tapping mode imaging in water is shown in figures 3.5a and 3.5b respectively.

Though there is some distortion in two areas on the leaf in both the topography and phase image it can be seen that there is correlation between the two images again. Though this could be indicative of surface homogeneity as seen in the previous air tapping images it is also possible that this is a result of a significant reduction in surface/tip interaction which is seen in phase data in liquid tapping mode due to a reduction in potential capillary and electrostatic force. As with the images in figure 3.3a and 3.3b there appears to be a layering of the surface. Though it is not to the same extent as the features in the previous images this could be further evidence of wax layers present in the cuticle of the plant which have stayed intact after the processing of the leaf into its dried form. The size in these features range from 410 nm x 350 nm to 1.2 μm x 950 nm. Though the largest of these is much larger than those seen in air tapping mode with the black tea leaves these are still comparable. As the cuticle is a wax layer the water would not be expected to have an effect on the surface.

The cells under the cuticle may change with the effects of the water and this was seen to disrupt scans within the first two hours of adding water. There was movement within the leaf and some swelling suggesting uptake of water.

3.3.1.5 Green tea leaves with AFM – tapping mode in air.

As a comparison to the black tea leaves and to examine if there was any difference between the surface of the leaf fragments due to the processing of the tea leaf to finished product, green tea leaf fragments were examined by AFM. Figure 3.6a displays an example of the topographical image obtained from one of the samples and figure 3.6b displays the corresponding phase image.

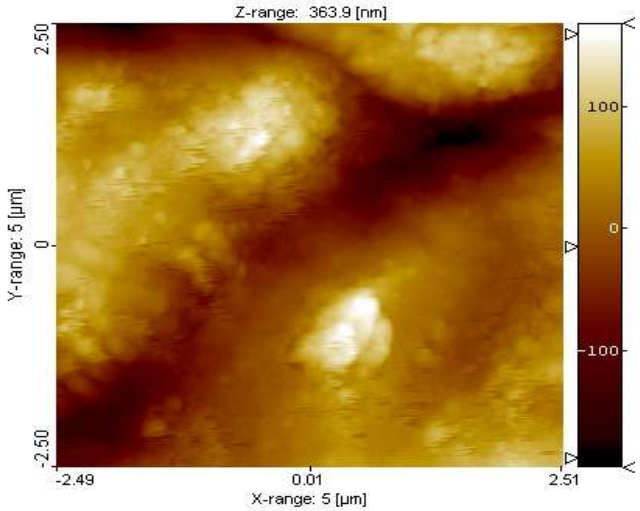

Figure 3.6a - Green untreated tea topography Image (Scan size 5 µm^2)

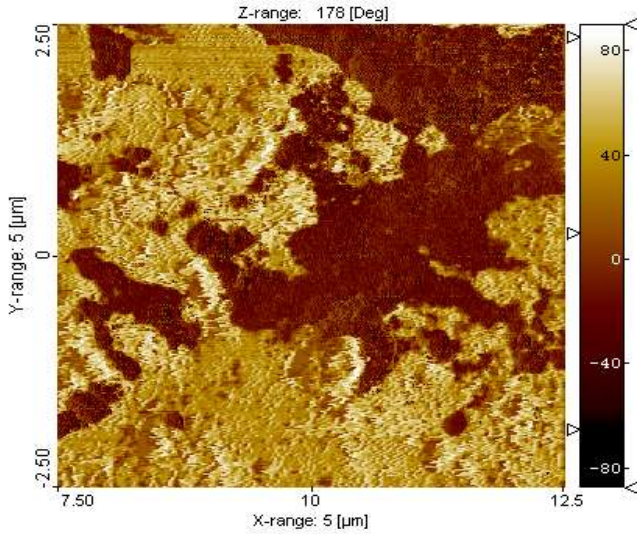

Figure 3.6b - Green untreated tea phase image (Scan size 5 µm^2)

3.3.1.6 Green tea leaves with AFM – tapping mode in air.

Production of green tea is not as destructive to the leaf as for black tea. Drying occurs before cutting so the surface of the leaf would be expected to show less debris than with black tea. The images in figures 3.6a and 3.6b show an example AFM scan in air of the topography and corresponding phase image of a green tea leaf fragment. There is in general less of a variation in height than for black tea, (here 360 nm). The phase image shows some differences from the topography image indicating there may be different properties between sections of the leaf. For example in the top right hand corner of the image there is evidence of changes in height. When this is compared with the phase image, the same area appears dark and relatively flat. The phase image indicates two types of surface features. This could be due to a change in the composition of the cuticle or a feature under the cuticle which is having an effect on the surface. When the topography is compared with the phase images, light areas in the phase generally correspond with higher areas in the topography, whereas the lower areas in topography generally correspond with the darker areas in the phase image. The darker areas of the phase image show more tip-sample interaction and a different structure to the lighter areas. The changes in phase indicate a difference in physico-chemical properties in the structure of the cuticle of the leaf. Use of

fuctionalised tips might be able to describe the differences in the properties of these regions, such as if they were more hydrophobic or hydrophilic. Previous studies have shown that the differences in the cuticle can be attributed to amorphous and crystalline wax layers (Perkins et al., 2005).

3.3.1.7 Green tea leaves with AFM – tapping mode in water.

To supplement the data gathered from the examination of green tea leaf fragments with air tapping mode, green tea leaves were imaged using the in water. Figures 3.7a and 3.7b display representative images of the topographical data gathered and the corresponding phase image.

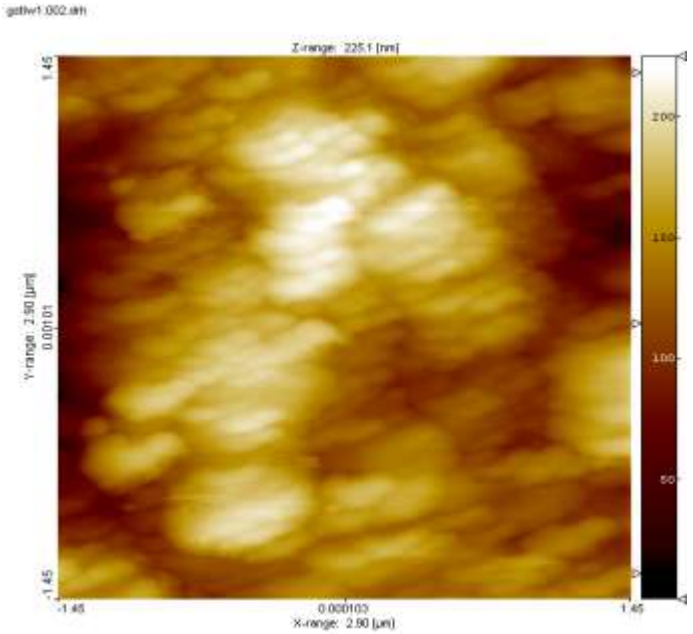

Figure 3.7a - Green untreated tea topography Image (Scan size 2.9 μm^2)

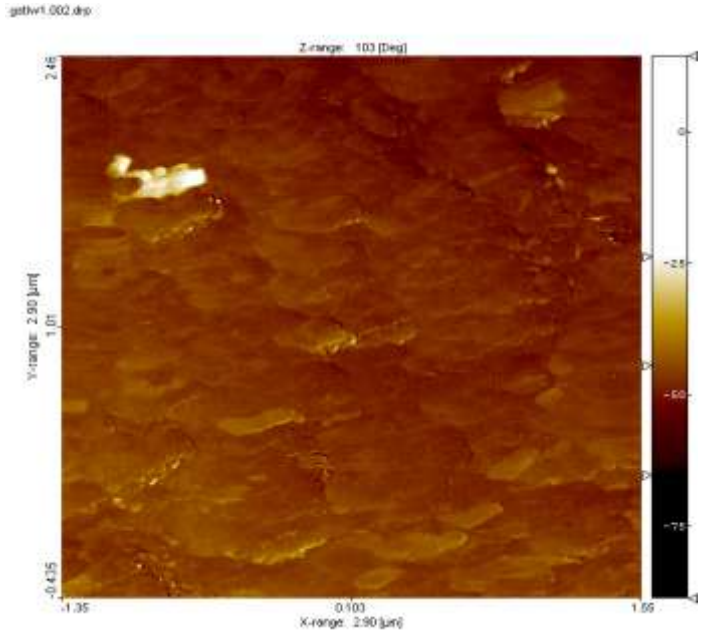

Figure 3.7b - Green untreated tea phase image (Scan size 2.9 μm^2)

3.3.1.8 Green tea leaves with AFM – tapping mode in water.

As with the black tea leaf fragments the samples were left in deionised water for two hours to equilibrate and then scanned.

An example topography image is shown in figure 3.7a and the corresponding phase image is shown in figure 3.7b. The topography and phase images indicate a homogeneous surface. These images are interesting as they show the overlapping of layers of wax on the surface of the leaf as previously seen in other scans. The layers of wax are comparable with those previously seen on the black tea leaves with sizes of the black tea leaf (air tapping). As with the image of the black tea leaf fragment the phase is not as pronounced as the interaction of the tip with the surface can be reduced when tapping in water.

With the exception of figure 3.6b, the phase image for the green tea leaf the surface appears to be homogenous. The lack of changes in interaction between the cantilever tip and surface of the cuticle of the leaf would suggest that the composition of the cuticle was uniform over the leaf. Confirmation of this would be possible with further experimentation with flatter leaves. The comparison of the layering of the cuticular waxes on the black and green tea leaves show that the different temperatures that these leaves are processed at have no effect on the surface morphology of the

leaf. The appearance of what could be epicuticular wax crystals in figure 3.2b and the change in phase in two distinct regions in figure 3.6b show that as well as having a layered structure there is also evidence of crystalline wax formation on the surface of the leaf. Further examination of these samples with hydrophilic probes would be able to confirm if the features seen in figure 3.2b are in fact epicuticular wax crystals as the probe would interact with these samples differently to the majority of the surface as would re-examination of the leaves in figure 3.6b to identify any changes in interaction between the two distinct layers on the green tea leaf surface. Examination of these leaves was tried with the functionalised probes but unsuccessfully.

3.3.2. SEM of tea leaves

3.3.2.1 SEM of tea leaves

Tea leaf samples were examined using SEM to compare with the AFM images. Figure 3.8 a, b and c are examples of SEM micrographs of the surface of black tea leaf fragments. Examples of the surface of green tea leaf fragments are shown in figure 3.9 a, b and c.

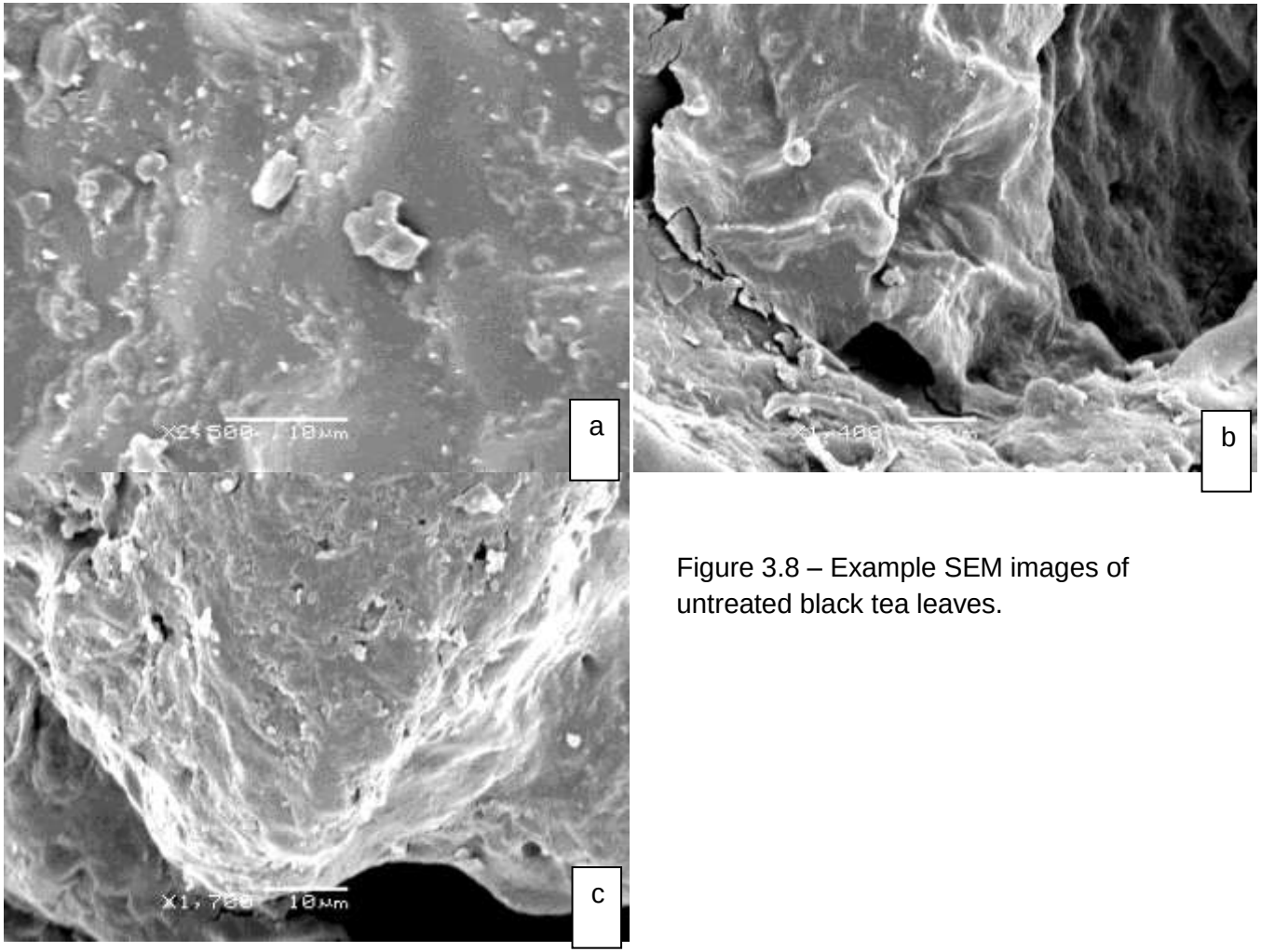

Figure 3.8 – Example SEM images of untreated black tea leaves.

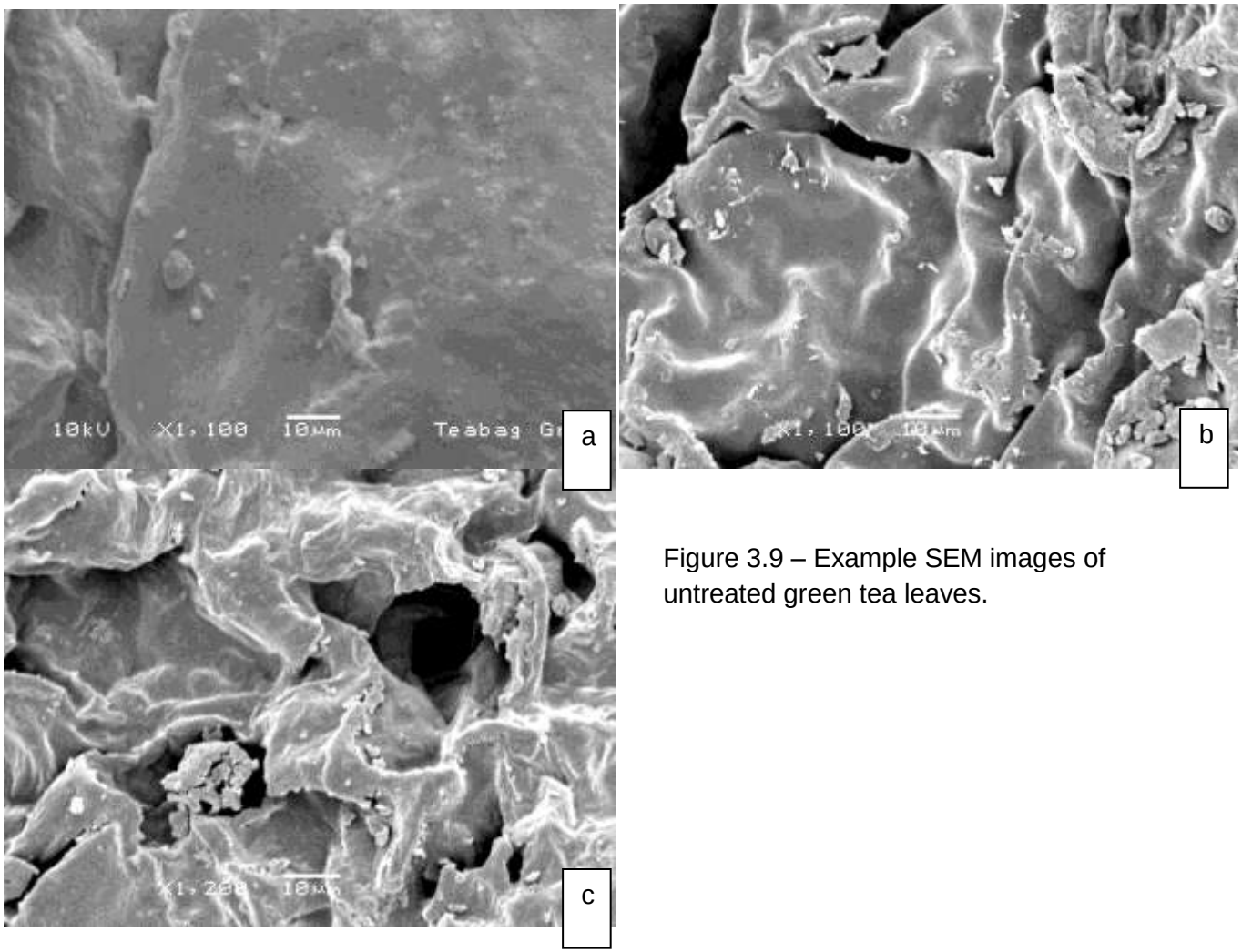

Figure 3.9 – Example SEM images of untreated green tea leaves.

3.3.2.2 SEM Images of Tea

Figure 3.8a, b and c show 3 different examples of SEM images of untreated black tea leaves. The magnification of the images is different for all 3 samples as the topography of the surface of each leaf was different. The maximum magnification achievable was dependent on a smoother, flatter surface, as in figure 3.8a. Though the magnification of the figure 3.8 b and c were lower, details of the surface can still be seen. Initially in figure 3.8 a, the surface shows large pieces of debris. One of the sections of debris is approximately 7 x 6 μm. Smaller debris is also visible on the surface, 1 x 1 μm. The surface wax also appears in layers on top of each other as also shown in the AFM images. Figure 3.8 b shows a varied topography. There is a section of the leaf which is lower than the rest of the micrograph to the right of the image. The bottom edge is higher and folds are visible on the leaf. Debris can also be seen in this image. It is difficult to say whether the cuticular wax is layered on top of the surface due to the folding of the leaf and the variation in height. With the large variation in topography seen in this image, the difficulty in scanning a whole leaf using the AFM can also be seen. The large differences in topography mean that a section of leaf which is lower than the rest will not be able to be scanned. The cantilever could interact with a larger ridge on the outside of one of these deeper areas so the actual area would not be

imaged. Holes can be seen in the cuticle and the largest is approximately 15 x 19 μm. The surface of the tea leaf fragment in figure 3.8 c is rougher than the previous two images. Layering of the surface cuticular wax can be seen on the leaf. Debris is evident on the surface and a large variation in height in topography can also be seen.

The presence of debris on all images indicates that the processing of the tea from its natural leaf state to the finished dry product is quite damaging to the tea leaf. With the size of the debris fragments on the surface and the frequency of them this indicates why there were some problems with obtaining stable images using the AFM. The variability seen in the 3 different images with regards to the height changes in topography also explain the difficulty in gaining stable large images with the AFM. Height of surrounding areas and also large changes in height in a short space in the x and y axis would affect the AFM instrument.

There are some indications that the images taken with the AFM correspond with the electron micrographs. The images for figures 3.1 to 3.3 do appear to be similar to the roughness of image 3.8 c. The smoother surface example of figure 3.5 to 3.7 do show similarities with the topography of figure 3.8 a.

Electron micrographs of green tea leaves were also taken. These are shown in figure 3.9a, b and c. As with the black tea leaves three examples are shown. Figure 3.9a shows a smooth surface on the leaf when compared to 3.9b and c. Some folding of the leaf is evident in the bottom centre of the micrograph, as is some debris. The roughness is more obvious in figure 3.9b. More debris is evident, though there appears to be a flatter area in the left hand side of the image. Finally, figure 3.9c shows the roughest topography. Much more debris is evident in the image and an attempt to get a successful AFM image from a sample like this would be difficult.

From the micrographs it can be seen that the rougher the surface on both black and green tea leaves, the more debris there is evident. Structures that were seen on the AFM are hard to recognise with the micrographs but there is some layering in the flatter images. As a difference was seen in the phase imaging for a green and black tea leaf there may be a difference in the leaf properties from the other tea leaves seen. As the top 3 leaves of the plant are used to produce the tea, then these leaves where cuticular micro-crystals may have been seen, figure 3.2b, and where distinct differences are seen in the green tea leaf, figure 3.6b may have been from a younger leaf and therefore not fully developed.

3.3.3 ToF-SIMS cluster source

3.3.3.1 ToF-SIMS of tea leaves.

Before experimentation could begin on tea leaves using the ToF-SIMS an examination of sample tea leaves was performed using the Bi_3^+ and C_{60}^+ cluster sources. Figure 3.10 displays the normalised intensity of selected molecular species from the spectra obtained for these samples using these sources.

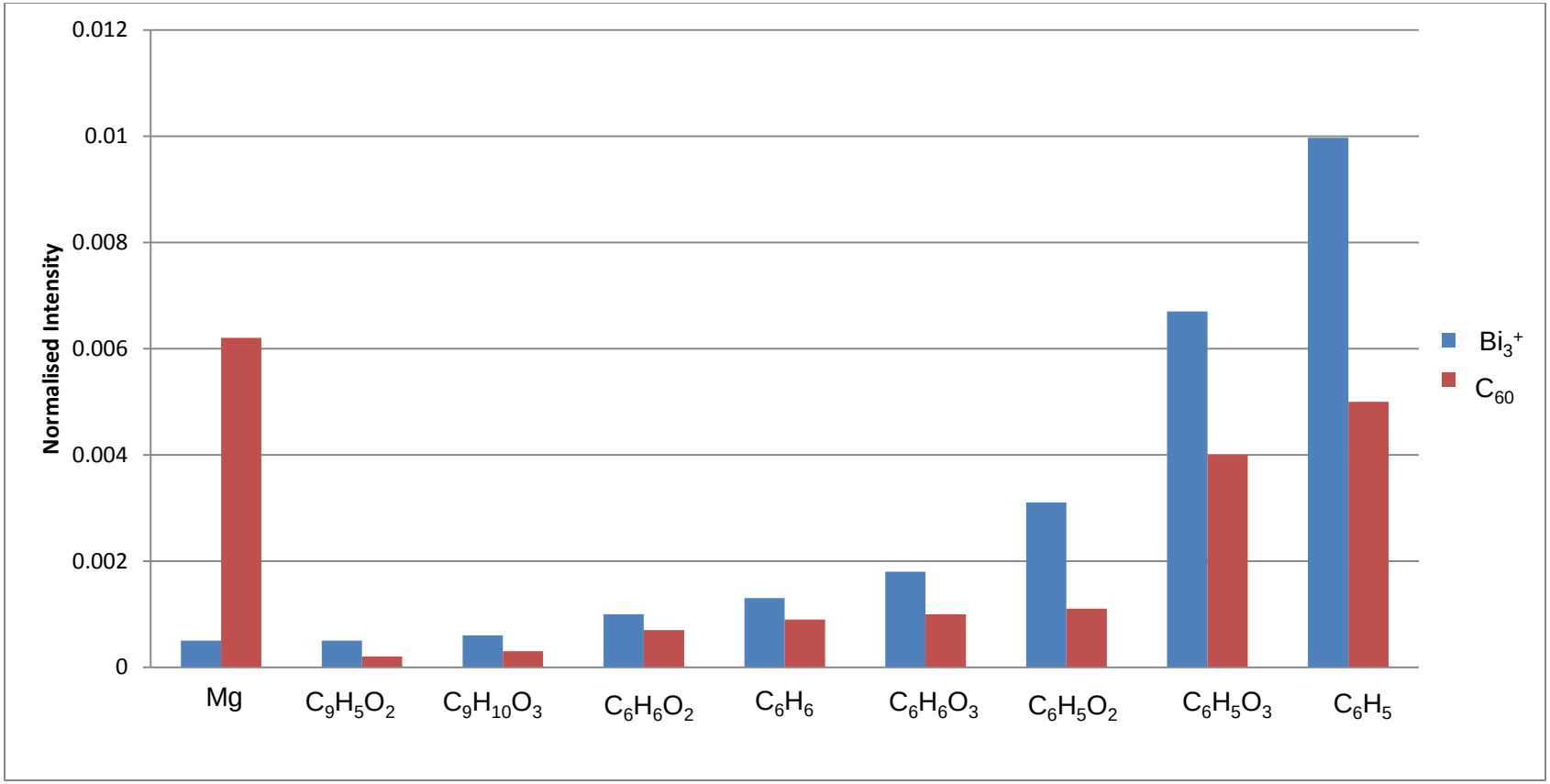

Figure 3.10 – Comparison of small and large molecular weight fragments obtained by using a Bi_3^+ and C_{60}^+ cluster source.

3.3.3.2 Use of cluster sources for ToF-SIMS of tea leaves

To initially characterise the chemical constituents of the tea leaves a decision as to which primary source to use was needed. Tea leaf samples were examined using the bismuth source of the ToF-SIMS instrumentation. Bi_3^+ is used for organic samples and other cluster sources, such as a C_{60}^+ can also be used.

In figure 3.10 a comparison of the normalized intensity of scans of a tea leaf using both the Bi_3^+ and C_{60}^+. When the fragment is more complex, $C_6H_5O_3$, then the intensity of the fragment is higher when the Bi_3^+ source is used. This increase in intensity would be beneficial given the later work that was planned of examining subtle changes due to the effects of infusion and if aroma molecules could be identified after addition to the surface of the tea leaf. Following this experiment Bi_3^+ was used for all analysis of the tea leaf fragments. C_{60}^+ was to be used again but in the depth profiling work as a high energy primary ion for removing layers of the leaf for examination of what was chemically present in the leaf.

3.3.4 ToF-SIMS scans of the surface of tea leaves.

Samples of black and green tea leaf fragments were examined using ToF-SIMS. Figures 3.11 and 3.12 show example spectra for the positive and negative spectra of black tea leaf fragments. Species marked on the spectra are of an intensity over 20% of the frame to show examples of identified peaks.

Figures 3.13 and 3.14 are examples of positive and negative spectra obtained when examining green tea leaf fragments. The species marked are again of the same order of intensity as with the black tea leaf fragments.

As all of the molecular species identified could not be included on the spectra, figure 3.15 is a table of the hydrocarbons identified as being on the surface of tea leaf from the positive spectra. Figure 3.16 shows the oxygenated hydrocarbon groups and other molecular species that were identified in the positive spectra for tea leaf samples.

The identification of peaks in the negative spectra is shown in figure 3.17 and includes hydrocarbons, oxygenated hydrocarbons and other groups.

Examples of the mean normalised intensity of some of the species identified on the positive spectra are shown in figure 3.18 a and b. A comparison of the normalised intensities for both green and black tea leaf fragments are shown for examples of all of the groups identified on the spectra.

Examples of the difference in mean normalised intensity for some of the species identified on the negative spectra are shown in figure 3.19.

As well as identifying any difference between the spectra for green and black tea leaf fragments ion images were acquired. The examples of the molecular species used in figures 3.18 and 3.19 are displayed with the total ion image for examples of black and green tea leaf fragments in a positive and negative regime. Figure 3.20 is an example of the black

positive spectra and 3.21 is an example of the black tea negative spectra. Figure 3.22 is an example of the ion images for the green tea positive spectra and figure 3.23 is for the negative spectra. These images display the distribution on the surface of the selected molecular species to examine if there is any difference in where the species are appearing on the scan.

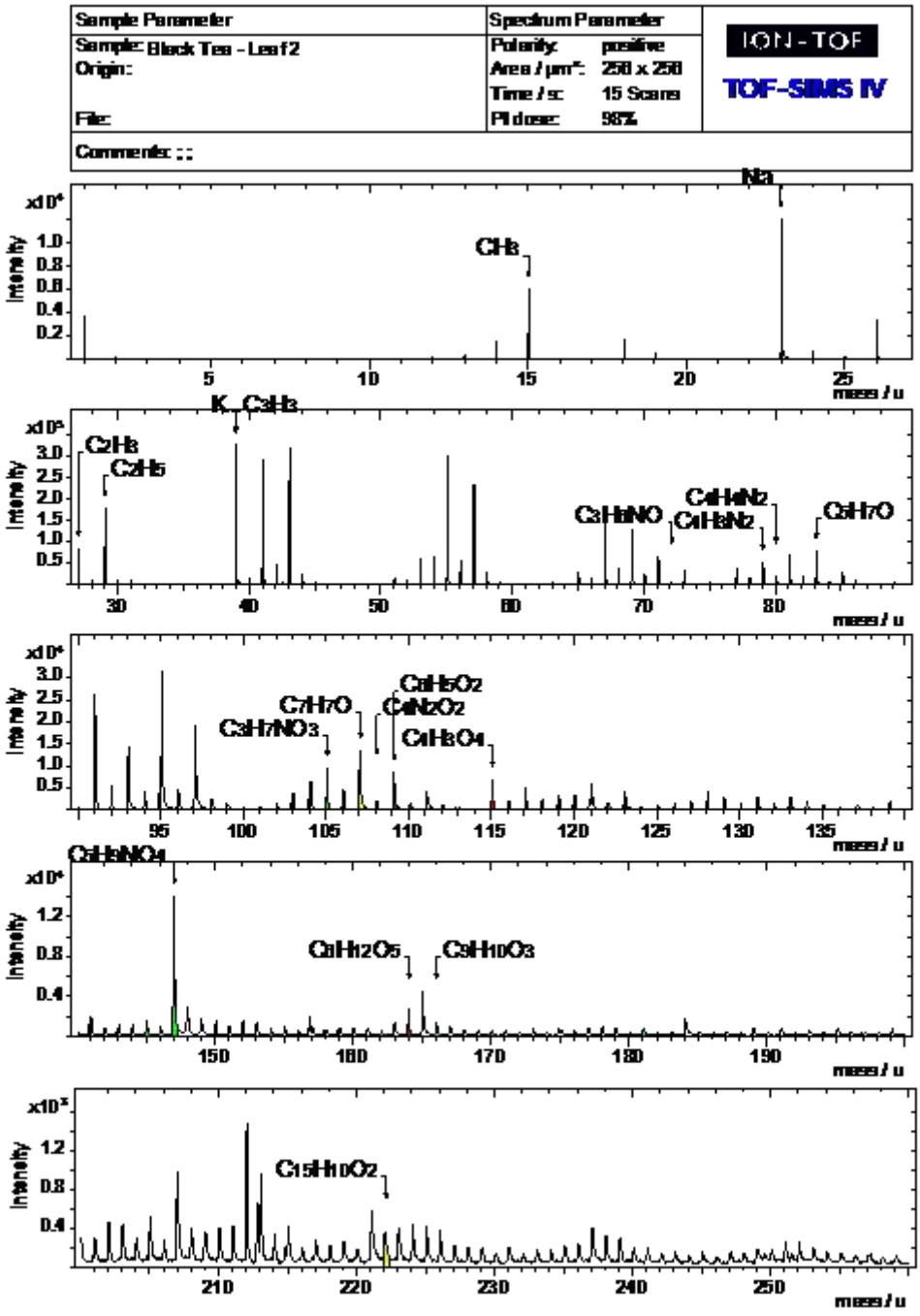

Figure 3.11 – Example positive spectra of black tea leaf using ToF-SIMS.

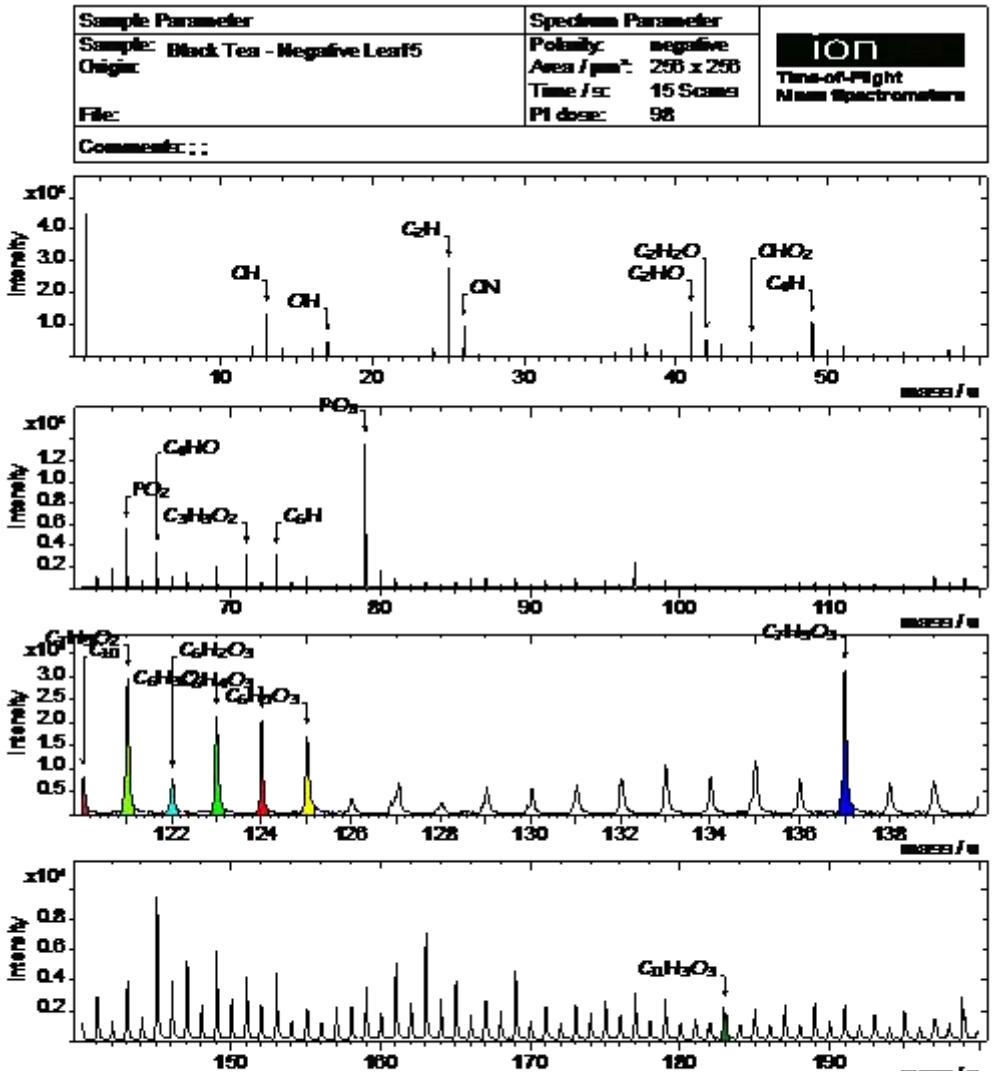

Figure 3.12 – Example negative spectra of black tea leaf using ToF-SIMS.

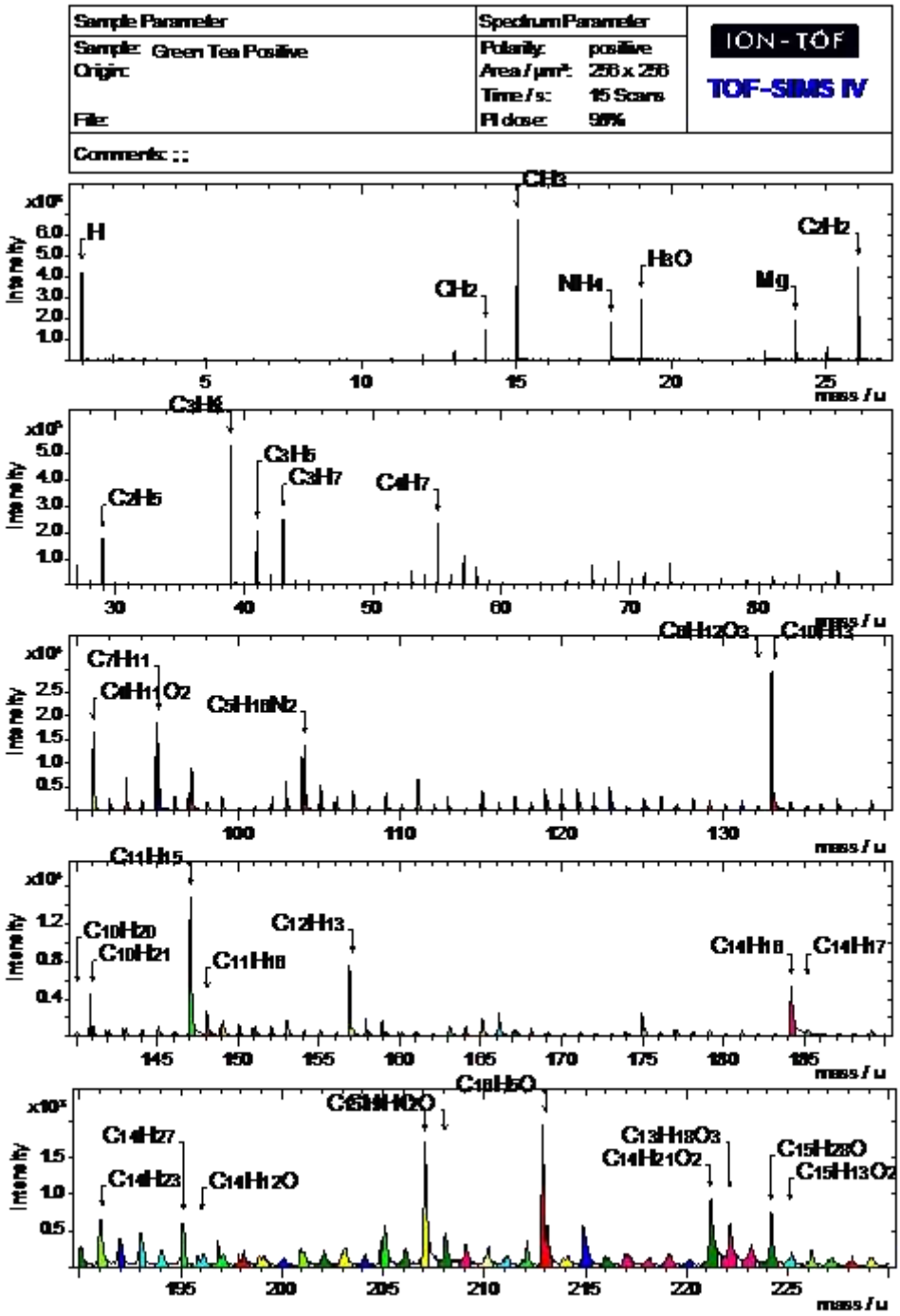

Figure 3.13 – Example positive spectra of green tea leaf using ToF-SIMS.

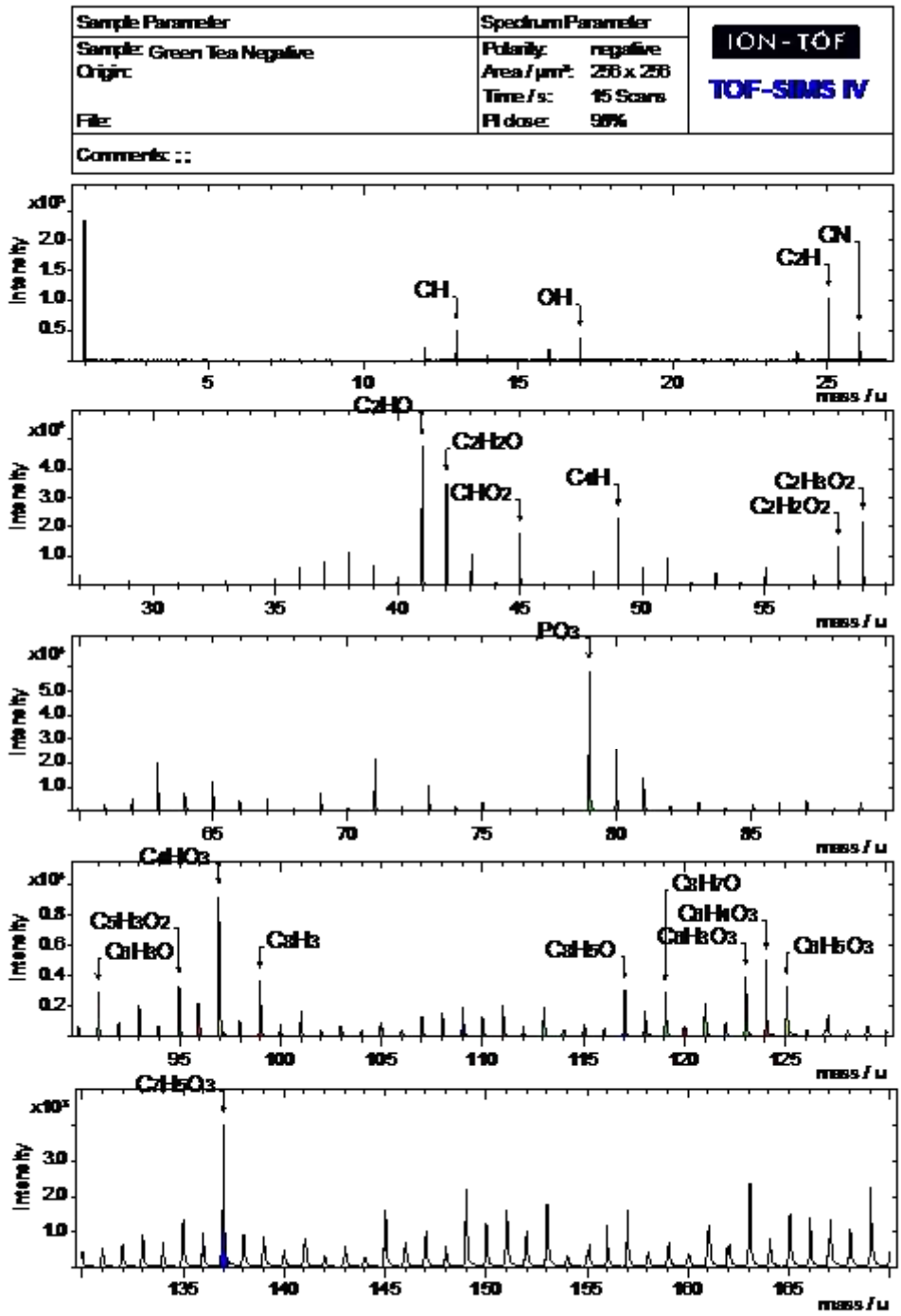

Figure 3.14 – Example negative spectra of green tea leaf using ToF-SIMS.

Ion	(m/z)	m dev. (ppm)	Ion	(m/z)	m dev. (ppm)	Ion	(m/z)	m dev. (ppm)	Ion	(m/z)	m dev. (ppm)	Ion	(m/z)	m dev. (ppm)	Ion	(m/z)	m dev. (ppm)
CH	13.00	-97.86	C_5H_7	67.07	68.23	C_9H_{10}	118.09	-78.12	$C_{12}H_8$	152.09	-41.18	$C_{14}H_{20}$	188.14	-122.80	$C_{17}H_{12}$	216.08	-6.76
CH_2	14.01	-0.19	C_5H_8	68.07	18.83	C_9H_{11}	119.11	-25.86	$C_{12}H_9$	153.08	-69.77	$C_{14}H_{21}$	189.15	-166.63	$C_{18}H_{11}$	227.03	-4.27
CH_3	15.02	42.31	C_5H_9	69.08	93.84	C_9H_{12}	120.10	-76.69	$C_{12}H_{10}$	154.10	52.05	$C_{14}H_{22}$	190.16	-145.16	$C_{18}H_{12}$	228.08	-48.80
C_2H_2	26.02	32.77	C_5H_{10}	70.09	0.80	C_9H_{13}	121.13	-83.12	$C_{12}H_{11}$	155.11	-11.49	$C_{14}H_{23}$	191.17	-139.78	$C_{19}H$	229.05	105.29
C_2H_3	27.03	75.40	C_5H_{11}	71.11	45.85	C_9H_{14}	122.13	-118.82	$C_{12}H_{12}$	156.12	-2.06	$C_{15}H_{12}$	192.11	-93.62	$C_{19}H_2$	230.04	63.46
C_2H_4	28.03	52.17	C_6H_5	77.05	52.69	C_9H_{15}	123.16	-28.51	$C_{12}H_{13}$	157.11	-168.52	$C_{14}H_{27}$	195.18	-186.78	$C_{18}H_{15}$	231.05	-115.28
C_2H_5	29.04	43.75	C_6H_6	78.05	-26.91	C_9H_{16}	124.15	-60.61	$C_{12}H_{15}$	159.15	-60.58	$C_{16}H_7$	199.06	30.37	$C_{18}H_{16}$	232.03	-112.16
C_2H_6	30.05	-98.93	C_6H_9	81.09	82.45	$C_{10}H_7$	127.08	19.72	$C_{12}H_{16}$	160.15	-92.94	$C_{16}H_8$	200.06	-2.78	$C_{19}H_9$	237.05	56.62
C_3H_2	38.02	-0.50	C_6H_{10}	82.10	81.29	$C_{10}H_8$	128.07	-54.95	$C_{12}H_{17}$	161.16	-82.80	$C_{16}H_{12}$	204.06	-76.70	$C_{19}H_{11}$	239.07	14.66
C_3H_3	39.03	72.82	C_6H_{11}	83.10	106.17	$C_{10}H_{11}$	131.11	-91.91	$C_{12}H_{19}$	163.15	-104.91	$C_{16}H_{13}$	205.11	-31.33	$C_{19}H_{13}$	241.03	-86.57
C_3H_4	40.03	28.67	C_6H_{12}	84.11	18.62	$C_{10}H_{13}$	133.13	-55.25	$C_{12}H_{20}$	164.10	-110.42	$C_{16}H_{14}$	206.05	-106.51	$C_{21}H_{27}$	279.17	-129.28
C_3H_5	41.04	61.86	C_6H_{13}	85.14	27.11	$C_{10}H_{14}$	134.12	-108.83	$C_{12}H_{23}$	167.11	-117.92	$C_{17}H_7$	211.05	81.97	$C_{22}H_{19}$	283.11	-55.19
C_3H_6	42.05	-3.14	C_7H_{11}	95.11	127.29	$C_{10}H_{15}$	135.15	-88.26	$C_{13}H_{12}$	168.10	-83.55	$C_{17}H_{11}$	215.03	-81.03	$C_{23}H_{11}$	287.07	-62.17
C_3H_7	43.06	97.66	C_7H_{12}	96.13	82.81	$C_{10}H_{16}$	136.14	-109.16	$C_{13}H_{16}$	172.14	-99.44	$C_{17}H_{12}$	216.08	-6.76			
C_4H_2	50.02	-2.37	C_7H_{13}	97.14	95.34	$C_{10}H_{17}$	137.16	-98.39	$C_{13}H_{17}$	173.14	-92.38	$C_{18}H_{11}$	227.03	-4.27			
C_4H_3	51.03	2.26	C_7H_{14}	98.13	14.74	$C_{10}H_{19}$	139.13	-104.14	$C_{14}H_6$	174.14	101.42	$C_{18}H_{12}$	228.08	-48.80			
C_4H_4	52.03	-24.87	C_7H_{15}	99.11	-119.10	$C_{10}H_{20}$	140.12	-109.80	$C_{13}H_{19}$	175.12	-105.62	$C_{19}H$	229.05	105.29			
C_4H_5	53.04	22.47	C_8H_9	105.09	27.87	$C_{10}H_{21}$	141.09	-92.40	$C_{13}H_{20}$	176.13	-122.56	$C_{19}H_2$	230.04	63.46			
C_4H_6	54.05	10.39	C_8H_{10}	106.09	-7.70	$C_{10}H_{22}$	142.10	-80.02	$C_{13}H_{21}$	177.13	-194.16	$C_{18}H_{15}$	231.05	-115.28			
C_4H_7	55.06	97.38	C_8H_{11}	107.11	-39.96	$C_{10}H_{23}$	143.11	-102.09	$C_{13}H_{22}$	178.11	-125.82	$C_{16}H_8$	200.06	-2.78			
C_4H_8	56.07	4.66	C_8H_{15}	111.18	74.75	$C_{11}H_{15}$	147.12	-92.22	$C_{14}H_{11}$	179.14	24.26	$C_{16}H_{12}$	204.06	-76.70			
C_4H_9	57.08	110.84	C_8H_{16}	112.16	-96.23	$C_{11}H_{16}$	148.13	-67.99	$C_{14}H_{16}$	184.15	28.00	$C_{16}H_{13}$	205.11	-31.33			
C_5H_2	62.02	-4.46	C_8H_{17}	113.12	-106.08	$C_{11}H_{17}$	149.16	-76.26	$C_{14}H_{17}$	185.16	-97.37	$C_{16}H_{14}$	206.05	-106.51			
C_5H_3	63.02	-43.89	C_9H_8	116.08	-38.55	$C_{11}H_{18}$	150.13	-86.26	$C_{14}H_{18}$	186.15	-42.57	$C_{17}H_7$	211.05	81.97			
C_5H_6	66.05	-13.20	C_9H_9	117.09	-16.64	$C_{12}H_7$	151.13	77.37	$C_{14}H_{19}$	187.17	-80.02	$C_{17}H_{11}$	215.03	-81.03			

Figure 3.15 – Hydrocarbons identified from the positive spectra of black and green tea leaves using ToF-SIMS.

Ion	(m/z)	m dev. (ppm)	Ion	(m/z)	m dev. (ppm)	Ion	(m/z)	m dev. (ppm)	Ion	(m/z)	m dev. (ppm)	Ion	(m/z)	m dev. (ppm)
CHO	29.00	66.26	$C_7H_5O_5$	169.14	93.15	$C_{13}H_{18}O_3$	222.12	-80.80	H	1.01	43.08	$C_4H_{12}N_2$	88.10	-121.33
CH_2O	30.01	9.25	$C_7H_6O_5$	170.06	88.19	$C_{14}H_7O_3$	223.07	48.36	H_2	2.02	-28.74	C_3H_7SN	89.03	64.91
CH_3O	31.02	82.18	$C_7H_7O_5$	171.14	107.00	$C_{15}H_{28}O$	224.15	-102.40	H_3	3.02	-22.67	$C_3H_{10}NO_2$	92.07	3.08
CH_4O	32.05	88.11	$C_6H_{12}O_6$	180.12	145.88	$C_{15}H_{13}O_2$	225.10	9.08	C	12.00	-85.16	$C_2H_{11}N_3O$	93.09	-3.90
C_2H_3O	43.02	43.63	$C_9H_9O_4$	181.05	90.83	$C_{15}H_{14}O_2$	226.10	-89.44	NH_2	16.03	83.33	$C_2H_{12}N_3O$	94.10	-99.66
CHO_2	45.04	88.82	$C_9H_{10}O_4$	182.05	-28.25	$C_{12}H_9O_5$	233.05	-34.84	NH_4	18.04	90.56	$C_4H_6NO_2$	100.08	107.31
C_2H_6O	46.04	53.88	$C_{12}H_{23}O$	183.15	63.54	$C_{15}H_{22}O_2$	234.05	-113.23	H_3O	19.02	93.28	$C_4H_7NO_2$	101.05	-7.63
C_3H_6O	58.08	107.79	$C_{10}H_9O_4$	193.14	183.86	$C_{16}H_{11}O_2$	235.06	33.92	Na	22.99	77.73	$C_5H_{16}N_2$	104.13	-48.03
$C_2H_4O_2$	60.08	116.22	$C_{14}H_{12}O$	196.08	-62.45	$C_{14}H_{20}O_3$	236.08	-104.43	Mg	23.99	96.85	$C_4N_2O_2$	108.06	130.07
$C_2H_5O_2$	61.04	69.17	$C_{10}H_{13}O_4$	197.04	-4.82	$C_{16}H_{14}O_2$	238.08	-53.79	MgH	24.99	60.05	$C_5H_3N_2O_2$	122.96	108.35
$C_3H_5O_2$	73.06	97.67	$C_{11}H_{18}O_3$	198.12	-42.11	$C_{15}H_{12}O_3$	240.09	74.60	Si	27.97	26.43	$C_6H_{11}NO_2$	129.09	-69.35
$C_5H_{10}O$	86.14	-80.12	$C_{15}H_5O$	201.01	40.56	$C_{12}H_9O_6$	249.00	-69.56	CH_2Na	37.00	84.25	$C_6H_{12}NO_2$	130.10	-95.11
$C_4H_{10}O_2$	90.06	14.74	$C_{12}H_{10}O_3$	202.06	92.58	$C_{16}H_{32}O_2$	256.06	-137.13	K	38.97	-16.11	$C_6H_6N_2O_2$	138.03	94.53
$C_6H_{14}O$	102.09	-62.84	$C_{12}H_{11}O_3$	203.06	101.52	$C_{19}H_5O_2$	265.05	57.24	C_2H_6N	44.06	67.59	$C_7H_{14}N_2O_2$	158.11	-104.84
$C_6H_5O_2$	109.14	131.61	$C_{15}H_{12}O$	208.06	13.36	$C_{17}H_{15}O_3$	267.04	-93.53	Na_2H	47.00	71.15	$C_6H_{15}SNO_2$	165.13	-35.98
$C_6H_6O_2$	110.14	105.26	$C_{14}H_9O_2$	209.07	53.56	$C_{18}H_7O_3$	271.07	87.44	C_3H_9N	59.08	-69.24	$C_8H_{10}N4O_2$	194.05	-58.65
$C_4H_2O_4$	114.08	112.03	$C_{15}H_{14}O$	210.09	-97.93	$C_{11}H_{21}O_8$	281.13	-81.21	C_3N_2	64.03	108.44	$C_{14}H_9NO$	207.07	-4.01
$C_4H_3O_4$	115.07	105.43	$C_{14}H_{12}O_2$	212.08	-84.89	$C_{18}H_{34}O_2$	282.12	-145.43	C_3HN_2	65.03	106.90			
$C_6H_5O_3$	125.15	0.34	$C_{16}H_5O$	213.04	61.88	$C_{18}H_{36}O_2$	284.08	-149.78	C_3H_6NO	72.11	105.26			
$C_6H_6O_3$	126.13	104.39	$C_{16}H_6O$	214.06	72.07	$C_{16}H_{30}O_4$	286.08	-138.07	$C_2H_4NO_2$	74.08	83.32			
$C_6H_{12}O_3$	132.11	-21.72	$C_{15}H_5O_2$	217.04	43.55	$C_{17}H_{36}O_3$	288.09	-87.76	$C_2H_5NO_2$	75.04	70.99			
$C_9H_5O_2$	145.07	106.58	$C_{12}H_{26}O_3$	218.08	-121.43				C_4N_2	76.03	100.31			
$C_9H_6O_2$	146.07	107.88	$C_{13}H_{15}O_3$	219.06	-14.98				$C_4H_3N_2$	79.05	92.78			
$C_6H_{10}O_5$	162.15	106.50	$C_{13}H_{16}O_3$	220.05	122.11				$C_4H_4N_2$	80.05	114.32			
$C_9H_{10}O_3$	166.07	57.96	$C_{14}H_{21}O_2$	221.16	44.79				$C_3H_9N_3$	87.08	-97.91			

Figure 3.16 – Oxygenated hydrocarbons and other species identified from the positive spectra of black and green tea leaves using ToF-SIMS.

Ion	(m/z)	m dev. (ppm)	Ion	(m/z)	m dev. (ppm)	Ion	(m/z)	m dev. (ppm)	Ion	(m/z)	m dev. (ppm)	Ion	(m/z)	m dev. (ppm)
CH	13.01	2.69	CHO	28.99	64.99	C_5H_3O	78.95	17.36	$C_5H_6O_3$	114.02	19.46	H	1.01	68.10
CH_2	14.01	-0.62	C_2HO	41.00	85.73	C_4HO_2	80.98	-113.00	C_8H_3O	115.02	106.39	C	12.00	-9.36
CH_3	15.03	105.34	C_2H_2O	42.00	-109.39	$C_4H_2O_2$	81.99	71.66	C_8H_4O	116.02	39.87	O	16.01	-40.17
C_2H	25.00	65.70	C_2H_3O	43.02	68.13	$C_4H_3O_2$	83.01	102.59	C_8H_5O	117.03	9.11	OH	17.00	20.24
C_2H_3	27.02	104.01	CHO_2	45.00	43.42	$C_4H_4O_2$	84.01	-109.81	C_8H_6O	118.04	75.60	C_2	24.00	-4.64
C_3H	37.00	3.48	C_3HO	53.01	23.02	$C_4H_5O_2$	85.02	-106.99	C_8H_7O	119.04	16.81	CN	26.00	110.60
C_3H_2	38.01	14.32	C_3H_2O	54.01	113.92	$C_3H_3O_3$	87.01	95.81	$C_7H_5O_2$	121.01	-5.71	C_3	36.00	-3.20
C_3H_3	39.02	51.31	C_3H_3O	55.02	85.07	$C_3H_4O_3$	88.01	93.94	$C_6H_2O_3$	122.01	103.53	C_2O	40.00	-2.63
C_4H	49.01	29.67	C_2HO_2	57.01	-0.53	$C_3H_5O_3$	89.02	-109.38	$C_6H_3O_3$	123.01	31.03	CO_2	44.00	13.59
C_4H_2	50.01	-97.18	$C_2H_2O_2$	58.00	40.43	C_6H_2O	90.01	3.61	$C_6H_4O_3$	124.02	19.14	C_4	48.00	-2.75
C_4H_3	51.02	37.04	$C_2H_3O_2$	59.01	27.85	C_6H_3O	91.02	57.74	$C_6H_5O_3$	125.03	92.21	C_3O	52.00	3.38
C_5H_2	62.01	-6.66	CHO_3	60.99	101.23	C_6H_4O	92.02	3.82	$C_7H_5O_3$	137.02	32.34	CO_3	59.98	115.93
C_5H_3	62.97	-2.30	C_4O	63.99	-501.41	$C_2H_5O_4$	93.02	102.01	$C_{11}H_3O_3$	183.00	56.25	C_6	72.00	58.36
C_6H	73.00	-16.80	C_4HO	65.00	29.34	$C_5H_2O_2$	94.00	112.37	$C_{10}H_{11}O_5$	211.06	89.61	PO_3	78.95	34.08
C_7H_2	86.01	-35.67	C_4H_2O	66.00	-81.37	$C_5H_3O_2$	95.01	58.05	$C_{20}H_{23}O_3$	311.16	-385.94	C_4O_2	79.96	-111.44
C_8H_2	98.01	-57.01	C_4H_3O	67.02	39.62	C_4O_3	95.98	-104.32	$C_{24}H_{21}O$	325.17	-352.68	C_{10}	120.00	101.74
C_8H_3	99.01	-17.94	C_4H_4O	68.01	-111.81	C_4HO_3	96.98	-37.30						
C_8H_4	100.02	-67.72	C_3HO_2	69.00	16.35	C_7H_2O	102.01	64.96						
C_8H_5	101.03	-61.28	C_4H_6O	70.02	-103.92	$C_3H_3O_4$	103.00	108.64						
C_9H_2	110.00	-72.79	$C_3H_3O_2$	71.01	94.45	$C_3H_4O_4$	104.01	94.80						
C_9H_3	111.02	-32.45	$C_2H_2O_3$	74.00	99.27	$C_3H_5O_4$	105.01	108.99						

Figure 3.17 – Molecular species identified from the negative spectra of black and green tea leaves using ToF-SIMS.

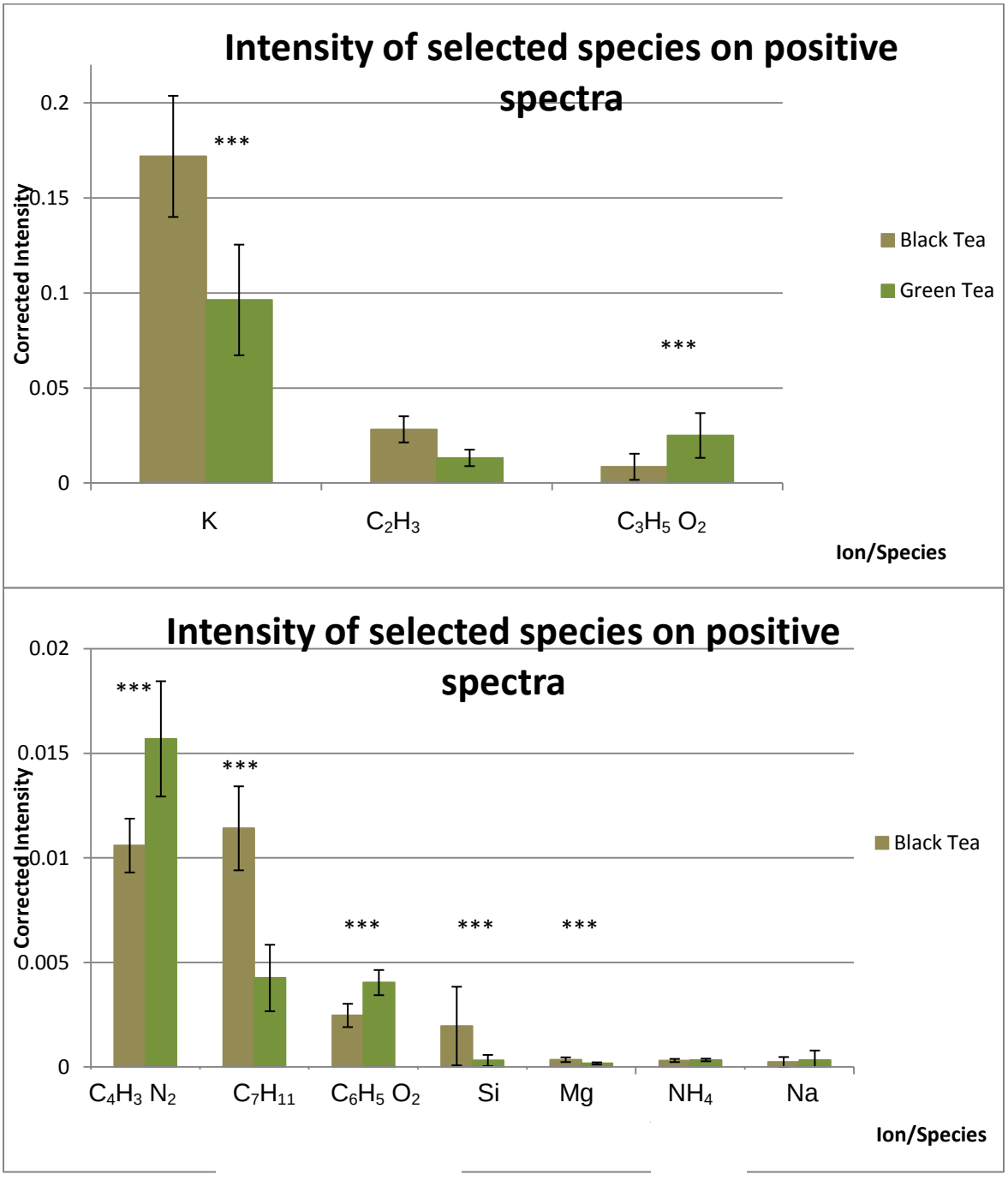

Figure 3.18 –Normalised intensity of a variety of positive species identified on black and green tea leaves using ToF-SIMS. (***) Signifies a 99.9% confidence level of a difference in mean normalized intensity.

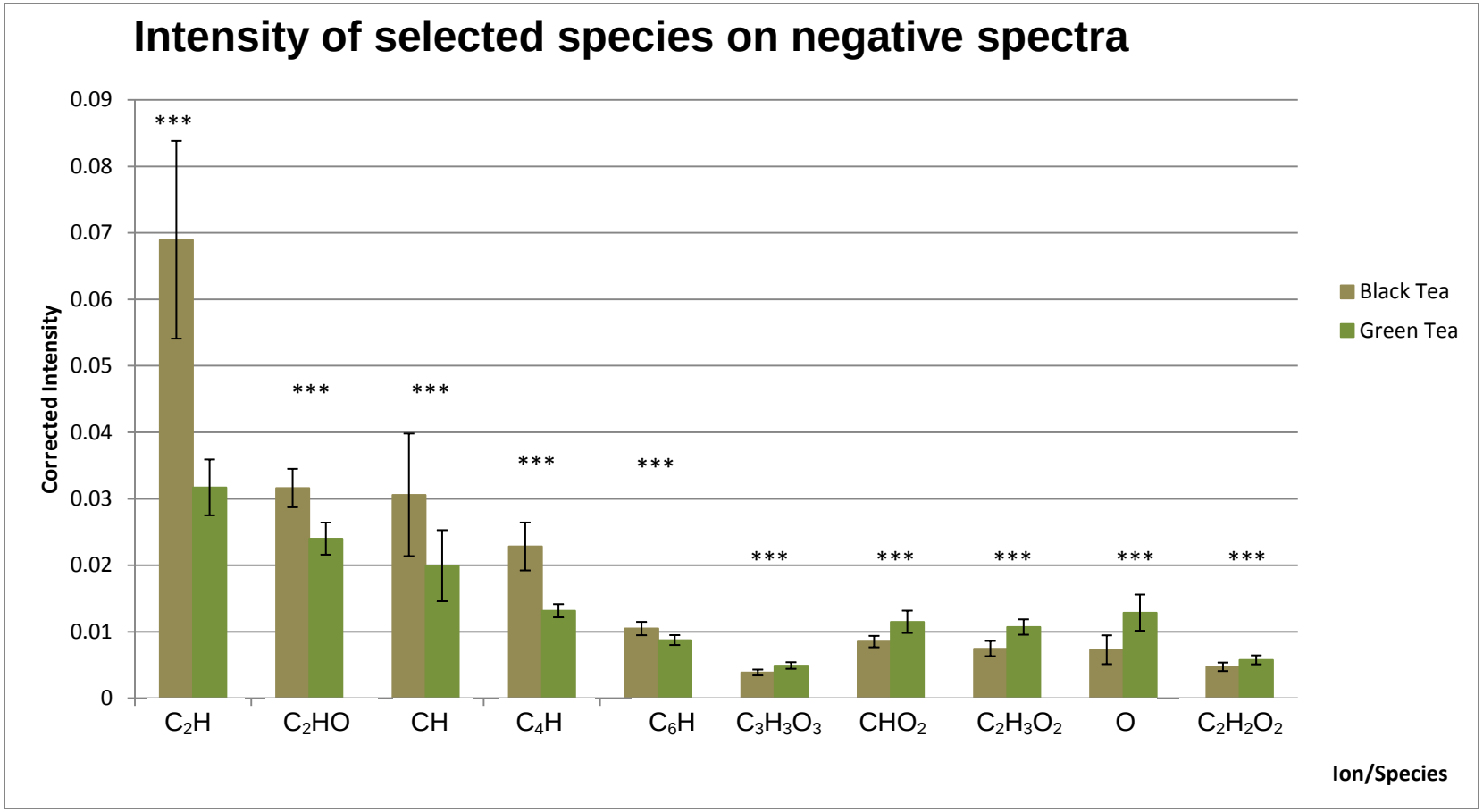

Figure 3.19 – Normalised intensity of a variety of negative species identified on black and green tea leaves using ToF-SIMS. (***) Signifies a 99.9% confidence level of a difference in mean normalized intensity.

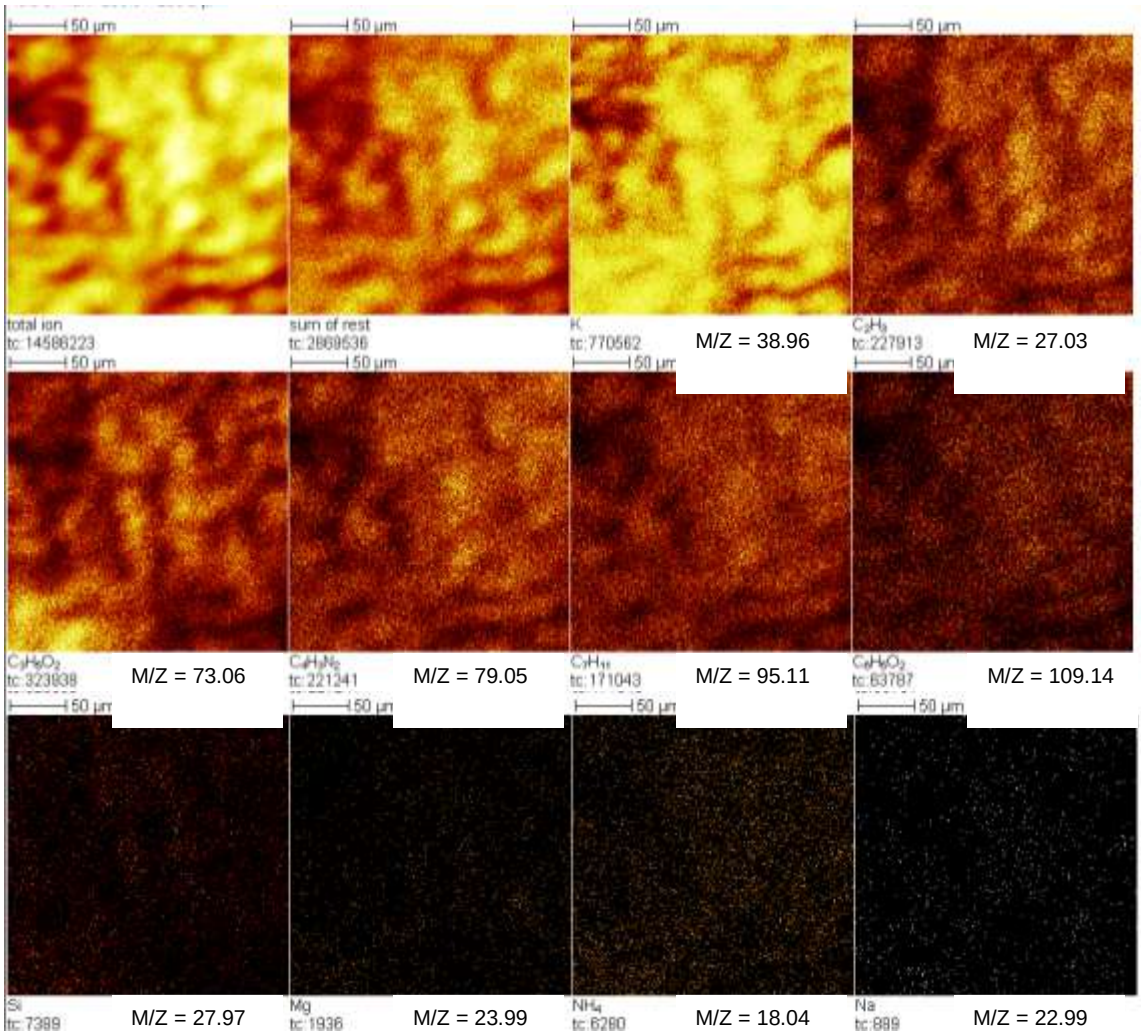

Figure 3.20 – Example Ion Images of a selection of positive species identified on black tea leaves using ToF-SIMS.

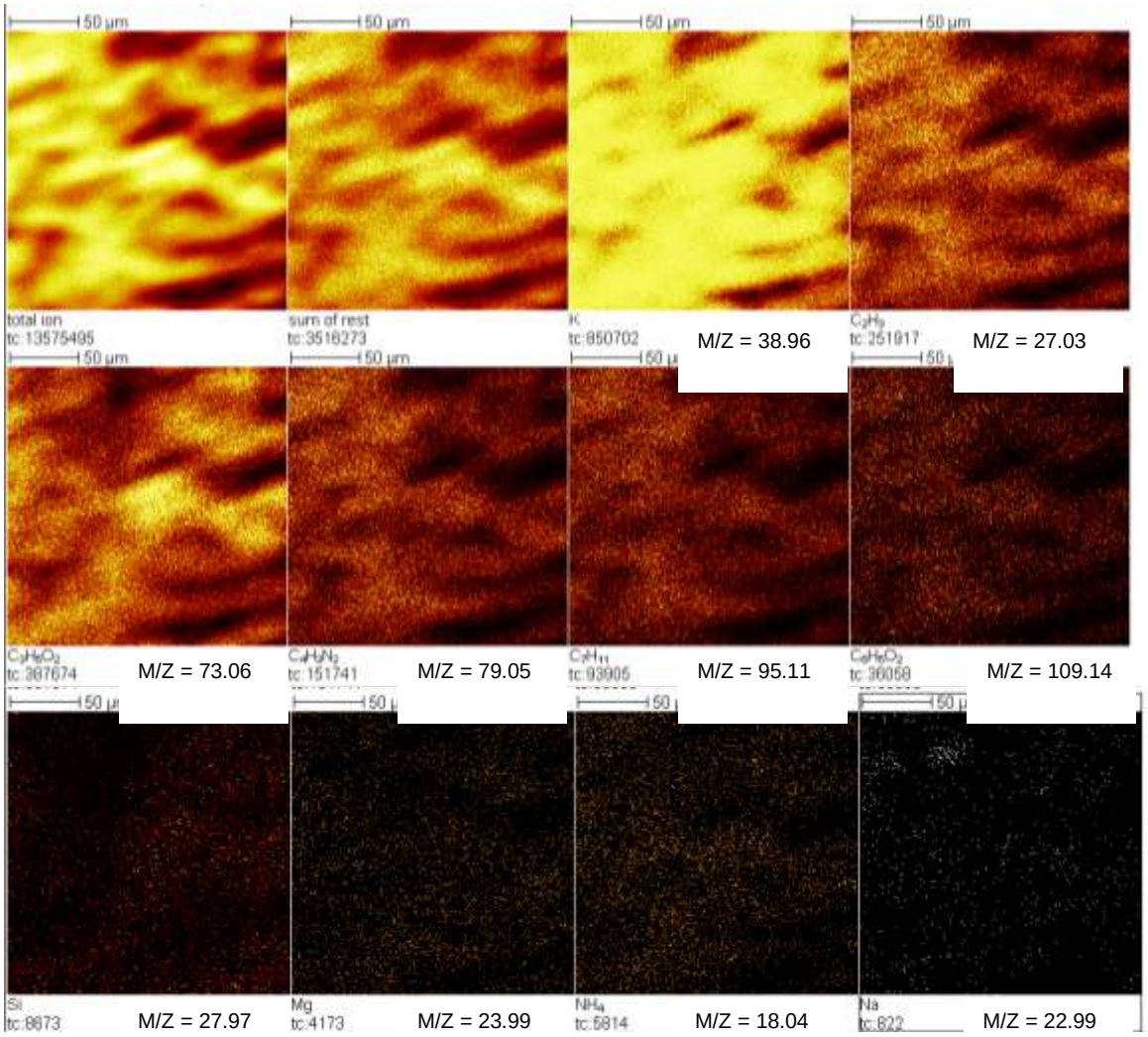

Figure 3.21 – Example Ion Images of a selection of positive species identified on green tea leaves using ToF-SIMS.

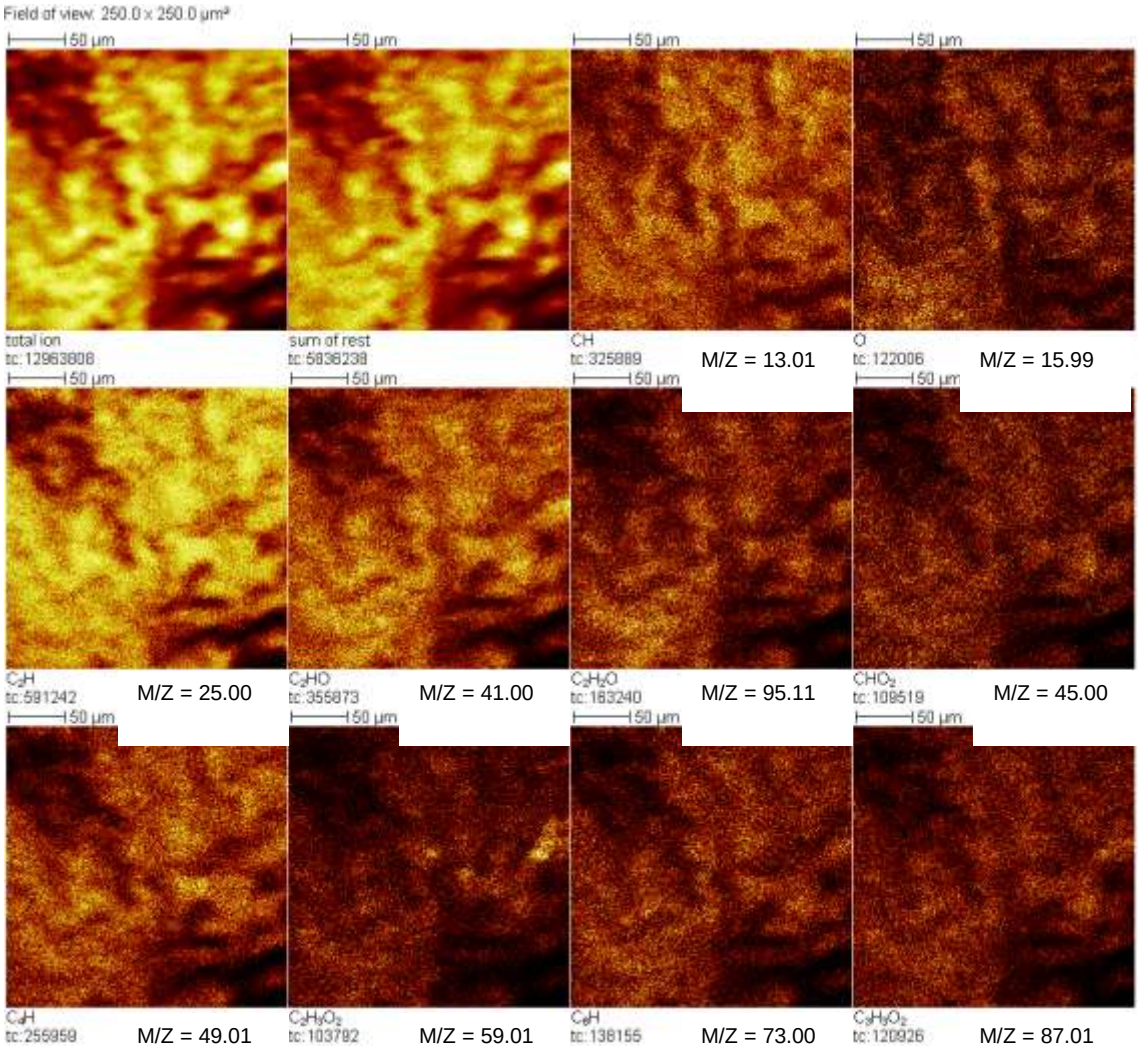

Figure 3.22 – Example Ion Images of a selection of negative species identified on black tea leaves using ToF-SIMS.

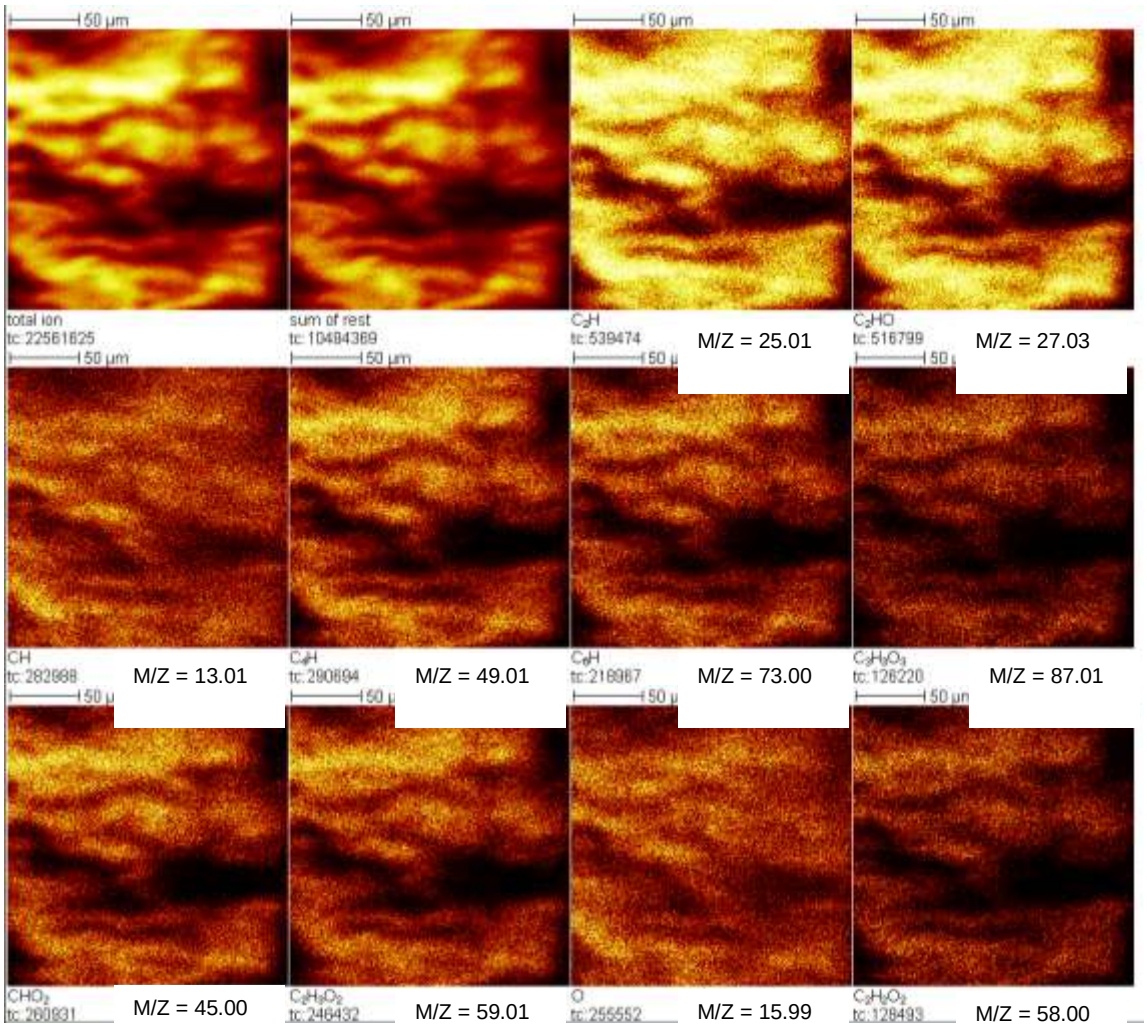

Figure 3.23 – Example Ion Images of a selection of negative species identified on green tea leaves using ToF-SIMS.

3.3.5 Examination of tea leaves with ToF-SIMS

As the electron micrographs of the tea leaves can only display topographical information and the AFM images showed homogeneity of the surface of the black tea leaves and a difference in the surface properties of the green tea leaves, a method of examining the surface chemistry of the leaves was needed. ToF-SIMS can measure the secondary ions released when a primary ion impacts on the surface of a sample.

Examples of positive and negative ToF-SIMS spectra for black tea leaves are shown in figures 3.11 and 3.12, with the corresponding spectra for green tea leaves shown in figures 3.13 and 3.14. The spectra show molecular species which have a high intensity in the scans. These range in size from the most basic hydrocarbon, CH to species of a larger m/z such as $C_{23}H_{11}$ was observed.

In total 138 hydrocarbons were identified in the positive spectra, these are listed in figure 3.15. The surface of the leaf is covered in the cuticle. This contains lipids and hydrocarbon groups with the cuticular waxes and cutin membrane. The presence on these hydrocarbons is indicative of the presence of lipid molecules and hydrocarbon molecules (Vickerman et al. 2002).

Oxygenated hydrocarbons and other species of interest were identified and listed in figure 3.16. With the identification of peaks present in the

ToF-SIMS spectra for epicuticular waxes in samples of compounds has lead to the identification of the possible presence of some of these epicuticular waxes. The fragment $C_{12}H_{23}O$, m/z 183.15, is an indication of the presence of Dodecyl aldehyde on the surface of the leaf. Also present were $C_2H_5O_2$, m/z 61.03, and C_2H_3O, m/z 43.02, which were identified as protonated acetic acid and a peak for behenyl acetate (Perkins et al., 2005).

Also in figure 3.16 are the other species identified in the positive spectra. The presence of hydrogen and carbon is most likely due to the various constituents of the cuticle. Nitrogen containing groups are also present. The nitrates are needed in the plant for the protein synthesis and the production of amino acids. With the nitrogen being present on the surface then protein synthesis and amino acid production is either occurring on or near the surface of the leaf or the presence on the surface is due to some part of the processing that the leaves undergo. The species NH_4^+ could indicate the presence of amino acids on the surface of the leaf. This fragment has been seen in an examination of all amino acids with ToF-SIMS. Individual fragments were also identified for each amino acid and C_2H_6N was identified as a unique fragment for the amino acid alanine (Sanni et al. 2002). Other nitrogen containing species could be evidence of amino acids on the surface of the tea leaves.

Potassium and sodium are also needed for growth in plants. The presence of both potassium and sodium containing species are found in the positive spectra. Potassium is needed in a plant for growth, starch storage and protein synthesis in a plant. It is also necessary for enzyme activation including the activation of enzymes that are involved in nitrogen metabolism. Sodium is used for absorbing water, maintaining rigidity of the plant and maintaining osmotic potential within the plant cells. The presence of both potassium and sodium containing species could either be due to the processing the leaves undergo or it is naturally occurring on the surface.

Magnesium is found in the palisade mesophyll layer of the plants where the chloroplasts are located. The presence of magnesium on the surface is probably due to the disruption to the cell structure of the processed leaf.

Finally silicon is also seen in the positive spectra. Some contamination is to be expected with the leaf fragments so the presence of silicon is not unexpected. Given the processing, packing, transport and storage of the leaves, then some small level of contamination is to be expected.

Information from the negative spectra was also obtained. Figure 3.17 is a list of all species identified in the negative spectra for tea leaves. The first two columns show the hydrocarbon groups identified. The hydrocarbons range from CH to C_9H_5 and again the presence of these hydrocarbons is due to the waxy layer of the cuticle of the leaf fragments A total of 23

hydrocarbons were present. The oxygenated hydrocarbons are also shown, ranging from CHO to $C_{24}H_{21}O$, these as before, are present due to the cuticle. In total 66 oxygenated hydrocarbons were identified on the negative spectra. As with the positive spectra these can be assigned to the lipid waxes on the surface of the cuticle.

Finally in the negative spectra groups such as carbon, oxygen and hydrogen were also seen, as well as examples of mixtures of these which didn't fall into the hydrocarbon or oxygenated hydrocarbon groups. Also a nitrogen containing group was identified, as in the positive spectra.

Comparison between the mean normalised intensity of some of the example peaks identified was performed. A difference in intensity could be due to the effects of processing on the leaf. Error bars of the standard deviation were included. A two tailed T-test was performed to examine if there was a significant difference between the intensity on the black tea leaf samples compared with the green tea leaf samples. A two tailed test allows the data to be examined, in this case, for differences in mean intensity of fragments between green and black tea and if these differences are statistically significant. Examples of the positive spectra are shown in figure 3.18.

Though the intensity was high for the fragments of C_2H_3, NH_4 and Na, there was no significant difference between the mean normalized

intensities of these fragments. All other fragments shown in figure 3.18 show a 99.9% confidence level of the difference.

The mean normalised intensity of potassium is much higher in black tea leaf fragments than in green tea leaf fragments. As the black tea leaves are cut and crushed before drying then the potassium could be released onto the surface as a byproduct of the crushing and cutting. With the mean normalised intensity still being high in the green tea leaf fragments there is also some potassium that will cover the surface during the processing.

The larger hydrocarbon group of C_7H_{11} shows that the mean normalised intensity is higher for black tea leaf fragments than green.

Examples of the oxygenated hydrocarbons show a reverse where the normalised intensity is slightly higher for green tea rather than black, as shown with $C_3H_5O_2$ and $C_6H_5O_2$.

The release of oxidative enzymes in the processing of black tea could change the composition of some of the cuticular waxes. If the oxidative enzymes were responsible than an increase in the presence of oxygen containing species would be expected to be seen on the surface of the black tea leaves than the green if this was happening though. As the AFM showed that the size of the wax plates had not changed during the processing for both green and black leaves then the difference in heat that is used in the processing appears to have a limited effect on the surface structure of the leaves. The difference in the levels of oxygenated

hydrocarbons could come from part of the processing of the leaves in conjunction with the oxidation of the leaves.

Silicon has a higher mean normalised intensity in the black tea leaves than the green tea leaves. This could be an effect of the use of a CTC (Cut Tear Crush) machine on the black tea leading to greater contamination.

The observation of nitrogen containing species is interesting. If the nitrogen is bound with a hydrocarbon, as with $C_4H_3N_2$, then the mean normalised intensity is much higher in green tea than in black. If the nitrogen is just bound to hydrogen as in NH_4 then there is a slight increase for green tea but no significant difference. As this has previously been seen as a group to identify the presence of amino acids then the fact there is no significant difference in the presence of this species indicates that there may be the same amount of amino acids on the surface of both leaves. When the peak for C_2H_6N was compared between green and black tea leaves there was no significant difference in the intensity for both leaves (Sanni et al. 2002).

Magnesium, as previously mentioned is a component of chlorophyll and is found in the palisade mesophyll layer of the leaf. Though only a low intensity was found on the surface of both green and black leaves the intensity was higher for black leaves. As both are rolled the more

mechanical treatment of the black leaf would account for the increase of pushing chlorophyll to the surface.

Examples of the negative spectra were examined is shown in figure 3.19. The hydrocarbons again showed a larger mean normalised intensity for black tea leaf fragments when compared to green tea leaf fragments. Generally the oxygenated hydrocarbons behaved in the same way as in the positive spectra. The mean normalised intensity for $C_3H_3O_3$, CHO_2, $C_2H_3O_2$ and $C_2H_2O_2$ all were higher for green tea leaf fragments, but only by a small amount. The intensity for Oxygen was nearly double for green tea leaf fragments than for black tea. There was one exception which was included. C_2HO had a higher intensity for black tea than for green tea. As C_2HO was identified as being present in the spectra for behenyl acetate (Perkins et al. 2005) this could be an indication that there was a change in the presence of this epicuticular wax after processing. The other species identified from behenyl acetate, $C_2H_3O_2$ showed a slight but significant (99.9%) increase in intensity in the green tea leaves when compared with black tea leaves. As the species is quite small there may be another explanation for the difference in this result. The fragment of C_2HO, as a small molecule, could have come from a different source on the surface of the leaf (and this could explain why there was a change in intensity).

Finally the distribution of the fragments on the surface was examined. The ToF-SIMS has a functionality which allows the mapping of the surface

from with the spectra. A total ion image is constructed showing where all fragments came from on the surface. Any identified peaks can also be mapped and the raster is rebuilt to show the position on the surface of the leaf that the peak came from. Figure 3.20 shows the ion images of the species discussed previously from figure 3.18 on black tea leaf fragments and figure 3.21 shows the same species on green tea leaf fragments. It can be seen that the hydrocarbon groups and oxygenated hydrocarbon groups on both of these figures match the topography of the total ion image indicating that the distribution on the surface is homogeneous. The difference in the phase images of the AFM between the black and green tea leaf fragments do not appear to have any chemical difference in relation to the cuticle. Although it should be noted the much reduced spatial resolution of ToF-SIMS compared to AFM, so ToF-SIMS may not be able to resolve small areas of heterogeneity. The presence of potassium in both teas of a high intensity and this too is comparable to the total ion image and topography indicating homogeneous surface distribution.

The other chemical groups identified have low intensity but it can be seen that there is no special region on the surface that the distribution can be attributed to. The distribution of Si is all over the surface, even though it is of a low intensity.

The species identified in figure 3.19 are examined using the ion image functionality in figure 3.22 for black tea leaf fragments and 3.23 for green

tea leaf fragments. Again, as with the positive ion images, it can be seen that the distribution of the hydrocarbons and oxygenated hydrocarbon are over the whole surface of the scanned area as opposed to certain areas indicating that the chemical composition of the cuticle is constant at the scale of observation of ToF-SIMS.

3.4 Conclusions

AFM shows that the surface of the black tea leaf fragments appears to be homogeneous in terms of composition. The scans were able to show differences in surface structure, such as rougher areas, areas with debris and areas with a layered like structure. One image showed the presence of what could be cuticular wax crystals. Green tea fragments appear to from AFM imaging have a heterogeneous structure at least in some areas with two different types of areas. Comparison of the layered structure shows that the size of these layers is comparable and that the different methods of processing of these leaves do not change the morphology of the cuticular waxes in this instance.

SEM of black tea leaf fragments showed that the surface was covered in debris, more so than the green tea leaf fragments and had a varied topography. The green tea leaves showed a smoother topography than

black and a reduction in the surface debris. This is consistent with the observation from AFM but is made from reviewing a large number of leaf fragments.

Chemically the two types of tea leaves show some minor differences. The ToF-SIMS data shows the same groups were identified but with subtle differences in terms of normalised intensity form certain mass fragments. The presence of hydrocarbons on the surface of the tea leaves is related to the epicuticular waxes, this was also true of the oxygenated hydrocarbons. Known components of the epicuticular waxes were identified from the ToF-SIMS spectra. The possible presence of amino acids was also identified with the identification of NH_4 and C_2H_6N, a previously identified species associated with the spectra for alanine.

Potassium and magnesium had a higher intensity in the black tea leaves than in the green tea leaves. As the treatment of the leaves is rougher in the mechanized stage of cutting, crushing and tearing for the black tea leaves these could be signs of damage to the leaf.

Given the temperature difference in processing, the slight increase in sodium intensity may be due to cell damage due to heat where the cells rupture and release their contents, which end up on the surface.

The spatial distribution of all of these groups identified was compared and all groups showed a uniform distribution at the micron scale over the surface of the leaves indicating no real difference in chemical composition.

References

Brunelle, A., Toubel, D., Laprevote, O. Biological tissue imaging with time-of-flight secondary ion mass spectrometry and cluster ion sources. J. Mass Spectrom. 2005; 40:985-999.

Butt, H. J., Wolff, E. K., Gould, S. A. C., Dixon Northern, B., Peterson, C. M., Hansma, P. K. (1990). "Imaging cells with the atomic force microscope." Journal of Structural Biology 105(1-3): 54-61.

Chen, H. X., Wang, Z. S., Qu, Z. S., Fu, L. L., Dong, P., Zhang, X. (2009). "Physicochemical characterization and antioxidant activity of a polysaccharide isolated from oolong tea." European Food Research and Technology 229(4): 629-635.

Cliff, B., Weibel, D. E, Lockyer, N. P., Jungnickel, H., Stephens, G., Vickerman, J. C. (2003). "Detection of chlorinated pesticides on the surface of fungus using ToF-SIMS." Applied Surface Science 203: 710-713.

Kirby, A. R., Gunning, A. P., Waldron, K. W., Morris, V. J., Ng, A. (1996). "Visualization of plant cell walls by atomic force microscopy." Biophysical Journal 70(3): 1138-1143.

Koch, K., Neinhuis, C., Ensikat, H. J., Barthlott, W. (2004). "Self assembly of epicuticular waxes on living plant surfaces imaged by atomic force microscopy (AFM)." Journal of Experimental Botany 55(397): 711-718.

Metzner, R., Schneider, H. U., Breuer, U., Schroeder, W. H. (2008). "Imaging Nutrient Distributions in Plant Tissue Using Time-of-Flight Secondary Ion Mass Spectrometry and Scanning Electron Microscopy." Plant physiology (Bethesda) 147(4): 1774-1787.

Mitchell, R., Carr, C. M., Parfitt, M., Vickerman, J. C., Jones, C. (2005).

"Surface chemical analysis of raw cotton fibres and associated materials." Cellulose 12(6): 629-639.

Perkins, M. C., Roberts, C. J., Briggs, D., Davies, M. C., Friedmann, A., Hart, C. A., Bell, G. A. (2005). "Surface morphology and chemistry of Prunus laurocerasus L. leaves: a study using X-ray photoelectron spectroscopy, time-of-flight secondary-ion mass spectrometry, atomic-force microscopy and scanning-electron microscopy." Planta 221(1): 123-134.

Sanni, O. D., Wagner, M. S., Briggs, D., Castner, D. G., Vickerman, J. C. (2002). "Classification of adsorbed protein static ToF-SIMS spectra by principal component analysis and neural networks." Surface and Interface Analysis 33(9): 715-728.

Vickerman, J. C., Briggs, D., Henderson, A. (2002). The static SIMS library, Surface Spectra Ltd.

Yi, W. S., Qin, L. H., Cao, J. B. (2011). "Investigation of morphological change of green tea polysaccharides by SEM and AFM." Scanning: n/a-n/a.

Zhong, Q., Inniss, D., Kjoller, K., Elings, V. B. (1993). "Fractured polymer/silica fiber surface studied by tapping mode atomic force microscopy." Surface Science Letters 290(1-2): L688-L692.

Chapter 4.

The effect of hot water infusion on the morphology and chemical composition of the surface of tea leaves.

4.1 Introduction

Previously studies have been conducted in the contents of the liquid infusion of the leaves of the *Camellia sinensis* plant. These have shown the presence of vitamins, mineral, alkaloids and polyphenols (Kenney et al. 1983; Owour et al. 1986; Kawakami et al. 1995; Ferrara et al. 2001; Peterson et al. 2005; Mizukami et al. 2007). Enzymes, such as polyphenol oxidase, cause oxidation, polymerisation and other modifications to the components within the leaf during processing (Hara 1999). The following experiments examine the effect on the leaf surface morphology and composition due to the infusion process.

Cutin on the tea leaf has been found to be composed of hexadecanoic ($C_{16}H_{32}O_2$), octadecenoic ($C_{18}H_{34}O_2$) and octadecanoic ($C_{18}H_{36}O_2$) acids, and derivatives of these acids (Tsubaki et al. 2008). The effects of the infusing process on the surface morphology and composition of the leaf, which we hypothesise will be related to the release of flavour and aroma, have not been reported. Given that the leaf, even when dried is covered in a protective cutin layer, release of the flavor constituents from the tea

would be dependent on the interaction of the boiling water with the internal structure of the leaf during the infusion process.

4.2 Experimental

For each section of the time course of infusion, five separate tea leaf fragments were selected using the leaf selection model discussed in the experimental methods section (Chapter 2. Black tea leaves (medium grade – 0.85 – 1.4 mm, ex Unilever, Kenya), were then infused for the following times.

A- 15 seconds

B- 30 seconds

C- 60 seconds

D- 150 seconds

E- 300 seconds

A group of leaves that had not been infused were also examined as a control.

Glassware was cleaned using piranha etching (see Chapter 2) to remove organic contamination in preparation for the addition of boiling water and the infusion process. The leaf fragments were placed into cleaned beakers and deionised water was heated on a hot plate to 100 ^{o}C. Once the water had reached boiling point it was added to the beakers containing the leaf fragments and infused for the required time. The leaves were then removed using filter paper.

The recovered leaves were then placed on piranha etched glass slides and dried overnight in a vacuum oven (17 hours). The leaves were then re-examined under a microscope to correctly orientate them so that the adaxial side was facing upwards for analysis.

The leaves were then analysed using a ToF-SIMS IV Instrument (ION-TOF GmbH, Münster, Germany). The primary ion beam was produced from a Bi_3^+ liquid metal ion source using an acceleration voltage of 25 kV and an AC target current of 1.26 pA with a bunched pulse width of less than 0.7 ns. Both positive and negative secondary ion species were analysed using a raster of 256 × 256 pixels was used. Five random areas were examined for each leaf fragment that was used. The total primary ion beam dose for every analysed area was kept below 10^{12} ions cm^{-2} throughout the analysis to ensure “static” conditions.

The leaves were also imaged using SEM, leaf samples were coated with a thin gold layer using a Balzers SCD 030 Gold Splutter coater (Balzers Union Ltd., Leichtenstein) in Argon at a vacuum of 0.15 mbar. The samples were examined using a JEOL 6060LV SEM (Jeol (UK) Ltd, Herts., UK). This was to compare visually any differences that may have occurred during the infusion process.

4.3 Analysis

Data analysis was carried out using software supplied by the instrument manufacturer, IonSpec (Version 4). The data was calibrated to known

peaks initially and then peaks were identified automatically using the software. Each peak was then examined individually and assignments checked for what was known to be on the surface of tea leaves. The intensity of the assigned peaks were normalised against the total ion count for each spectrum to allow for any topographical differences between the samples.

The data from these spectra were then input into Matlab V7.0.4 and analysed using the PLS toolbox V5.2.1. (The Mathworks UK, Cambridge, UK).

4.4 Results

4.4.1 SEM of infused leaves

By comparing the SEM scans of the leaves, changes at the micron scale that could have occurred during the infusion process would be noticeable.

Figures 4.1-4.3 shows SEM images of tea leaves that have not been infused.

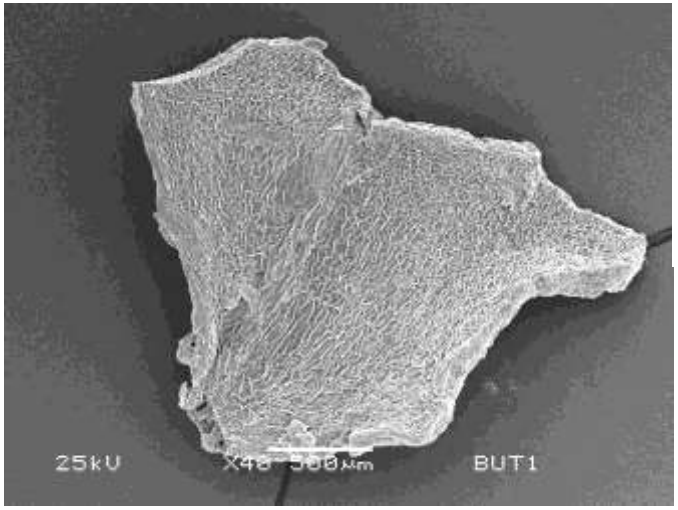

Figure 4.1 – Whole black tea leaf – not infused

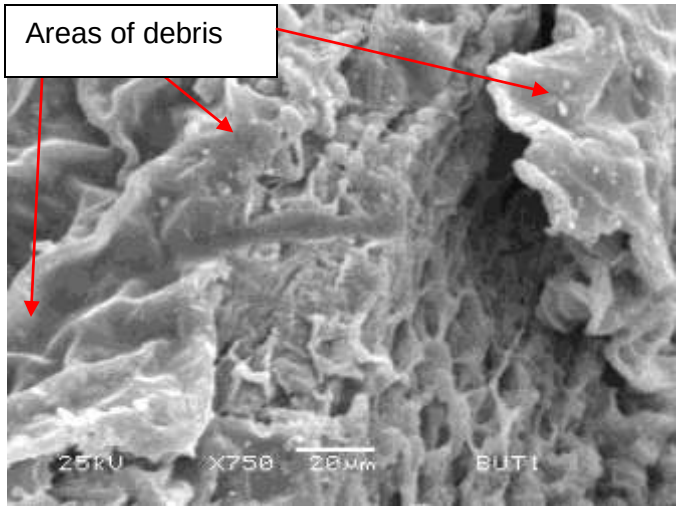

Figure 4.2 – Black tea leaf – not infused. Debris is noticeable on the leaf surface and is believed to be a result of the tea production process.

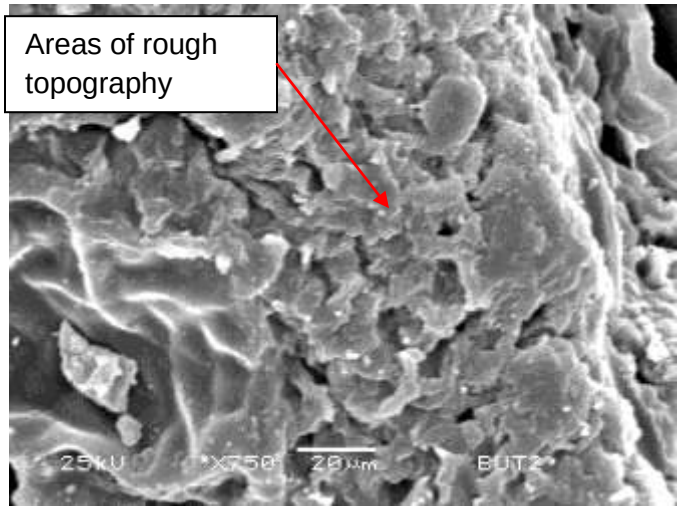

Figure 4.3 – Black tea leaf – not infused. More areas of debris are noticeable on this section. Rough topographical features can also be seen.

Figures 4.4-4.6 show the effects of 15 seconds of infusion time.

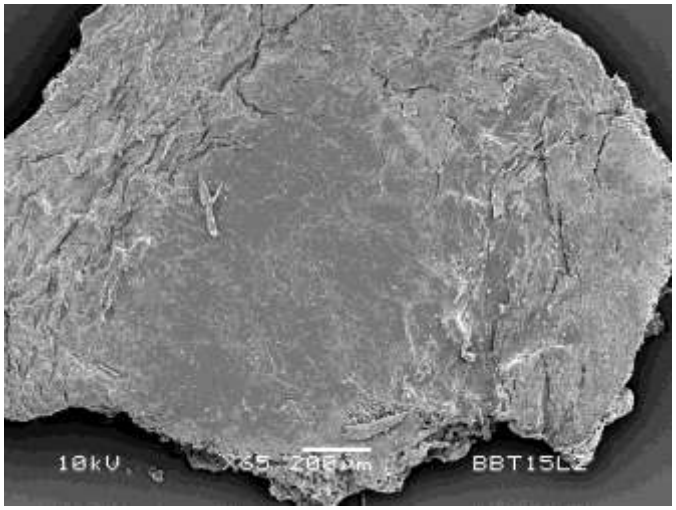

Figure 4.4 – Whole black tea leaf infused for 15 seconds.

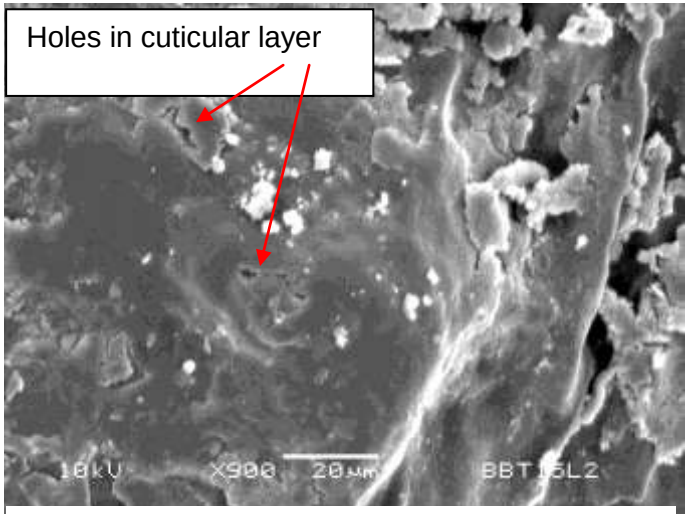

Figure 4.5 – Black tea infused for 15 seconds. Surface is rougher than tea leaves which have not been infused and holes are starting to appear in the cuticular layer. Some debris is still evident.

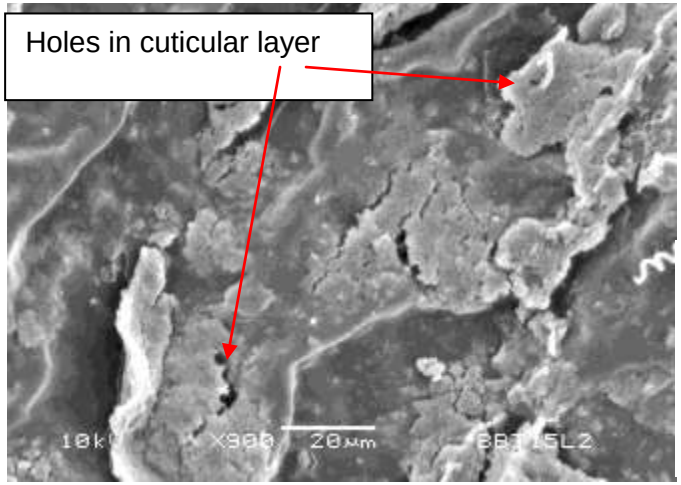

Figure 4.6 – Black tea leaf infused for 15 seconds. This, again, shows roughness of the surface and less cohesive cutin layer. Debris is still evident on the surface of the cutin layer.

Figures 4.7 to 4.9 show electron micrographs of tea leaves infused for 30 seconds.

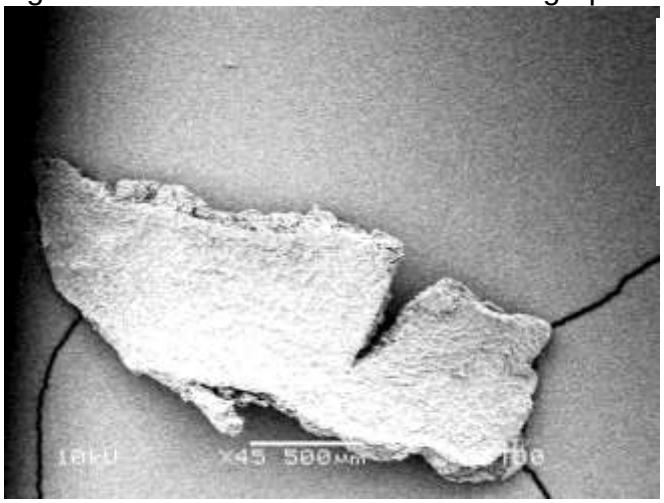

Figure 4.7 – Whole black tea leaf infused for 30 seconds.

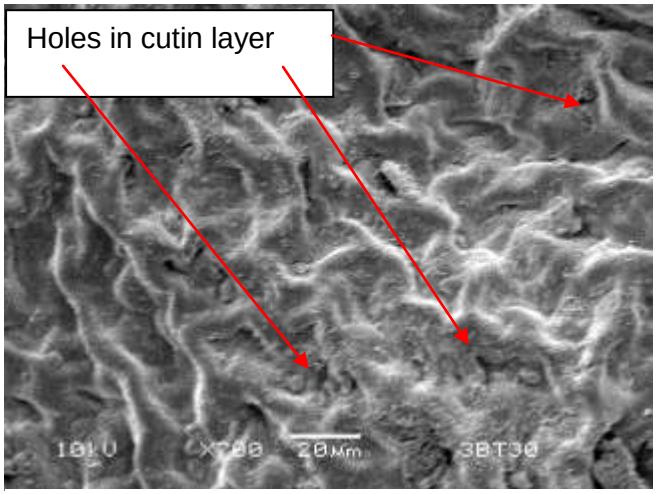

Figure 4.8 – Black tea leaf infused for 30 seconds. More holes in the surface of the cutin layer are visible. Less debris is visible than for 15 s infusion or no infusion.

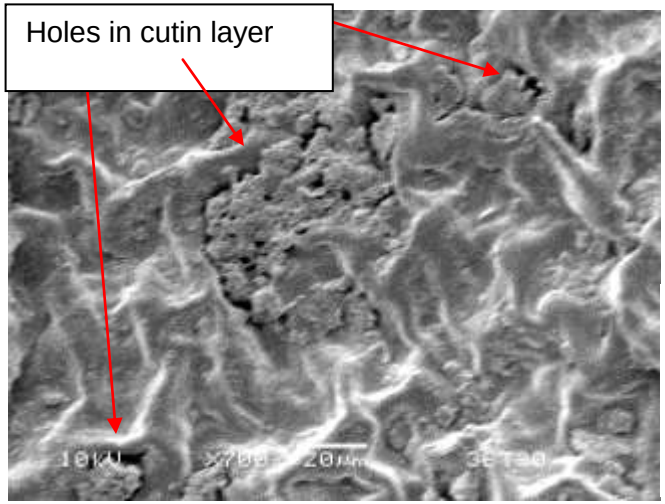

Figure 4.9 – Black tea infused for 30 seconds. The holes appear on surface of the cutin layer. Some debris can still seen on the surface.

Figures 4.10 to 4.12 show electron micrographs of tea leaves infused in boiling water for 60 seconds.

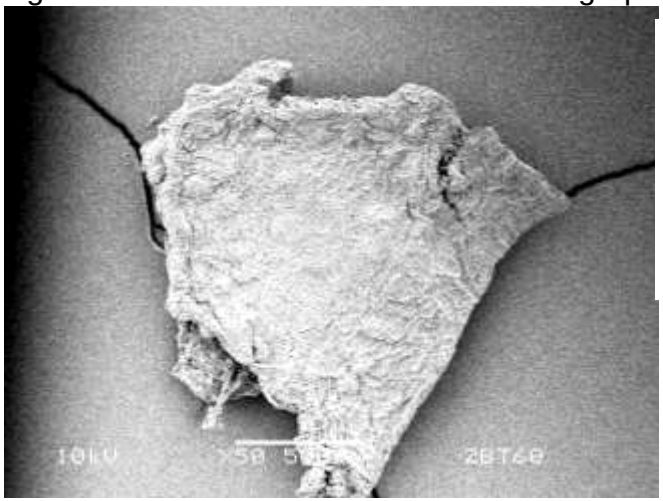

Figure 4.10 – Whole Black tea leaf infused for 60 seconds. No visible difference to previous leaves.

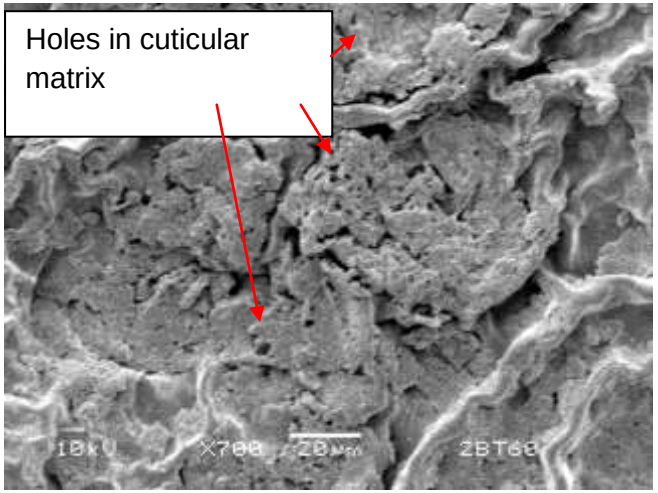

Figure 4.11 – Black tea leaf infused for 60 seconds. More disruption to the cutin layer are evident than for 30 or 15 s of infusion.

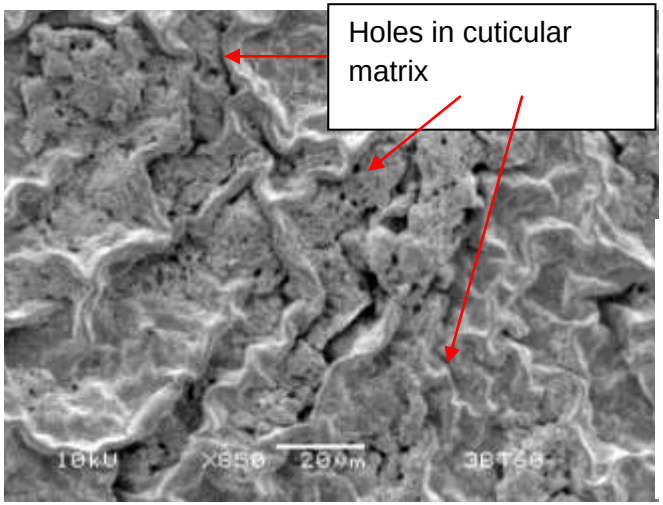

Figure 4.12 – Black tea leaf infused for 60 seconds. Again area of changes on cutin layer more evident than on 15 or 30 s of infusion time.

Figures 4.13 to 4.15 are of tea leaves infused in boiling water for 150 seconds.

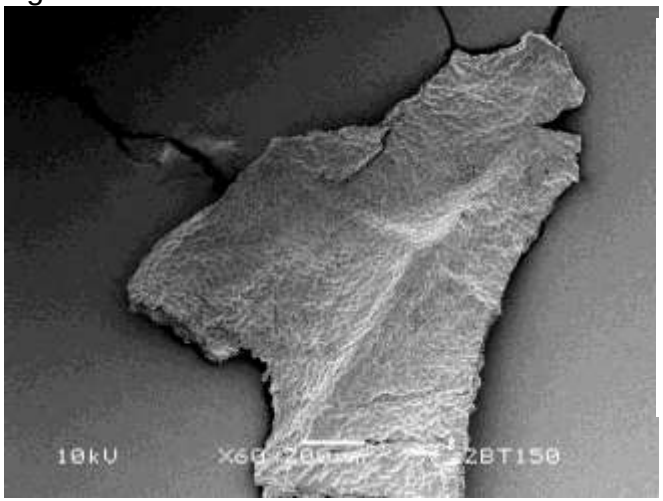

Figure 4.13 – Whole Black tea leaf infused for 150 seconds. Again there is no visible difference to previous leaves at this magnification.

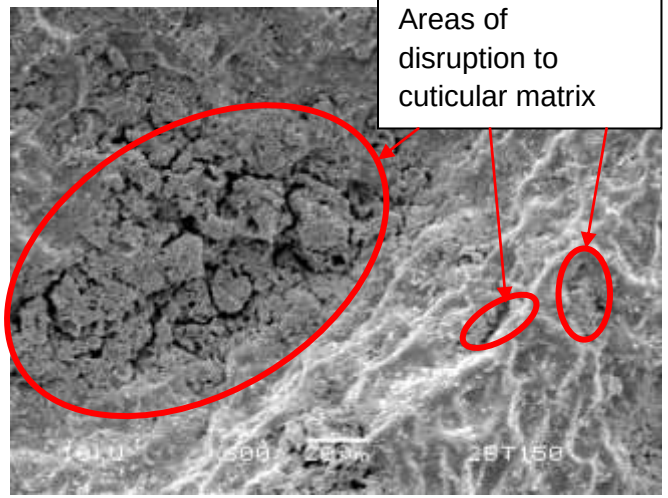

Figure 4.14 – Black tea leaf infused for 150 seconds. A larger area of disruption is visible as the infusion time has increased.

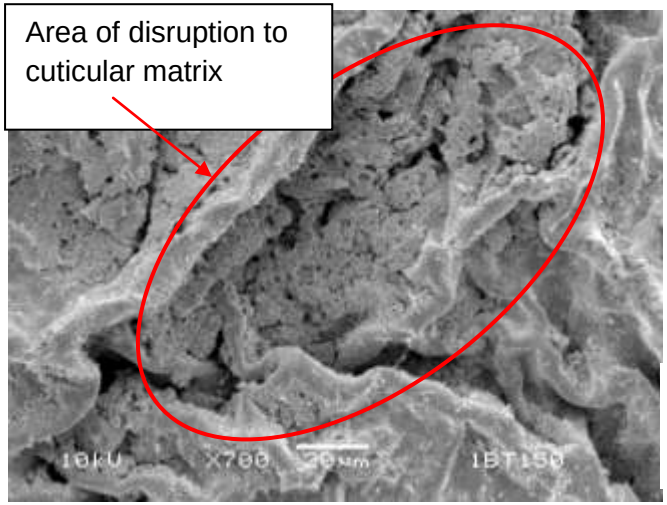

Figure 4.15 – Black tea leaf infused for 150 seconds. Again, a larger area of disruption is visible as the infusion time has increased.

Figures 4.16 to 4.18 are of tea leaves infused for 300 seconds.

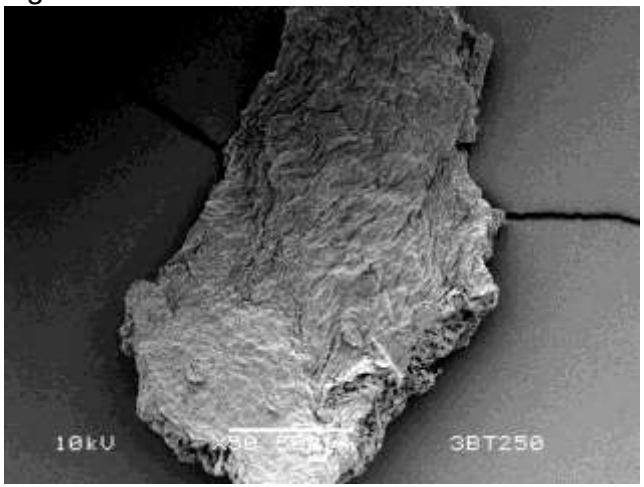

Figure 4.16 – Whole Black tea leaf infused for 300 seconds. The cuticular layer of the leaf is beginning to look damaged and cracks appear in the cuticular matrix.

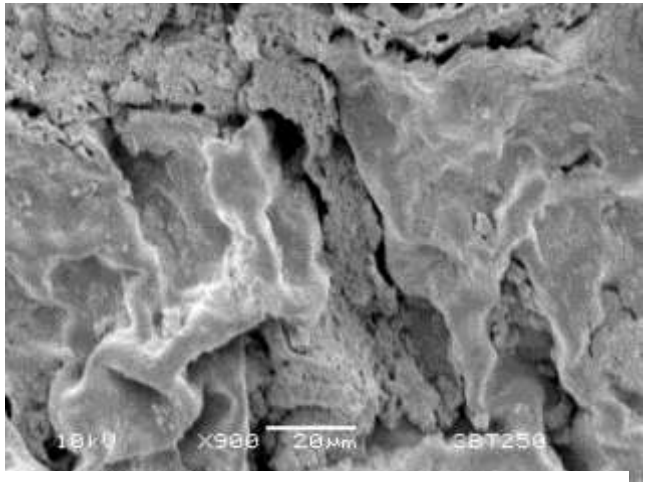

Figure 4.17 – Black tea leaf infused for 300 seconds. The disruption to the surface of the leaf has resulted in a sponge like appearance where the holes are occurring.

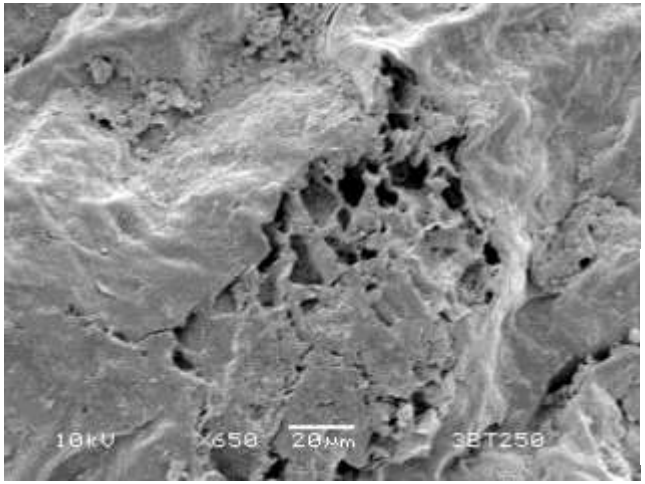

Figure 4.17 – Black tea leaf infused for 300 seconds. The disruption to the surface of the leaf has increased the size of the holes that appear. The shape and size of these holes could be indicative of the cellular structure of the upper Epidermal layer of a leaf.

4.4.2 ToF-SIMS results

Figure 4.18 shows an example of a mass spectra (positive ions), for untreated tea leaves. Both positive and negative spectra were examined for each of the random areas that were scanned. The circled peaks show the differences that can be seen in untreated leaves versus the scans for leaves that have been infused for 30 s.

From this we can see that the peaks at 58 ($C_2H_4NO^+$), 86($C_4H_8NO^+$), 105($C_8H_9^+$), 116($C_9H_8^+$), 133($C_{10}H_{13}^+$) and 224($C_{15}H_{28}O^+$) mass/charge are different from those in the positive spectra produced for 30 s of infusion.

Figure 4.19 shows an example of a spectra for 30 s of infusion time of a tea leaf. When this is compared with the spectra for untreated leaves, Figure 4.18 then the peaks at 42($C_3H_6^+$), 73($C_3H_5O_2^+$), 79($C_4H_3N_2^+$), 81($C_6H_9^+$), 84($C_6H_{12}^+$), 106($C_8H_{10}^+$), 115($C_4H_3O_4^+$), 121($C_9H_{13}^+$), 207($C_{14}H_9NO^+$), 213($C_{16}H_5O^+$), 221($C_{14}H_{21}O_2^+$) and 281($C_{11}H_{21}O_8^+$) mass/charge are of a higher intensity than those in Figure 4.17 of an untreated tea leaf fragment.

Figure 4.20 shows an example of a negative spectra for a tea leaf that has not been treated. The circled peaks show the differences that can be seen in untreated leaves versus the scans for leaves that have been infused for 30 s. Peaks at 25 (C_2H^-), 25(C_2H^-), 41(C_2HO^-), 43($C_2H_3O^-$), 49(C_4H^-) and

75($C_2H_3O_3^-$) mass/charge are different from those in the positive spectra produced for 30 s of infusion.

Figure 4.21 shows an example of a negative spectra for 30 s of infusion time of a tea leaf. When this is compared with the spectra for untreated leaves, Figure 4.20 then the peaks at 17(OH^-), 63($C_5H_3^-$), 71($C_3H_3O_2^-$), 78($C_5H_3O^-$) and 97($C_4HO_3^-$) mass/charge are of a higher intensity than those in Figure 4.22 of an untreated tea leaf fragment.

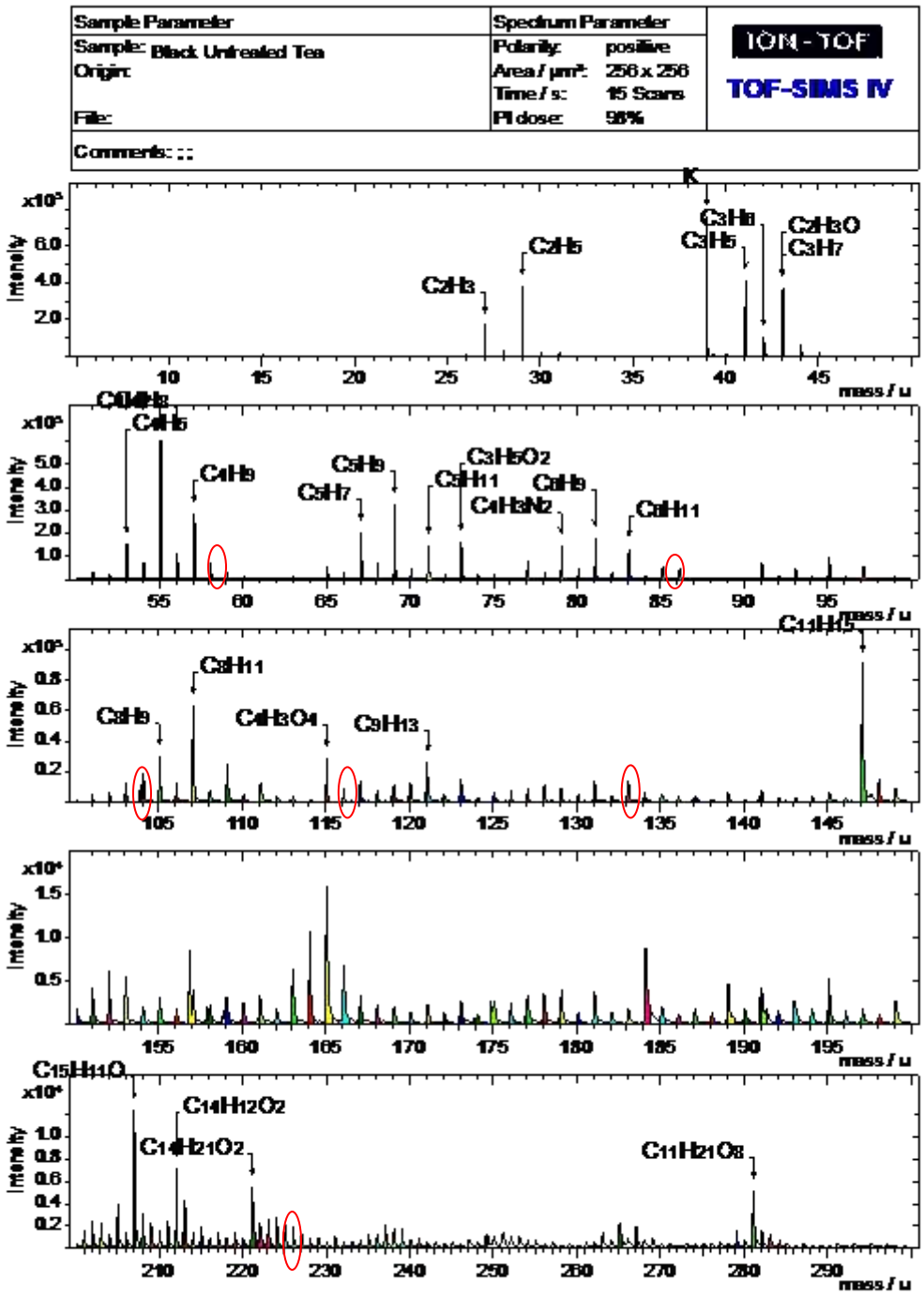

Figure 4.18 – ToF-SIMS spectra of untreated tea leaf. The peaks which have been circled indicate a difference with the spectra obtained for 30 s of infusion time.

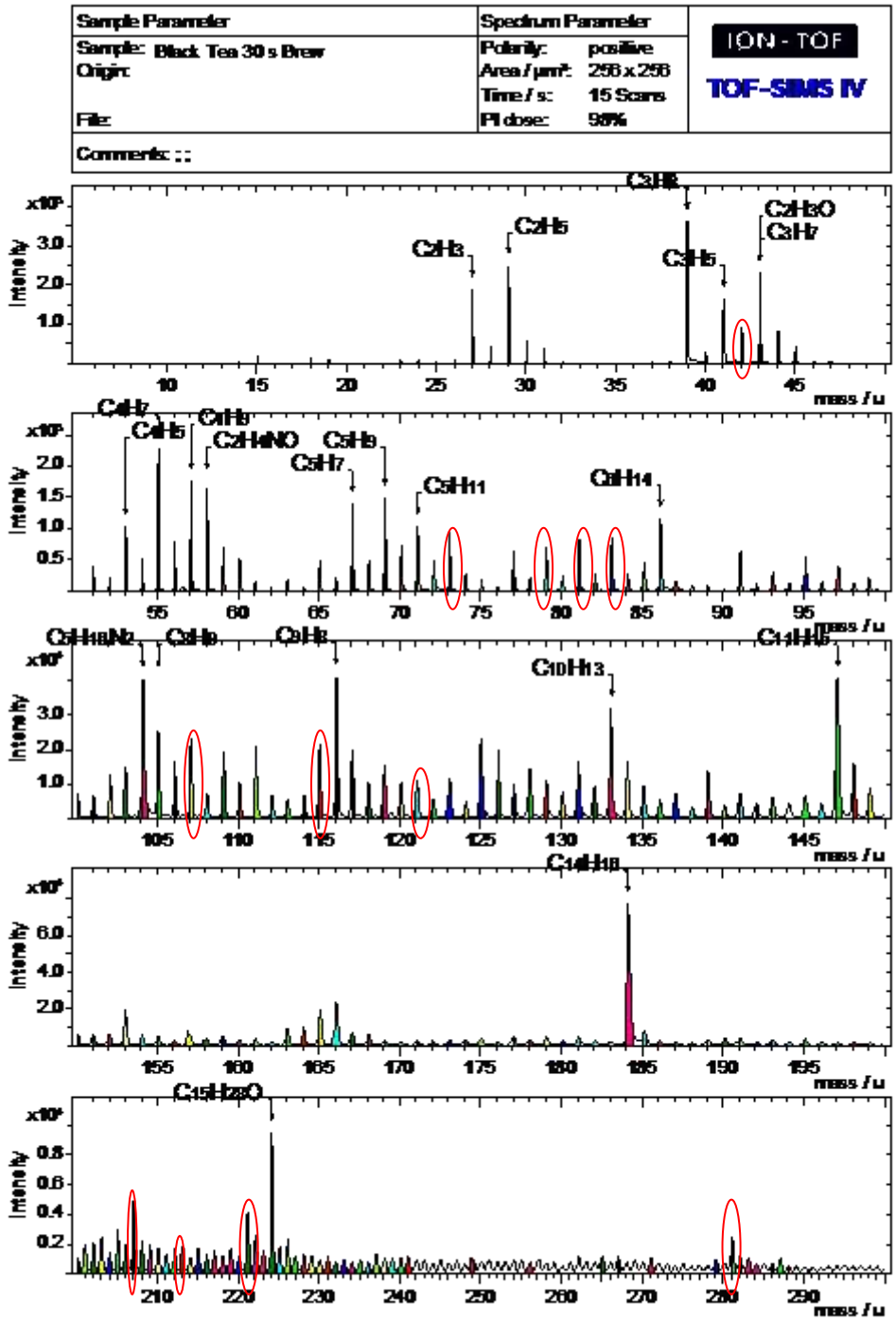

Figure 4.19 – ToF-SIMS Spectra (positive) of a tea leaf infused for 30 s. Peaks circled indicate a difference with the spectra for untreated leaves (Figure 4.18)

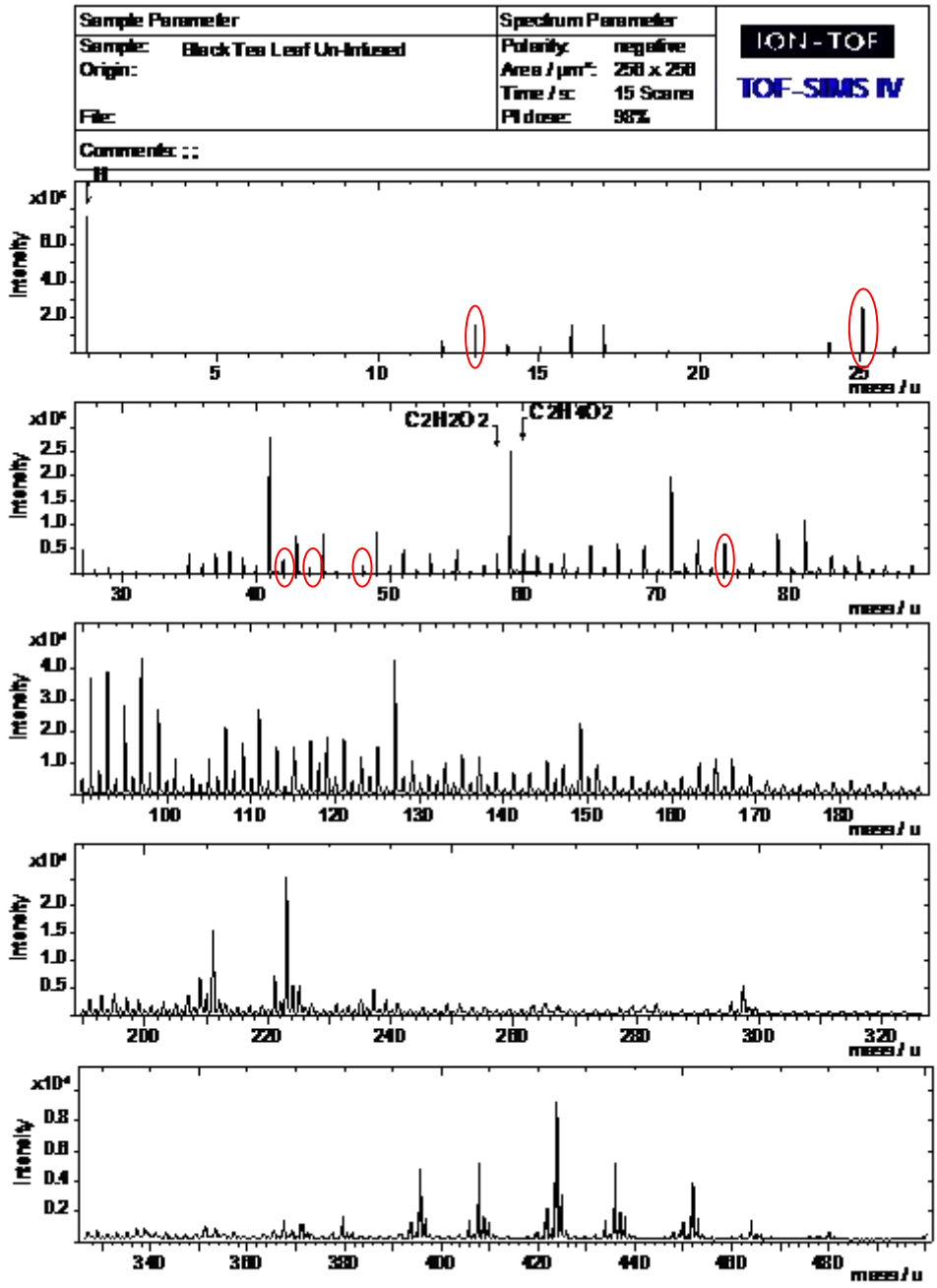

Figure 4.20 – ToF-SIMS Spectra (negative) of untreated tea leaf. The peaks which have been circled indicate a difference with the spectra obtained for 30 s of infusion time (Figure 4.21).

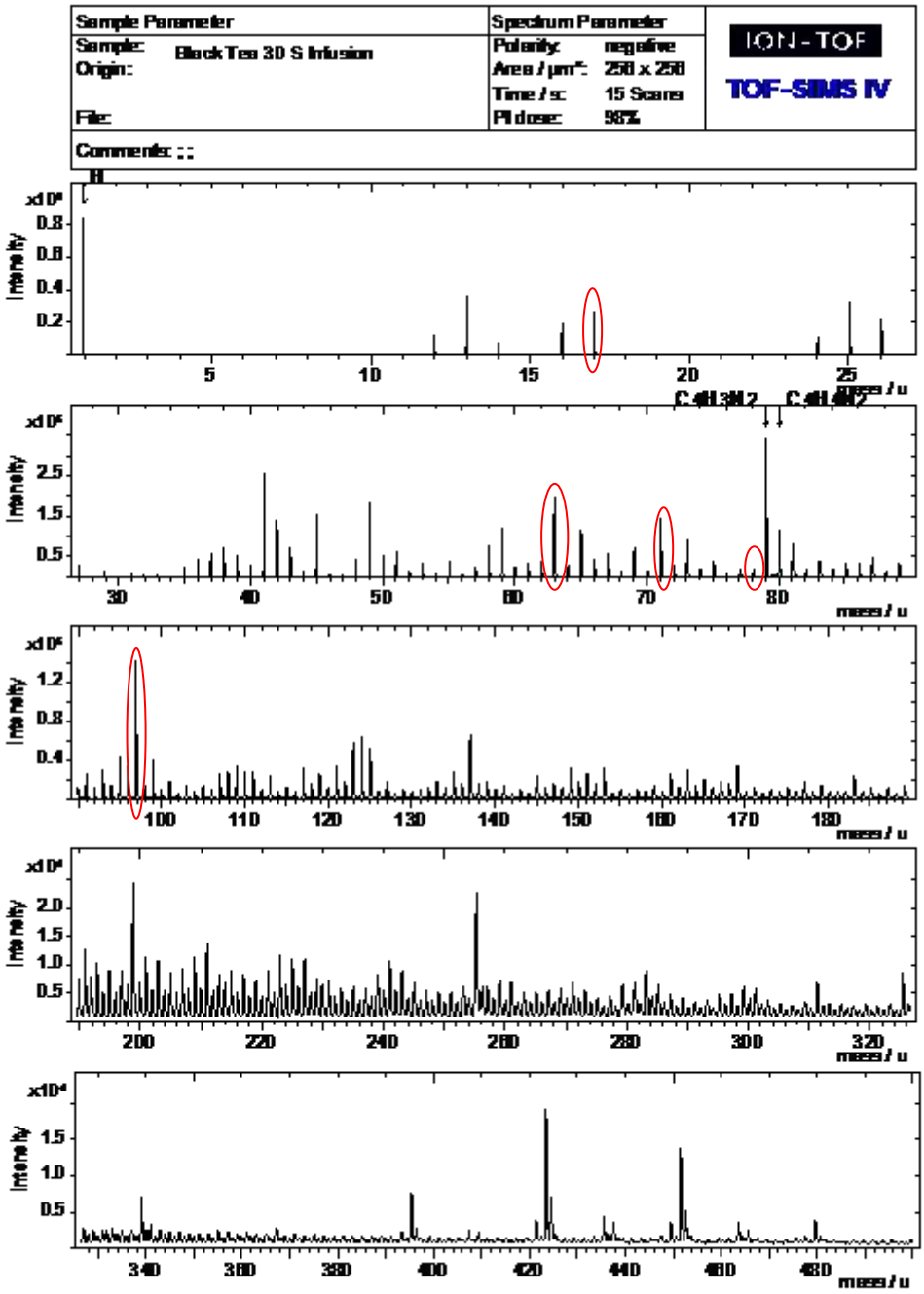

Figure 4.21 – ToF-SIMS Spectra (negative) of a tea leaf infused for 30 s. Peaks circled indicate a difference with the spectra for untreated leaves (Figure 4.20)

4.4.3 Principal component analysis of ToF-SIMS data.

Given the amount of data generated by the use of the ToF-SIMS for this experiment, a robust and accurate method of analysing the data was required. Each data set comprised of a positive and negative scan from five different areas of five different leaves, ie. 25 positive and 25 negative scans per condition. A total of 60 data sets would have been compared with each other.

Principal component analysis (PCA) allows for the pre-processing of data so the results that are given can be analysed more accurately (As previously discussed in the introduction. Figure 4.22 shows an example of a loadings plot of a sample of data without pre-processing. When this is compared with figure 4.24, when mean centred pre-processing has been performed on the whole data set, it can be seen that the data generated by the loadings can be more readily analysed.

Pre-processing by mean centre is where the mean is subtracted from the mean of the whole data set from every point in the data set. Any variation within the data from the mean can then be more readily seen.

As well as producing a loadings plot for all the data points within a set of data, a scores plot can be generated by the use of PCA. This scores plot transforms the whole data set, in this case a list of ions and molecular species identified by ToF-SIMS, into numbers which can then be considered as X and Y co-ordinates. These scores depend on the amount

of variance between each data set. Principal component one will always have the largest amount of variance and this will decrease with each subsequent principal component. The transformation of these principal components into X/Y co-ordinates depends on taking the score for adjacent principal components (eg. 1 and 2, 3 and 4 etc., but never 2 and 3, 4 and 5). Each scan of each leaf was transformed into an X and Y score and these scores can be seen plotted in Figure 4.23.

Each of the Principal Components that are generated also produce a loadings plot as previously discussed. Figure 4.24 shows the loadings plot for Principal Component 1 of figure 4.23. The majority of the points on this plot, which represent ions and species from both the positive and the negative scans of the leaves, have loadings of 0 or close to 0. This shows that they do not have any effect on the positioning of the whole score for the leaves in Figure 4.23. When the loadings are positive, for example K, C_3H_7, C_4H_7 etc., these are responsible for the shift in positioning of some of the leaves on the scores plot onto the positive side of the graph. This has separated out the leaves with no infusion or 15 seconds of infusion. The negative loadings of Figure 4.23, show that $C_3H_5O_2$, PO_3, C_2H, CH, C and others are responsible for the shift to the negative side of the graph for the leaves that have been infused for 30 to 300 seconds.

Figure 4.24 is the plot of the loadings for Principal Component 2. This component is on the Y axis. Positive scores on this component show by placing the leaves about the 0 point and negative loadings are shown

below the 0 point. Small chain hydrocarbons, such as CH, C_2H, C_3H_7 and C_4H_7 are shown to be on the positive side of the loadings plot. This means they are vary between untreated tea leaves and leaves that have been infused for 300 seconds from the rest of the treatment times, as well as some of the data for 15, 60 and 150 seconds of infusion. PO_2, Oxygen and Potassium also appear on the positive side of the plot. The species that appear on the negative side of the loading plot are either long chain hydrocarbons such as $C_{14}H_{16}$, $C_{11}H_{16}$, $C_{10}H_9$ and C_8H_{15}. Also two oxygenated hydrocarbons appear to be having an effect as well. Both C_3H_6O and $C_5H_{10}O$ are on the negative side of the loading plot. Combined with the long chain hydrocarbons these are what are responsible for separating some of the data for 15 to 150 seconds of infusion time for the scores plot.

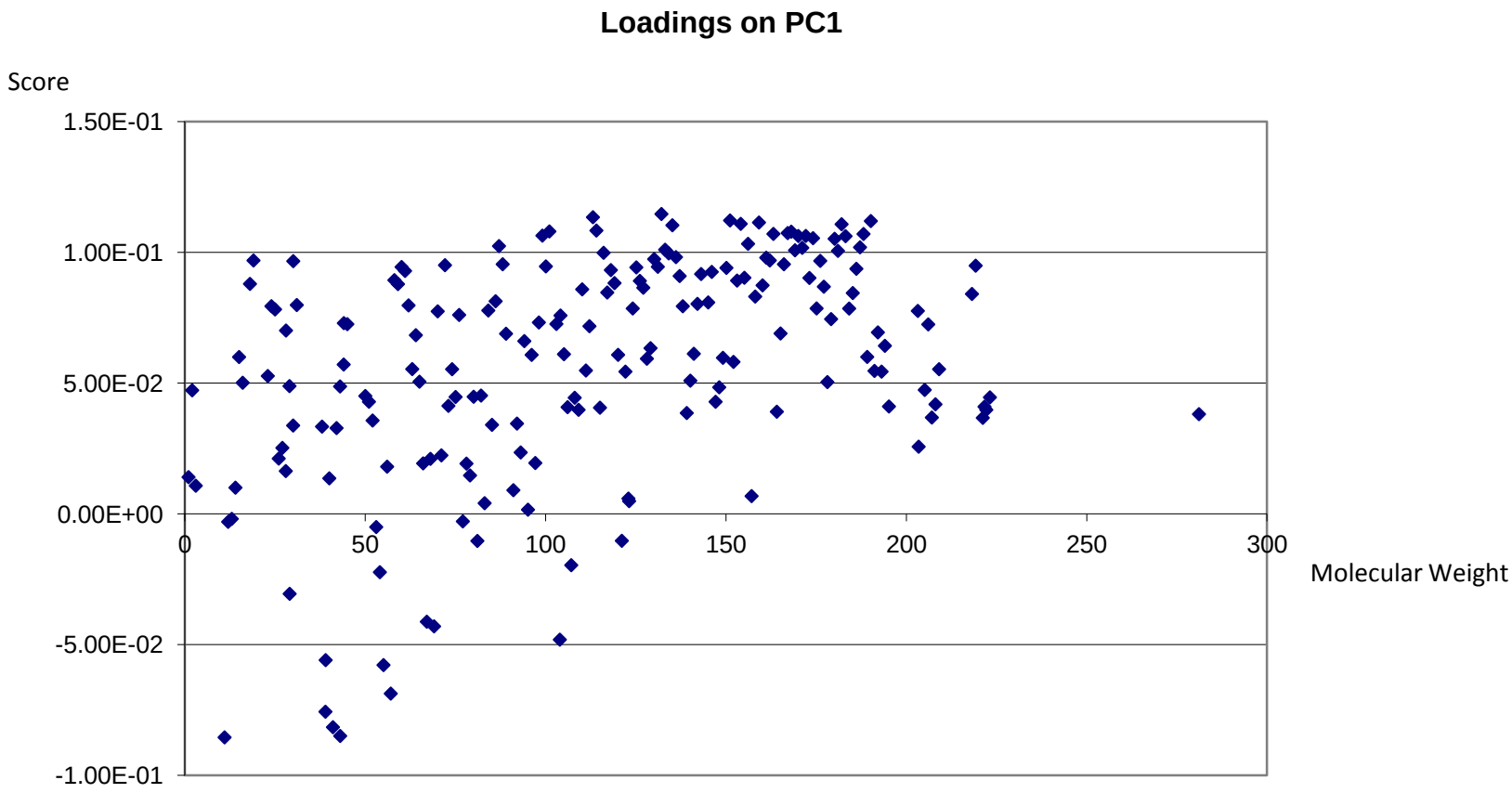

Figure 4.22 - Example Loadings scores of small sample of data from positive spectra without preprocessing.

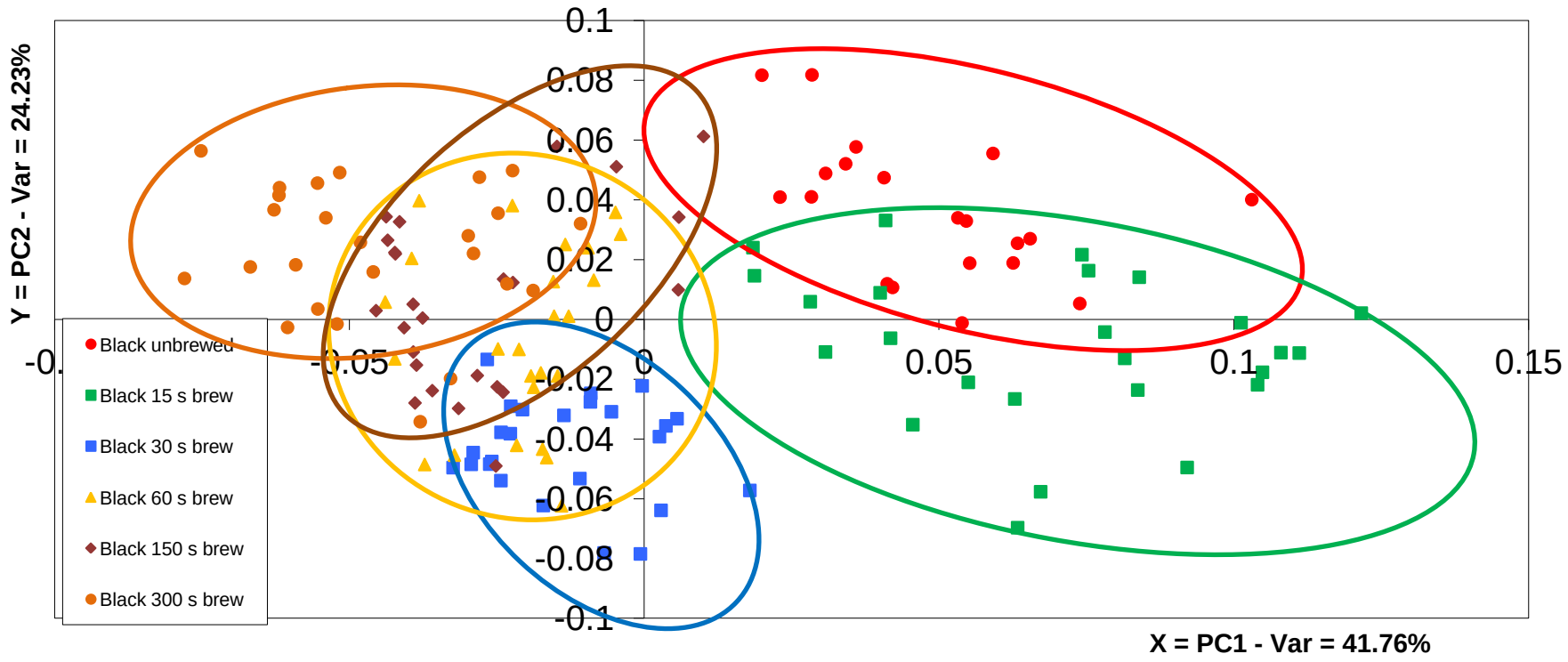

Figure 4.23 - Results of PCA for the normalised positive and negative spectra for black tea leaves. Areas circled show the correlation between multiple samples treated by the same infusion conditions.

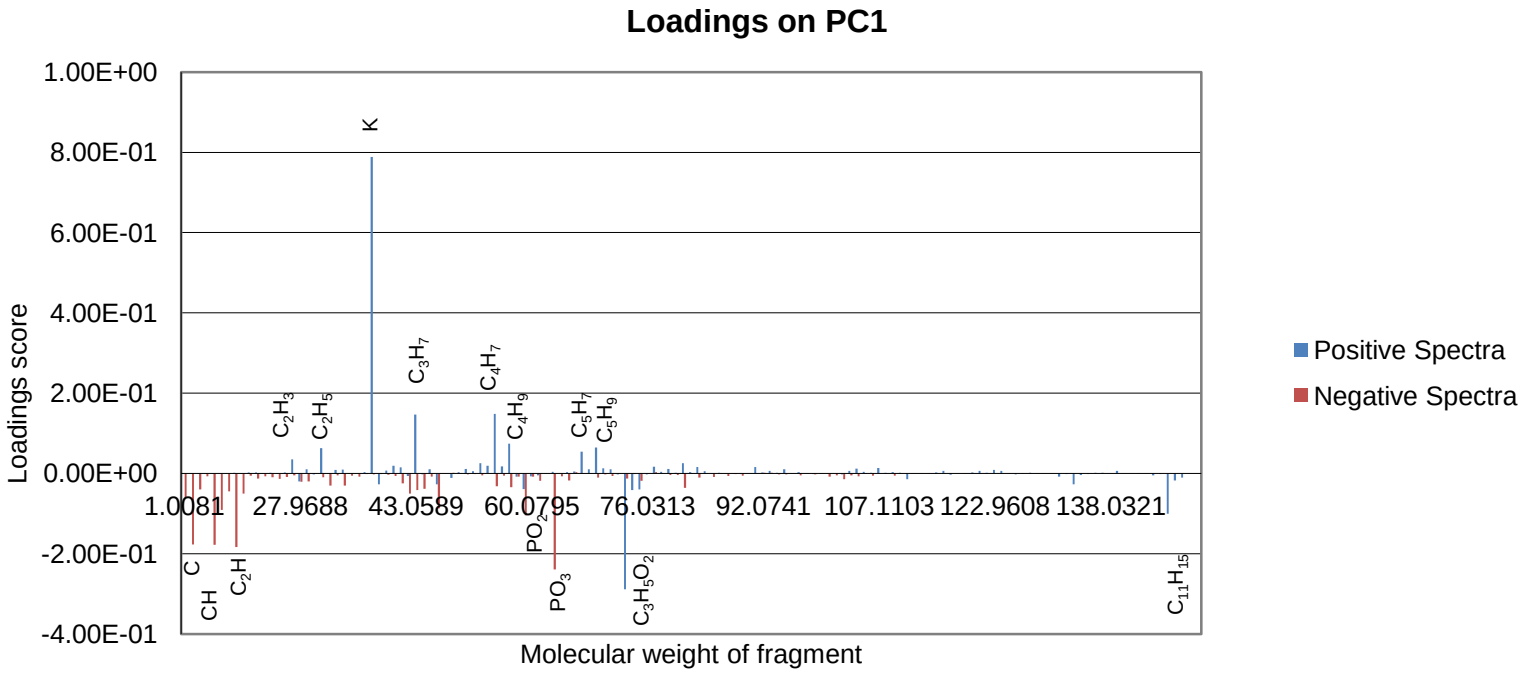

Figure 4.24 - Loadings plot of the positive and negative spectra of tea on PC1. Labelled peaks which have had an effect on the data.

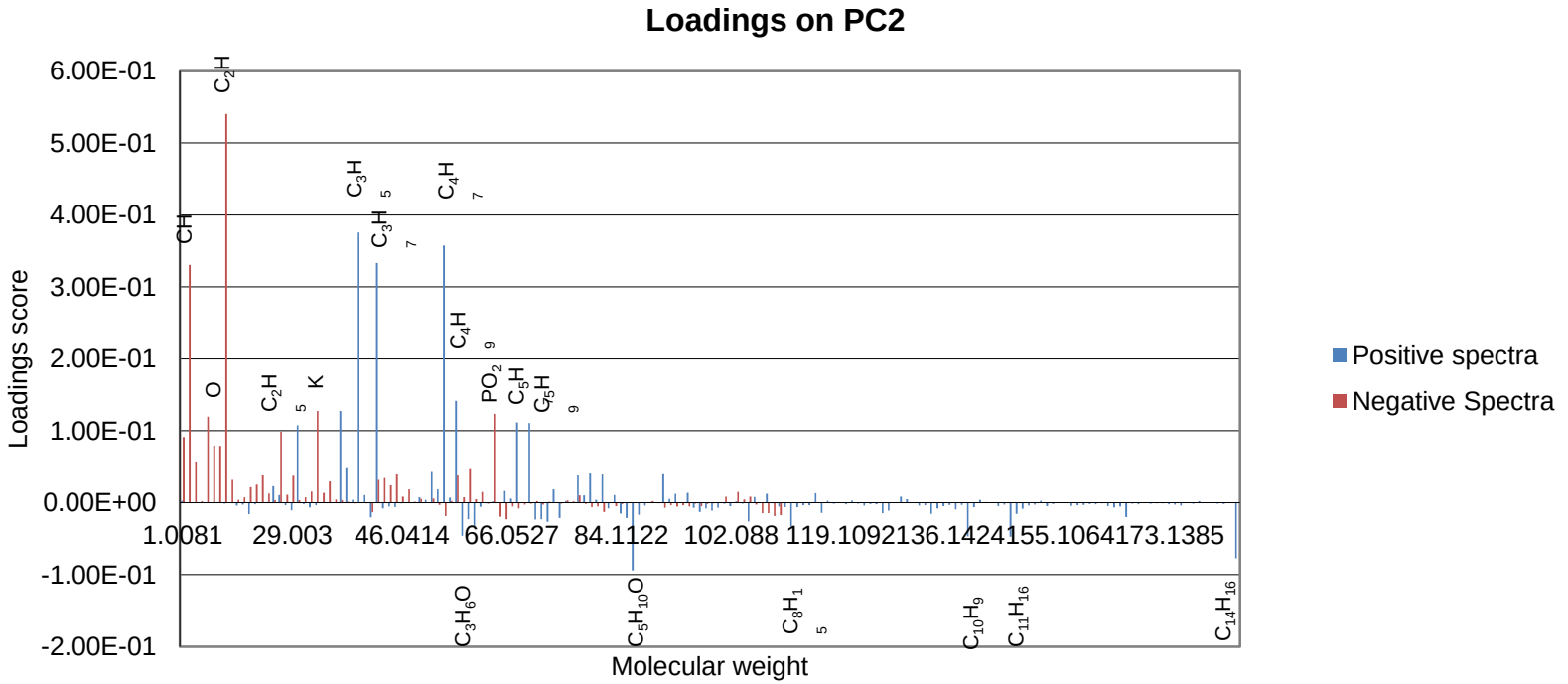

Figure 4.25 - Loadings plot of the positive and negative spectra of tea on PC2. Labelled peaks which have had an effect on the data.

Figure 4.26 shows the mean normalised peak intensity for some of the species that were highlighted as of interest and having an affect on the loadings and scores plots for PCA. By plotting the mean normalised intensity, changes in intensity that are caused by infusion can be seen and also the effect of increasing the time of infusion. For example potassium shows an initial increase of intensity after 15 seconds of infusion and then the intensity decreases sharply to 150 seconds. A slight increase is seen at 300 seconds of infusion. Oxygen in contrast shows an increase in intensity as the infusion time increases.

Figure 4.27 shows in tabulated form all the molecules and species that appear of interest due to the loadings plots for principal component 1 and 2. Species marked in bold are from negative ToF-SIMS spectra.

Three marker species were identified for hexadecanoic, octadecenoic and octadecanoic acids. The mean normalised intesity of these markers are shown in figure 4.28. The marker fragment for hexadecanoic acid is $C_{16}H_{31}O$. Because of the chemical similarities between octadecenoic and octadecanoic acids (2 extra hydrogen atoms) a marker was found that could be for octadecenoic acid, $C_{18}H_{33}O$, but as the pattern of change in intensity for infusion time is the same as the marker for octadecanoic acid, $C_{18}H_{35}O$, this could be another indication of the presence of octadecanoic acid.

Figure 4.29 shows species that show a similar change in intensity for infusion time as the markers in figure 4.28. The species shown are also highlighted in the loadings of the PCA analysis. This change in intensity is ten times greater than that of the marker species in figure 4.28 which is why they have appeared on the loadings plot when the markers did not.

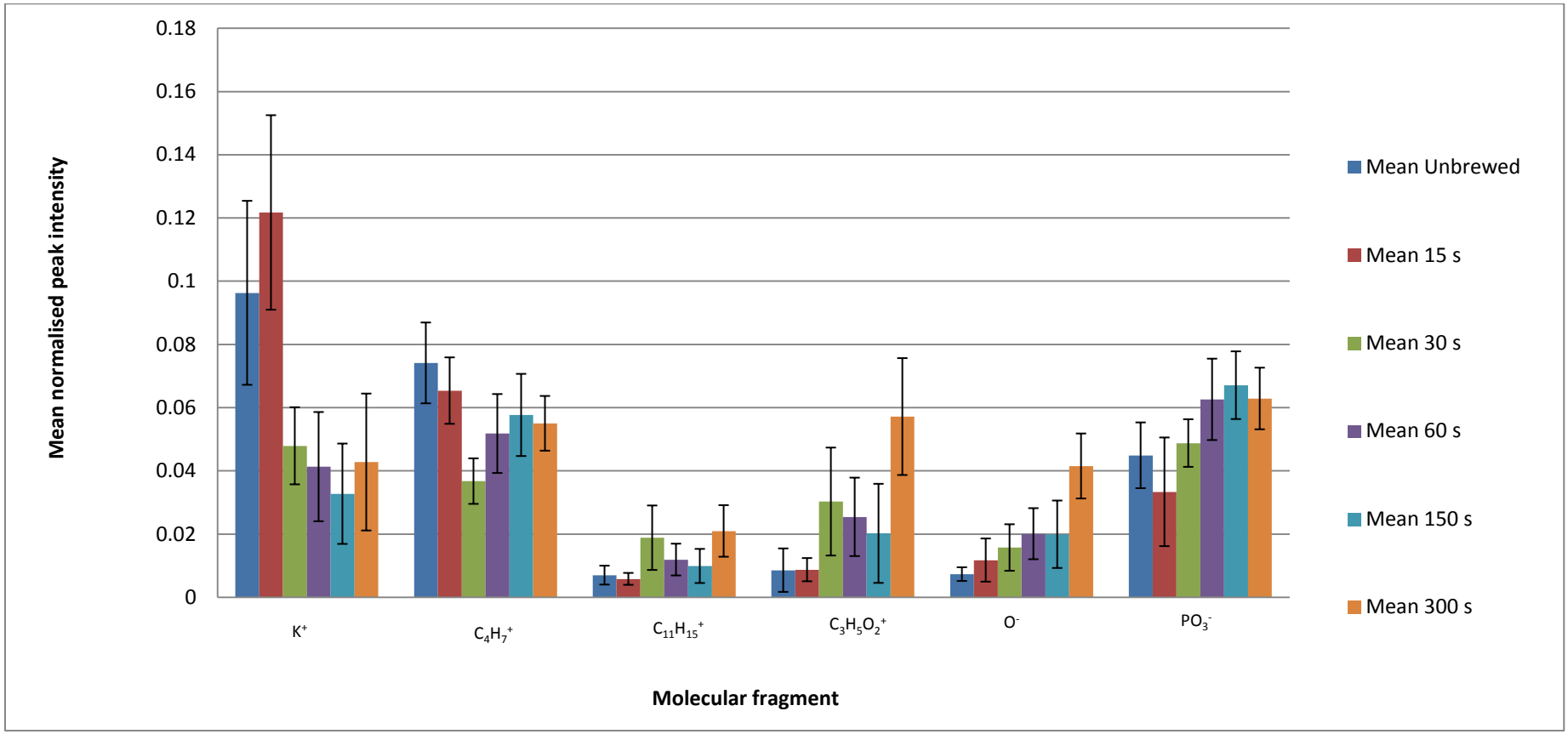

Figure 4.26 Mean normalised peak intensity of some of the fragments identified by PCA.

PC1		PC2	
Positive effect	Negative effect	Positive effect	Negative effect
K	**C**	**C_2H**	C_8H_{15}
C_4H_7	**PO_2**	C_3H_5	C_3H_6O
C_3H_7	**OH**	C_4H_7	$C_{10}H_{19}$
C_4H_9	$C_{11}H_{15}$	C_3H_7	$C_{11}H_{15}$
C_5H_9	**$C_2H_3O_3$**	**CH**	$C_{14}H_{16}$
C_2H_5	**CH**	C_4H_9	$C_5H_{10}O$
C_5H_7	**O**	**C_4H**	
C_2H_3	**C_2H**	K	
	PO_3	**PO_3**	
	$C_3H_5O_2$	**O**	
		C_5H_7	
		C_5H_9	
		C_2H_5	

Figure 4.27 List of molecular species and ions which are influencing the data spread for PCA in both a positive and negative way. Species in Bold are from negative scans.

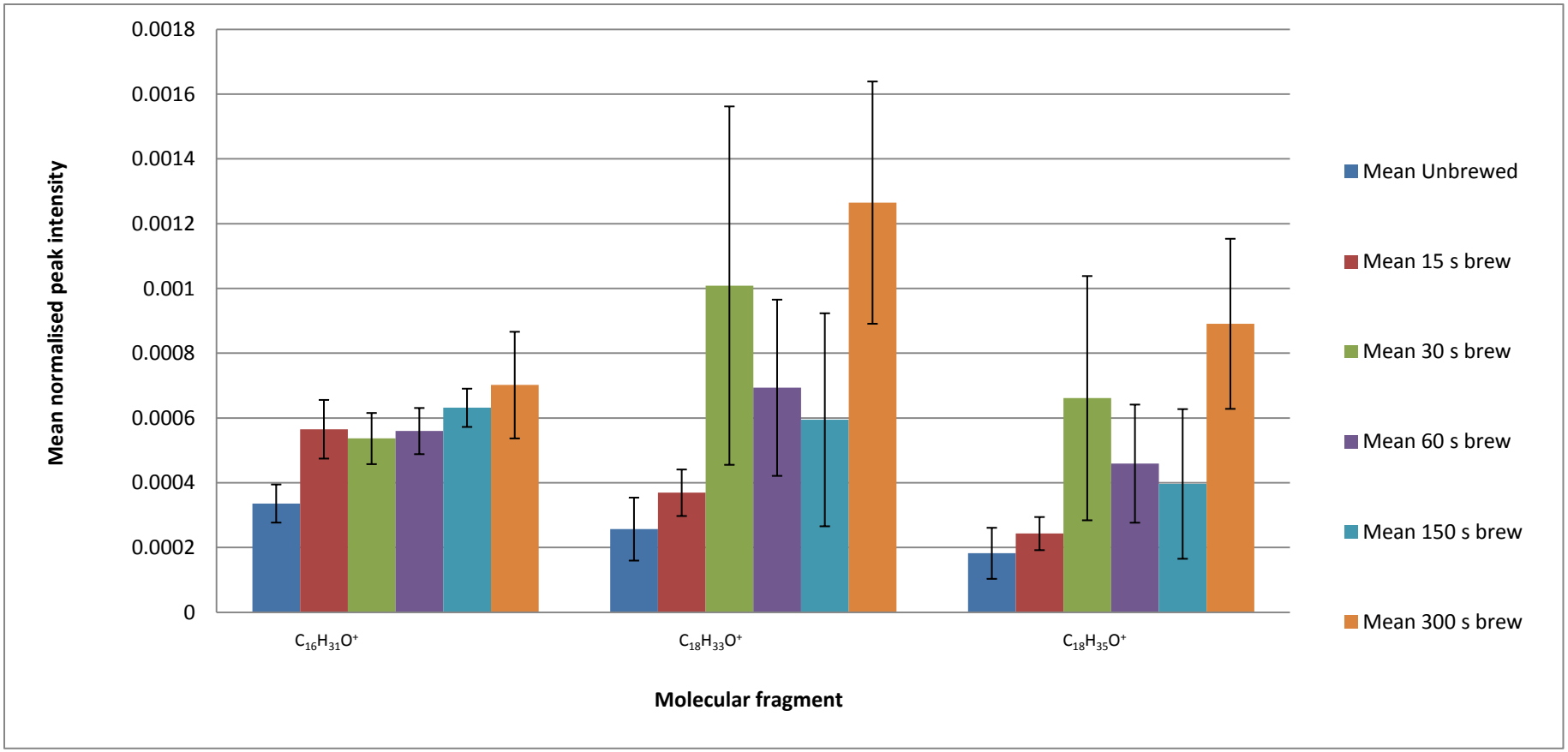

Figure 4.28 Mean normalised peak intensity of molecular fragments that are present in the cutin layer.

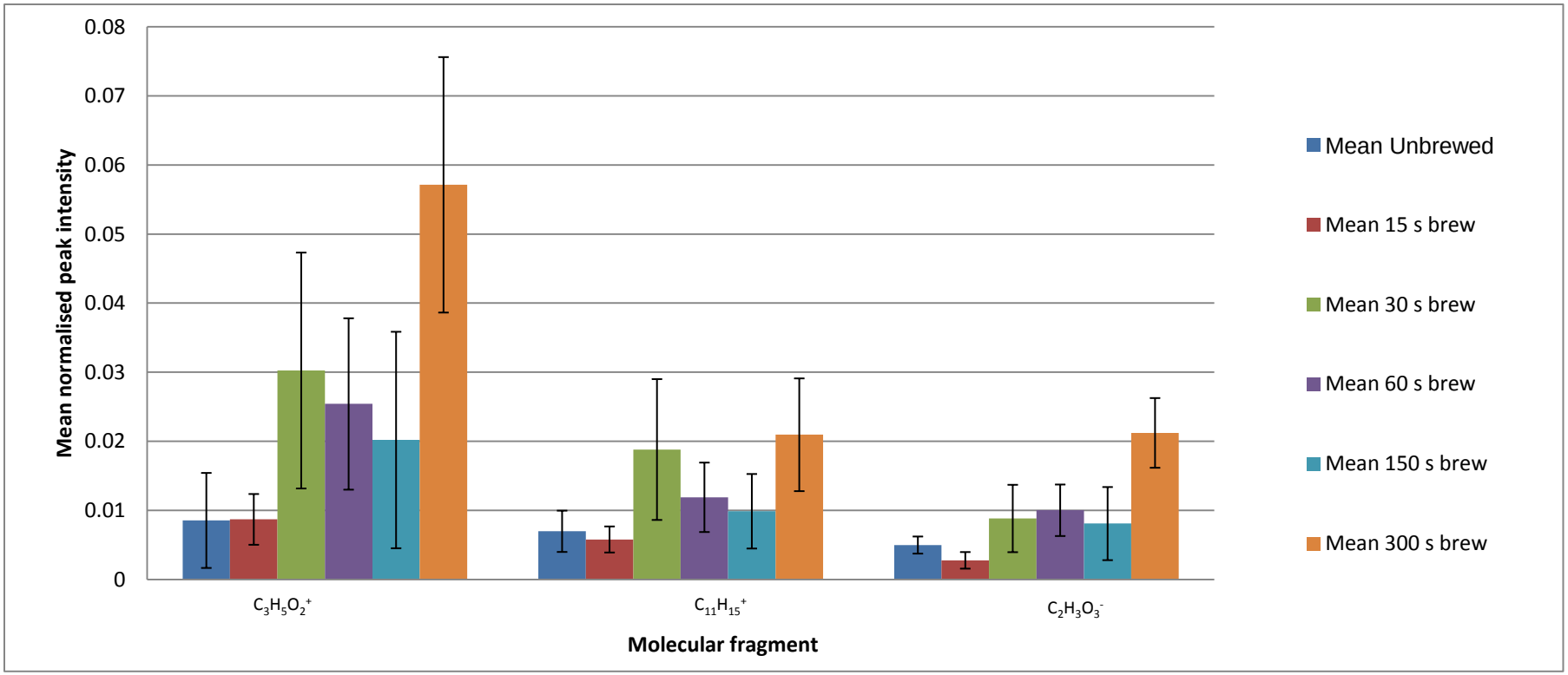

Figure 4.29 Mean normalised peak intensity of fragments that show the changes in intensity with infusion time as the identified species for Cutin monomers.

4.5 Discussion

4.5.1 Discussion of the effects of infusion on the surface of tea leaves as seen by SEM.

Comparison of the images aquired from examination of the tea leaves using SEM show a difference in the microstructure of the cutin layer on the adaxial side of the leaf with infusion in boiling water.

Initial comparisons of the electron micrographs with lower magnification (x40 to x65 magnification) showing the entire fragment of the tea leaf display little difference when the leaf has been infused. (Figures 4.1, 4.4, 4.7, 4.10, 4.13 and 4.16).When the magnification is increased to x700 to x900 then differences can be seen.

Initially, (Figures 4.2 and 4.3) the surface of the leaf fragment shows a lot of debris on the surface. Given the amount of processing steps that the leaf has to undergo from plucking to final product these are probably an artifact of the heating and tearing stages.

When comparing these images to the images obtained after 15 seconds of infusion time (Figures 4.5 and 4.6) it can be seen that the debris is still evident on the surface but that there are in addition a small number of pits in the cuticular layer.

The pits in the cuticular layer are more evident after 30 seconds of infusion (Figures 4.8 to 4.9). These features are more numerous than at 15 seconds of infusion and can be seen at random parts of the leaf (Figure 4.8) or in groups as seen in Figure 4.9. The debris can still be seen on the

cutin layer of the leaf but it is less apparent than for the infusion time of 15 seconds or no infusion at all.

Figures 4.11 and 4.12 show the effects of infusion for 60 seconds. By 60 seconds the cuticular matrix is disrupted by the infusion and the number of holes has sharply increased. The distribution of these holes is more regular and affects a larger area of the cuticular matrix. By 60 seconds there is no sign of debris from production of the finished tea product.

At 150 seconds, (Figures 4.14 and 4.15), the holes on the surface of the cutin layer have increased in size. The frequency of the holes seems to be the same as at 60 seconds and is occuring in regions of the surface rather than on the whole surface. In figure 4.14 it can be seen that there is a large area of cutin matrix disruption from infusion in the centre of the electron micrograph. The area surrounding this area of disruption shows some smoother topography which are free from holes. This is again evident in figure 4.15.

The effects of the final infusion time of 300 seconds are shown in Figures 4.17 and 4.16. As seen previously in Figures 4.14 and 4.15 the size of the holes is increasing when compared to shorter infusion times. This is particularly evident in figure 4.15.

The adaxial surface of the leaf was initially mostly covered in a waxy layer, the cuticle. The main component of this cuticular layer is Cutin. Cutin is one of the two polymers that constitute the plant leaf surface. The other polymer is cutan. This polymer is sometimes described as a biopolyester.

The cuticule was damaged and progressively removed during infusion, being melted by the hot water and reforming in a disordered manner during the drying stage. Previously, monomers of 9, 10-epoxy-18-hydroxyoctadecanoic acid, dihydroxyhexadecanoic acid and 9, 10, 18-trihydroxyoctadecanoic acid have been identified as the primary cutin constituents of tea, as well hexadecanoic, octadecanoic and octadecenoic acids (Tsubaki, 2008). Octadecenoic acid, and its derivatives, would melt first in the boiling water, as these have a melting point of 13-14 $^{\circ}$C, followed by hexadecanoic acid (63 $^{\circ}$C) and octadecanoic acid (69.6 $^{\circ}$C) and their derivatives. The initial holes that appear in the cutin are, we propose related to the early preferential loss of the lower melting point components before more widespread damage occurs. As the cuticular layer is melting the cuticular waxes could be reforming on the leaf so that the wax fills any broken or disrupted cells from the upper epidemal layer. Tof-SIMS analysis was carried out to address this question.

4.5.2 ToF-SIMS and Principal Component Analysis.

Figure 4.23 shows the result of PCA for comparison of the positive spectra of black tea leaves. A control group of leaves which had not been infused in boiling water was taken for comparison with the leaves infused for different times.

From the PCA plot in figure 4.23 it can be seen that for principal component 1 (PC1) both the untreated tea samples and 15 s brew are positioned on the positive side of the plot and the longer infused samples are mainly positioned towards the negative side. Detectable changes are clearly occurring within 15s of infusion.

The grouping of the untreated samples, 15s, 30s and 300s show how the data is spread with the scores from the PCA. By examining the loadings for each of the principle components, it can be seen which ions and ion species are responsible for this differentiation between the data (Joliffe, I.T. 2002). By examining the loadings on PC1 (Figures 4.24 and 4.27) it can be seen that the molecular species which have a positive effect on the data separation are in descending order K^+, $C_4H_7^+$, $C_3H_7^+$, $C_4H_9^+$, $C_3H_5^+$, $C_5H_9^+$, $C_2H_5^+$, $C_5H_7^+$ and $C_2H_3^+$. With the exception of potassium, these are all hydrocarbon groups. The surface wax constitutes a layer of cutin comprising of hydrocarbon monomers. These monomers are either of a C16 or C18 chain length and vary in plant species. The potassium may either be as a result of fertilizers, which are applied to the tea plant as it this has been shown to increase the polyphenol and amino acid content of the tea leaf, or from residual potassium which would be present on the leaf following transport through the vascular bundles for the control of opening of stoma and maintenance of the ion channels with the leaf cells (Venkatesan et al. 2004). The negative loadings are related to $C_3H_5O_2^+$,

PO_3^-, C_2H^-, O^-, CH^-, $C_2H_3O_3^-$, $C_{11}H_{15}^+$, OH^-, PO_2^- and C^- ion fragments. The negative loadings include a higher mass hydrocarbon than the positive loadings and are dominated by the oxygenated species but also include the presence of phosphor groups. The oxygenated species also likely to be due to the change of surface waxes. The presence of phosphate groups can be either from phosphate containing enzymes within the leaf, which are part of the chemical process for producing catechins or from the phospholipid bilayer that covers cell membranes. As the intensity of these peaks increases with infusion time, this suggests that the phosphate containing groups are leaching from the damaged cell membranes within the leaf onto the surface as part of the infusion process or being revealed by the movement of the cutin wax layer.

By comparison of the positioning of the data on PC2 (Figures 4.25 and 4.27), it can be seen that there is a change within 15 s of infusion. This change in positioning is more pronounced for the samples that were infused for 30s. The scores for 60s and 150s are intermingled with the positioning of the scores for 30s and 300s.

The molecular species shown to be responsible for the positive positioning of the data on PC2 (Figure 4.25) are C_2H^-, $C_3H_5^+$, $C_4H_7^+$, $C_3H_7^+$, CH^-, $C_4H_9^+$, C_4H^-, K^+, PO_3^-, O, $C_5H_7^+$, $C_5H_9^+$ and $C_2H_5^+$. A higher intensity of these fragments can be seen in the untreated tea compared with the different infused samples. When the molecular species are examined for the negative positioning on PC2 it can be seen that they are $C_8H_{15}^+$,

$C_3H_6O^+$, $C_{10}H_{19}^+$, $C_{11}H_{15}^+$, $C_{14}H_{16}^+$ and $C_5H_{10}O^+$. These are all large hydrocarbon fragments or oxygenated hydrocarbons. These results are summarised in figure 4.27. The smaller molecular fragments, C^-, OH^-, CH^-, O^-, and C_2H^-, are seen to have an effect on the positioning of the various infusion times in the PCA plot (Figure 4.23).

By plotting the mean intensities of example fragments of all the groups raised by the PCA, (Figure 4.26), the compositional changes that occur on the surface of the leaf become evident. Potassium intensity increases initially after 15s of infusing time and then shows a sharp decrease at 30 s and a further decrease to 150s. At 300s of infusing there is another increase in intensity. This initial increase, then decrease and further increase in intensity could be due to an initial release of potassium from the cutin matrix; this is then washed away until potassium from within the leaf is leeched to the surface.

Oxygen shows an increase with infusion time. The level of oxygen for 60 and 150s of infusing is equal but there is a further increase in intensity at 300s of infusing. The monomers which are part of the cutin layer all contain oxygen. For a change in intensity to occur this oxygen must become more readily available on the surface to be analysed. This suggests a re-orientation of the monomers when the cutin layer is drying and reforming after the infusion process and potential melting.

The hydrocarbon groups, shown in Figure 4.27 as C_4H_7 and $C_{11}H_{15}$ seem to act in two different ways. Any hydrocarbon with a chain length below C_8

shows an initial decrease in peak intensity to 60s, an increase to 150s and then a small decrease in intensity to 300s. Hydrocarbons of C_8 and above show an initial decrease at 15s of infusion with an increase at 30s. This intensity decreases for 60 and 150s but is still at a level above untreated tea. Finally, there is an increase at 300s of infusion which is the highest intensity for all of the infusing times. After 30s of infusion time if there is an increase in intensity for short chain hydrocarbons then there is a decrease for long chain hydrocarbons suggesting that different parts of the monomer are available. Increases in intensity for long chain hydrocarbons result in a decrease in intensity for short term hydrocarbons as well. Oxygenated hydrocarbons, $C_3H_5O_2$ in figure 4.26, show a slight increase in intensity at 15s, with a much larger increase at 30s. This then decreases for 60 and 150s, again still at a level above untreated tea leaves, with a large increase for 300s. This again is an example of the reorientation of the monomeric units of cutin.

Finally phosphate groups, for example PO_3, show an initial decrease in intensity at 15s. This intensity increases to 150s and then shows a slight decrease at 300s. The change in the phosphate groups could show an increase in the revelation of the cell wall and damage due to the phospholipid bilayer covering the cells below the cuticle. After an initial removal of the phosphate groups from the surface of tea, and increase could be indicative of the leeching of these groups from within the leaf.

The changes in the intensity of these molecular ions could be related to the availability of the larger monomers which make up the cutin layer and the fragmentation from these larger monomers with the ToF-SIMS analysis.

Further examination (Figures 4.28 and 4.29) of the mean intensity of these molecular fragments shows a similarity between the pattern of change of intensity for some of the molecular species when the leaves are infused. This can be indicative of the fragments in question being related to the surface. Figure 4.28 shows how the fragments $C_3H_5O_2^{+,}$ $C_{11}H_{15}^{+}$, and $C_2H_3O_3^{-}$ display a similar pattern in the changes of the normalised intensity as a function of infusion, of the fragments as $C_{18}H_{31}O^{+}$ and $C_{18}H_{35}O^{+}$ in Figure 4.29, these peaks are identified as fragments of both octadecenoic acid and octadecanoic acid. These changes in intensity show no resemblance to the changes on the leaf surface for hexadecanoic acid as seen in Figure 4.29. The monomers are insoluble in water so there wouldn't be lost into the water used for infusing (O'Neil 2006), but could be redistributed as a reformed wax layer on the surface. With the increase of intensity for the molecular markers (Figure 4.29) for these acids increasing with infusion time at 30s, the first point of a significant change in the surface chemistry of the leaf, the cutin layer would be redistributed over the surface of the leaf. After infusing the leaves are taken out of the water and placed on a slide and dried. When the leaves are dried, these wax components would reform on the leaf surface. There is a slight drop in

peak intensity for these molecular markers for 60 and 150s, but the intensity is still higher than for untreated and 15s brew of the tea. The highest intensity for these peaks is at 300 s infusing time.

One of the peaks identified as influencing the scores in the negative region in PC1 is $C_3H_5O_2$. This has been identified as being a fragment from cellulose (Mitchell et al. 2005). As infusion time increased, the mean intensity of this fragment also increased. With a change in the surface cutin layer, the material underneath the layer would be exposed. If the cutin has melted and been redistributed then the appearance of a specific cellulose fragment is not unexpected. With the changes in the cutin layer occurring during the infusion process then the boiling water would be allowed to access the layers below the cutin. Flavour release from the leaf would be able to occur as the water was able to interact with compounds held within the spongy mesophyll and palisade mesophyll layers of the leaf.

4.6 Conclusions

It can be seen that significant morphological and chemical changes are occuring in the leaf fragments upon infusion in boiling water. This is evident from the first 15 to 30 seconds of infusion. Visually, the surface of the tea leaf displays more prominent changes from 30s of infusion time relatted to the melting of some of the wax components of the cuticle, with an increasing effect with time of infusion. Chemical changes occur

primarily within the first 15 to 30 seconds of infusion, although continuing effects are also seen up to 300 s. The effect on the surface of the leaf is to alter the composition of the cutin layer. The presence in the positive ToF-SIMS spectra of $C_3H_5O_2$, and its subsequent increase with infusion time, could be a marker for cellulose (Mitchell et al. 2005) from the remains of the cells in the upper epidermal layer of the leaf revealed as the cutin being removed during infusion. The hydrocarbon groups in both positive and negative spectra are indicative of a change in the waxy cuticular layer of the plant surface. Some of the fragments indicate the presence of derivatives of octadecanoic acid, previously noted as the major monomer in the cutin layer of *Camellia sinensis*. Taken together these data indicate that the melting of the cutin layer during infusion may be related to release of flavour, aroma and constituents such as polyphenols during the early stages of infusion.

References

Ferrara, L., Montesano, D., Senatore, A. (2001). "The distribution of minerals and flavonoids in the tea plant (Camellia sinensis)." Farmaco **56**(5-7): 397-401.

Hara, Y., Kuroda, Y. (1999). "Antimutagenic and Anticarcinogenic activity of tea polyphenols." Mutation Reseach/Reviews in Mutation Research **436**(1): 28.

Kawakami, M., Ganguly, S. N., Banerjee, J., Kobayashi, A. (1995). "Aroma composition of Oolong tea and black tea by brewed extraction

method and characterizing compounds of Darjeeling tea aroma." Journal of Agricultural and Food Chemistry **43**(1): 200-207.

Kenney, M. A., Thimaya, S. (1983). "Copper content of tea." Journal of the American Dietetic Association **82**(5): 509-510.

Mitchell, R., Carr, C. M., Parfitt, M., Vickerman, J. C., Jones, C. (2005). "Surface chemical analysis of raw cotton fibres and associated materials." Cellulose **12**(6): 629-639.

Mizukami, Y., Sawai, Y., Yamaguchi, Y. (2007). "Simultaneous analysis of catechins, gallic acid, strictinin, and purine alkaloids in green tea by using catechol as an internal standard." Journal of Agricultural and Food Chemistry **55**(13): 4957-4964.

O'Neil M J. Editor. The Merck Index: an encyclopedia of chemicals, drugsand biological. 14th Edition. Merck Research Laboratories, Whitehouse Station, NJ, USA. 2006

Owuor, P. O., Chavanji, A. M. (1986). "Caffeine contents of Clonal Tea - Seasonal-Variations and effects of plucking standards under Kenyan conditions." Food Chemistry **20**(3): 225-233.

Peterson, J., Dwyer, J., Bhagwat, S., Haytowitz, D., Holden, J., Eldridge, A. L., Beecher, G., Aladesanmi, J. (2005). "Major flavonoids in dry tea." Journal of Food Composition and Analysis **18**(6): 487-501.

Tsubaki, S., Iida, H., Sakamoto, M., Azuma, J. (2008). "Microwave Heating of Tea Residue Yields Polysaccharides, Polyphenols, and Plant Biopolyester." Journal of Agricultural and Food Chemistry **56**(23): 11293-11299.

Venkatesan, S., Murugesan, S., Ganapathy, M. N. K., Verma, D. P. (2004). "Long-term impact of nitrogen and potassium fertilizers on yield, soil nutrients and biochemical parameters of tea." Journal of the Science of Food and Agriculture **84**(14): 1939-1944.

Chapter 5.

ToF-SIMS surface and near-surface analysis of aroma distribution in tea leaves.

5.1 Introduction

Following on from the effects of infusion on tea leaves, the addition of aroma molecules was studied. Three aroma chemicals were selected from the complex matrix of aromas that are present in tea. These were methyl salicylate, linalool and trans-2-hexenal. The three aromas have different chemical properties so experimentation with these aromas would indicate if the properties of the volatile aromas in tea led to different interactions with the surface of the tea leaves.

Tea aroma is a complex mix of components (Kawakami et al. 1995). Previous studies concentrated on examining the components that are present in the aroma released from leaves during infusion (Takeo et al. 1981; Morita et al. 1994; Gulati et al. 1996, Zhang et al. 2006; Li et al., 2006; Rawat et al. 2007; Rawat et al. 2008).

As some of the aroma is lost during the processing of tea (Ravichandran et al. 1998), the standard industrial practice is to collect the natural aroma that is released in processing, mix it with water and spray the aroma cocktail back onto the processed leaves. By using ToF-SIMS depth

profiling with three aroma samples that are naturally found in tea, the location of where these molecules interact with the leaf can be discovered.

During these experiments three of the naturally occurring aromas will be added to the surface of the tea leaves in solution and ToF-SIMS depth profiling will be performed on the leaves to identify where in the leaf they can be found.

Methyl salicylate, $C_8H_8O_3$, is an organic ester, containing a functional alcohol group and ester group. It is an oily liquid, pale yellow and clear in colour, with a molecular weight of 152.15 g/mol. It is slightly soluble in water (1g/1500ml water) (Merck 2006), but is highly soluble in chloroform, alcohols, ether and glacial acetic acid. The difference between acetic acid and glacial acetic acid it that the glacial form is anhydrous and ice like crystals form at 16.6^{o}C. Methyl salicylate is described as having an aroma like chewing gum or toothpaste as it has been used in both of these products in the past. Because of the close proximity of the hydroxyl and ester groups there is a strong intramolecular binding of methyl salicylate (Aparicio et al. 2010). Plants produce methyl salicylate as part of a defence mechanism. It has been shown that it can act as a signaling compound as part of a systemic acquired response (Tzellos et al. 2011; Park et al. 2007). It can induce early flowering as part of an effort to reproduce prior to death in stressed plants (Martinez et al. 2004). It has also been shown that if one plant is attacked that the release of this aroma

from an area of attack will induce the production of defensive chemicals within other parts of the plant (Vlot et al. 2008). Methyl salicylate has a partition coefficient of 2.55 K_{ow} (Lyman et al. 1993). A partition coefficient of 1 or over indicates that the material is lipophilic in nature.

Trans-2-hexenal, $C_6H_{10}O$, is also known as leaf aldehyde. It has a molecular weight of 98.14 g/mol and is only slightly soluble in water, but is soluble in alcohol. It is a pale clear oily liquid. It is known that trans-2-hexenal is produced when a plants is damaged or wounded. By increasing the concentration of trans-2-hexenal experimentally it was shown that some genes that were involved in a plants defense response were induced (Bate et al. 1998).

In response to a bacterial infection of the plant *Phaseolus vulgaris*, trans-2-hexenal was released and shown to have been bactericidal in low concentrations (Croft et al. 1993). Trans-2-hexenal has a partition coefficient of 1.58 K_{ow} (Merck 2006), so though it is still lipophilic it is less so than the other 2 aromas (Naknean et al. 2010). Trans-2-hexenal is said to smell like cut grass.

Linalool, $C_{10}H_{18}O$ is a terpene alcohol, one of 3 isomeric alcohols. It has a molecular weight of 154.25 g/mol (Merck 2006). A clear liquid, that is slightly soluble in water but is miscible in alcohol and ether. Linalool is

described as having a pleasant floral smell, with a touch of spiciness. Linalool can be used to help increase the symbiotic relationship between certain plants and insects. *Manduca sexta*, a moth and the jimsonweed plant, *Datura wrightii*, though the moth is herbivorous the release of linalool increases the production of eggs by the moth rather than attracting it for feeding (Reisenman et al. 2010). Linalool has a partition coefficient of 2.97 K_{ow}. Linalool is slightly more lipophilic than methyl salicylate (Merck 2006).

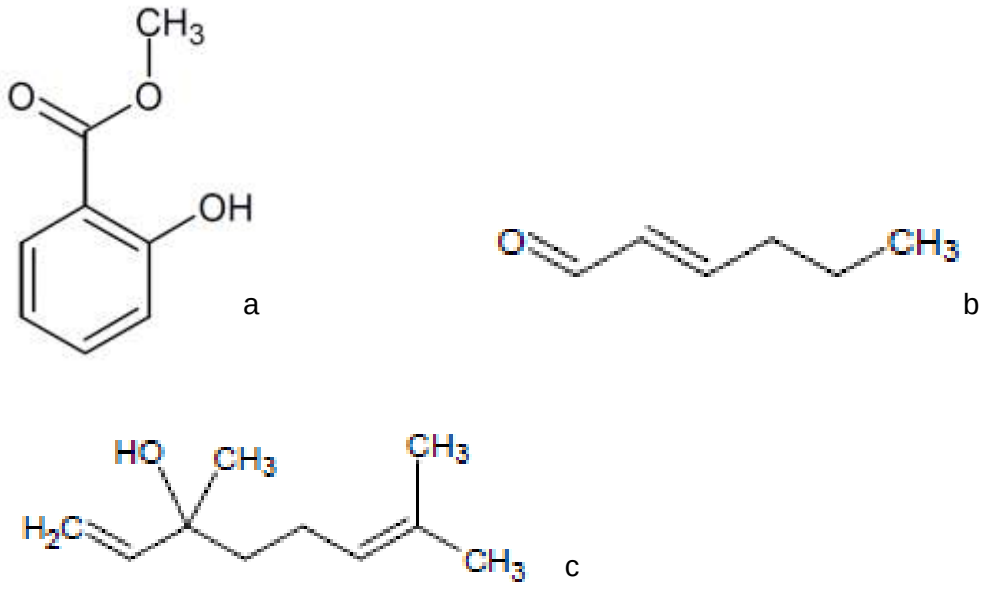

Figure 5.1 – Chemical structure of (a) methyl salicylate, (b) trans-2-hexenal and (c) linalool.

5.2 Experimental

5.2.1 Leaf selection and flattening

Leaves were chosen using the leaf selection process described in chapter 2. As these leaf fragments had a rough topography they were placed in a glass beaker (which had been piranha etched) of cold distilled water for 2 hours to soak them. The soaking of the leaves would allow them to be artificially flattened without affecting the chemical composition of the leaf fragments by infusion in boiling water.

The soaked leaves were then placed between two glass slides that had been cleaned using Piranha etching (Method described in chapter 3). The leaf fragments were then left for 24 hours to dry with weights placed on top of them to aid in the flattening of the surface.

After drying the leaf fragments were re-examined under an optical microscope to ensure the correct orientation of the adaxial side for analysis

5.2.2 Aroma preparation

Three aromas that are naturally found in tea were chosen. These were methyl salicylate, trans-2-hexenal and linalool (Takeo et al. 1981; Morita et al. 1994; Gulati et al. 1996; Ravichandran et al. 1998; Wang et al. 2000; Zhang et al. 2006; Rawat et al 2007; Rawat et al. 2008). The aromas prepared following the aroma preparation protocol in Chapter 2. 1 µl of diluted aroma was then placed on the surface of a leaf selected for analysis and left for 24 hours before experimentation.

5.2.3 ToF-SIMS Depth Profiling

For depth profiling with the ToF-SIMS, multiple samples were prepared 24 hours before experimentation. This ensured that conditions were similar to how tea aroma is re-sprayed back onto the surface currently in industry.

Samples were then loaded onto a cold stage and placed in the primary air lock. Liquid nitrogen was used in conjunction with a cold finger to cool the samples down to -100°C before applying a vacuum to them. This ensured that volatile aromas were not released into the vacuum.

After the initial cooling stage the samples were transferred to the main chamber of the ToF-SIMS and a cold finger was used again to ensure the

temperate was kept as close to -100 $^{\circ}$C during the experiments as possible.

An initial scan of the area to be depth profiled was taken using the standard SIMS settings as described in chapters 4 and 5. This area was 250 x 250 microns. This scan was then calibrated as described in the methods and materials chapter, against three known peaks and known peaks in the mass spectrum were identified on a peak list. For example potassium, magnesium, cellulose and some hydrocarbons were used in this small sample peak list. Depth profiling was performed on the samples to examine where the aroma could be found on within the structure of the leaf. A C_{60}^{+} source was used for sputtering to remove layers of the surface during the depth profile (Cheng et al. 2006) and the Bi_3^{+} source was used for analysis as described previously. The sputter gun of C_{60}^{+} (400pA) was set to sputter for an area of 100 x 100 microns on the surface and the analysis gun (2nA) was also set to this size and calibrated to ensure the area analysed was the same area as that sputtered. The two sources were used in interlaced mode. Depth profiles were acquired for approximately 30 minutes (at this time the signals for the aroma had reached a low intensity and the palisade mesophyll layer of the leaf had been reached). A final scan was recorded on the area that had been depth profiled but the size for this was 250 x 250 microns to ensure coverage of the area of

depth profile and the surrounding surface that had not been profiled for comparison.

After the depth profiles had been produced the data was fully analysed. All peaks were identified and assignments for molecular species and ions were automatically performed using the Iontof software. This data was then plotted and similarities were found between known peaks and peaks that acted in the same way. The assignment of these peaks was then double checked to ensure they were correctly identified.

5.3 Results and discussion

5.3.1 ToF-SIMS Depth profiling results untreated leaves

Black tea leaves that had not been treated with aroma were examined first. Figure 5.2 shows an example depth profile for one of the untreated tea leaves. These data show an initial increase in the rise of the potassium marker with depth with all other groups showing an initial sharp drop in the intensity of their associated signal. This is thought to be an artefact due to the rough topography of the surface and was seen in all samples that were examined (Wucher et al. 2008). With the surface of the leaf being uneven, the effect of the C_{60}^{+} sputtering would not be even until the higher topographical features were removed. As there would be higher features on the surface a false signal of intensity would be given. When the surface was the same height, the proper depth profile could be recorded.

Given the strength of the signal for potassium, the peaks identified were broken down into subgroups so a clearer idea of the composition of the depth profile could be seen. All of these groups were compared with a marker for cellulose, $C_3H_5O_2$, which was identified in the previous experiments on the effects of infusion on the tea leaf in chapter 4. Figure 5.3 shows the traces of species assigned to be from the cellulose when compared to the $C_3H_5O_2$ marker. The profiles for CH_3O, $C_2H_5O_2$ and $C_4H_5O_2$ showed identical patterns. The intensity of these species start to increase from approx 250 s and then are of a more stable higher intensity from 1000 s into the depth profile.

Figure 5.4 compares a group of hydrocarbons with the known cellulose marker. As another distinct group of hydrocarbons were also identified this group was termed hydrocarbon group one. Figure 5.5 compares the second group of hydrocarbons identified, termed, hydrocarbon group two, with the cellulose marker. Figure 5.6 shows the cellulose marker compared with magnesium groups found during the depth profile. Magnesium is found within the leaf and is associated with chlorophyll and will be discussed later. Two species containing nitrogen are compared with the cellulose marker in figure 5.7 and potassium and calcium containing species are compared in figure 5.8. Following experimentation with the three different aromas and the identification of peaks which could be used as markers for these aromas the depth profile of the tea leaf with no aroma

added was examined for the identified aroma markers to examine if there was any evidence of the aroma before addition. This is shown in figure 5.9.

Ion images, a feature on the ToF-SIMS, show the spatial location of the ions and molecular species in the scan area. An example of each group found in the depth profile data are shown in figure 5.10. These examples are compared with an image called the total ion image. This is a composite image of all of the ions and molecular species that were recorded by the depth profile and compared against the total ion image, a composite image of the surface examined showing all ions and molecular species present. Further analysis was performed by adding together different Ion images to produce a composite image of each grouping found on the depth profile (figure 5.11). Another of the functions available with IonImage is a XZ reconstruction of the depth profile. An area of depth profile can be chosen, in the XY range and then the Z range can be included into this image to show if there is any difference in the positioning of molecular species when the depth profile is occurring. Figure 5.12 shows an example of this for the untreated tea leaf. The groups previously identified from the graphs are compared with the cellulose marker of $C_3H_5O_2$ to examine the positioning of these groups within the leaf structure.

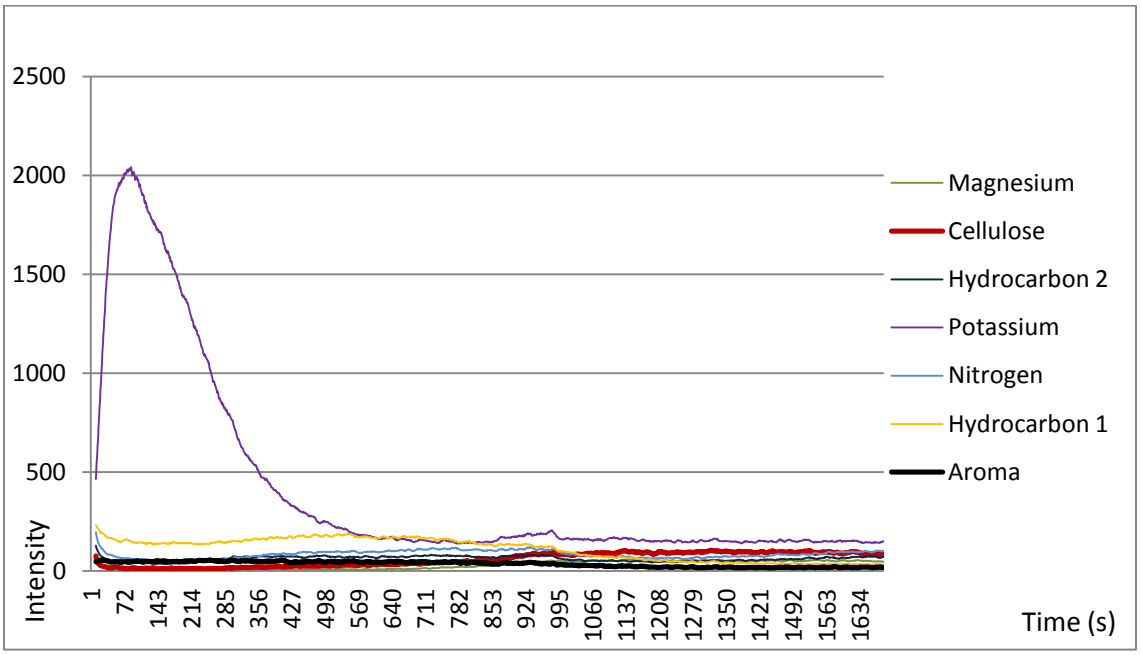

Figure 5.2 - Example trace for depth profiling of an uninfused tea leaf.

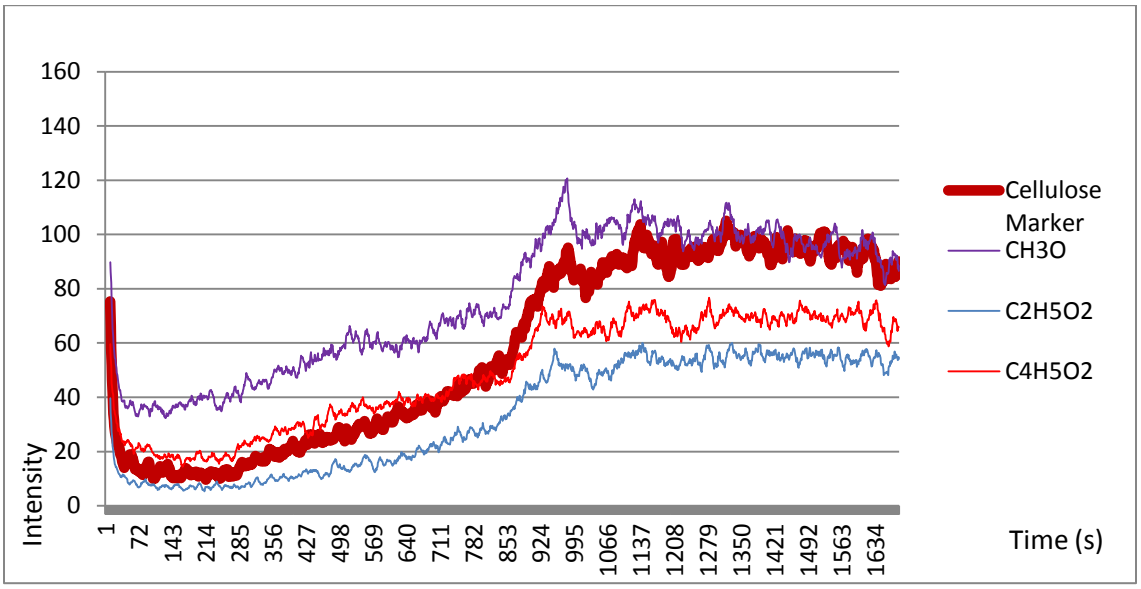

Figure 5.3 - Depth profile trace of markers for cellulose when compared with a known marker for cellulose.

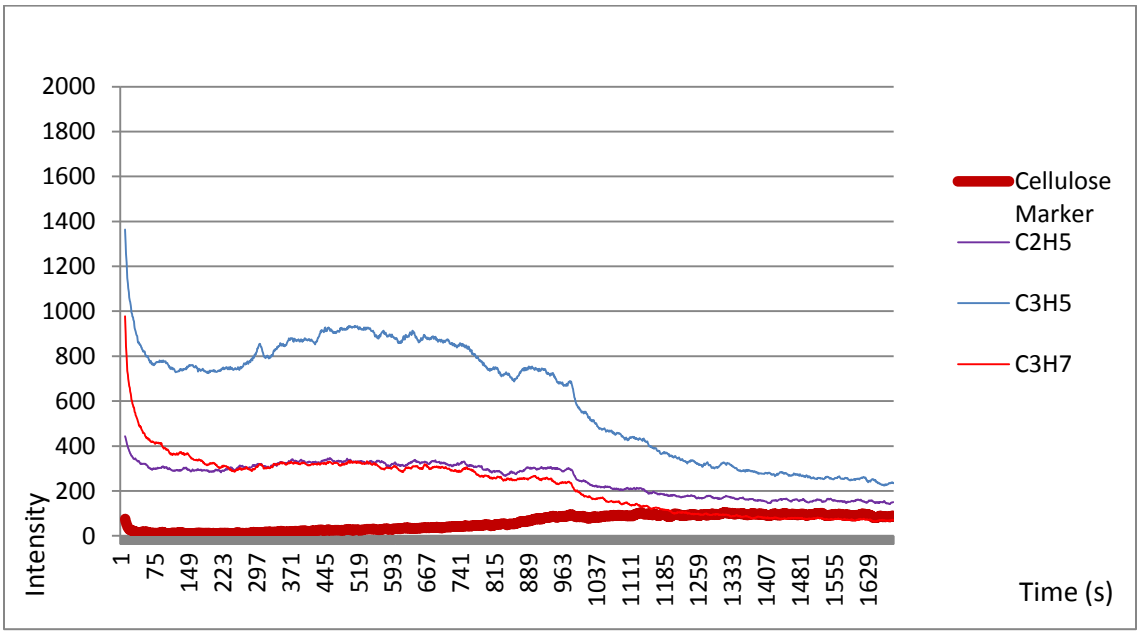

Figure 5.4 - Depth profile showing a comparison of group one of hydrocarbons with a cellulose marker.

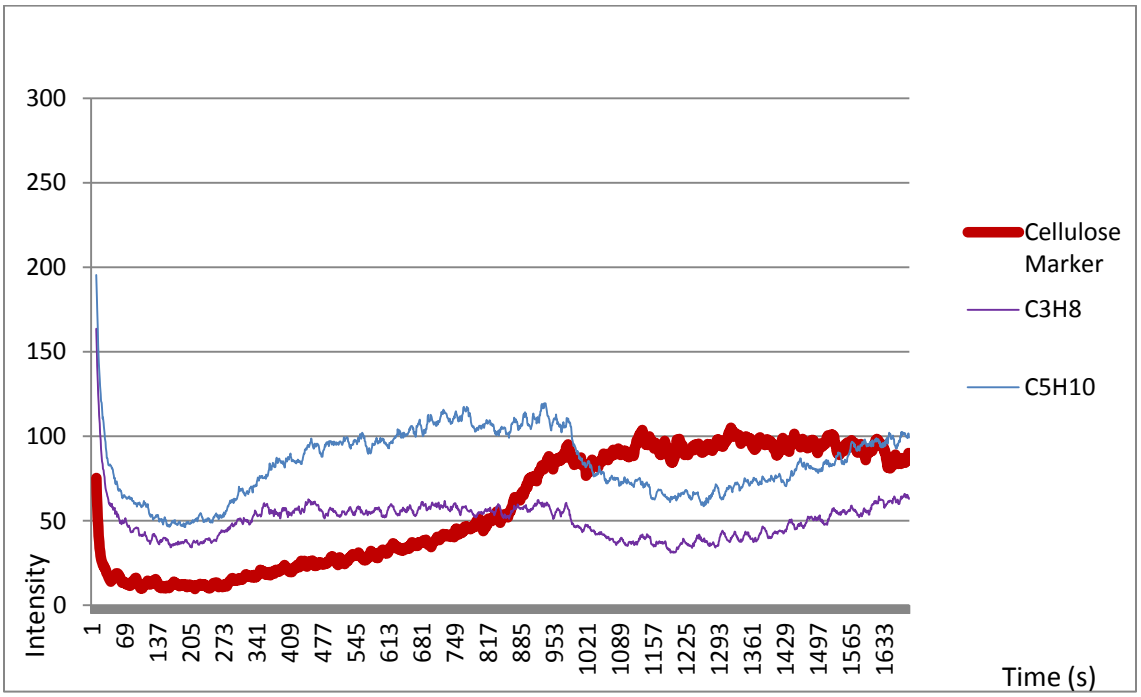

Figure 5.5 - Depth profile showing a comparison of group two of hydrocarbons with a cellulose marker.

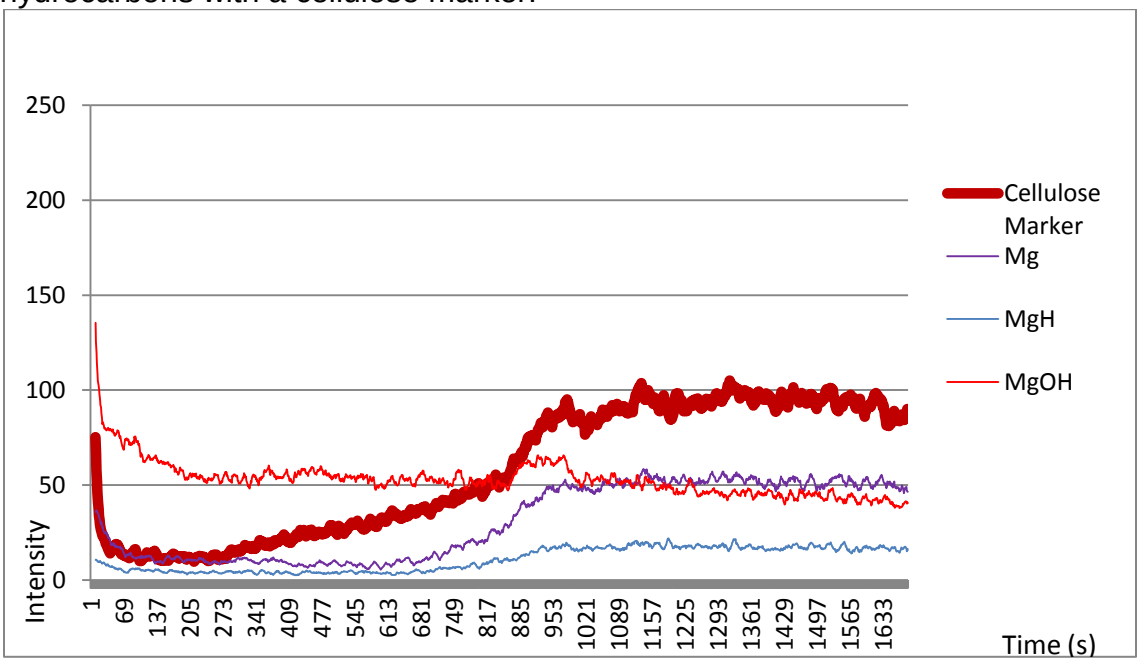

Figure 5.6 - Depth profile showing a comparison of magnesium containing species with a cellulose marker.

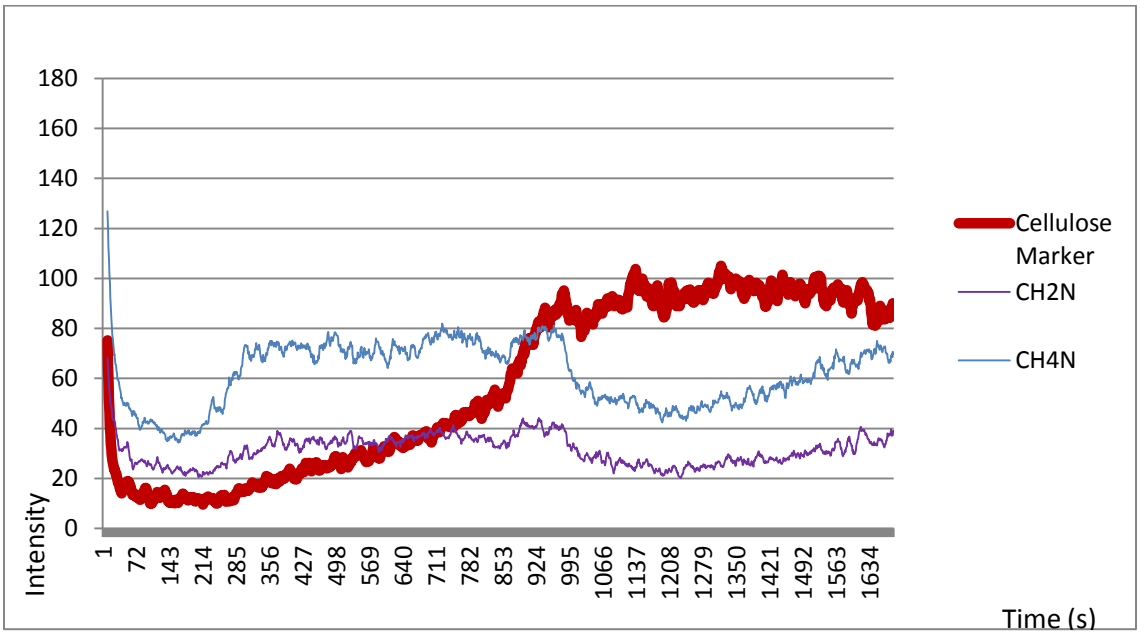

Figure 5.7 - Depth profile showing a comparison of nitrogen containing species with a cellulose marker.

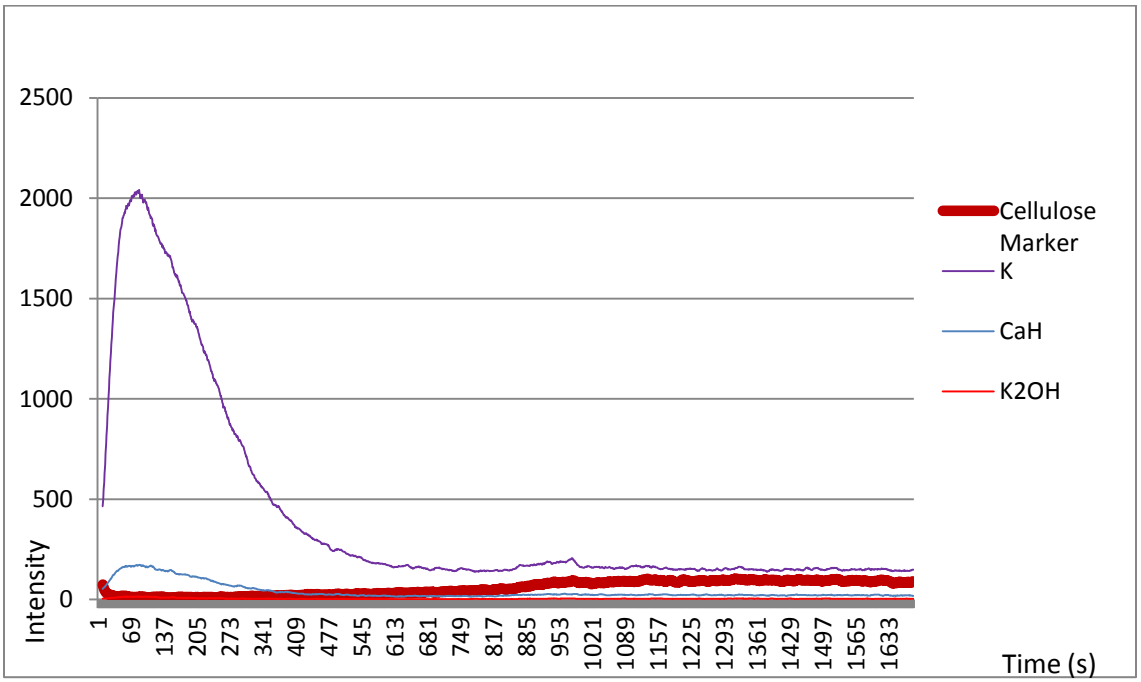

Figure 5.8 - Depth profile showing a comparison of potassium and a calcium containing species with a cellulose marker.

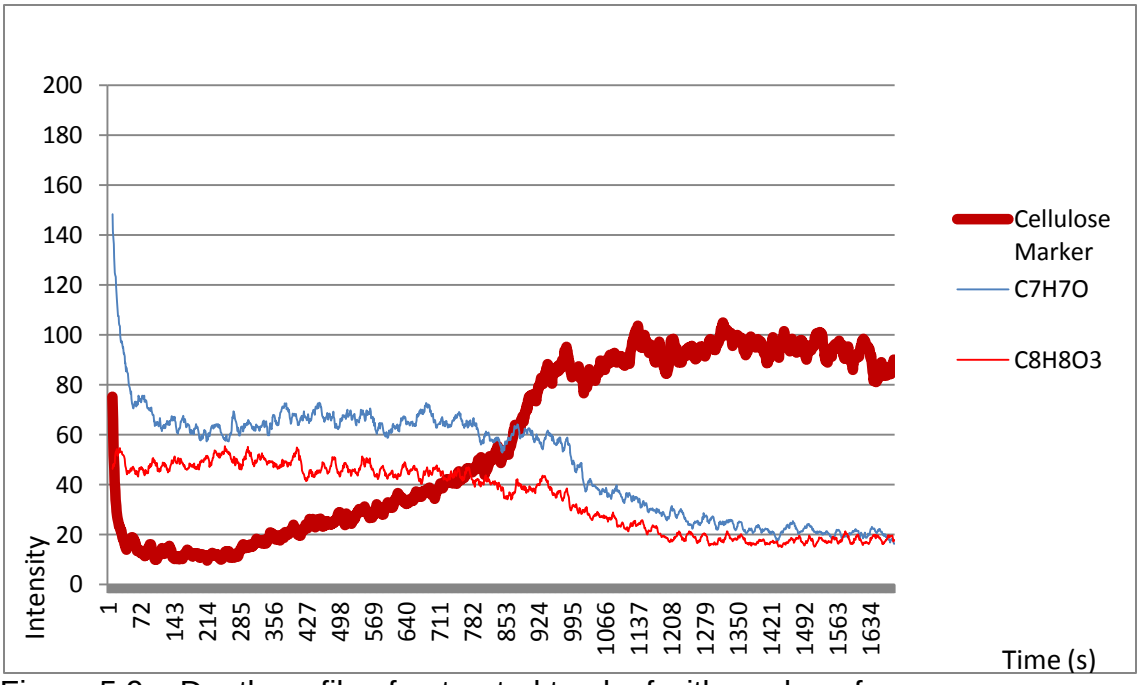

Figure 5.9 – Depth profile of untreated tea leaf with markers for aromas.

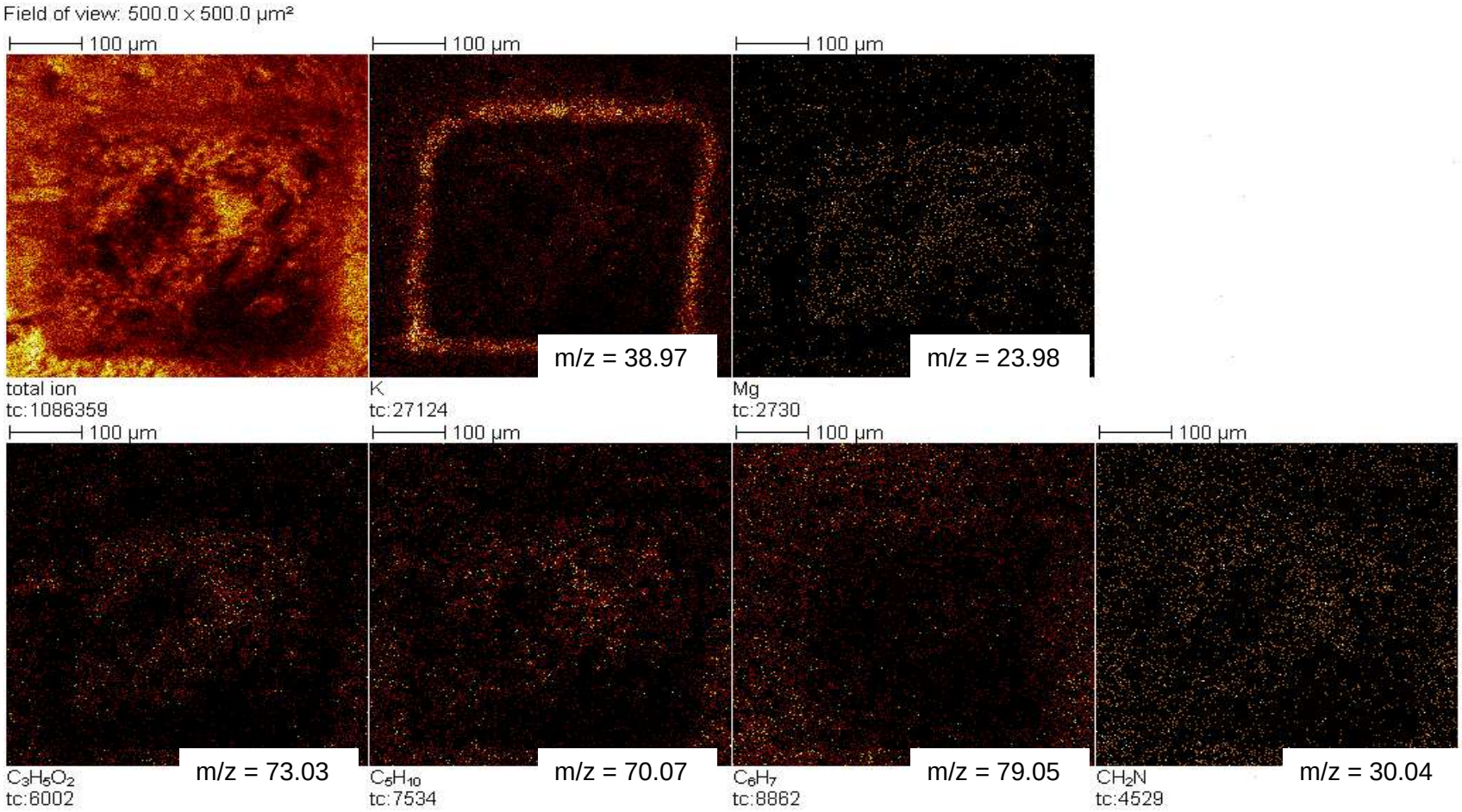

Figure 5.10 - Ion images showing examples of all groups identified on an untreated tea leaf after depth profiling.

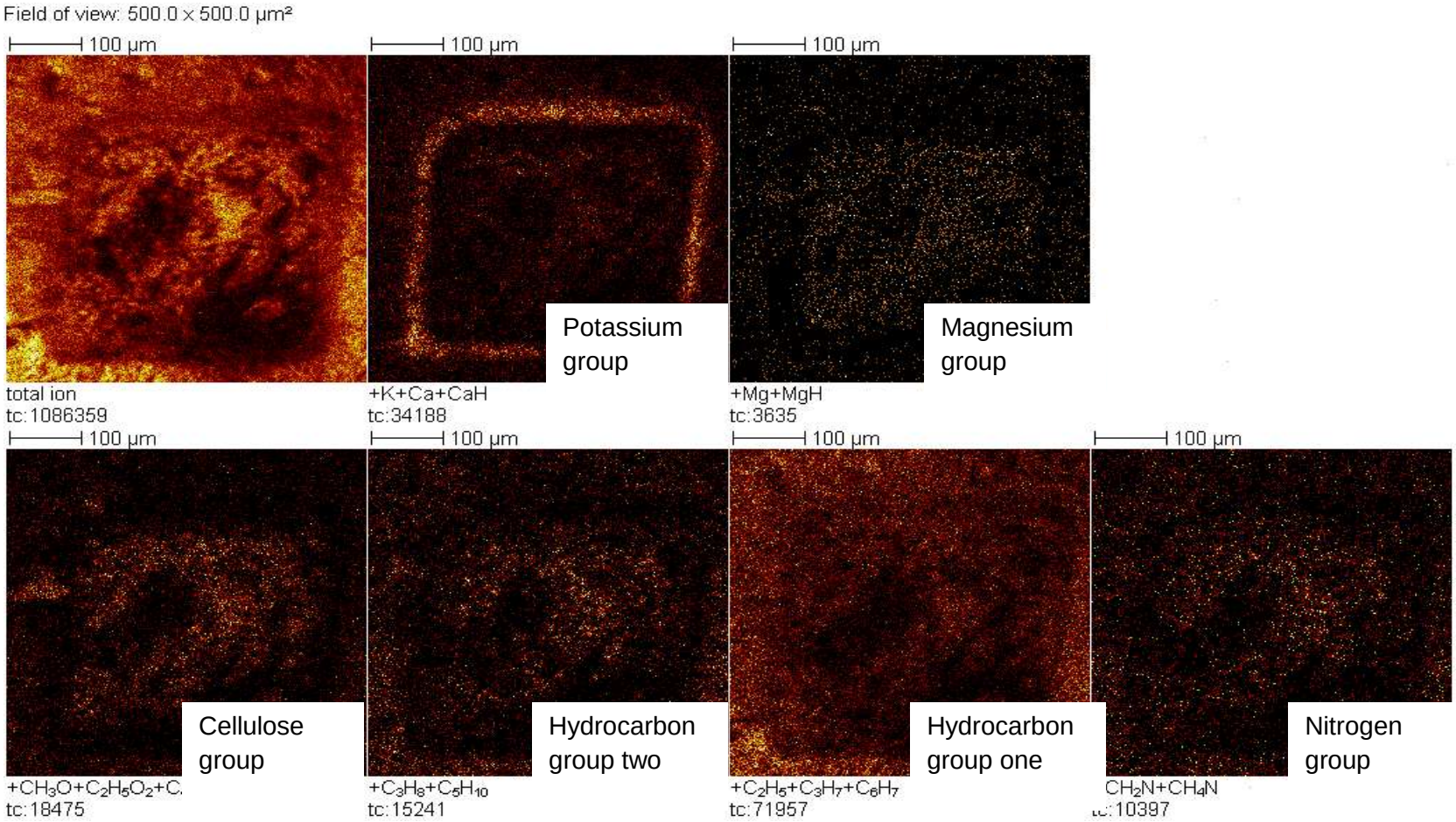

Figure 5.11 - Ion images showing composite images of all species identified on an untreated tea leaf after depth profiling.

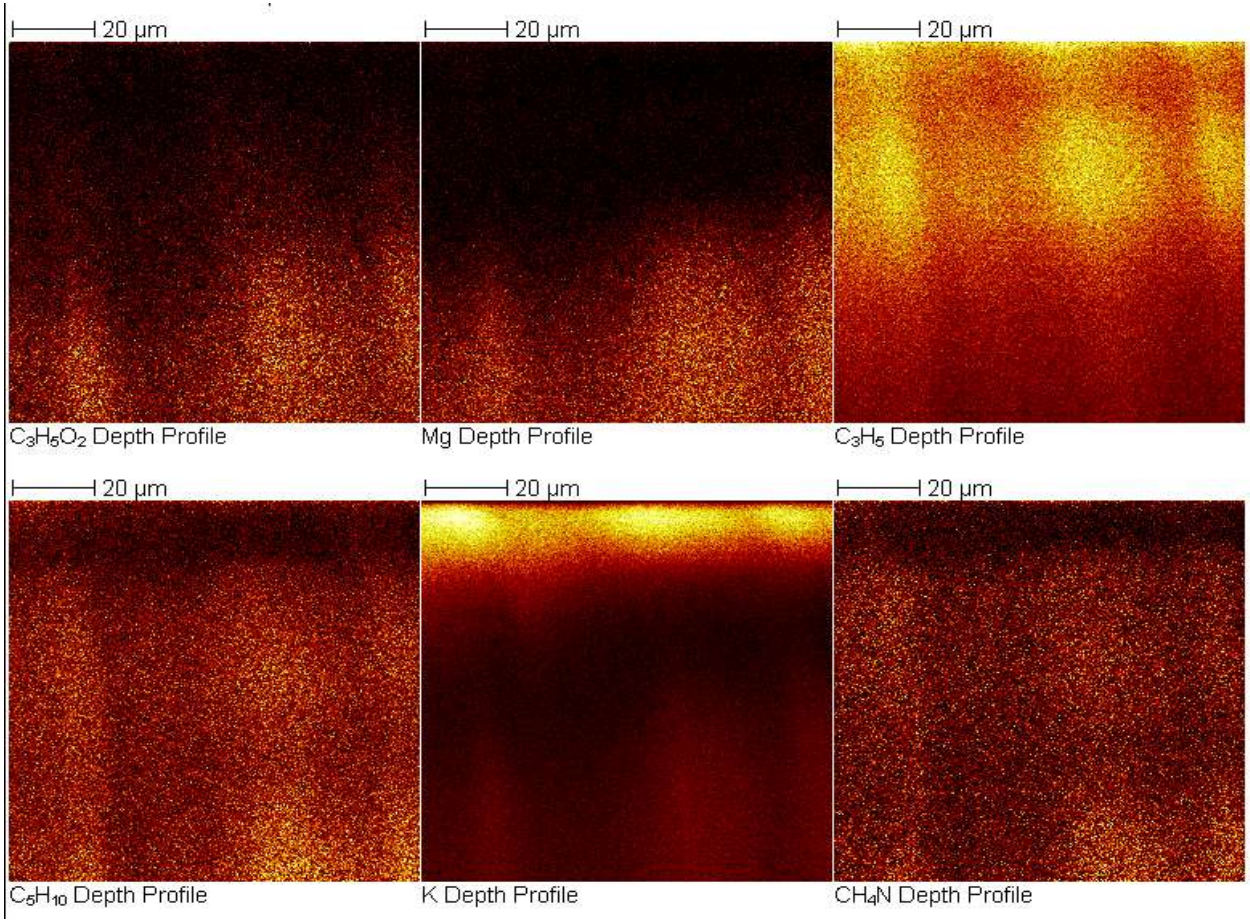

Figure 5.12 – XZ reconstruction of depth profile using markers previously described in the untreated tea data

5.3.2 Discussion of ToF-SIMS Depth profiling of untreated leaves

Figure 5.2 shows an overview trace of groups identified from the data set for a depth profile where the tea leaf has been left untreated. Because of the high intensity of the potassium peak when compared with the rest of the peaks identified on the depth profile, other traces have been masked. To compensate for this the data was broken down into groupings where they were compared with a known marker for cellulose, $C_3H_5O_2$. This marker was identified in the experiments detailed in chapter 4 as a fragment of cellulose. By comparing the traces for other elements and species with this marker an idea can be formed as to where in the leaf the element or species is appearing.

Initial comparisons were made with species thought to be present in cellulose with the $C_3H_5O_2$ fragment. Previous experiments of depth profiling with cluster ions on a cellulose based material were difficult. It had been shown that the use of the C_{60}^+ source in a depth profile of filter paper was able to produce a stable depth profile but this technique had never been published about on a leaf sample (Fletcher et al. 2006). In figure 5.3 it can be seen that with the exception of intensity the traces for CH_3O, $C_2H_5O_2$ and $C_4H_5O_2$ all follow the same trace pattern as $C_3H_5O_2$. The fragment of $C_4H_5O_2$ had been seen in the experiments with the filter paper. All of these species can now be used as a marker for the presence of

cellulose within the leaf. These species show a low intensity at the start of the trace, following the previously discussed drop, and then a sharp increase from around 850s. Given that cellulose will start to appear in the palisade mesophyll layer (see figure 1.7 in introduction) it can surmised that the depth profile has gone to level below the cuticle and upper epidermis. Any comparison between the levels of cellulose and any markers for aroma will be able to take this into account.

Two distinct groups of hydrocarbons were discovered during the depth profile measurements, namely hydrocarbon group one and two. In figure 5.4 the traces for markers of hydrocarbon group one are compared with the cellulose marker. It can be seen that there is a slight rise in intensity for C_3H_5 and a leveling off for C_3H_7 and C_2H_5. The intensity of all of these groups drops at approximately 967 seconds, after the depth profile has reached the palisade mesophyll layer indicating that this group of hydrocarbons are present in the cutin layer of the cuticle and also are present in the epidermis itself.

The second group of hydrocarbons are shown in figure 5.5 compared with the cellulose marker. These groups of C_3H_8 and C_5H_{10} show an initial decrease in intensity. The intensity starts to increase from approximately 250 s into the profile and then drops at approximately 967 s. The difference between hydrocarbon group two when compared to

hydrocarbon group one is that the intensity of these markers start to increase again at around 1250 s of profiling. As with the hydrocarbon group one markers they are present in the cuticular layer, the slight increase at 250 s could be an effect of the roughness of the interface between the cuticle and the epidermis. The increase after the known level of the palisade mesophyll layer could be an indication of either the depth profile reaching the spongy mesophyll layer or the presence of hydrocarbon containing features within the palisade mesophyll layer. Given that the structure of chlorophyll contains large molecular weight hydrocarbons, it is more than likely that the increase in these hydrocarbon groups is related to the distribution of the chlorophyll molecules in the palisade mesophyll layer.

The presence of magnesium and magnesium containing species were compared with the cellulose marker in figure 5.6. Magnesium is a component of chlorophyll. In most plants there are two types of chlorophyll present. Chlorophyll A, $C_{55}H_{72}O_5N_4Mg$, which is universal to all chlorophyll containing life forms and Chlorophyll B, $C_{55}H_{70}O_6N_4Mg$ which is specific to plants and not found in algae etc. Chlorophyll containing cells are not encountered in leaves until the palisade mesophyll layer which is below the upper epidermal layer and the cuticle. When the magnesium level in the depth profile rises then the depth achieved is to the palisade mesophyll layer. MgOH intensity generally decreases over the time of the

depth profile, with an exception of an increase from 870 s to 967 s, MgH and Mg show an increase in intensity from 691 s, the increase in intensity being much higher for Mg than MgH. With the presence of magnesium being detected in the depth profile and the fact that Mg and MgH increase when the depth profile reaches the palisade mesophyll layer, as shown by the cellulose marker, it can be seen that the cellulose marker is a good indication as to the depth reached in the profile.

The presence of nitrogen containing species was compared with the cellulose marker in figure 5.7. After an initial drop in intensity to 210 s the intensity of CH_2N and CH_4N increases and then drops again after 967 s of the trace. As with the first part of the trace for hydrocarbon group two this could be indicative of an increase in nitrogen containing groups in the epidermal layer as opposed to the cuticle. The presence of the nitrogen containing group's decreases after the trace reaches the palisade mesophyll layer but starts to increase as the trace progresses at around 1381 s. As the transport of minerals and fluids is through the xylem and phloem in the leaf structure this could indicate the closeness of the leaf transport system or the movement of nitrogen containing compounds through the leaf.

The majority of elements and species examined showed an initial decrease in intensity for the first 200 s of the depth profile trace, with potassium, CaH and K_2OH showing an initial increase in intensity to 70 s which then drops and plateaus at 565 s. This is shown in figure 5.8. The presence of potassium is interesting as it was one of the main elements that showed changes during the infusion time experiments of chapter 4. With the data of the depth profile it can be seen that the potassium is situated in the cuticle and epidermal layers of the leaf with a small amount in the palisade mesophyll layer and below.

Whereas the evidence from the experiments in chapter 4 indicated changes in potassium intensity when the leaves were infused, the evidence of the depth profile indicates the potassium is associated with the cutin layer.

With the identification of markers for the three different aromas, the depth profiles for the tea leaf fragments that had not been treated with aroma were re-examined to identify any of the markers (figure 5.9). No markers were found for linalool or trans-2-hexenal but two of the markers for methyl salicylate were found. C_7H_7O and $C_8H_8O_3$ were present on the untreated tea leaves but in a lower intensity when compared with figure 5.2. The tea leaf fragments were produced in the standard way, as previously

described, and the aroma cocktail was sprayed back onto the leaves. These were then stored in a foil container until experimentation. This means that the aroma methyl salicylate can be stay on leaf after respraying.

Figure 5.10 showed another capability of ToF-SIMS. As well as being able to produce spectra of the surface for the area being analysed it is also able to show an ion image, where each mass fragment can be spatially located on the leaf surface. This can be done for each main group identified in the depth profile analysis. The total Ion image (all mass data summed at each pixel) clearly shows the area of the depth profile analysis in the centre of the image. Potassium is seen at its most intense on the rim of the crater of the area of depth profile. This corresponds with the full depth profile with the highest point for potassium being between the cuticle and the palisade mesophyll layer. Magnesium and the marker for cellulose are observed in the centre of the depth profile confirming that the palisade mesophyll layer was entered during depth analysis. The marker for hydrocarbon group two and the nitrogen containing species show a presence both in the crater of the depth profile and the unablated surface. As the profile showed a high intensity on the surface and then an increased intensity in the palisade mesophyll layer this is to be expected.

Finally the marker for hydrocarbon group one is only detectable on the surface of the leaf that was unablated.

Analysis can be performed by adding ions and molecular species together to obtain a composite image of all the markers for each group (figure 5.11). The markers for potassium and calcium, when combined confirm their strongest presence on the rim of the crater as before. The markers for cellulose and magnesium again show the strongest intensity in the crater of the depth profiled region. Whilst previously the marker for hydrocarbon group two had a high intensity on both the surface and within the crater, here it can be seen to have a higher intensity within the crater of depth profiling. With the addition of all the images for hydrocarbon group two, this differentiation can be made.

Nitrogen containing groups were present in roughly the same intensity on the surface and in the depth profile crater whereas the markers for hydrocarbon group one are present in a high intensity on the surface of the leaf and only a lower intensity within the crater.

When the depth profile is examined in the Z axis, it can be seen where the species are occurring, figure 5.12. Though there is evidence of the

presence of $C_3H_5O_2$ and Mg in the start of the depth profile, the intensity of these species increases as the depth profile progresses. This correlates to the graphs of the depth profile in figures 5.3 and 5.6. The change in intensity for hydrocarbon group 1, C_3H_5, shows an initial large intensity which drops slightly to increase again and then a large decrease in the presence of this species as the profile continues. The decrease also correlates to the occurrence of the large increase in the intensity for Mg and $C_3H_5O_2$. Both C_5H_{10}, the marker for hydrocarbon group 2 and NH_4, the nitrate group marker behave in the same way. At the surface of the profile there is an initial large intensity. This decreases so an almost black line appears indicating very little of these two species. The intensity then increases again as the profile continue to a steady level. At the bottom right of these images there is a section of large intensity for both. This indicates that the hydrocarbon group 2 and nitrate groups may be related in structure to each other. Finally, the potassium marker shows a large intensity at the start of the profile which decreases rapidly. There is then a very minimal amount present which starts to increase as the palisade mesophyll layer is entered. It can be seen that interfaces between the groups are not a straight line, as expected due to the biological nature of the samples. For example, the potassium shows a larger variation between sections on the surface with thicker areas of high intensity. This variation would need to be considered with the results for when aromas are added to the leaves.

When a depth profile has been performed it is usual to measure how deep the depth of the crater created is so as to ascertain the sputter rate. This can for example be performed with an AFM. From this measurement the scale of the depth profile would be changed to nanometres instead of time taken. Given the rough topography of the leaves, as previously discussed in chapter four, this wasn't possible even though it was attempted. The areas of the depth profile were not visible on the AFM instrument and a wide scan of areas on the leaf was not possible. An alternative method to the use of the AFM to obtain this data would be the use of an optical profileometer. This method of profiling a surface is in a non contact regime; this allows the scan of the surface to be much faster than with a stylus (as in standard profileometry) or a cantilever in AFM. As well as a speed advantage there is no chance of damage to the optics from the scan as can happen with cantilevers and tips. Though this technique is possible it was not used on these samples, hence the depth profile is referred to in time units.

5.3.3 ToF-SIMS Depth profiling results of leaves with methyl salicylate added

Figure 5.13 is the positive spectra obtained from a sample of methyl salicylate on aluminium foil. Figure 5.14 shows an overview example of the surface mass spectra obtained when examining a leaf which had been infused with the aroma, methyl salicylate. Whereas the data in figure 5.2 showed an initial drop in intensity for all species with the exception of potassium, here there is an initial drop in intensity with potassium as well.

Hence the peaks for hydrocarbon group one is of a high enough intensity to be examined directly. Figure 5.15 shows the markers for the aroma methyl salicylate when compared to a known fragment of cellulose, $C_3H_5O_2$. With the strength of intensity for the potassium fragment and the marker for hydrocarbon group one being so intense initially, figure 5.16 shows the depth profile with these groups removed so a clearer understanding of the positioning of the species identified can be seen.

Figures 5.17 and 5.18 show the Ion Images created from the ToF-SIMS instrument after the depth profile was complete. Figure 5.17 shows the markers that were used for figure 5.15 and their positioning on the depth profile and around it. Figure 5.18 shows a composite of all species identified in each group to show a clearer image of the surface after the depth profile. The IonImage XZ reconstructions of the markers for methyl

salicylate are shown compared with the cellulose marker in figure 5.19. The markers for the potassium, nitrate, magnesium and both hydrocarbon groups are shown in figure 5.20 compared with the cellulose marker.

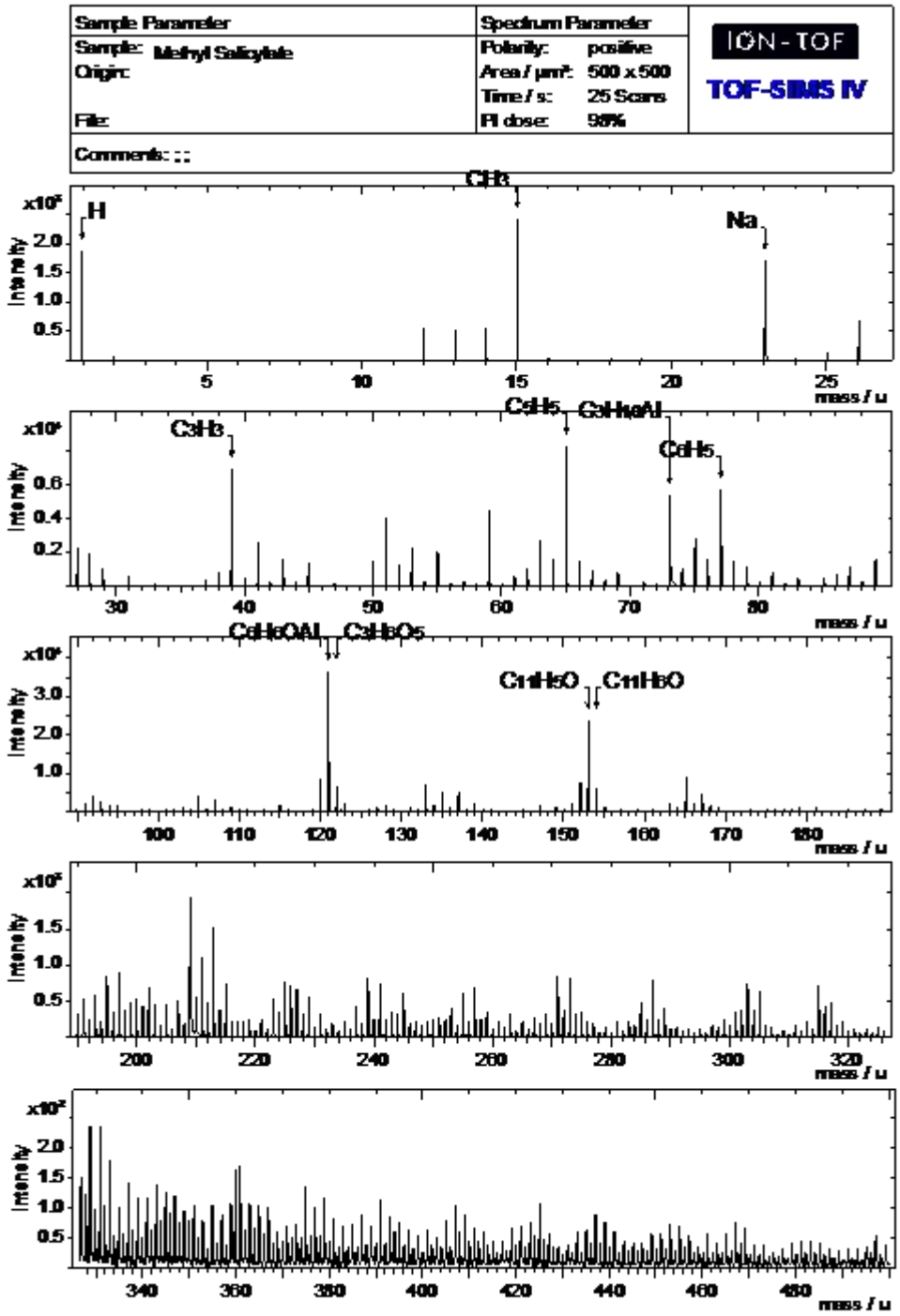

Figure 5.13 – Spectra (positive) for sample of methyl salicylate on aluminium foil.

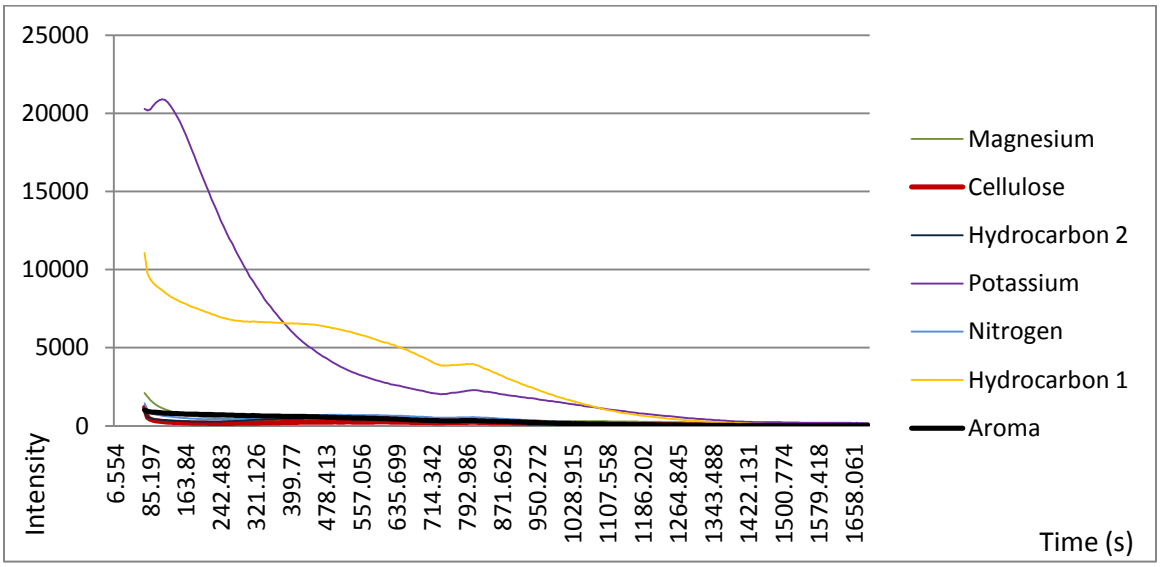

Figure 5.14 - Example trace for depth profiling of a tea leaf infused with methyl salicylate.

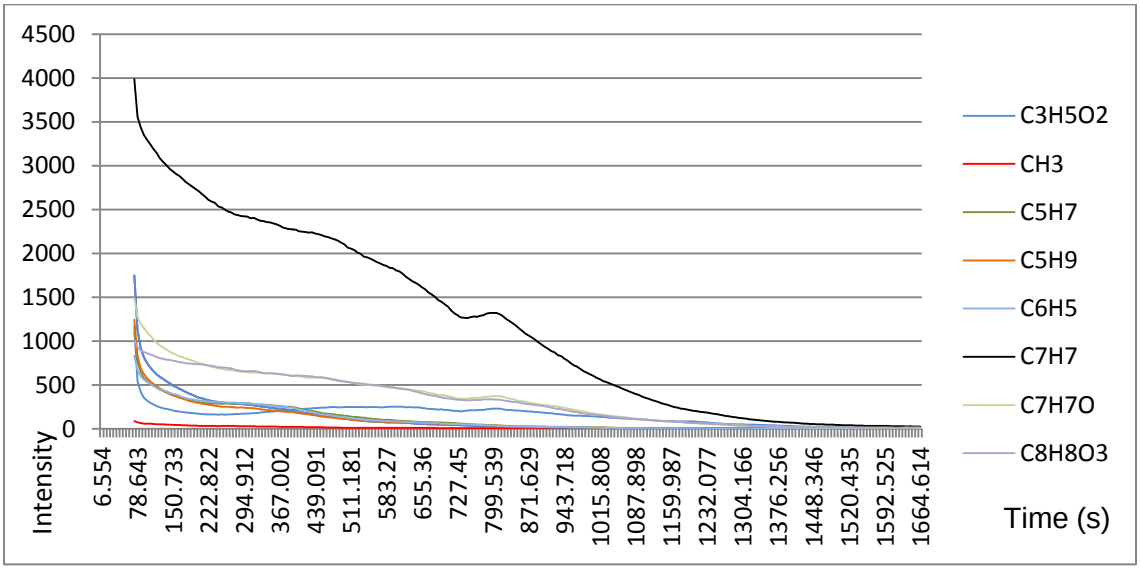

Figure 5.15 - Depth profile of markers for methyl salicylate when compared to other possible fragments of cellulose.

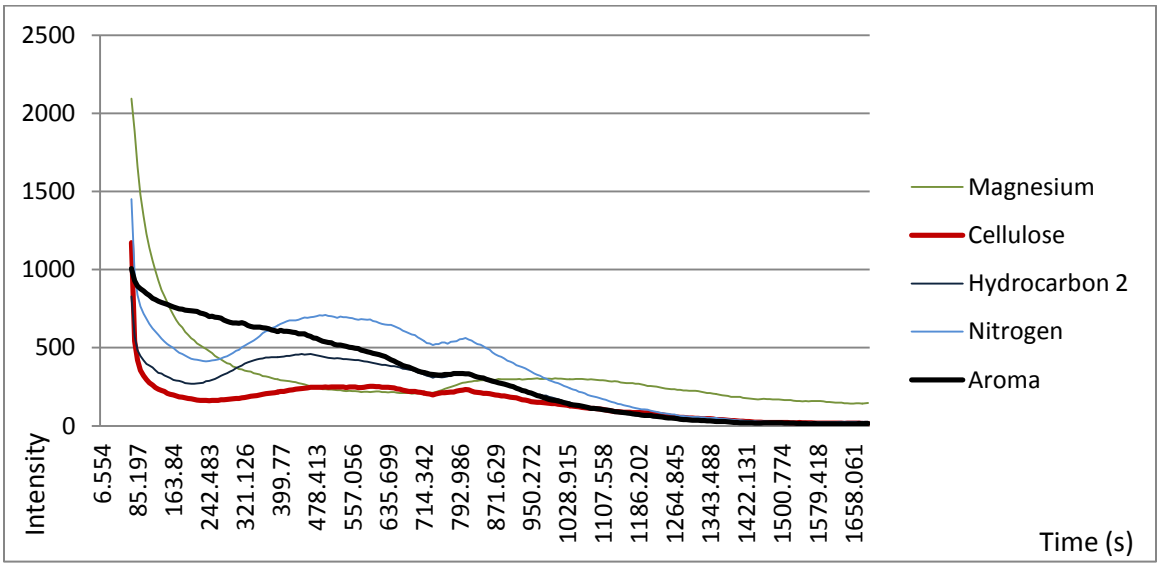

Figure 5.16 - Depth profile showing a comparison of examples of all species except potassium and hydrocarbon group 1.

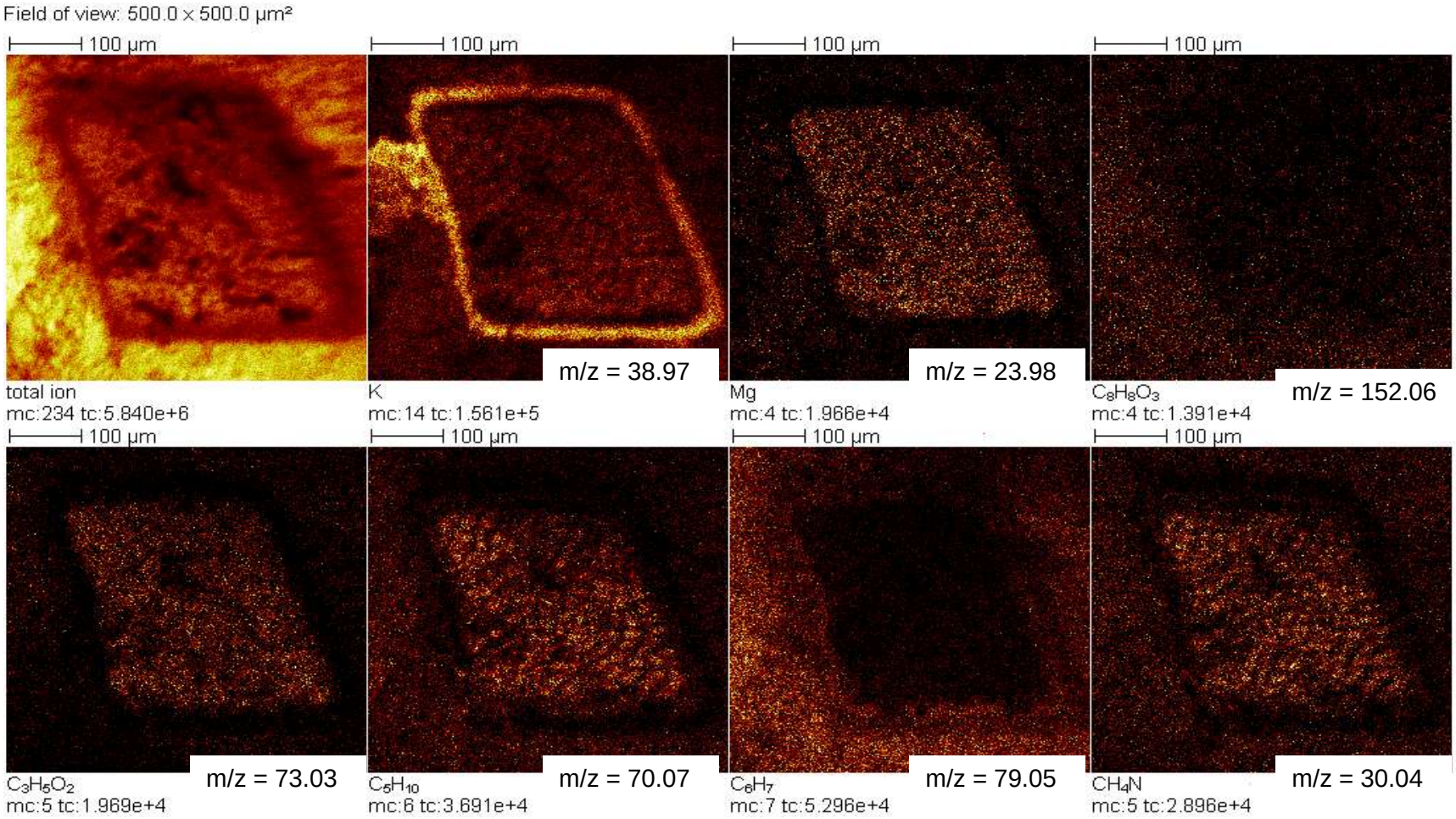

Figure 5.17 - Ion images showing examples of all groups identified on a leaf treated with methyl salicylate after depth profiling.

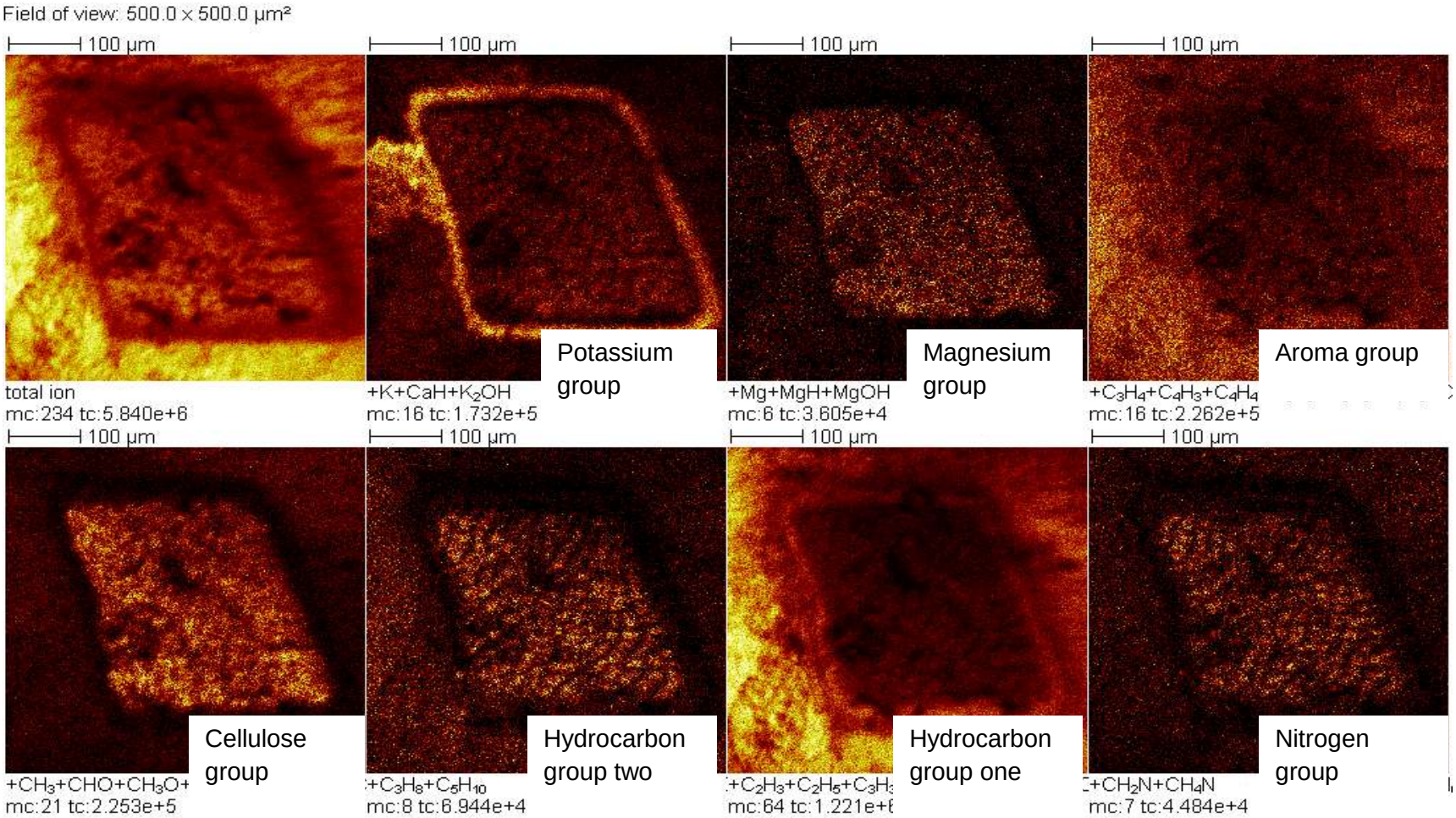

Figure 5.18 - Ion images showing composite images of all species identified on a tea leaf treated with methyl salicylate after depth profiling.

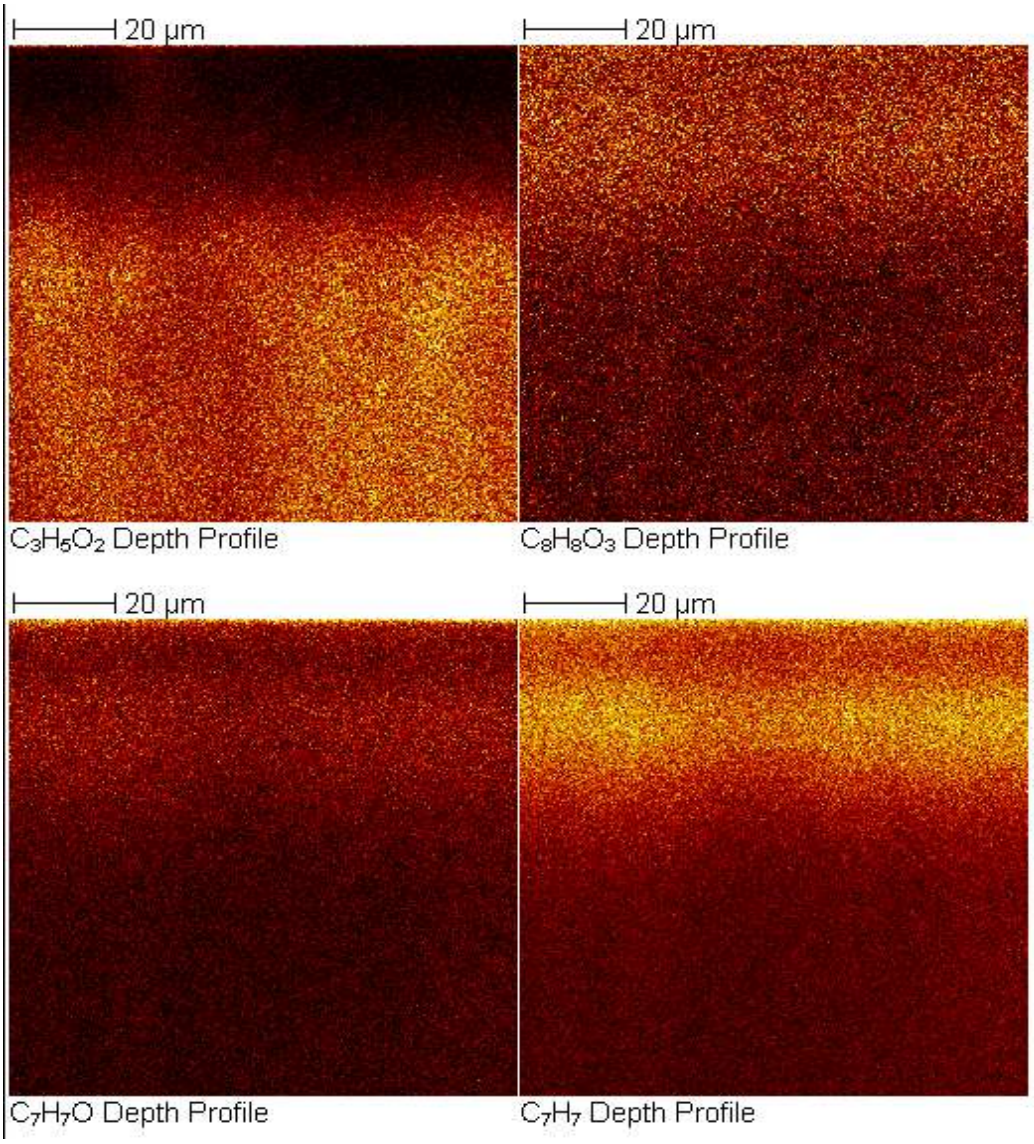

Figure 5.19 - Ion images showing XZ reconstruction of ions identified as being markers for methyl salicylate compared with cellulose marker.

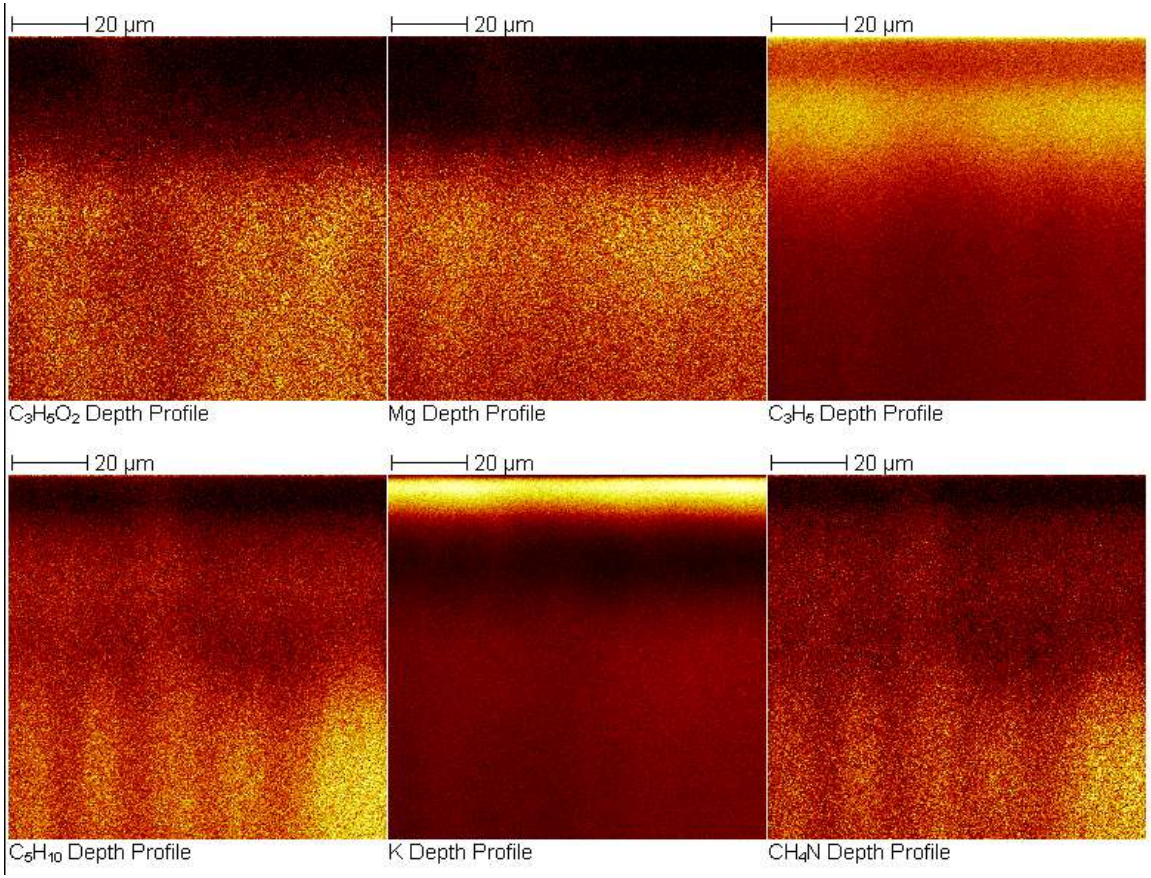

Figure 5.20 - Ion images showing XZ reconstruction of ions identified as being markers for other groups identified on tea leaves for a tea leaf treated with methyl salicylate.

5.3.4 Discussion of ToF-SIMS Depth profiling of leaves with methyl salicylate added

After depth profiling the tea that had no aroma added to the surface, tea leaves with aroma were examined using the same conditions. In figure 5.14 the overall trace for a tea leaf with methyl salicylate added shows the different groups that were present and identifiable by similar trace patterns, as with figure 5.2. Because of the high intensity of the potassium example peak the traces for the other species have been masked. Again the cellulose marker of $C_3H_5O_2$ was used as a comparison.

Markers for the aroma methyl salicylate were found and are displayed in figure 5.15. As well as being able to detect the presence of the molecular ion of the aroma itself, $C_8H_8O_3$, markers at C_7H_7O, C_7H_7, C_6H_5, C_5H_9, C_5H_7, C_3H_7, C_2H_5 and CH_3 were also present. The spectra was examined for the possibility of other fragments of the aroma but the deviation in ppm was too high to confirm the presence of C_6H_7O, C_7H_5O and $C_7H_5O_2$. After the initial dip of the trace at 100 seconds, the presence of the aroma continued to reduce until a time of 240 s and then there was an increase. This increase lasted to approx 560s and then there was a steady decrease in the presence of all markers. The time of 560 s is interesting as the presence of the cellulose marker showed a marked increase from this

time. This would indicate that the aroma had been present on the cuticle of the leaf and had also managed to penetrate through the cuticle to the upper epidermis of the leaf. When the cellulose increased, the trace for the aroma decreased indicating some aroma was present, but at a lower intensity than in the upper epidermal layer. The decrease in intensity means that the aroma has been able to penetrate the cuticle and the upper epidermis.

Given the strength of the intensities for the potassium marker and hydrocarbon group one marker, figure 5.16 shows what is occurring in the depth profile with these two markers removed.

Figure 5.17 shows the ion image for an example of each of the markers for the 7 different groups already mentioned. The marker for the aroma, $C_8H_8O_3$, and hydrocarbon group one, C_6H_7, can be seen to be brighter on the surface of the leaf and not in the depression caused by the depth profile. Potassium is brightest on the interface between the area of depth profile and the surface at the interface of etching. All of the other groups are brighter within the area where the depth profile occurred. Figure 5.18 shows an amalgamation of all the markers that were identified within the depth profile for the different groups already mentioned. Again the aroma markers and those for hydrocarbon group one is brighter on the surface of the tea leaf as opposed to the area of depth profiling. The magnesium

group, nitrogen containing group, cellulose group and hydrocarbon group two are brightest within the area of depth profiling and the image appears to show a delineation of the cells within the leaf at this level of the depth profile. Again the potassium grouping shows a brighter signal on the edge of where the depth profile occurred indicating it has a stronger intensity within the layers between cuticle and palisade mesophyll layer.

Figure 5.19 shows the depth profile of the methyl salicylate markers compared with $C_3H_5O_2$ in the Z (height) direction. All three of the markers show a higher intensity before the palisade mesophyll layer is reached but there are still signs that the aroma has reached into palisade mesophyll. The intensity of the markers all show an even spread through the trace in the xy direction. The diffusion of the aroma seems to have concentrated it at the cuticle and the bottom of the upper epidermal layer whilst there is still penetration through to the palisade mesophyll layer.

Figure 5.20 shows the IonImage reconstruction of the depth profile for examples of the other groups identified for the untreated tea leaves. The distribution of these groups corresponds with figure 5.14.

As discussed in the introduction the cuticle of the leaf is composed of an insoluble membrane which is surrounded and impregnated with soluble cuticular lipids, often referred to as cuticular waxes. The best known component of the cuticular membrane is cutin. In effect the cuticle can be

seen as a polymeric lipid membrane. The sorption capacity of the lipophilic compounds has been show to be high in experiments (Riederer et al. 1984; Riederer et al. 1985).

As the aroma is mixed with water the transport of the aroma molecules into the leaf must occur by diffusion through the cuticular membrane. With the electron micrographs shown in chapter 3, the effect of the processing of the tea leaves must also be considered. Though the samples used were examined for damage to the cuticle there is a possibility that there are tears in the cuticle that would have allowed the diluted aroma through to the epidermis and then further diffusion into lower layers of the leaf could occur. As methyl salicylate has a K_{ow} >1 then it is expected that it will be able to pass through the cutin layers in the cuticle and surrounding the epidermal cells.

As the amount of diluted aroma, 1 µl, was small and was left for 24 hours before experimentation, evaporation of the water would occur leaving the aroma on the surface. If there was any transport of the aroma past the cuticle of the leaf then there would be a measurable intensity as the depth profile occurs. The longer the time of the depth profile than the deeper it goes.

The markers for methyl salicylate do show a high intensity on the surface of the leaf indicating that the evaporation of water has left some of the aroma on the surface. There is also a high intensity at the interface between the epidermal layer and the palisade mesophyll layer (indicated by the increase in intensity of $C_3H_5O_2$). This shows that the aroma has been able to penetrate the epidermis of the leaf and has started to diffuse through to the palisade mesophyll layer. Though the intensity is lower for the aroma markers in the palisade mesophyll layer it can be seen that the aroma has diffused through to it. As the epidermal cells can be covered in cutin to help prevent water loss, the high intensity of the aroma markers in the epidermis of the leaf could indicate that there is another membrane like barrier that the aroma must diffuse through to reach the lower layers. As a small amount of diluted aroma had been used for the experiments there is also the possibility that with more of the dilute aroma added there would have been deeper penetration through the dehydrated leaf before the water containing the aroma evaporated.

Methyl salicylate has two functional groups, an ester and an alcohol group. The size of the molecule and the reactivity with itself must also be taken into account. A smaller lipophilic molecule will pass through the cuticle more easily than a large molecule. Methyl salicylate is a large molecule in relation to trans-2-hexenal, it contains a carbon ring and the functional ester and alcohol groups can bond with other molecules of methyl

salicylate (Aparicio et al. 2010). This doubling of the size of the molecule which may cause difficulties in the diffusion of the aroma through the cutin layers. As methyl salicylate is not very water soluble there would be a lower concentration of molecules that have been dissolved in solution which leads to a lower sorption through the cuticle (Kerier et al. 1988; Buchholz et al. 2006; Schreiber et al. 2006). By dissolving the aroma in either ether or glacial acetic acid and applying this to the leaf, further penetration could be observed.

Confirmation of the depth profile is similar to the depth profile for untreated leaves is shown in figure 5.20 when the cellulose marker is compared with the magnesium, potassium and nitrogen containing species and markers for hydrocarbon groups 1 and 2. The profile corresponds with what had been seen in the samples of untreated leaves indicating that the addition of the aroma did not have an effect on the other groups seen.

5.3.5 ToF-SIMS Depth profiling results of leaves with trans-2-hexenal added

The same experiment was repeated for leaf samples that had been treated with trans-2-hexenal. The positive spectra for the aroma on aluminium foil is shown in figure 5.21. Figure 5.22 shows the depth profile with examples of each group identified. The intensity for the peaks for hydrocarbon group one and potassium are higher than the other groups as with the example

depth profile for methyl salicylate infused leaves which masks the depth profile for the aroma molecule.

Figure 5.23 shows the identification of markers for the aroma trans-2-hexenal when compared with a marker for cellulose. This was to correlate the depth at which the aroma pentrated the leaf structure. The cellulose marker was $C_3H_5O_2$. As the intensity for the potassium and hydrocarbon group one markers were so high another overview of the group markers can be seen in figure 5.24 so an overall view of the depth profile of the leaf can be seen.

From the information gathered from previous depth profiles an estimation of the actual layers seen as the depth profile occurs is shown in figure 5.25.

Figures 5.26 and 5.27 show the Ion images for the leaf fragment treated with trans-2-hexenal. An initial image of examples of the different groupings found on the leaf is shown in figure 5.26 and composite images of the species that make up the groups are shown in figure 5.27.

An IonImage XZ reconstruction of the markers for trans-2-hexenal is shown compared with the cellulose marker in figure 5.28. The markers for

the potassium, nitrate, magnesium and both hydrocarbon groups are shown in figure 5.29 compared with the cellulose marker.

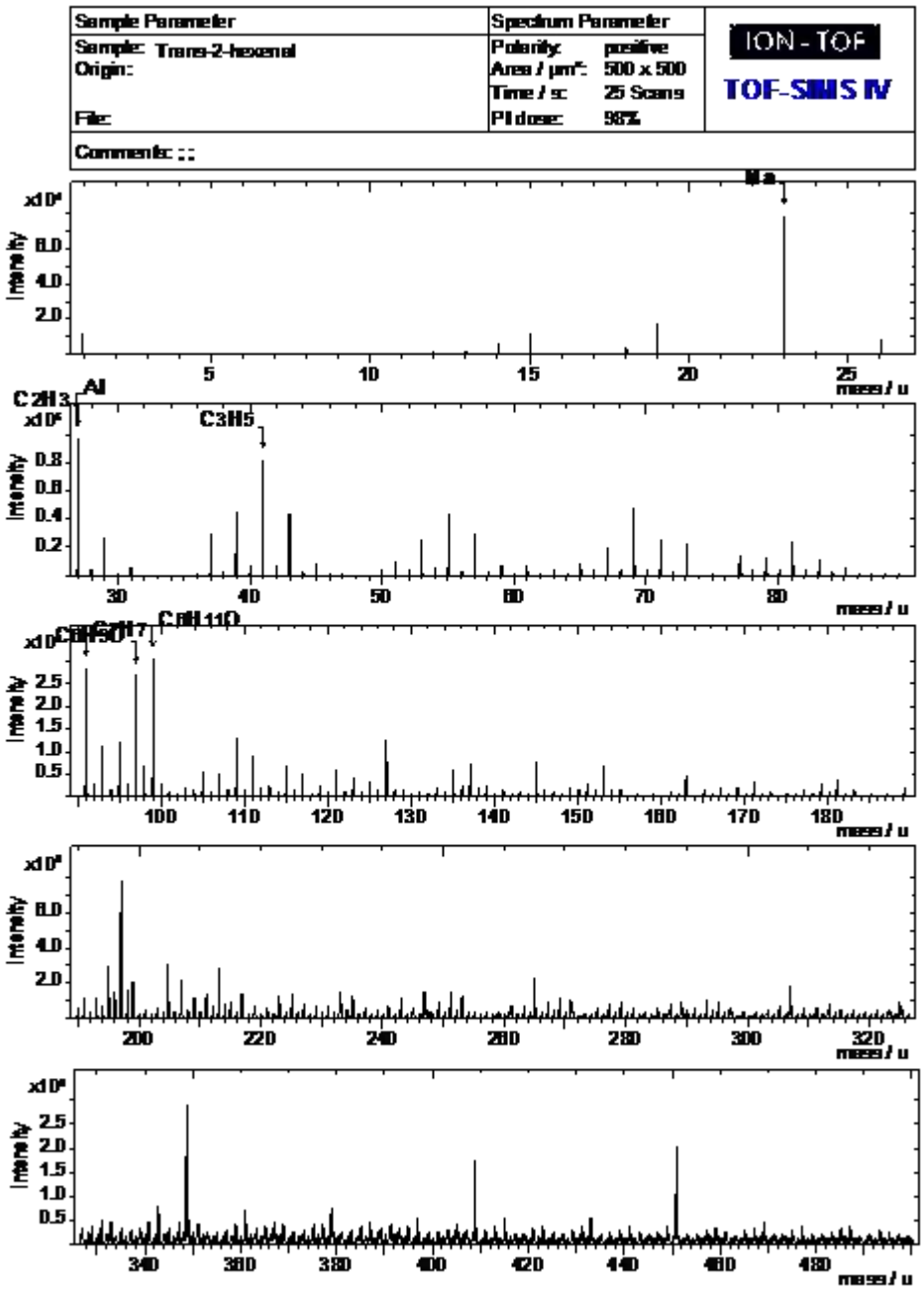

Figure 5.21 – Spectra of sample of trans-2-hexenal on aluminium foil.

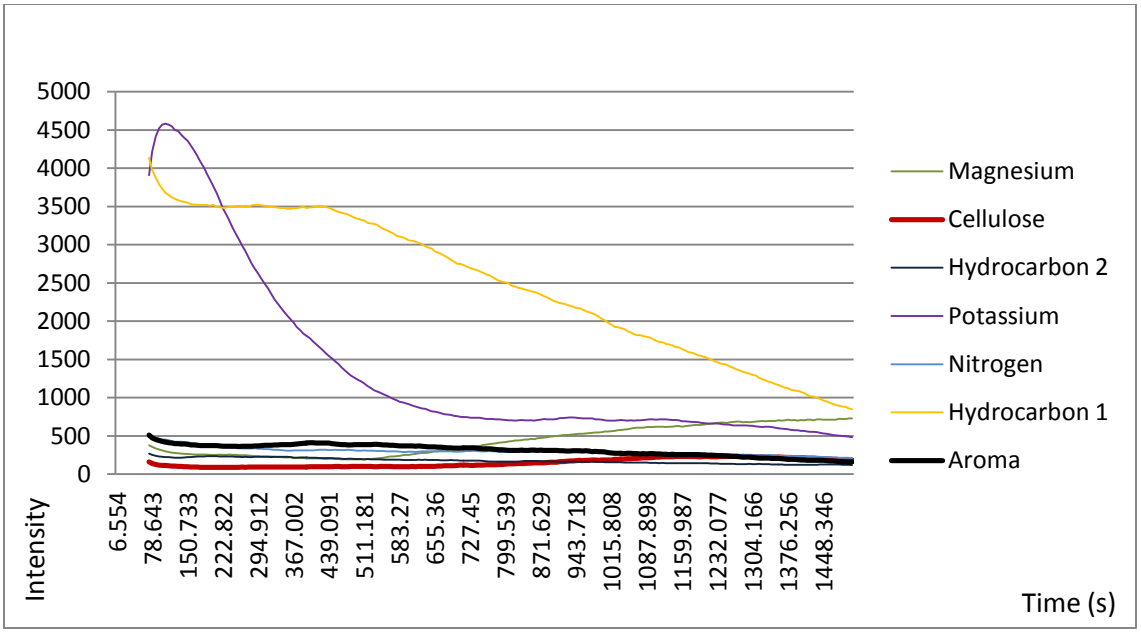

Figure 5.22 - Example trace for depth profiling of a tea leaf infused with trans-2-hexenal.

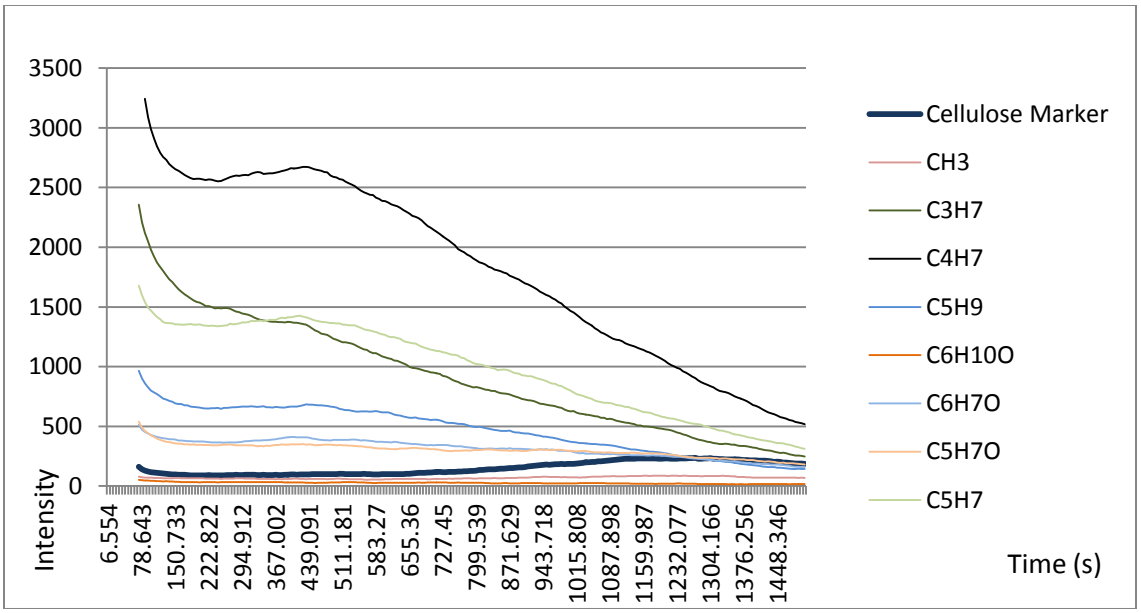

Figure 5.23 - Depth profile trace of markers for the aroma trans-2-hexenal when compared with a marker for cellulose.

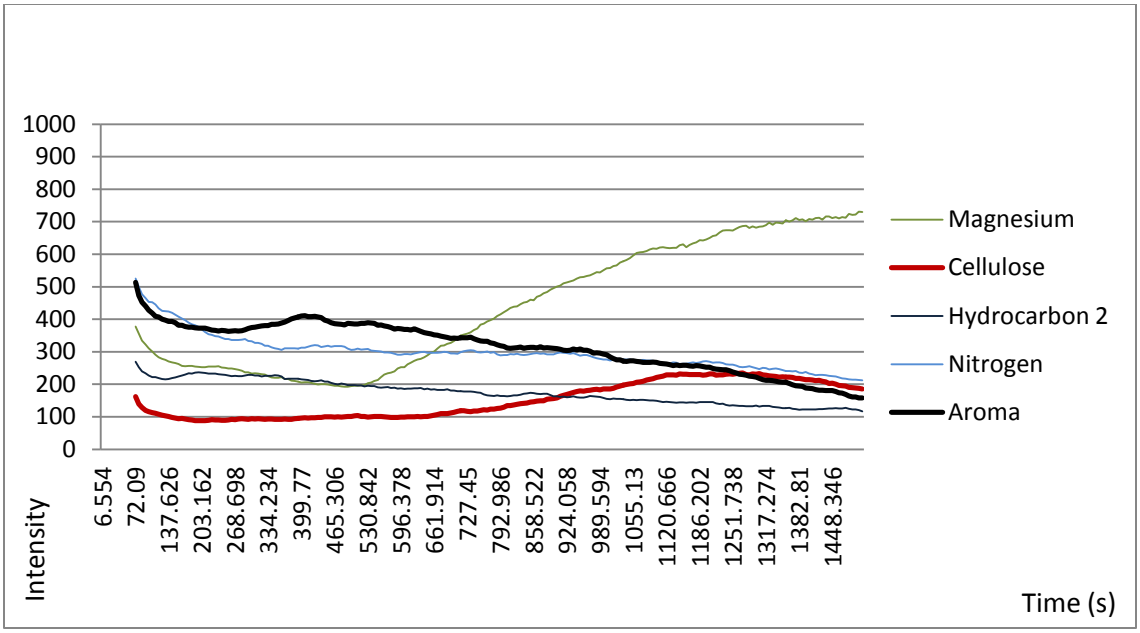

Figure 5.24 - Depth profile showing a comparison of examples of all species except potassium and hydrocarbon group 1.

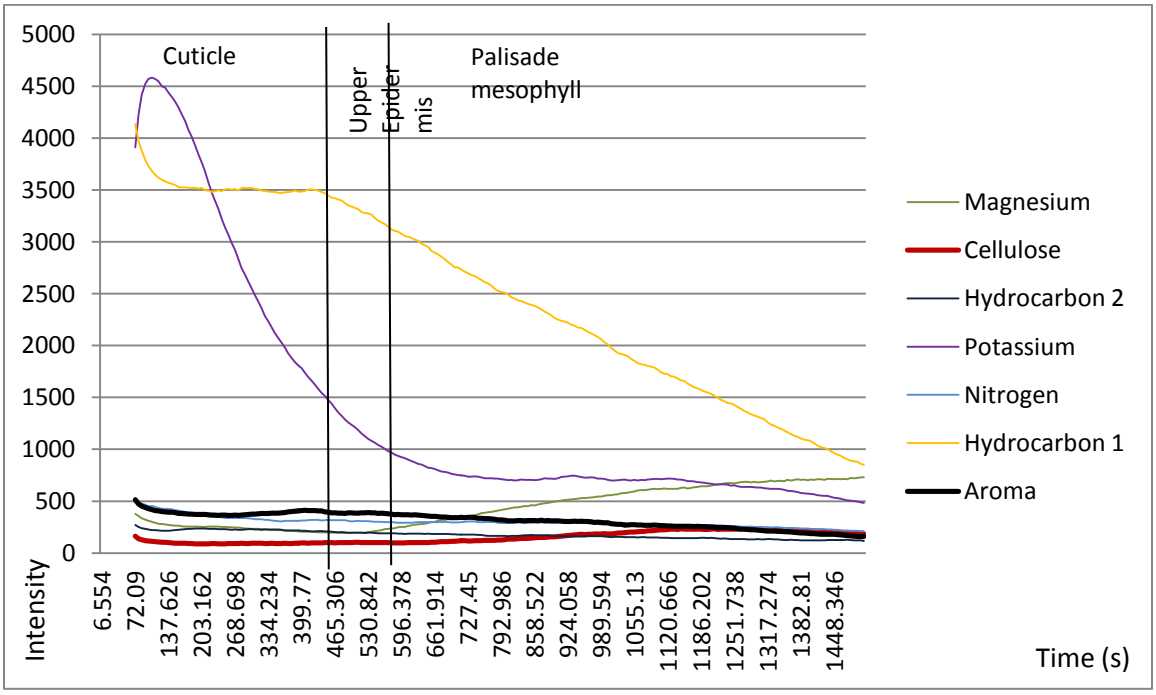

Figure 5.25 – Annotated depth profile of tea leaf treated with trans-2-hexenal to indicate the interfaces of the different layers of the leaf.

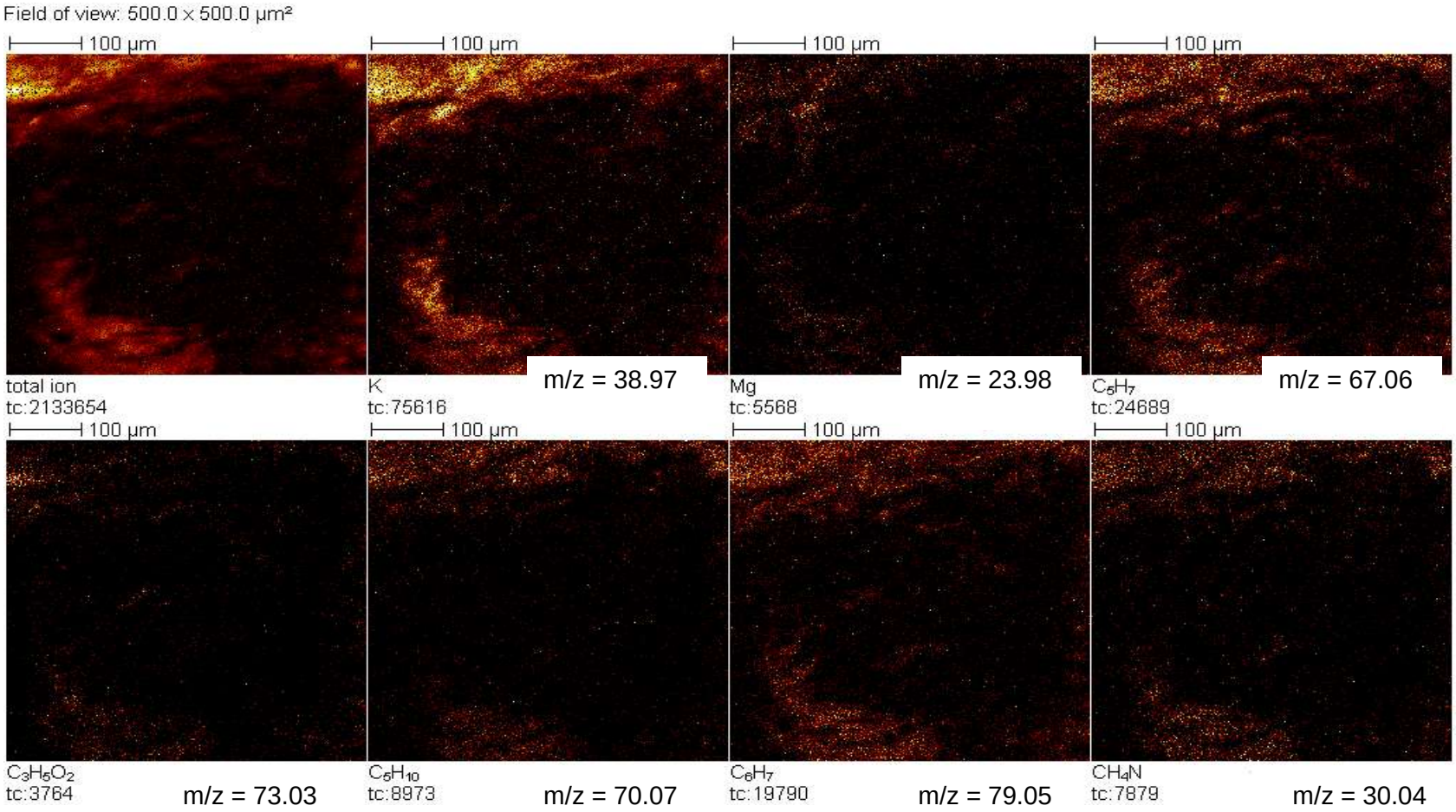

Figure 5.26 - Ion images showing examples of all groups identified when trans-2-hexenal is added to the surface of the leaf after depth profiling.

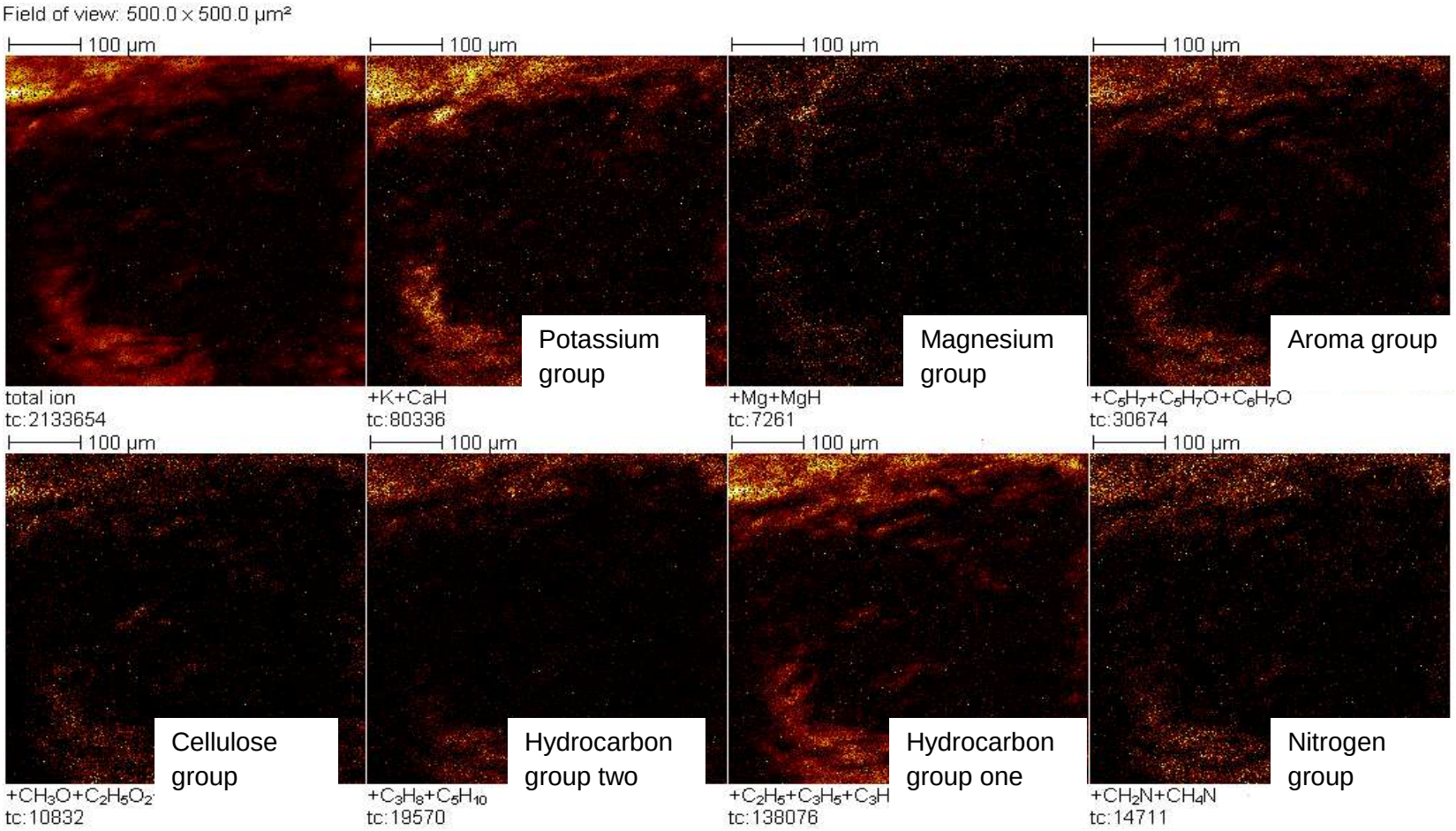

Figure 5.27 - Ion images showing composite images of all species identified when Trans-2-hexenal is added to the surface of the leaf after depth profiling.

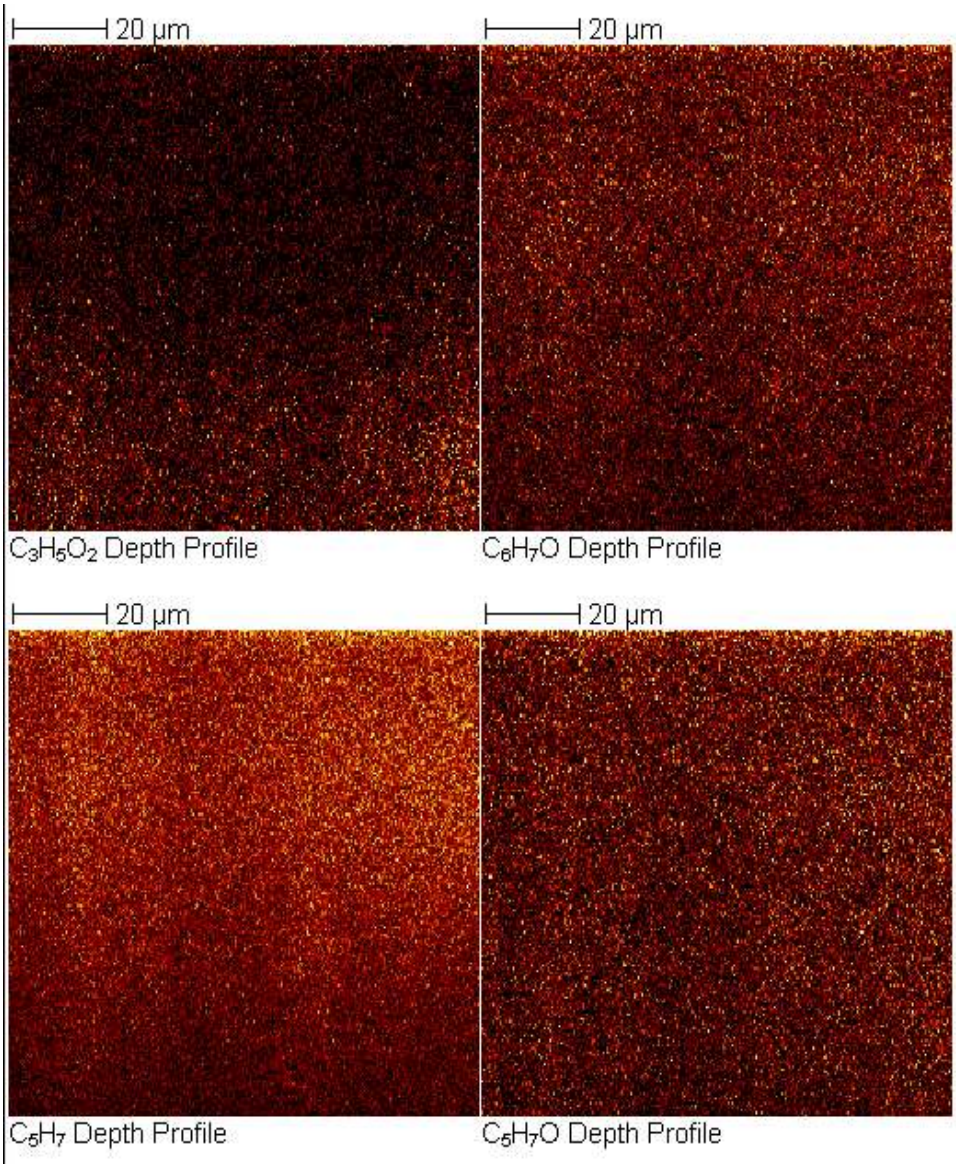

Figure 5.28 - Ion images showing XZ reconstruction of ions identified as being markers for trans-2-hexenal compared with cellulose marker.

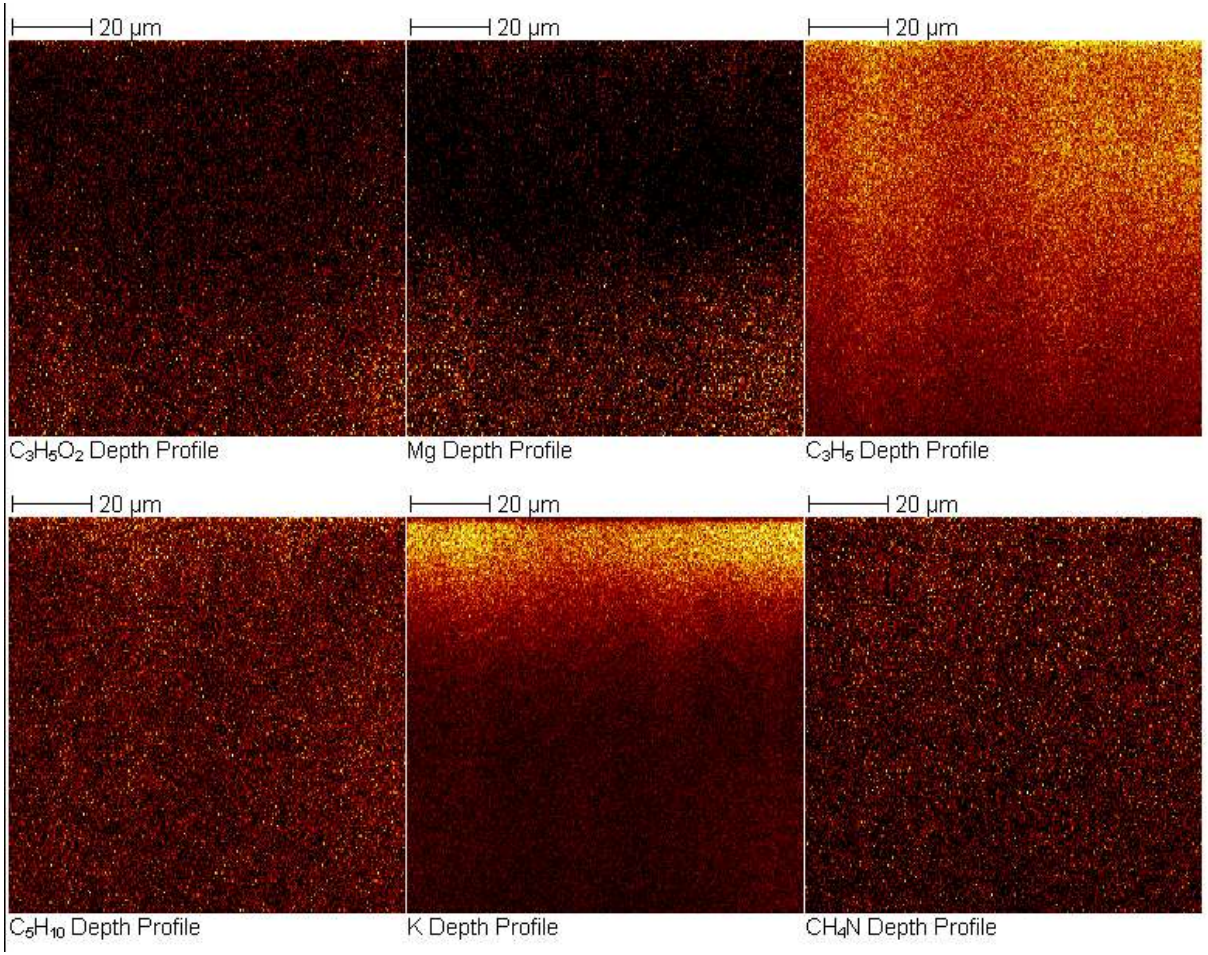

Figure 5.29 - Ion images showing XZ reconstruction of ions identified as being markers for other groups identified on tea leaves for a tea leaf treated with trans-2-hexenal.

5.3.6 Discussion of ToF-SIMS Depth profiling results of leaves with trans-2-hexenal added

Figure 5.22 shows the overview trace of the depth profile. As with the previous overviews, figures 5.2 and 5.14, the markers for potassium and hydrocarbon group one are of such a high intensity that they mask detail within the depth profile.

When the aroma Trans-2-hexenal was added, figure 5.23, possible markers were found for it, CH_3, C_3H_7, C_4H_7, C_5H_7, C_5H_9, C_5H_7O, C_6H_7O and $C_6H_{10}O$ were seen to decrease in intensity from 399 s, before the cellulose marker of $C_3H_5O_2$ increased in intensity from approximately 635 s into the depth profile. This would show that the aroma was adsorbed to the surface of the cuticle and had diffused into the epidermal layer of the leaf. With the decrease in intensity it can be seen that some aroma had diffused into the palisade mesophyll layer.

Figure 5.24 shows an overview of the depth profile with the markers for hydrocarbon group one and potassium removed. As with the depth profile for methyl salicylate, the marker for magnesium and cellulose increase from approximately 635 s into the depth profile. The presence of the aroma decreases with time but it is not a slower decrease than was previously seen with methyl salicylate. This could be indicative of the aroma reaching into a greater depth of the leaf fragments.

Given the information from the depth profiles for all of the leaves, with the exception of those treated with linalool it is possible to see where the interfaces are between the cuticle of the leaf and the epidermal layer, and also the epidermal layer and the palisade mesophyll layer. Figure 5.25 shows an amended scan of a leaf with trans-2-hexenal added. Given that the presence of both magnesium and cellulose are markers in the palisade mesophyll layer it can be seen that the intensity of these markers is reached at approximately 520 seconds of profiling. The sharp drop in the intensity of hydrocarbon group one at approximately 430 seconds is indicative of the cuticle having been profiled through and reaching the upper epidermal layer. Variation will obviously occur because of biological differences between leaves but the processing that the leaves go through from their fresh state to a processed state will also have an effect on sample variation.

The ion images in figure 5.26 and 5.27 are not as clear as those recorded for an untreated tea leaf or with methyl salicylate but the area of depth profiling can still be seen. If the sample had been completely flat then the image would have been square, given the topography of the leaf and that it had to be artificially flattened it is not surprising that some images are clearer than others. What can be seen is that the aroma marker of C_5H_7 and the composite of all aroma markers are on the surface of leaf in the

depth profile data, with a small amount heterogeneously distributed within the area of depth profile.

The XZ representation of the presence of aroma markers in the height of the depth profile is shown in figure 5.28. The intensity of the markers is uniformly high until it reaches the palisade mesophyll, as indicated by the increased intensity of $C_3H_5O_2$, this is clearer with the species C_5H_7. Whereas with the methyl salicylate there appeared to be partitioning of the aroma at the interface between the epidermis and the palisade mesophyll layer, here the aroma shows a constant high intensity indicating there was no partitioning.

As trans-2-hexenal has a lower K_{ow} than methyl salicylate, it was assumed that this aroma would have been able to diffuse over the cutin layers but not to the same extent. Experimentally it can be seen that there is a greater diffusion through the leaf with a constant high intensity. As one of the markers identified was of the pure aroma, any reductive or oxidative interactions within the structure of the leaf can be discounted. There may be some reactivity but the presence of the whole aroma was checked with the other markers for it to find out how deep it penetrated. As with methyl salicylate there was a decrease in the intensity of the aroma in the palisade mesophyll layer indicating that the aroma is not diffusing as freely as it could if these layers were not present. This aroma is insoluble in

water. It is also smaller than methyl salicylate. The small size of trans-2-hexenal may have helped with the level of diffusion across the cuticle given its lipophilicity (Buchholz et al. 2006; Schreiber et al. 2006).

To ensure that the aroma did not have any other effects on the rest of the leaf sample, the nitrogen, magnesium and potassium containing groups, and the markers for hydrocarbon groups 1 and 2 were compared with the cellulose marker in figure 5.29. The XZ representation shows the same general behaviour, though the depth profile is not as sharp as with the untreated leaf or methyl salicylate treated leaf. With the variable topography of the leaves and the fact that a small section of the depth profile, in the XY directions of the raster, are used, the lack of sharp detail could be a result of this. Many different sections were observed that showed this patterning. Previously the marker for C_3H_5 showed a high intensity at the surface and the interface between the epidermis and palisade mesophyll layer. This is not seen for these samples. The C_5H_{10} and CH_4N markers showed an increase in intensity from the epidermis layer down to the palisade mesophyll layer, in the leaves treated with trans-2-hexenal, this cannot be seen. Mg and $C_3H_5O_2$ still show an increase in intensity from when the depth profile reaches the palisade mesophyll layer and K shows an initial high intensity in the cuticle of the leaf which decreases as the profile decreases. The chemistry of the leaf

has not been changed but the topography could be masking the clarity of the profile.

5.3.7 ToF-SIMS Depth profiling results of leaves with linalool added

The experiment was repeated again for leaf samples that had been treated with a final aroma, linalool. The positive spectra for linalool on aluminium foil is shown in figure 5.30. Figure 5.31 shows the depth profile with examples of each group that was identified. As with the leaves that had methyl salicylate and trans-2-hexenal added to the surface, the markers for potassium and hydrocarbon group one are of such a high intensity that the rest of the depth profile is masked.

Figure 5.32 shows three markers that were identified for the aroma linalool, these were compared with the marker for cellulose as in the previous depth profiles. The IonImages for the markers of each grouping are compared with the total ion image for leaves treated with linalool in figure 5.33. The composite images of each of the members of each grouping compared with the total ion image are shown in figure 5.34.

An IonImage XZ reconstruction of the markers for linalool is shown compared with the cellulose marker in figure 5.35. The markers for the potassium, nitrate, magnesium and both hydrocarbon groups are shown in figure 5.31 compared with the cellulose marker are shown in figure 5.36.

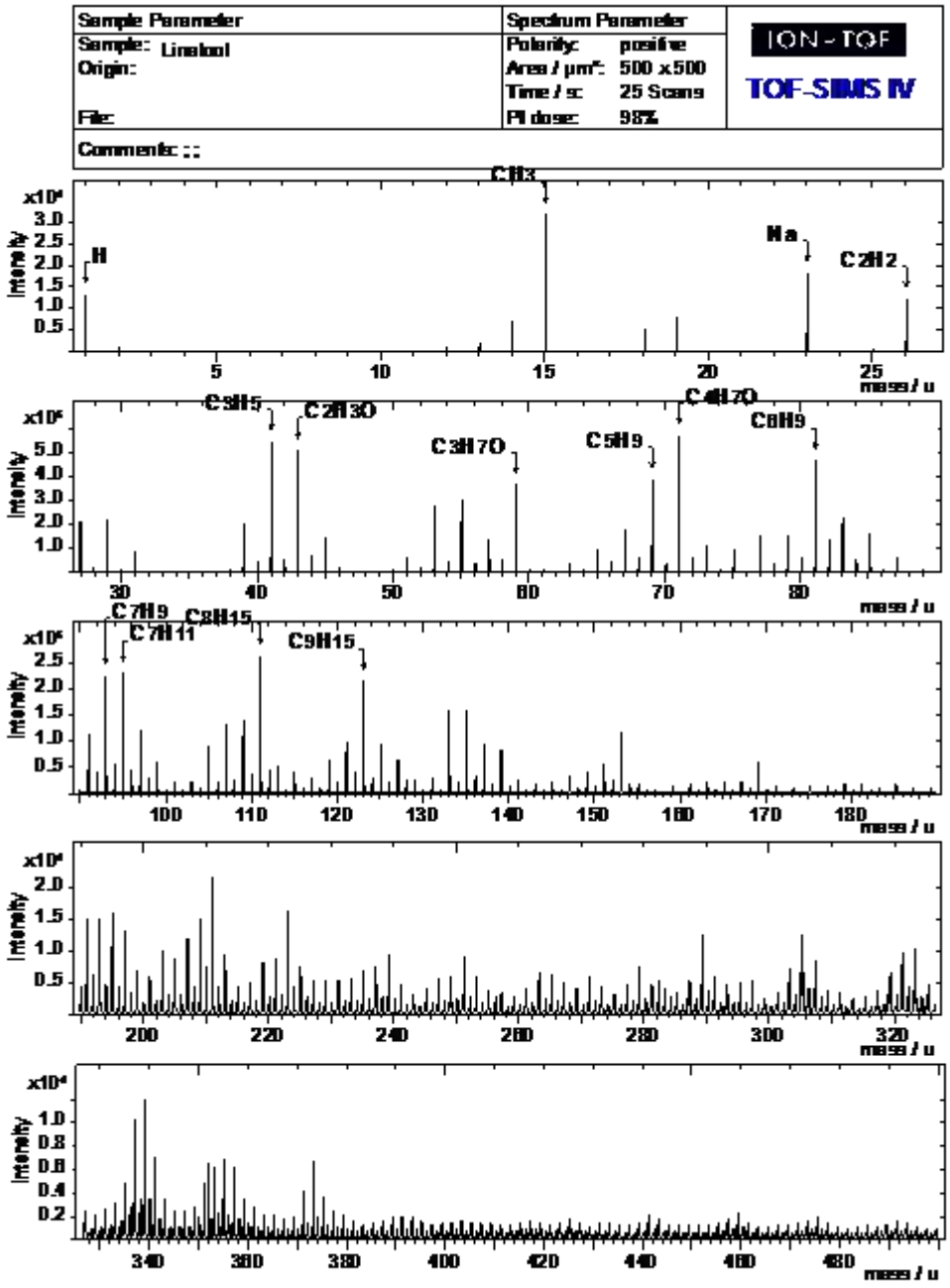

Figure 5.30 – Spectra of linalool sample on aluminium foil.

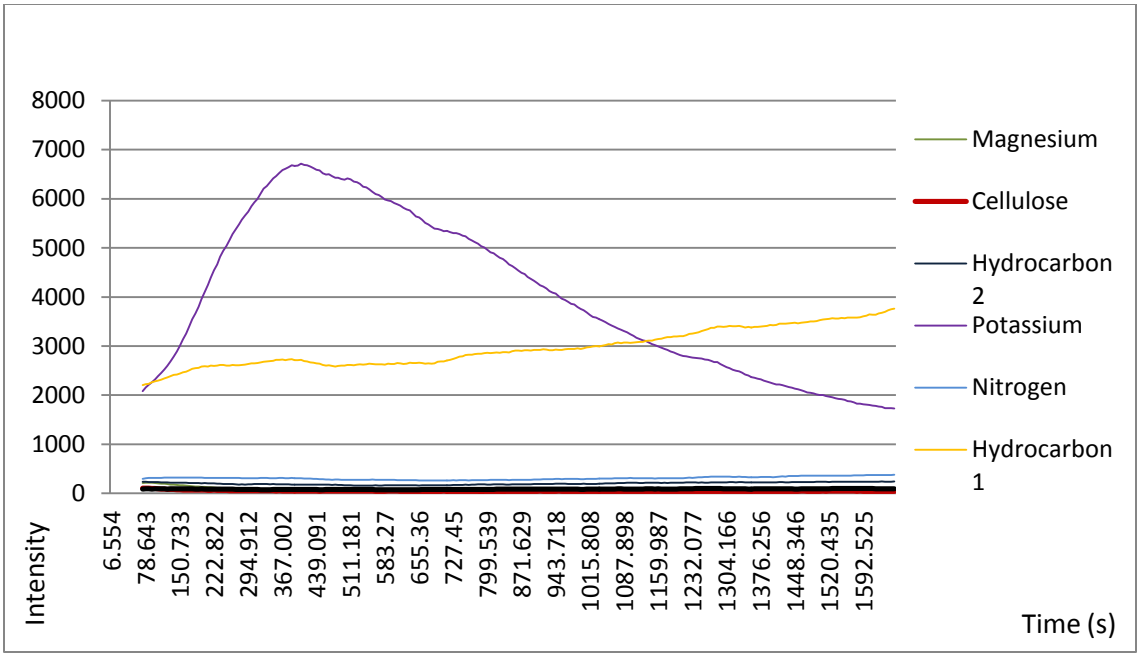

Figure 5.31 - Example trace for depth profiling of a tea leaf infused with linalool, overview of all groups.

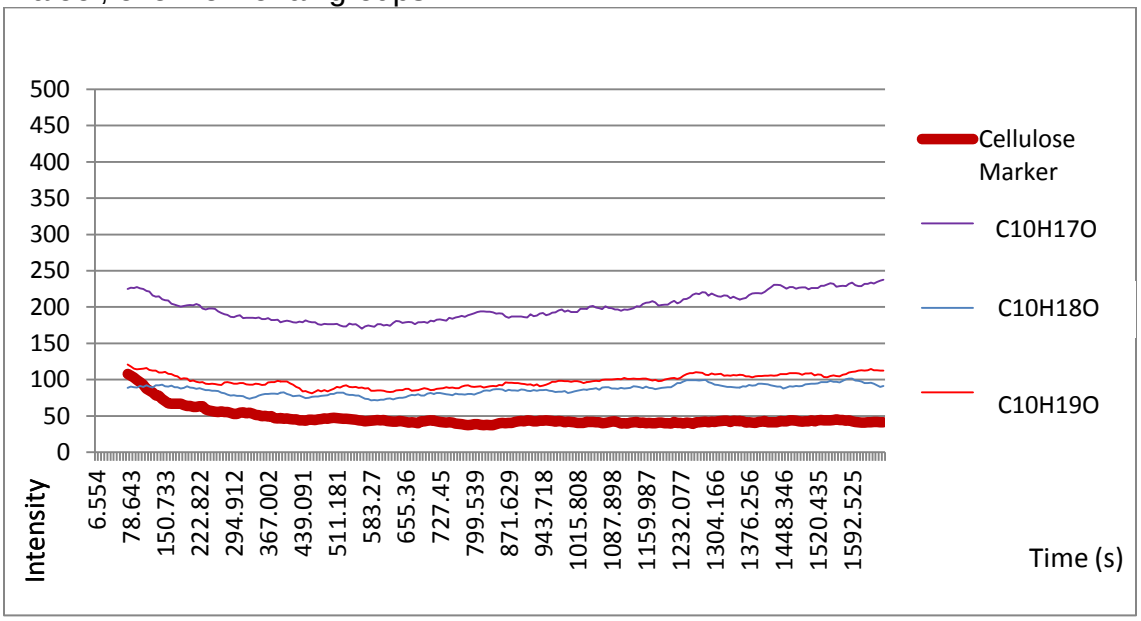

Figure 5.32 - Depth profile trace of markers for the aroma linalool when compared with a marker for cellulose.

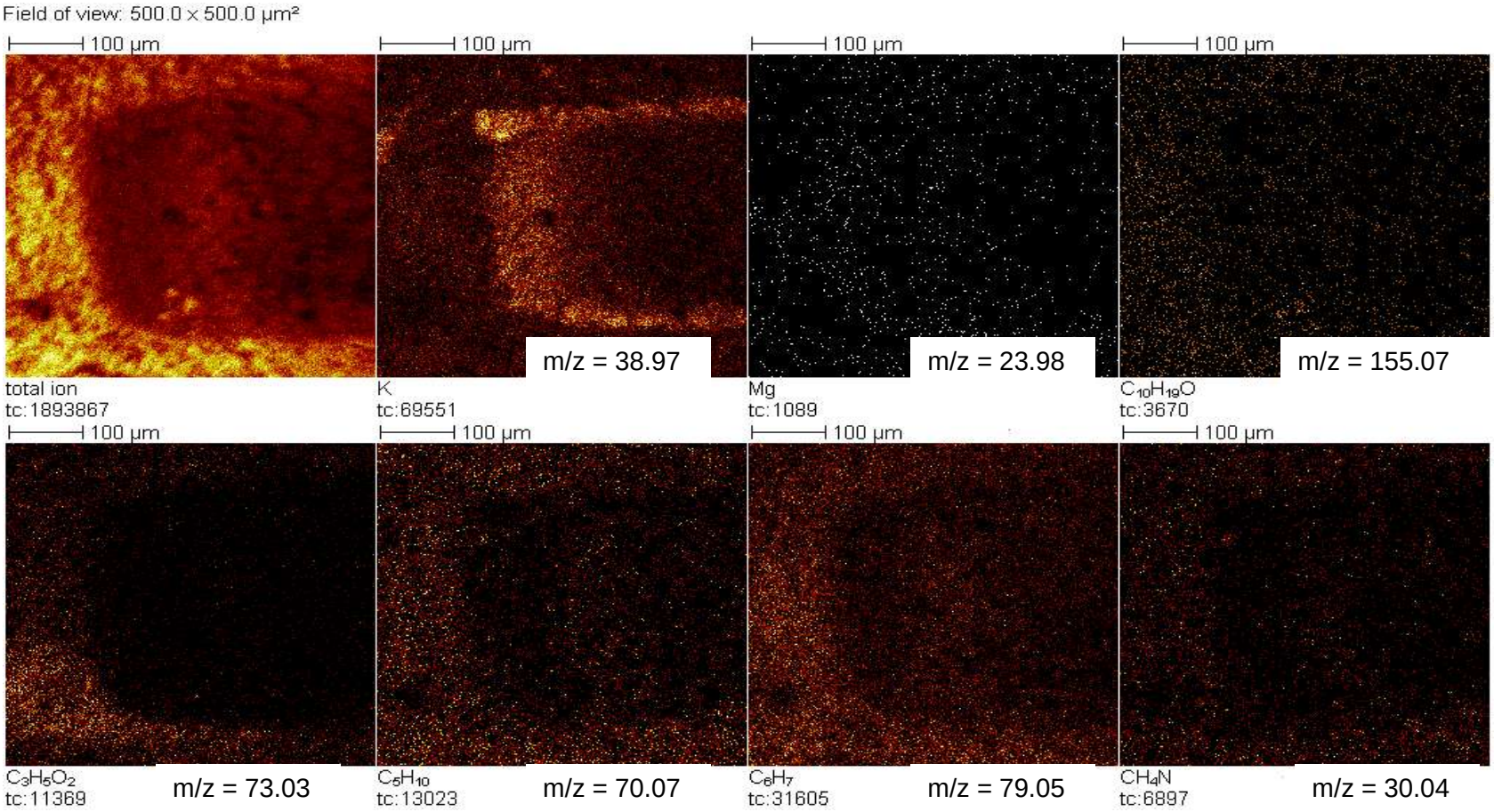

Figure 5.33 - Depth profile Ion images showing examples of all groups identified when linalool is added to the surface of the leaf.

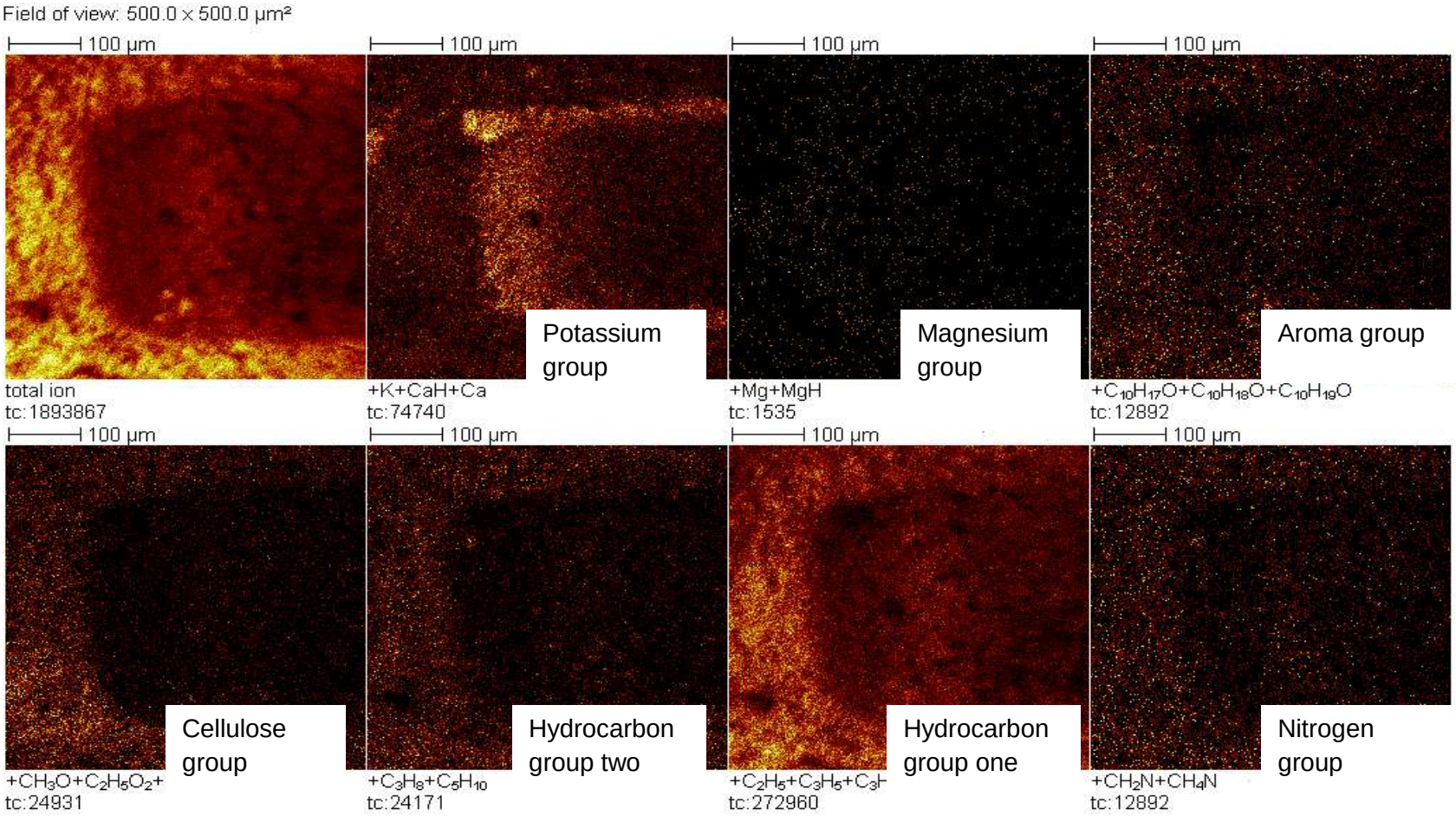

Figure 5.34 - Depth profile Ion images showing composite images of all species identified when linalool is added to the surface of the leaf.

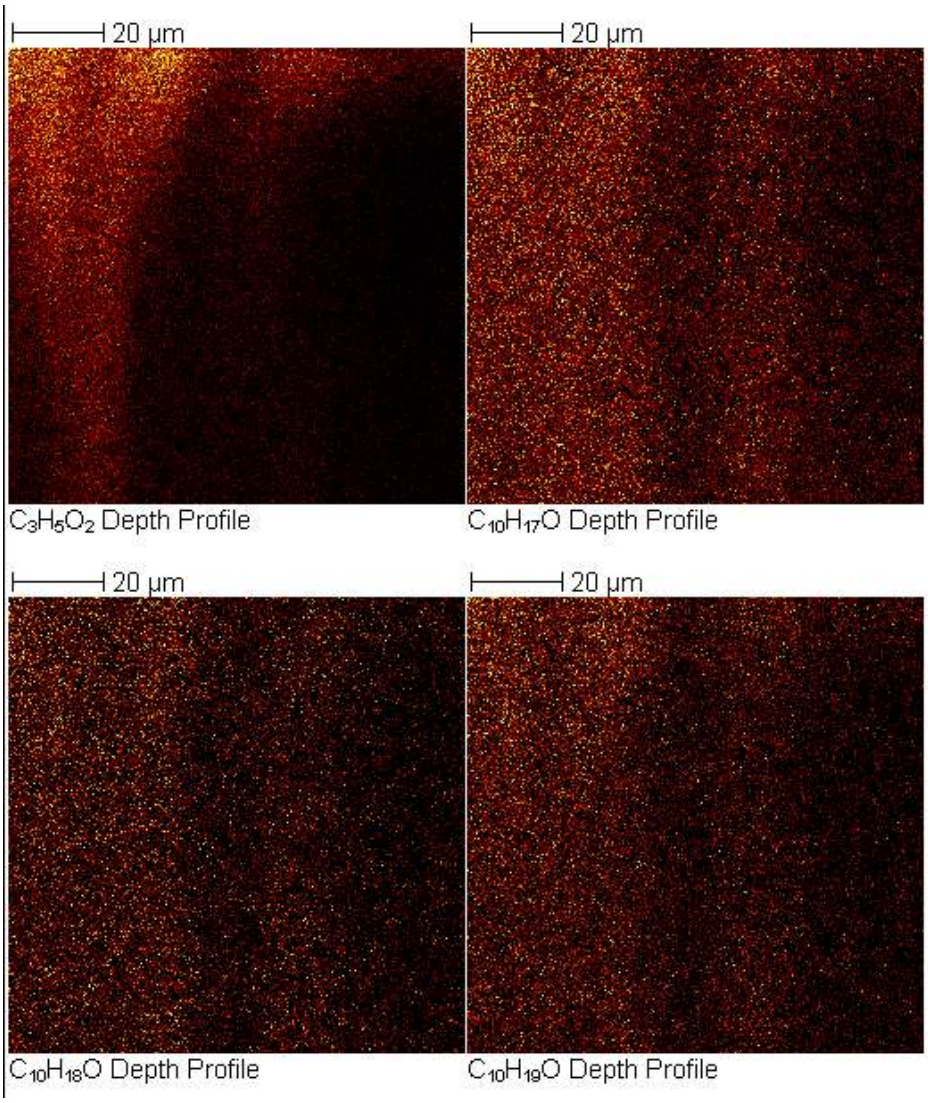

Figure 5.35 - Ion images showing XZ reconstruction of ions identified as being markers for linalool compared with cellulose marker.

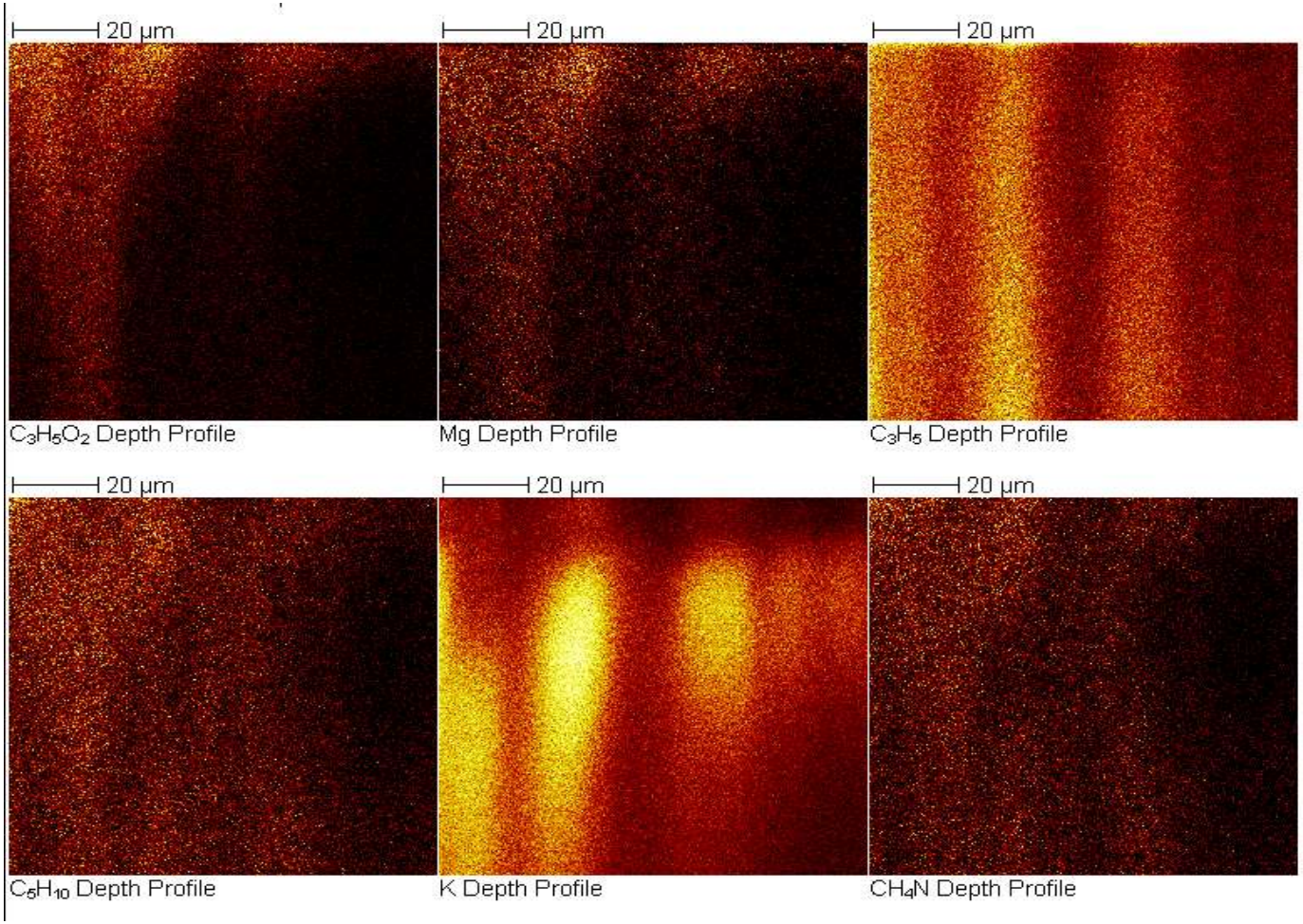

Figure 5.36 - Ion images showing XZ reconstruction of ions identified as being markers for other groups identified on tea leaves for a tea leaf treated with linalool.

5.3.8 Discussion of ToF-SIMS Depth profiling results of leaves with linalool added

When linalool was added to the tea leaf surface there was a significant change in the depth profile data (figure 5.31). The depth profiles for the untreated tea leaves and tea leaves treated with methyl salicylate and trans-2-hexenal showed an initial increase in the intensity for potassium and the marker for hydrocarbon group one, C_3H_5, followed by a sharp decrease in intensity, whilst the other markers increase. This depth profiles for leaves treated with linalool showed a slow increase in the hydrocarbon group one marker and potassium. All other markers are masked by the high intensity for these. The amount of time it took for the potassium and hydrocarbon group one peak to start to decrease in intensity is as long as the usual depth profile for the other aromas. The cuticle could be thicker on these leaf samples for this to occur.

The markers for linalool were examined in figure 5.32. After an initial decrease the intensity for the standard marker that has been used in the previous data sets, this is level for the rest of the trace. There is some increase in the intensity of the markers for the aroma. $C_{10}H_{17}O$, $C_{10}H_{18}O$

and $C_{10}H_{19}O$ all start to increase in intensity from 583 seconds into the depth profile. The increase was higher for $C_{10}H_{17}O$.

The IonImages of the depth profile of the marker species is shown in figure 5.33. The markers for cellulose and magnesium are of a very low intensity confirming that the palisade mesophyll layer has not been reached from the depth profile. This is also confirmed in figure 5.34 with the composite images of all identified marker species. The aroma markers in both of these figures can be seen to have a higher intensity on the surface of the leaf around the etch pit.

The XZ representation of the depth profile for the aroma markers compared with the marker for cellulose is shown in figure 5.34. These images appear different to the examples for untreated leaves and leaves treated with methyl salicylate and trans-2-hexenal. There is evidence of etching with the $C_3H_5O_2$ marker as the band on the right hand side of the image decreases in width as the time of the profile increases. This is also seen on the right hand side of the image with a small area of intensity. The aroma markers correlate to these areas of intensity for cellulose but appear at a constant intensity. As with the XZ representation of the depth profile for methyl salicylate there appears to be partitioning of the aroma in

the cuticle. As linalool is a large molecule, 154.25g/mol, the diffusion through the epicuticular waxes and the cutin membrane could be affected by the size of the molecule. The larger molecules could have difficulty in diffusion through the cutin membrane. As it is also the most lipophilic of the aromas then linalool is only slightly soluble in water so even though the diluted sample was thoroughly mixed before application it was not in a proper solution.

When the XZ representation of the depth profile is examined for all markers of the potassium, magnesium and nitrogen containing species and hydrocarbon groups 1 and 2, the same vertical banding pattern is seen (Figure 5.36).

Potassium, which is usually seen as having a high intensity on the cuticle and then increasing after the interface between the palisade mesophyll and epidermis layer shows a high intensity through the whole profile. The intensity starts to decrease towards the end of the profile. There is no increase, as expected for the cellulose or magnesium markers. C_3H_5 is showing a constant high intensity in vertical bands which correspond to the banding of the potassium. Though C_5H_{10} and CH_4N are showing similar patterns in the profile, the expected horizontal layers are not seen. If this was due to a thicker cuticle then the horizontal banding of potassium

would be of a high intensity for the duration of the scan, as seen. Given that there are vertical stripes in the image, this would indicate an effect from the topography of the leaf fragment. It can be said with confidence that they are definitely on the surface but not how far into the leaf they diffuse.

An overview of the penetration of all of the aromas through the leaf is shown in figure 5.37 showing that trans-2-hexenal penetrated the furthest; methyl salicylate also was able to penetrate through to the palisade mesophyll layer but with a lower intensity. Finally linalool was present in the cuticle but with the thickness of the cuticle it was not possible to see if the aroma was able to penetrate the palisade mesophyll layer. Given the similarity in size to methyl salicylate it can be assumed that it would but with a lower intensity that trans-2-hexenal.

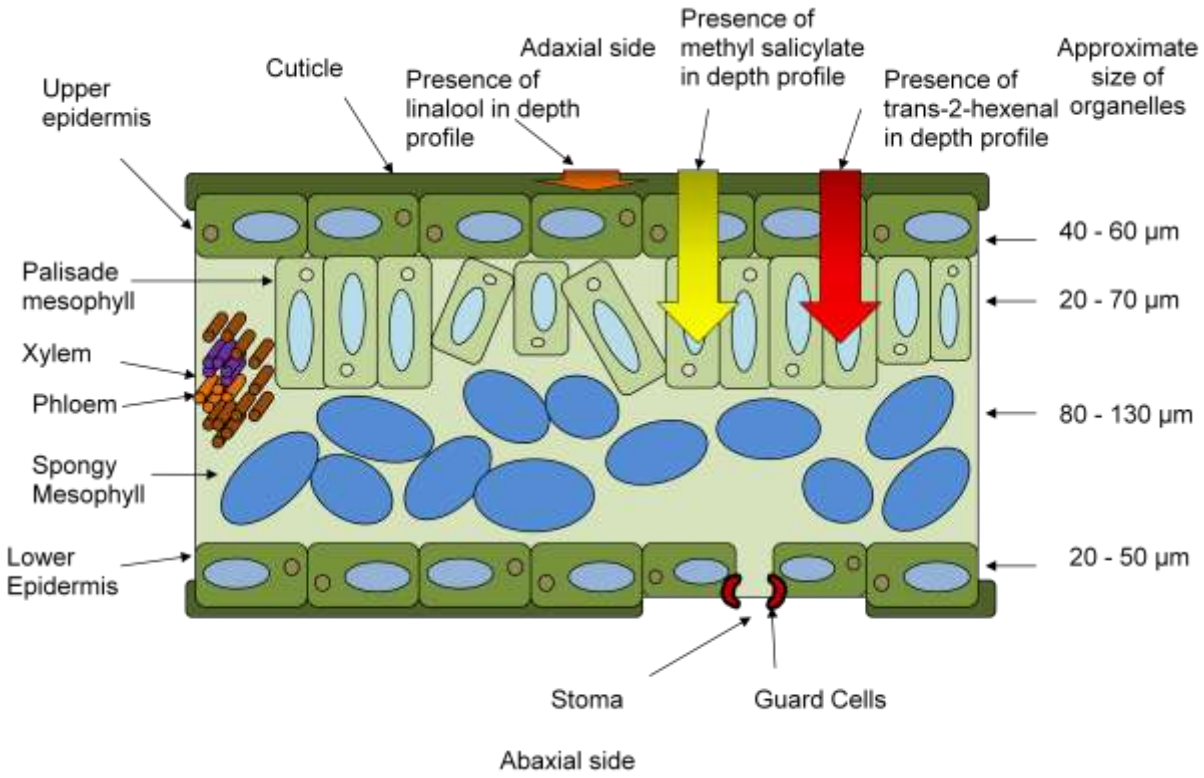

Figure 5.37 – Penetration of aromas through the leaf from depth profile results.

5.4 Conclusions

Depth profiling of tea leaf fragments without aroma added revealed the presence of distinct groups of fragments on the surface of the leaf and an altered chemical composition as the depth profile progressed into the upper epidermis and the palisade mesophyll layer. K, Ca and K_2OH were seen to have a high intensity on the cuticle of the leaf which reduced as the depth profile continued to the palisade mesophyll layer. A group of markers, $C_4H_5O_2$, $C_2H_5O_2$ and CH_3O, indicate the presence of cellulose. Previous experiments using cluster sources to depth profile cellulose were unsuccessful and this experiments shows that the use of a C_{60}^+ source allows the depth profiling of cellulose containing biological materials.

Confirmation that the cellulose markers did, in fact, indicate the spongy mesophyll layer had been reached was shown with the presence of magnesium and other markers containing magnesium. These were Mg, MgH and MgOH. The presence of chlorophyll was indicated by these markers.

Nitrogen containing groups, CH_2N and CH_4N, appeared to increase in intensity after 200 seconds and then decrease in intensity when the palisade mesophyll layer was reached. The increase after 200 second could be indicative of penetration of the upper epidermis.

Two distinct groups of hydrocarbons were found during the depth profiles. Hydrocarbon group one, consisting of C_2H_5, C_3H_5 and C_3H_7, showed an increase in intensity after 200 seconds and a decrease of intensity after the palisade mesophyll layer had been reached. The initial intensity was high indicating the presence of more hydrocarbon group one in the upper epidermis, a little less in the cuticle and a small amount in the palisade mesophyll layer. Hydrocarbon group two, which consisted of C_3H_8 and C_5H_{10}, showing an increase in intensity when the depth profile reaches the upper epidermis and then a decrease in the palisade mesophyll layer. The intensity then starts to increase again, which is where the profile differs from that of hydrocarbon group one.

When methyl salicylate was added to the surface of the tea leaf, the depth profile showed that the intensity of the aroma markers of CH_3, C_2H_5, C_3H_7, C_5H_7, C_5H_9, C_6H_5, C_7H_7, C_7H_7O and $C_8H_8O_3$ were high in the cuticle, with an even higher intensity at the area between the upper epidermis and the palisade mesophyll layer. The intensity decreased in the palisade mesophyll layer indicating the aroma had penetrated the cutin membrane in the cuticle and surrounding the epidermal cells. Partitioning could be seen by the intensity at these two areas indicating the diffusion was hampered by the size and that the aroma was sparingly soluble.

When trans-2-hexenal was added to the leaf surface, the depth profiles showed the markers for this aroma, CH_3, C_3H_7, C_4H_7, C_5H_7, C_5H_9, C_5H_7O, C_6H_7O and $C_6H_{10}O$, having a high intensity in the cuticle and upper epidermal layer and then a steady decrease in intensity during the profiling of the palisade mesophyll layer. There was no partition at the cuticle and the interface between the upper epidermis and the palisade mesophyll layer. The aroma had diffused to the palisade mesophyll layer but, again, to a lesser extent than the cuticle and upper epidermis.

The presence of markers for linalool, $C_{10}H_{17}O$, $C_{10}H_{18}O$ and $C_{10}H_{19}O$, were seen on the cuticle of the leaf. Due to the thickness of the cuticle it was not seen how far into the leaf linalool was able to diffuse but given the data for methyl salicylate it can be assumed that some would be seen in the palisade mesophyll layer. Given these data shown the size of the molecule is important in how far the molecule can penetrate into the leaf. The smallest of the molecules, trans-2-hexenal was able to penetrate the cuticle with no signs of partitioning at either the cuticle or the epidermal layer. As it was lipophilic it was able to penetrate the cuticle and cutin membrane within the leaf. Methyl salicylate showed that it was able to diffuse through the cuticle and epidermis and there was a low intensity of the aroma in the palisade mesophyll layer. The size of this aroma was much larger than trans-2-hexenal. Methyl salicylate was more lipophilic than trans-2-hexenal but showed partitioning within the cuticle and the

interface between the epidermal and palisade mesophyll layer. With methyl salicylate being more lipophilic it should have been able to penetrate the cuticle more easily, this was not the case due to the size of the molecule. Finally, linalool, the largest molecule was present in the surface and showed signs of partitioning in the cuticle as methyl salicylate did. The diffusion of the aroma appears to be dependent on the size of the aroma molecule and a lower partition coefficient. The smaller, less lipophilic molecules are able to penetrate the cuticle and the intensity in the palisade mesophyll is higher than the larger, more lipophilic aromas. To confirm this, further depth profiling of different aroma molecules is needed, ideally small molecular weight aromas which have high partition coefficients and a range of aromas with molecular weights between trans-2-hexenal and methyl salicylate.

References

Aparicio, S., Alcaide, R. (2010). "On the Structure of Liquid Methyl Salicylate: the Role of Intramolecular Hydrogen Bonding." European journal of chemistry 1(3): 162-167.

Bate, N. J., Rothstein, S. J. (1998). "C6-volatiles derived from the lipoxygenase pathway induce a subset of defense-related genes." The Plant journal : for cell and molecular biology 16(5): 561-569.

Buchholz, A. (2006). "Characterization of the diffusion of non-electrolytes across plant cuticles: properties of the lipophilic pathway." Journal of Experimental Botany 57(11): 2501-2513.

Cheng, J., Wucher, A., Winograd, N. (2006). "Molecular Depth Profiling with Cluster Ion Beams." The journal of physical chemistry. B 110(16): 8329-8336.

Croft, K. P. C., Juttner, F., Slusrenko, A. J. (1993). "Volatile products of the lipoxygenase pathway evolved from Phaseolus vulgaris (L.) leaves inoculated with Pseudomonas syringae pv phaseolicola." Plant physiology (Bethesda) 101(1): 13.

Fletcher, J. S., Conlan, X. A., Lockyer, N. P., Vickerman, J. C. (2006). "Molecular depth profiling of organic and biological materials." Applied Surface Science 252(19): 6513-6516.

Gulati, A., Ravindranath, S. D. (1996). "Seasonal variations in quality of Kangra tea (Camellia sinensis (L) O Kuntze) in Himachal Pradesh." Journal of the Science of Food and Agriculture 71(2): 231-236.

Kawakami, M., Ganguly, S. N., Banerjee, J., Kobayashi, A. (1995). "Aroma composition of Oolong tea and black tea by brewed extraction method and characterizing compounds of Darjeeling tea aroma." Journal of Agricultural and Food Chemistry 43(1): 200-207.

Kerier, F., Schonherr, J. (1988). "Permeation of lipophilic chemicals across plant cuticles: prediction from partition coefficients and molar volumes." Archives of environmental contamination and toxicology 17(1): 7-12.

Lyman, W. J., Reehl, W. F. Rosenblatt, D. H. (1993). Handbook of Chemical Property Estimation Methods, American Chemical Society.

Martínez, C., Pons, E., Prats, G., Leon, J. (2004). "Salicylic acid regulates

flowering time and links defence responses and reproductive development Salicylic acid and flowering time in Arabidopsis." The Plant journal : for cell and molecular biology 37(2): 209-217.

Merck (2006). The Merck Index: An Encyclopaedia of Chemicals, Drugs and Biologicals: An Encyclopedia of Chemicals, Drugs, and Biologicals (Merck Index: Encyclopedia of Chemicals, Drugs & Biologicals), Merck Manuals.

Morita, K., Wakabayashi, M., Kubota, K., Kobayashi, A., Herath, N. L. (1994). "Glycoside precursor of tea aroma .2. Aglycone constituents in fresh tea leaves cultivated for green and black tea." Bioscience Biotechnology and Biochemistry 58(4): 687-690.

Naknean, P., Meenune, M. (2010). "Factors affecting retention and release of flavour compounds in food carbohydrates." International Food Research Journal(17): 23-34.

Park, S. W., Kaimoyo, E., Kumar, D., Mosher, S., Klessig, D. F. (2007). "Methyl Salicylate Is a Critical Mobile Signal for Plant Systemic Acquired Resistance." Science 318(5847): 113-116.

Ravichandran, R., Parthiban, R. (1998). "The impact of processing techniques on tea volatiles." Food Chemistry 62(3): 347-353.

Rawat, R., Gulati, A. (2008). "Seasonal and clonal variations in some major glycosidic bound volatiles in Kangra tea (Camellia sinensis (L.) O. Kuntze)." European Food Research and Technology 226(6): 1241-1249.

Rawat, R., Gulati, A., Babu G. D. K., Acharya, R., Kaul, V. K., Singh, B. (2007). "Characterization of volatile components of Kangra orthodox black tea by gas chromatography-mass spectrometry." Food Chemistry 105(1): 229-235.

Reisenman, C. E., Riffell, J. A., Bernays, E. A., Hildebrand, J. G. (2010). "Antagonistic effects of floral scent in an insect–plant interaction." Proceedings of the Royal Society B: Biological Sciences 277(1692): 2371-2379.

Riederer, M., Schönherr, J. (1984). "Accumulation and transport of (2,4-dichlorophenoxy)acetic acid in plant cuticles: I. Sorption in the cuticular membrane and its components." Ecotoxicology and Environmental Safety 8(3): 236-247.

Riederer, M., Schönherr, J. (1985). "Accumulation and transport of (2,4-dichlorophenoxy)acetic acid in plant cuticles: II. Permeability of the cuticular membrane." Ecotoxicology and Environmental Safety 9(2): 196-208.

Schreiber, L. (2006). "Review of sorption and diffusion of lipophilic molecules in cuticular waxes and the effects of accelerators on solute mobilities." Journal of Experimental Botany 57(11): 2515-2523.

Takeo, T. (1981). "Black tea aroma and its formation .2. Variation in amounts of linalol and geraniol produced in tea shoots by mechanical injury." Phytochemistry 20(9): 2149-2151.

Tzellos, T. G., Sardeli, C., Lallas, A., Papzisis, G., Chourdakis, M., Kouvelas, D. (2011). "Efficacy, safety and tolerability of green tea catechins in the treatment of external anogenital warts: a systematic review and meta-analysis." Journal of the European Academy of Dermatology and Venereology 25(3): 345-353.

Vlot, A. C. (2008). "Systemic acquired resistance: the elusive signal (s)." Current Opinion in Plant Biology 11(4): 436.

Wang, D. M., Yoshimura, T., Kubota, K., Kobayashi, A. (2000). "Analysis of glycosidically bound aroma precursors in tea leaves. 1. Qualitative and quantitative analyses of glycosides with aglycons as aroma compounds." Journal of Agricultural and Food Chemistry 48(11): 5411-5418.

Wucher, A. (2008). "Molecular Depth Profiling Using a C60 Cluster Beam: The Role of Impact Energy." Journal of physical chemistry. C 112(42): 16550-16555.

Zhang, Z. Z., Li, Y. B., Qi, L., Wan, X. C. (2006). "Antifungal activities of major tea leaf volatile constituents toward Colletorichum camelliae Massea." Journal of Agricultural and Food Chemistry 54(11): 3936-3940.

Chapter 6.

Discussion

6.1 Introduction

The surface chemistry and morphology of the tea leaves were investigated using AFM, SEM and ToF-SIMS. Visually, black tea leaves show more surface debris and a rougher topography than green tea leaves using the SEM. As there is a mechanistic approach to the production of black tea leaves and as the leaves are damaged to allow oxidation of the leaf this is to be expected.

The AFM showed what appear to be layers of waxes on the surface of both green and black tea leaves of a comparable size. This indicates that although the leaves were treated at different heats in the processing from fresh leaf to finished product there is little evidence that the morphology of the leaf changes due to the processing steps. It was also seen that structures were visible on one of the black tea leaf samples of what appear to be wax micro-crystals. In the green tea leaf samples, there was evidence of a difference in tip interaction between the sample and the probe indicating a difference in composition of the cuticle. This difference may be due to the age of the original leaf.

The surface chemistry of the tea leaves were examined with ToF-SIMS. Both leaves were composed of hydrocarbon groups and oxygenated hydrocarbons, indicative of lipids on the surface of the leaf.

Differences in the mean normalised intensity of potassium and magnesium were observed where the intensity was higher in black leaves compared with green tea leaves. The presence of dodecyl aldehyde was indicated by the peak for $C_{12}H_{23}O$, whilst $C_2H_5O_2$ and C_2H_3O were also seen indicating the presence of protonated acetic acid and behenyl acetate, known epicuticular waxes (Perkins et al. 2005). This may have been due to the release of these species when the leaves were cut, torn and crushed to start the oxidative process of producing black tea leaves.

The effects different lengths of infusion in hot water on the surface chemistry and morphology of the tea leaf has been displayed as well. Whilst previous work have examined what is released from tea leaves during infusion, either as aroma by capturing and analysing the head space of infusions or by examining the resultant infusion, this is the first examination of what happens to the actual leaf during this process. Chemical changes are apparent at 15 seconds of infusion and these changes continue until the end point of 300 seconds.

The morphology of the surface changes from 30 seconds of infusion time with the melting of the cuticular waxes on the surface. Waxes that had been identified in the cuticular layer had a melting point of 69.6 ^{o}C and

were insoluble. The effects of infusion and then drying showed a visual change in the morphology of the leaf with the appearance of holes in the cuticle which increased in frequency and then size as time progressed.

Chemical changes are apparent at 15 seconds of infusion and these changes continue until the end point of 300 seconds. The increase in the intensity of $C_3H_5O_2$, a species that had previously been seen in the examination of cotton fibres, was seen to increase with infusion time. The increase was attributed to the change in the structure of the cuticular wax following infusion and an increase in the amount of material seen in the epidermal layer following a movement of the cuticular waxes. The intensity of hydrocarbon groups on the surface of the leaf changed during the infusion process. Long chain hydrocarbons, oxygenated hydrocarbons and oxygen all increased in intensity from the un-infused leaf to the final infusion time. Shorter chain hydrocarbons decreased in intensity as infusion time increased.

Monomers of previously identified components of the cutin layer, such as octadecanoic acid were identified on the surface of the leaf and the changes in these species were observed. These increased with infusion time (Tsubaki et al. 2008).

Overall these data suggest that the melting of the cuticle and cutin layer during infusion may be related to the release of aroma, flavour and other constituents of the tea leaf. As the cuticle melts in the boiling water, more

liquid is allowed to diffuse into the leaf. As the cuticle is the main barrier for this to occur, a change in the structure of the cuticle would ease this problem. As the changes occur rapidly this may be related to an early stage of infusion.

It has been shown for the first time that the C_{60}^{+} source on the ToF-SIMS is a useful diagnostic tool for the analysis of cellulosic material, which had previously been theorised. Whereas before cellulose membrane was used, in these data a complex bio matrix was analysed. The condition of the samples was also problematic. Some previous studies have used leaves or sections of leaves where the material was reasonably fresh or still attached to the plant and alive. In these experiments all samples had been processed and dehydrated prior to experimentation. The use of the C_{60}^{+} source on the analysis of complex bio molecules, even in a degraded state could allow detailed molecular profiling of the surface composition and with its ability to ablate the surface depth profiling into the bulk of a biological material.

In earlier experiments $C_3H_5O_2$ was used as a marker for the presence of cellulose and with the use of the depth profiles this was confirmed by the presence of Magnesium. By being able to identify cellulose the estimation

of where in the leaf molecules could be found was improved. Two distinct hydrocarbon groups were also identified.

The addition of the aroma samples showed varied results. Whereas trans-2-hexenal, a lipophilic aroma which is insoluble in water, was able to diffuse through the cuticle, epidermal layer and palisade mesophyll layer easily methyl salicylate, a larger, more lipophilic aroma slightly soluble in water, showed partitioning when diffusing through the leaf. The intensity for methyl salicylate was increased when the depth profile examined the cuticle and the epidermal layer of the leaf. Some methyl salicylate was present in the palisade mesophyll layer showing that the aroma was able to diffuse through the epicuticular waxes and the cutin membrane of the leaf but the higher intensity of the markers for the aroma showed that the cutin membrane was the rate limiting step in the diffusion with a higher intensity at the cuticle and the interface between the epidermis and the palisade mesophyll layer. This was also partially seen with the aroma linalool, a large lipophilic molecule. The diffusion of the aroma appears to be controlled by the size and shape of the molecule. Trans-2-hexenal is a small chained aldehyde whereas methyl salicylate has a large ring structure with an alcohol and ester group which can bond to itself causing a large increase in molecule size and linalool is a long chain terpene alcohol.

With agrichemical and fertilizers the addition of surfactants and adjunctives have been shown to increase the diffusion of materials through the cuticle

of the leaf. As the aromas are mixed with water a better delivery system could be useful in ensuring the aroma fully penetrates the cuticle so that it is released during infusion to ensure a better sensory experience of the tea drinker. Experiments using Polyethelyne Glycol have been shown to help in the diffusion of agrichemical but the effects of using a compound such as this could affect the taste of the tea and given the possibilities of side effects, due to contamination during polymerisation or its laxative effect, would not be an ideal candidate for a surfactant on a foodstuff. The ideal surfactant would show the same characteristics but not be toxic or harmful and not affect the taste or smell of the finished tea drink.

References

Perkins, M. C., Roberts, C. J., Briggs, D., Davies, M. C., Friedmann, A., Hart, C. A., Bell, G. A. (2005). "Surface morphology and chemistry of Prunus laurocerasus L. leaves: a study using X-ray photoelectron spectroscopy, time-of-flight secondary-ion mass spectrometry, atomic-force microscopy and scanning-electron microscopy." Planta 221(1): 123-134.

Tsubaki, S., H. Iida, et al. (2008). "Microwave Heating of Tea Residue Yields Polysaccharides, Polyphenols, and Plant Biopolyester." Journal of Agricultural and Food Chemistry 56(23): 11293-11299.